BULGARIAN CHEMICAL COMMUNICATIONS

Eccentric Connectivity Polynomial of C_{18n+10} Fullerenes

Modjtaba Ghorbani[1], Ali Reza Ashrafi[2,3] and Mahsa Hemmasi[4]

[1]Department of Mathematics, Faculty of Science, Shahid Rajaee Teacher Training University, Tehran, 16785 – 136, I. R. Iran

[2]Department of Mathematics, Statistics and Computer Science, University of Kashan, Kashan, 87317 – 51167, I. R. Iran

[3]Institute of Nanoscience and Nanotechnology, University of Kashan, Kashan 87317−51167, I. R. Iran

[4]Department of Mathematics, Faculty of Science, Islamic Azad University, Kashan Branch, Kashan, I. R. Iran

The fullerene era was started in 1985 with the discovery of a stable C_{60} cluster and its interpretation as a cage structure with the familiar shape of a soccer ball by Kroto and co-authors. The eccentric connectivity polynomial of a molecular graph G is defined as $ECP(G, x) = \Sigma_{a \in V(G)} deg_G(a)x^{ecc(a)}$, where $ecc(a)$ is defined as the length of the maximum path connecting to another vertex of G. In this paper this polynomial is computed for C_{18n+10} fullerenes.

INTRODUCTION

We first recall some algebraic definitions that will be kept throughout. A pair $G = (V, E)$ such that V is a non-empty set and E is a subset of 2-element subsets of V is called a simple graph (graph for short). G is said to be connected if for arbitrary vertices x and y of G, there exists a sequence $x = x_0, x_1, x_2, ..., x_n = y$ such that x_i and x_{i+1} are adjacent in G. The vertex and edge sets of a graph G are denoted by $V(G)$ and $E(G)$, respectively. If $x, y \in V(G)$ then the distance $d(x, y)$ between x and y is defined as the length of the minimum path connecting x and y. The eccentric connectivity index of G, $\xi^c(G)$, was proposed by Sharma, Goswami and Madan [1]. It is defined as $\xi^c(G) = \Sigma_{u \in V(G)} deg_G(u)ecc(u)$, where $deg_G(x)$ denotes the degree of the vertex x in G and $ecc(u) = \text{Max}\{d(x, u) \mid x \in V(G)\}$ [2−6]. The radius and diameter of G are defined as the minimum and maximum eccentricity among vertices of G, respectively.

A fullerene is a molecule composed entirely of carbon atoms. The fullerene era was started in 1985 with the discovery of a stable C_{60} cluster [7, 8]. Let F be a fullerene graph with exactly p, h, n and m pentagons, hexagons, vertices and edges between them, respectively. Since each vertex lies in exactly 3 faces and each edge lies in 2 faces, the number of vertices is $n = (5p+6h)/3$, the number of edges is m $= (5p+6h)/2 = 3/2n$ and the number of faces is $f = p + h$. By Euler's formula $n − m + f = 2$, one can deduce that $(5p + 6h)/3 − (5p + 6h)/2 + p + h = 2$, and therefore $p = 12$, $v = 2h + 20$ and $e = 3h + 30$. Therefore, such molecules are made up entirely of n carbon atoms having 12 pentagonal and $(n/2 − 10)$ hexagonal faces, where $n \neq 22$ is a natural number equal or greater than 20.

We now define the eccentric connectivity polynomial of a graph G, as
$$\Xi(G,x) = \Sigma_{a \in V(G)} deg_G(a)x^{ecc(a)}.$$
Then the eccentric connectivity index is the first derivative of $\Xi(G,x)$ evaluated at $x = 1$. Herein, our notation is standard and taken from the standard book of graph theory [9–14].

RESULTS AND DISCUSSION

This paper describes significant updates to the fullerene chemistry. In other words, this is a synthesis of knowledge. The research is based on our earlier works [9, 11–14] on constructing new classes of fullerenes and providing good computer programs for discovering their topological properties. Our research in this field started with the classification of fullerenes by their molecular graphs [9]. In the field, it is generally observed that there are more than 20 infinite families of fullerene graphs. This problem has been known to partly arise from the stability of fullerenes. The aim of this section was to compute eccentric connectivity index of an infinite family of these series of

* To whom all correspondence should be sent:
E-mail: mghorbani@srttu.edu

fullerenes, namely, C_{18n+10}. To do this, we first drew these compounds by HeperChem [15] and then computed their adjacency and distance matrices by TopoCluj [16]. Next, we applied some GAP [17] programs to compute the $ecc(u)$ for a given vertex u of these nano-materials. The final step of this process is the analysis of the data obtained by our GAP programs. These programs are accessible from the authors upon request.

An automorphism of the graph $G = (V, E)$ is a bijection σ on V which preserves the edge set E, i.e., if $e = uv$ is an edge, then $\sigma(e)=\sigma(u)\,\sigma(v)$ is an edge of E, where $\sigma(u)$ is the image of the vertex u. Thus Aut(G), the set of all automorphisms of G, under composition of mappings, forms a group. Aut(G) acts transitively on V if for any vertices u and v in V there is $\alpha \in Aut(G)$ such that $\alpha(u) = v$.

To explain our method, we computed the eccentric connectivity polynomial of an icosahedral fullerene C_{20} with 20 vertices and a cube H_3 with 8 vertices. Since for every, $v \in V(C_{20})$, $ecc(v)= 5$, $\Xi(C_{20}, x) = 60x^5$. On the other hand, H_3 is 3-regular and so for every $v \in V(H_3)$, $ecc(v)= 3$. Hence $\Xi(H_3, x) = 24x^3$.
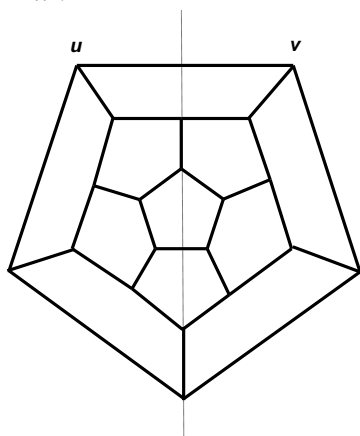

Fig. 1: The molecular graph of fullerene C_{20}.

We began by the following simple Lemma:

Lemma 1. Let $G = (V, E)$ be a graph. If Aut(G) acts transitively on V, then G is k-regular, where $|E| = k|V|/2$. Moreover, for every u in $V(G)$, $\Xi(G, x) = k|V| \times x^{ecc(u)}$.

The hypercube H_n is a graph consisting of all n-tuples $b_1 b_2 b_n$, $b_i \in \{0,1\}$, as vertices. Two vertices are adjacent if the corresponding tuples differ in precisely one place, so for every vertex a in $V(G)$, $ecc(a) = n$ and H_n is n - 1 regular. Darafsheh [14] proved that H_n is transitive. We now applied Lemma 1 to compute the eccentric connectivity polynomial of a hypercube H_n. We have $\Xi(H_n, x) = (n-1)2^n . x^{n-1}$. On the other hand, by considering the fullerene graph C_{20} shown in Figure 1, one can see that C_{20} is vertex transitive. But $ecc(u) = 5$, for

every u in $V(C_{20})$. This implies that $\Xi(C_{20}, x) = 60x^5$. The fullerenes C_{20} and C_{60} are the only vertex transitive fullerenes. So it is important how to compute $\Xi(G, x)$ polynomial for other fullerenes.

Lemma 2. Let $G = (V, E)$ be a graph. If orbits of Aut(G) under its action on V are V_1, V_2, V_s and u_i is a vertex of V_i, then:

$$\Xi(G, x) = \sum_{i=1}^{s} k_i \, |V_i| \, x^{ecc(u_i)}.$$

Proof. Suppose $V_i's$ $(1 \le i \le s)$ are orbits of Aut(G) on the set V. Clearly, for every u_i in V_i $deg_G u_i = k_i$ and Aut(G) acts transitively on V_i $(1 \le i \le s)$. By using Lemma 1 the proof is completed.

Now we used Lemma 2 to compute the polynomial $\Xi(G,x)$ for the fullerene graph C_{18n+10}. In Table 1, the $\Xi(G,x)$ polynomials of C_{18n+10} fullerenes (Figures 2 and 3) are computed, $4 \le n \le 13$. For $n \ge 14$ we have the following general formula for the $\Xi(G,x)$ polynomial of this class of fullerenes:
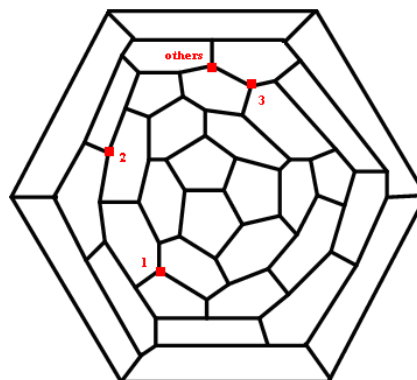

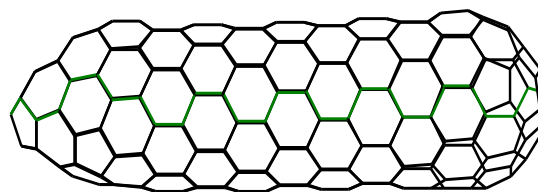**Fig. 2.** The molecular graph of the fullerene C_{18n+10}.

Fig. 3. The value of $ecc(x)$ for vertices of central and outer polygons.

Theorem 1. The $\Xi(G,x)$ polynomial of the fullerene C_{18n+10} $(n \ge 14)$, is computed as follows:

$$\Xi(C_{18n+10}, x) = 54x^{n+2} \times \frac{x^{n-2} - 1}{x - 1} + $$
$$+ 45(x^{2n} + x^{2n+1}) + 27x^{2n+2} + 21x^{2n+3}.$$

Proof. From Figure 2, one can see that Aut(G) has exactly four orbits on the vertices of C_{18n+10}. We named the representatives of these orbits as type 1, type 2, type 3 and type 4. In Table 1, we recorded our calculations:

Table 1: The type of vertices and their eccentricities

Vertices	ecc(x)	No.
Type 1 Vertices	$2n+3$	7
Type 2 Vertices	$2n+2$	9
Type 3 Vertices	$2n, 2n+1$	15
Type 4 Vertices	$n+i$ ($2 \leq i \leq n-1$)	18

By the calculations given in Table 1, and Figure 2, the theorem is proved.

Some exceptional cases are given in Table 2.

Corollary 1. The diameter of C_{18n+10} fullerene, $n \geq 4$, is $2n + 3$.

Table 2. Some exceptional cases of C_{18n+10} fullerenes.

Fullerenes	EC Polynomials
C_{82}	$67x^{10}+15x^{11}$
C_{100}	$18x^{10}+50x^{11}+22x^{12}+10x^{13}$
C_{118}	$36x^{11}+39x^{12}+21x^{13}+13x^{14}+9x^{15}$
C_{136}	$18x^{11}+36x^{12}+27x^{13}+21x^{14}+15x^{15}+12x^{16}+7x^{17}$
C_{154}	$36x^{12}+27x^{13}+21x^{14}+18x^{15}+21x^{16}+15x^{17}+9x^{18}+7x^{19}$
C_{172}	$18x^{12}+27x^{13}+21x^{14}+18x^{15}+21x^{16}+18x^{17}+15x^{18}+15x^{19}+ 9x^{20}+7x^{21}$
C_{190}	$27x^{13}+21x^{14}+18x^{15}+24x^{16}+18x^{17}+18x^{18}+18x^{19}+15x^{20}+15x^{21}+9x^{22}+7x^{23}$
C_{208}	$9x^{13}+21x^{14}+18x^{15}+24x^{16}+18x^{17}+18x^{18}+18x^{19}+ 18x^{20}+ 18x^{21}+ 15x^{22}+ 15x^{23}+9x^{24}+7x^{25}$
C_{226}	$21x^{14}+18x^{15}+24x^{16}+18x^{17}+18x^{18}+18x^{19}+18x^{20}+18x^{21}+18x^{22}+18x^{23}+15x^{24}+15x^{25}+9x^{26}+7x^{27}$
C_{244}	$12x^{15}+24x^{16}+18x^{17}+18x^{18}+18x^{19}+18x^{20}+18x^{21}+18x^{22}+18x^{23}+18x^{24}+18x^{25}+15x^{26}+ 15x^{27}+9x^{28}+7x^{29}$

CONCLUSION

This paper contains information about the topological property of an infinite class of fullerenes. The area of fullerene chemistry is relatively young and received a strong boost after the discovery of the C_{60} fullerene molecule by Kroto and his team. Our results are related to the mathematical properties of this new allotrope of carbon.

REFERENCES

1 V. Sharma, R. Goswami, A. K. Madan, *J. Chem. Inf. Comput. Sci*., **37,** 273 (1997).

2 B. Zhou, Z. Du, *MATCH Commun. Math. Comput. Chem*, **63**, 181 (2010).

3 A. A. Dobrynin, A. A. Kochetova, *J. Chem. Inf. Comput. Sci*., **34**, 1082 (1994).

4 I. Gutman, *J. Chem. Inf. Comput. Sci*., **34**, 1087 (1994).

5 I. Gutman, O.E. Polansky, *Mathematical Concepts in Organic Chemistry*, Springer-Verlag, New York, 1986.

6 M. A. Johnson, G. M. Maggiora, *Concepts and Applications of Molecular Similarity*, Wiley Interscience, New York, 1990.

7 H. W. Kroto, J. R. Heath, S. C. O'Brien, R. F. Curl, R. E. Smalley, *Nature*, **318,** 162 (1985).

8 H. W. Kroto, J. E. Fichier, D. E Cox, *The Fulerene*, Pergamon Press, New York, 1993.

9 M. V. Diudea, *Fullerenes, Nanotubes and Carbon Nanostructures*, **10**, 273 (2002).

10 A. R. Ashrafi, M. Ghorbani, M. Jalali, *Ind. J. Chem*., **47A**, 535 (2008).

11 M. Ghorbani, A. R. Ashrafi, *J. Comput. Theor. Nanosci*., **3**, 803 (2006).

12 A. R. Ashrafi, M. Jalali, M. Ghorbani, M. V. Diudea, *MATCH Commun. Math. Comput. Chem*, **60**, 905 (2008).

13 M. Ghorbani, M. Jalali, *Dig. J. Nanomat. Bios*., **3**, 269 (2008).

14 A. R. Ashrafi, M. Ghorbani, M. Jalali, *Dig. J. Nanomat. Bios*., **3**, 245 (2008).

15 HyperChem package Release 7.5 for Windows, *Hypercube Inc*., Florida, USA, 2002.

16 M. V. Diudea, O. Ursu, Cs. L. Nagy, *TOPOCLUJ*, Babes-Bolyai University, Cluj, 2002.

17 The GAP Team, *GAP, Groups, Algorithms and Programming*, Lehrstuhl fuer Mathematik, RWTH, Aachen, 1992.

ПОЛИНОМ НА ЕКСЦЕНТРИЧНА СВЪРЗАНОСТ НА C$_{18N+10}$ ФУЛЕРЕНИ

Моджитаба Гхорбани[1], Али Реза Ашрафи[2,3] и Махса Хемаси[4]

[1]*Катедра по математика, Факултет естествени науки, Университет за обучение на преподаватели Шахид Раджаи, Техеран 16785 – 136, Иран*

[2]*Катедра по математика, Статистика и компютърни науки, Университет Кашан, Кашан, 87317 – 51167, Иран*

[3]*Институт по нанонаука и нанотехнологии, Университет Кашан, Кашан, 87317 – 51167, Иран*

[4]*Катедра по математика, Факултет естествени науки, Ислямски университет Азад, Филиал Кашан, Кашан, Иран*

(Резюме)

Епохата на фулерените започва през 1985г. с откриването на стабилен C$_{60}$ клъстер и неговата интерпретация като клетъчна структура с познатата форма на футболна топка от Крото и съавтори. Полиномът на ексцентрична свързаност на молекулен граф G, определен като $ECP(G, x) = \Sigma_{a \varepsilon V(G)} deg_G(a) x^{ecc(a)}$, където $ecc(a)$ е дължината на максималния път до друг възел от G. В настоящата статия този полиномът е изчислен за C$_{18n+10}$ фулерени.

Retention modeling in gas chromatography by QSRR approach

M.N. Moskovkina*, I.P. Bangov, A.Zh. Patleeva

Department of Chemistry, Faculty of Natural Sciences, Shumen University, Shumen, 9712, 115 University str., Bulgaria

The Quantitative Structure–Retention Relationship (QSRR) approach was applied to model the retention behavior of substituted phenols in Gas Chromatography (GC). The experimental retention data for a set of 42 phenol derivates, including priority pollutants, separated on GC columns with different polarities – the non–polar SE–30 phase and the polar phases OV–225 and NGA, were taken from literature. The Multiple Linear Regression (MLR) statistical method was preferred for the QSRR developing. A charge–related topological index (CTI), developed by one of the authors (I.B.) was probed as a global descriptor in order to measure and compare its potential to contribute to QSRRs. Analysis of the equations derived with different descriptors proved the ability to describe and evaluate the participants in the chromatographic retention process. Comparison of the numerical values of the regression coefficients in similar QSRR models for different stationary phases exhibits the specific features of solute–stationary phase interactions in each case. The parametric values of the regression coefficients in similar models for different stationary phases correlate with McReynolds phase selectivity.

Keywords: QSRR; substituted phenols; molecular indices; gas chromatographic Kovats retention index; phase polarity; McReynolds constants.

1. INTRODUCTION

Phenol derivates are constantly a point of interest for analytic chemists. Most of phenol substituted derivates form the list of priority pollutants [1, 2] and bring harm to human health and environmental problems. Among the widespread analytical methods for phenol detection and identification is the gas chromatography. Experimental chromatographic methods for component testing in complex organic mixtures have some limits: you need to own expensive instruments and to collect a wide range of standards subjected to rigorous analytical testing to verify identity and determine purity. The quantitative relationships between the solute structure and its retention data (QSRR), proposed in 1979 [3], are often used to solve the identification problem to predict the chromatographic separation behaviour of the solutes. One of the main reasons to deal with the QSRR approach is due to its possibility to study the relationships between the solute structure and its chromatographic retention data.

A comprehensive look over the publications [4–10] dealing with the QSRR subject reveals its importance until today.

Linear methods are widely applied in the QSAR and QSRR area [11–14].

Support vector machine (SVM), a non-linear algorithm was developed for regression and classification [15] and gained popularity in QSPR studies for drug design and biological activity [16, 17].

Another non-linear regression method used in chemometric investigations, especially in chemomatics and bioinformatics, is the neural network (NN) method [18–24]. Three different mathematical approaches (SVM, NN and MLR) were used in [25] to investigate the relationship between structure and retention index and to derive QSRRs for data sets of 174 and 132 diverse compounds. The statistical models derived by these methods revealed similar prediction ability.

The preferable statistical method for QSRR remains the Multiple Linear Regression (MLR) developing.

The modern state of art in the QSRR approach gives the possibility to generate multivariable regression equations able to reflect the chromatographic retention behavior for different solute series in different chromatographic modes. The goal of QSRR is to predict the retention characteristics and to take a peep into the mechanism of chromatographic separations. Surely the anticipated development of more precise methods for solute structure parameterization will be advanced due to QSRR studies.

---

* To whom all correspondence should be sent:
E-mail mmarinan@abv.bg

When a multiple linear regression form is preferred for the QSRR modelling, each element of the matrix of regression coefficients has certain significance. The value of the correlation coefficient **r** indicates the physical meaning of the linear relationship between the retention parameter and the derived set of molecular descriptors. The statistical significance of the parameters included in a common regression can be used to render an account of the significance of the participation of each descriptor in intermolecular interactions during the separation process. This information can be used to quantify the nonspecific (dispersive) and specific (polar) interactions between the solutes and the chromatographic phases. Whereas quantifying of the nonspecific dispersive molecular interactions can be successfully carried out by using some global topological or constitutive molecular indices, the various specific polar interactions are quantified less precisely by numeric local molecular indices.

Generally for gas chromatographic practice, all problems dealing with solute separation to be reduced to phase selectivity end inevitably to McReynolds constants [26].

Despite a serious amount of critical publications against the theoretical base of McReynolds system [27 mmarinan@abv.bg 33]］, the usage of McReynolds constants is still popular in chromatographic laboratories and literature.

In the present investigation the experimental GC retention data are related to the separation in 3 different columns: non polar phase SE–30 (methylsilicone) and two polar phases: OV–225 (3–cyanopropyl methylphenyl polysiloxane) and NGA (neopentyl glycol adypate). The phases OV–225 and NGA have almost similar polarities according to McReynolds polarity scale (1849 and 1813), but differ in donor–acceptor characteristics. Both phases exhibit electron donor properties. The NGA phase structure contains the oxygen atom in a carboxyl group as an important electron pair donor and a center for hydrogen-bonding interactions. The OV–225 phase possesses cyano-groups – centers for electron pair donor - electron pair acceptor interactions.

The chemometric analysis of the gas chromatographic retention on stationary phases with similar polarities and small variance in McReynolds constants gives a chance to expose the ability to reflect the molecular solute–stationary phase interactions. A large number of solute sets (n

= 42) allows to derive regressions with a wide set of molecular descriptors to contribute significantly to the regression models and to rise the statistical accuracy of the resulting correlation.

The chromatographic phase selectivity is a complex term rendering an account for different kinds of solute–stationary phase interactions. According to Rohrschneider–McReynolds concept, the Kovats retention index difference ΔI_x of the test compound on the column (I_i) and squalane (I_{sq}) provides a measure of polarity [26, 34–35]. The polarity of squalane is defined to be 0 as a standard apolar reference phase.

The empirical McReynolds scale for stationary phase polarity/selectivity characterization deals with ten test compounds. The phase selectivity is expressed with 10 indices (McReynolds Stationary phase polarity constants).

In the present paper the Quantitative Structure–Retention Relationship (QSRR) approach was applied to model the retention behavior of a set of substituted phenols (n = 42) in gas chromatography (GC) separated on stationary phases with different polarities, to describe and evaluate the participants in the chromatographic retention process and to compare the information received from QSRRs with McReynolds Polarity Constants.

2. EXPERIMENTAL COMPUTATION METHODOLOGY

2.1. Retention data

The experimental retention data – the Kovats indices - for the set of 42 substituted phenols including priority pollutants separated on GC columns with different polarities – the nonpolar SE–30 phase and the polar phases OV–225 and NGA, were taken from the literature [37]. The McReynolds constants for the three phases of our investigation were taken from literature [36] and are shown in Table 1. The structures of the solute set are shown in Fig. 1.
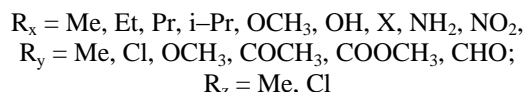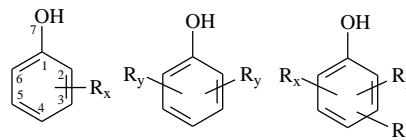

R_x = Me, Et, Pr, i–Pr, OCH$_3$, OH, X, NH$_2$, NO$_2$,
R_y = Me, Cl, OCH$_3$, COCH$_3$, COOCH$_3$, CHO;
R_z = Me, Cl
Fig. 1. General formulae of the phenol derivates.

Table1. McReynolds Stationary phase polarity constants

McR	I_1	ΔI_2	ΔI_3	ΔI_4	ΔI_5	ΔI_6	ΔI_7	ΔI_8	ΔI_9	ΔI_{10}
	X'	Y'	Z'	U'	S'	H'	I'	K'	L'	M'
SE–30	15	53	44	64	41	31	3I	22	44	2
OV–225	228	369	338	492	386	282	226	150	342	117
NGA	234	425	312	402	438	339	210	157	362	103

ΔI_1 (benzene) – X'; ΔI_2 (1-butanol) – Y'; ΔI_3 (2-pentanone) – Z'; ΔI_4 (1-nitropropane) – U'; ΔI_5 (pyridine) – S'; ΔI_6 (2-methyl-2-pentanol) – H'; ΔI_7 (1-iodobutane) – I'; ΔI_8 (2-octyne) – K'; ΔI_9 (1,4-dioxane) – L', ΔI_{10} (*cis*-hidrindane) – M'

Table 2.1. Experimental Gas Chromatographic Retention Data (*Kovats Indices)* for substituted phenols separated on three stationary phases (I phase- SE-30; II phase –OV-225; III phase-NGA).

№	Compounds	I_{SE-30}	I_{OV-225}	I_{NGA}	№	Compounds	I_{SE-30}	I_{OV-225}	I_{NGA}
1	2-Me Ph	1035	1587	1742	22	3-NH$_2$ Ph	1335	2219	2352
2	4-Me Ph	1059	1654	1813	23	2,4,6triCl Ph	1349	1928	2067
3	3-Me Ph	1065	1648	1782	24	2,4,5-triCl Ph	1362	2039	2158
4	2,6diMePh	1098	1593	1716	25	3-OH Ph	1368	2371	2576
5	2,4diMePh	1134	1660	1825	26	3,5-Cl Ph	1391	2217	2343
6	3-Et Ph	1160	1742	1898	27	4-I Ph	1398	2230	2348
7	4-Et Ph	1162	1746	1890	28	4-CO$_2$CH$_3$Ph	1500	2376	2461
8	3,5diMe Ph	1163	1706	1877	29	2-NH$_2$ Ph	1242	2039	2196
9	2,3diMe Ph	1169	1693	1857	30	3-Br Ph	1270	2069	2214
10	2.4diCl Ph	1183	1708	1877	31	2-I-Prop,5-Me Ph	1271	1776	1932
11	4-Cl Ph	1192	1922	2058	32	2-OCH$_3$ Ph	1095	1544	1627
12	3-Cl Ph	1194	1911	2061	33	2-NO$_2$Ph	1149	1556	1703
13	2,4,6-triMe Ph	1204	1612	1778	34	2.6-(OCH$_3$)$_2$Ph	1347	1936	2014
14	2,6diCl Ph	1206	1727	1871	35	2-OCH$_3$-4-Pr Ph	1392	1810	1884
15	4-OCH$_3$ Ph	1210	1930	2050	36	2-OCH$_3$-4-CHO Ph	1447	2199	2235
16	3-OCH$_3$ Ph	1211	1940	2083	37	2.6-(OCH$_3$)$_2$-4-CH$_3$ Ph	1473	2076	2106
17	2,3,5,-triMe Ph	1260	1823	1960	38	2-OCH3-4-COCH$_3$ Ph	1531	2283	2326
18	4-Br Ph	1274	2054	2191	39	4-COCH$_3$ Ph	1578	2478	2529
19	3-Me,4-Cl Ph	1283	2025	2135	40	2.6-(OCH$_3$)2-4-Pr Ph	1624	2254	2256
20	4-NH$_2$ Ph	1314	2154	2277	41	2.6-(OCH$_3$)2-4-COCH$_3$ Ph	1849	2685	2683
21	4-OH Ph	1334	2330	2515	42	(2-OCH$_3$-4-OCH$_2$CH=CH$_2$)Ph	1367	1848	1923

Table 2.2. Structural indicative descriptors for substituted phenols.

№	Compounds	R orto	R vic	OCH$_3$	Cl	Br	I	X	NO$_2$	NH$_2$	R keton	R aldh	R ester	alkyl	R o-Cl	R o-Me
1	2-MePh	1	0	0	0	0	0	0	0	0	0	0	0	1	0	1
2	4-MePh	0	0	0	0		0	0	0	0	0	0	0	1	0	0
3	3-MePh	0	0	0	0	0	0	0	0	0	0	0	0	1	0	0
4	2,6diMePh	2	0	0	0	0	0	0	0	0	0	0	0	2	0	2
5	2,4diMePh	1	0	0	0	0	0	0	0	0	0	0	0	2	0	1
6	3-EtPh	0	0	0	0	0	0	0	0	0	0	0	0	1	0	0
7	4-EtPh	0	0	0	0	0	0	0	0	0	0	0	0	1	0	0
8	3,5diMePh	0	0	0	0	0	0	0	0	0	0	0	0	2	0	0
9	2,3diMePh	1	1	0	0	0	0	0	0	0	0	0	0	2	0	1
10	2.4diCl	1	0	0	2	0	0	2	0	0	0	0	0	0	1	0
11	4-ClPh	0	0	0	1	0	0	1	0	0	0	0	0	0	0	0
12	3-ClPh	0	0	0	1	0	0	1	0	0	0	0	0	0	0	0
13	2,4,6-triMePh	2	0	0	0	0	0	0	0	0	0	0	0	3	0	2
14	2,6diCl Ph	2	0	0	2	0	0	2	0	0	0	0	0	0	2	0
15	4-OCH$_3$ Ph	0	0	1	0	0	0	0	0	0	0	0	0	0	0	0
16	3-OCH$_3$ Ph	0	0	1	0	0	0	0	0	0	0	0	0	0	0	0
17	2,3,5,-triMePh	1	1	0	0	0	0	0	0	0	0	0	0	3	0	1
18	4-Br Ph	0	0	0	0	1	0	1	0	0	0	0	0	0	0	0
19	3-Me,4-Cl Ph	0	0	0	1	0	0	1	0	0	0	0	0	1	0	0
20	4-NH$_2$ Ph	0	0	0	0	0	0	0	0	1	0	0	0	0	0	0
21	4-OH Ph	0	0	0	0	0	0	0	0	0	0	0	0	0	0	0
22	3-NH$_2$ Ph	0	0	0	0	0	0	0	0	1	0	0	0	0	0	0
23	2,4,6triCl Ph	2	0	0	3	0	0	3	0	0	0	0	0	0	2	0
24	2,4,5-triCl Ph	1	0	0	3	0	0	3	0	0	0	0	0	0	1	0
25	3-OH Ph	0	0	0	0	0	0	0	0	0	0	0	0	0	0	0
26	3,5-Cl Ph	0	0	0	2	0	0	2	0	0	0	0	0	0	0	0
27	4-I Ph	0	0	0	0	0	1	1	0	0	0	0	0	0	0	0
28	4-CO$_2$CH$_3$ Ph	0	0	0	0	0	0	0	0	0	0	0	1	0	0	0
29	2-NH$_2$ Ph	0	0	0	0	0	0	0	0	1	0	0	0	0	0	0
30	3-Br Ph	0	0	0	0	1	0	1	0	0	0	0	0	0	0	0
31	2-i-Prop,5-MePh	1	0	0	0	0	0	0	0	0	0	0	0	2	0	0
32	2-OCH$_3$ Ph	1	0	1	0	0	0	0	0	0	0	0	0	0	0	0
33	2-NO$_2$ Ph	1	0	0	0	0	0	0	1	0	0	0	0	0	0	0
34	2.6-(OCH$_3$)$_2$ Ph	2	0	2	0	0	0	0	0	0	0	0	0	0	0	0
35	2-OCH$_3$-4-Pr Ph	1	0	1	0	0	0	0	0	0	0	0	0	1	0	0
36	2-OCH$_3$-4-CHO Ph	1	0	1	0	0	0	0	0	0	0	1	0	0	0	0
37	2.6-(OCH$_3$)$_2$-4-CH$_3$ Ph	2	0	2	0	0	0	0	0	0	0	0	0	1	0	0
38	2-OCH$_3$-4-COCH$_3$ Ph	1	0	1	0	0	0	0	0	0	1	0	0	0	0	0
39	4-COCH$_3$ Ph	0	0	0	0	0	0	0	0	0	1	0	0	0	0	0
40	2.6-(OCH$_3$)$_2$-4-Pr Ph	2	0	2	0	0	0	0	0	0	0	0	0	1	0	0
41	2.6-(OCH3)$_2$-4-COCH$_3$ Ph	2	0	2	0	0	0	0	0	0	1	0	0	0	0	0
42	2-OCH$_3$-4-COCH$_2$CH=CH$_2$Ph	1	0	0	0	0	0	0	0	0	0	0	0	0	0	0

The solute set of substituted phenols and the experimental retention data (Kovats indices I$_i$) for the three stationary phases –SE-30, OV–225 and NGA, are listed in Table 2.1.

2.2. Descriptor calculation

The multiple linear regressions (MLR) were derived according to equation (1):

$$I = \sum d_i D_i + \sum p_i P_i + a_0, \qquad (1)$$

where I is the experimental retention value (the Kovats Retention Index); D$_i$ – a global structure molecular index to quantify the non–specific chromatographic interactions. We have checked some global molecule indices ("*bulk* indices") such as molecular mass (M), molar refractivity (MR), polarizability (α), and Wiener topology index (W) as a measure of solute dispersive properties (D = M, MR, α, W); for the P$_i$ indices specific molecular descriptors should be used to quantify the polar intermolecular interactions of the solute with the stationary phase; *a$_o$*, *d$_i$* and *p$_i$* are the regression coefficients depending on the properties of the stationary phases.

A charge–related topological index (CTI) developed by one of the authors (I.B.) [38–40] was probed as a D descriptor in order to measure and compare its ability to contribute to QSRRs.

The CTI index is expressed as:

$$CTI = \sum_i \sum_j \frac{L_i L_j}{D_{ij}} \qquad (2)$$

Here D_{ij} are the inter–atomic distances and L_i are local indices characterizing the separate heavy (non–hydrogen) atoms i which are expressed as follows:

$$L_i = L_o + N_H + q_i \qquad (3)$$

L_o are the constant values for each atom and for each hybridization state (they can be atom valences in some cases), N_H is the number of hydrogen atoms attached to a given heavy atom, and q_i are the corresponding charge densities computed by either the empirical method of Gasteiger or by any of the most sophisticated quantum chemistry methods at semiempirical or nonempirical level. In the present investigation two kinds of CTI indices were developed - CTI_{AM1} and CTI_{DFT}, calculated either at the semiempirical AM1 or at the nonempirical DFT level.

The molecular indices M, MR, α, were calculated in Excel [41]. The CTI index and Wiener index W were developed with a Str Manager Software program.

Some kinds of solute structure descriptors were used for the P_i variables: nonempirical quantum chemical indices (dipole moment μ, atomic charges q_i; energy of the highest occupied molecular orbital (HOMO) E_{Homo} and energy of the lowest unoccupied molecular orbital (LUMO) E_{Lumo}; energy of hydration E_{hydr}; total molecular energy E_{total} on one side and a set of structure indicative descriptors to reflect the presence of different functional groups in the solute structures: P_i = R_{ketone}, $R_{aldehide}$, R_{ester}, OH, NH_2, NO_2, Hal, Cl, Br, I, OCH_3, alkyl, on the other. Some additional indicative descriptors were used to reflect the presence of the substitutes in *ortho*-position towards the OH-group of the phenol ring: R_{orto}, $R_{o–OH}$, $R_{o–NO2}$, $R_{o–NH2}$, $R_{o–Cl}$, especially the presence of methyl substituents in vicinal position towards the

OH-group of the phenol ring – R_{vic}The values of the indicative structural descriptors used are listed in Table 2.2.

The geometries of the molecules were fully optimized at the semiempirical AM1 or DFT B3LYP/6–31+G(d,p) level of theory and were characterized as minima (no imaginary frequencies) at the potential energy surface (PES) by frequency calculations at the same computational level. All reported total energies were corrected by zero-point energy (unscaled), estimated from the harmonic frequency calculations at temperature 273 K and atmospheric pressure 1.01325×10^5 Pa. All calculations were performed using the PC GAMESS version 7.1 (Tornado) [42] of the GAMESS (US) QC package [43].

The molecular quantum indices calculated with AM1 and entered into the developed QSRR were: atomic charges Q_i ; (Q_1–Q_6 are the charges of the C-atoms in the benzene ring; Q_7 is the atomic charge of the O–atom in the phenyl group); the energy of hydration – E_{hydr}, the energy of the HOMO-orbitals $–E_{homo}$. The procedure of CTI index generation permits to use the atomic charge values calculated with different quantum methods. Since we have used both the semi-empirical AM1 and the DFT approach for atom charges calculation, two kinds of CTI indices were obtained – the CTI_{AM1} and the CTI_{DFT} one. The numeric values of the quantum indices developed with the AM1 approach, along with the global dispersive molecular descriptors, are presented in Table 2.3.

The similar quantum descriptors calculated with DFT and used for QSRR modeling were: atomic charges q_i (Lowdin); (q_1–q_6 are the charges of the C-atoms in the benzene ring; q_7 is the atomic charge of the O–atom in the phenyl group); dipole moment μ (Debye); E_{tot} – the total molecular energy (Hartree), the energy of HOMO-orbitals – $E_{Homo (DFT)}$ and CTI_{DFT} values, which are presented in Table 2.4.

Table 2.3. The Global dispersive molecular descriptors calculated for QSRR models (M – molecular mass; MR – molar refractivity; α – polarizability, W – Wiener topologic index), and quantum molecular descriptors, calculated at AM1 level: charge-relative topology index – CTI (AM1); HOMO-energy – E_{Homo}; E_{hydr} – hydratation energy; Q_i – atomic charges of resp. atoms.

№	Compounds	M	MR	a	W	CTI (AM1)	E_{Homo} (AM1)	E_{hydr} (AM1)	Q_1 (AM1)	Q_2 (AM1)	Q_6 (AM1)	Q_7 (AM1)
1	2-MePh	108.14	2.79	12.91	162	118.90	-8.997	-7.38	0.080	-0.151	-0.155	-0.255
2	4-MePh	108.14	32.79	12.91	182	117.94	-8.880	-7.66	0.073	-0.209	-0.154	-0.253
3	3-MePh	108.14	32.79	12.91	173	118.18	-9.012	-7.58	0.081	-0.213	-0.162	-0.253
4	2,6diMePh	122.17	37.83	14.74	207	128.26	-8.891	-5.01	0.084	-0.148	-0.089	-0.256
5	2,4diMePh	122.17	37.83	14.74	224	127.43	-8.786	-6.15	0.076	-0.148	-0.153	-0.254
6	3-EtPh	122.17	37.39	14.74	217	125.49	-9.019	-7.05	0.080	-0.211	-0.161	-0.253
7	4-EtPh	122.17	37.39	14.74	235	125.16	-8.910	-7.18	0.074	-0.155	-0.210	-0.253
8	3,5diMePh	122.17	37.83	14.74	229	126.94	-8.970	-6.19	0.085	-0.218	-0.165	-0.254
9	2,3diMePh	122.17	37.83	14.74	211	127.55	-8.916	-6.21	0.085	-0.146	-0.160	-0.257
10	2.4diCl	163	37.36	14.93	224	153.81	-9.271	-7.87	0.094	-0.144	-0.144	-0.241
11	4-ClPh	128.56	32.56	13	182	131.13	-9.125	-8.58	0.081	-0.207	-0.149	-0.248
12	3-ClPh	128.56	32.56	13	173	131.76	-9.300	-8.49	0.089	-0.212	-0.156	-0.248
13	2,4,6-triMePh	136.19	42.88	16.58	264	136.67	-8.698	-3.93	0.077	-0.145	-0.085	-0.256
14	2,6diCl Ph	163	37.36	14.93	207	155.12	-9.374	-6.85	0.100	-0.145	-0.087	-0.230
15	4-OCH$_3$ Ph	124.14	32.22	13.54	235	134.24	-8.636	-10.6?	0.044	-0.180	-0.124	-0.253
16	3-OCH$_3$ Ph	124.14	32.22	13.54	217	134.77	-8.966	-10.4?	0.110	-0.246	-0.190	-0.250
17	2,3,5,-triMePh	136.19	42.88	16.58	269	136.48	-8.850	-4.87	0.084	-0.147	-0.164	-0.258
18	4-Br Ph	173.01	35.37	13.7	182	130.93	-9.189	-8.56	0.093	-0.158	-0.216	-0.247
19	3-Me,4-Cl Ph	142.59	37.6	14.83	238	140.35	-9.035	-7.31	0.085	-0.210	-0.155	-0.249
20	4-NH$_2$ Ph	109.13	32.45	12.42	182	121.88	-7.957	-13	0.016	-0.159	-0.104	-0.256
21	4-OH Ph	110.11	29.45	11.71	182	126.43	-8.725	-15.8?	0.044	-0.178	-0.119	-0.253
22	3-NH$_2$ Ph	109.12	32.45	12.42	187	121.67	-8.281	-12.7?	0.126	-0.306	-0.217	-0.253
23	2,4,6triCl Ph	197.45	42.17	16.85	264	174.72	-9.390	-6.5	0.101	-0.139	-0.081	-0.226
24	2,4,5-triCl Ph	197.45	42.17	16.85	264	175.34	-9.388	-7.39	0.103	-0.146	-0.145	-0.237
25	3-OH Ph	110.4	29.45	11.71	187	126.78	-8.982	-15.7	0.117	-0.301	-0.192	-0.249
26	3,5-Cl Ph	163	37.36	14.93	229	153.35	-9.537	-7.95	0.099	-0.214	-0.155	-0.243
27	4-I Ph	220.01	40.16	16.1	182	130.80	-9.243	-8.55	0.097	-0.220	-0.162	-0.247
28	4-CO$_2$CH$_3$ Ph	152.15	39.28	15.46	355	166.90	-9.536	-9.16	0.114	-0.233	-0.178	-0.245
29	2-NH$_2$ Ph	109.13	32.45	12.42	169	122.41	-8.204	-12.3	-0.030	0.058	-0.110	-0.255
30	3-Br Ph	173.01	35.37	13.7	173	131.67	-9.337	-8.46	0.081	-0.191	-0.144	-0.248
31	2-i-Prop,5-MePh	150.22	46.98	18.41	321	141.79	-8.962	-5.32	0.085	-0.148	-0.160	-0.258
32	2-OCH$_3$ Ph	124.14	34.22	13.54	80	136.02	-8.783	-9.63	0.066	-0.004	-0.137	-0.250
33	2-NO$_2$ Ph	139.11	35.08	12.91	251	165.39	-9.911	-12.6?	0.177	-0.229	-0.180	-0.245
34	2.6-(OCH$_3$)$_2$ Ph	154.17	40.46	16.02	301	161.14	-8.745	-8.5	-0.003	0.030	0.083	-0.261
35	2-OCH$_3$-4-Pr Ph	166.22	48.46	19.05	438	156.52	-8.621	-7.46	0.061	-0.250	0.002	-0.135
36	2-OCH$_3$-4-CHO Ph	152.15	40.81	15.46	351	166.37	-9.126	3	0.100	-0.019	-0.156	-0.243
37	2.6-(OCH$_3$)$_2$-4-CH$_3$ Ph	168.19	45.72	17.85	372	169.49	-8.619	-7.31	-0.050	-0.261	0.032	0.085
38	2-OCH$_3$-4-COCH$_3$ Ph	166.18	43.62	17.3	389	174.23	-9.151	-8.62	0.050	-0.009	-0.143	-0.252
39	4-COCH$_3$ Ph	36.15	37.16	14.83	290	175.04	-9.428	-7.83	0.109	-0.230	-0.175	-0.246
40	2.6-(OCH$_3$)$_2$-4-Pr Ph	196.25	54.92	21.52	551	181.57	-8.636	-6.37	-0.003	0.030	0.083	-0.260
41	2.6-(OCH3)$_2$-4-COCH$_3$ Ph	196.2	50.09	19.77	540	198.12	-9.013	-7.42	0.015	0.026	-0.082	-0.265
42	2-OCH$_3$-4-COCH$_2$CH=CH$_2$ Ph	164.25	48.5	18.86	438	162.93	-8.657	-9.51	0.063	-0.002	-0.135	-0.250

Table 2.4. The quantum descriptors for QSRR models calculated at DFT level (CTI_{DFT} –charge-relative topology index; E_{Homo} –the Homo- energy; q_i –atomic charges (Lowdin); E_{total} – total energy (Hartree))

№	Compounds	E_{Homo} (DFT)	CTI (DFT)	E_{total} (Hartree)	q_1 (DFT)	q_2 (DFT)	q_6 (DFT)	q_7 (DFT)
1	2-MePh	-0.0063	128.2227	-346.66	0.113	-0.033	-0.107	-0.233
2	4-MePh	-0.0002	117.1808	-346.66	0.119	-0.140	-0.112	-0.234
3	3-MePh	-0.0022	117.8407	-346.66	0.122	-0.150	-0.117	-0.233
4	2,6diMePh	-0.0066	139.563	-385.95	0.108	-0.031	-0.008	-0.230
5	2,4diMePh	-0.0058	138.6126	-385.96	0.111	-0.029	-0.112	-0.234
6	3-EtPh	-0.0009	138.615	-385.95	0.122	-0.144	-0.117	-0.230
7	4-EtPh	-0.0018	136.6195	-385.95	0.120	-0.112	-0.139	-0.233
8	3,5diMePh	-0.002	136.1877	-385.96	0.125	-0.130	-0.158	-0.234
9	2,3diMePh	-0.0074	140.1745	-385.95	0.115	-0.040	-0.117	-0.228
10	2.4diCl	-0.0085	147.1098	-1226.6	0.111	-0.104	-0.096	-0.216
11	4-ClPh	-0.0099	120.8116	-766.97	0.123	-0.132	-0.104	-0.227
12	3-ClPh	-0.0078	121.9637	-766.9	0.127	-0.146	-0.112	-0.222
13	2,4,6-triMePh	-0.0061	161.3894	-425.25	0.103	-0.006	-0.031	-0.232
14	2,6diCl Ph	-0.0107	147.8288	-1226.6	0.101	-0.105	-0.090	-0.206
15	4-OCH$_3$ Ph	-0.0006	138.0317	-421.86	0.106	-0.129	-0.105	-0.240
16	3-OCH$_3$ Ph	-0.2131	139.9949	-421.86	0.355	-0.200	-0.130	-0.565
17	2,3,5,-triMePh	-0.0068	159.0513	-425.25	0.116	-0.046	-0.127	-0.228
18	4-Br Ph	-0.0007	120.9104	-2878.5	0.124	-0.133	-0.105	-0.227
19	3-Me,4-Cl Ph	-0.0083	139.9538	-806.27	0.123	-0.143	-0.112	-0.227
20	4-NH$_2$ Ph	-0.1853	115.4051	-362.71	0.101	-0.103	-0.130	-0.243
21	4-OH Ph	-0.0004	117.448	-382.58	0.106	-0.127	-0.103	-0.240
22	3-NH$_2$ Ph	-0.0043	113.891	-362.71	0.130	-0.181	-0.143	-0.230
23	2,4,6triCl Ph	-0.0028	174.7997	-1686.17	0.098	-0.086	-0.101	-0.203
24	2,4,5-triCl Ph	-0.0039	174.3801	-1686.17	0.113	-0.108	-0.109	-0.209
25	3-OH Ph	-0.0097	115.7902	-382.59	0.131	-0.193	-0.137	-0.226
26	3,5-Cl Ph	-0.0013	144.7492	-1226.58	0.361	-0.103	-0.131	-0.553
27	4-I Ph	-0.0034	120.6733	-7195.74	0.270	-0.141	-0.112	-0.475
28	4-CO$_2$CH$_3$ Ph	-0.0086	209.4104	-535.21	0.136	-0.140	-0.114	-0.219
29	2-NH$_2$ Ph	-0.1896	117.0761	-362.71	0.086	0.053	-0.129	-0.245
30	3-Br Ph	-0.0087	122.0323	-2878.53	0.127	-0.149	-0.110	-0.223
31	2-i-Prop,5-MePh	-0.007	183.2764	-464.53	0.116	-0.032	-0.122	-0.228
32	2-OCH$_3$ Ph	-0.0018	141.3289	-421.86	0.098	0.078	-0.113	-0.227
33	2-NO$_2$ Ph	-0.0014	195.7651	-511.88	0.141	-0.034	-0.108	-0.194
34	2.6-(OCH$_3$)$_2$ Ph	-0.0028	186.7031	-536.35	0.073	0.089	0.079	-0.227
35	2-OCH$_3$-4-Pr Ph	-0.0034	199.7381	-539.73	0.095	0.077	-0.110	-0.232
36	2-OCH$_3$-4-CHO Ph	-0.0051	213.9548	-535.18	0.118	0.077	-0.113	-0.210
37	2.6-(OCH$_3$)$_2$-4-CH$_3$ Ph	-0.0037	210.6052	-575.64	0.068	0.089	0.081	-0.230
38	2-OCH$_3$-4-COCH$_3$ Ph	-0.0019	240.3078	-574.48	0.114	0.075	-0.112	-0.214
39	4-COCH$_3$ Ph	-0.0102	186.8544	-459.98	0.350	-0.122	-0.143	-0.552
40	2.6-(OCH$_3$)$_2$-4-Pr Ph	-0.004	254.1766	-654.22	0.069	0.090	0.081	-0.227
41	2.6-(OCH3)$_2$-4-COCH$_3$ Ph	-0.0056	298.1189	-688.96	0.088	0.085	0.078	-0.212
42	2-OCH$_3$-4-COCH$_2$CH=CH$_2$ Ph	-0.0031	221.6187	-538.52	0.095	0.076	-0.107	-0.231

2.3. Calculation method

The chemometric approach for QSRRs development was executed with Excel program [41]. The regression linear models (MLR) were obtained by using forward stepwise multiple regression techniques.

The requirements for statistical accuracy [44] for all developed MLR models were fulfilled. The best regression model was selected on the basis of the highest values of the correlation coefficient (r), the square correlation coefficient (r^2), the value of the F-test, (a statistic for assessing the overall significance), the lowest standard error of estimation (S) and the maximum residual value between the experimental retention data and those calculated with equation derived Δ_{max}. The cross–correlation coefficients r_{ij} between the independent variables in the equation are presented in Table 3–1 for AM1-calculated descriptors and in Table 3–2 for DFT-calculated descriptors. In order to derive meaningful results, the independence of the

variables (their orthogonality) was checked. The occasionally observed colinearity of the structural parameters used in the same equation eliminates its informative value. When the number of cases (experimental data) analyzed is limited, high correlations can be obtained by including large numbers of independent variables in a process of regressions deriving. The correlations thus obtained can be statistically insignificant unless the F-test value for a given number of degrees of freedom is lower than the value calculated for the respective significance level. The sequential F-test allows one to decide whether an introduction of an individual independent variable into the regression equation is statistically justified [45].

3. RESULTS AND DISCUSSION

The QSRRs derived for three phases and their statistics are shown as three parts of Table 4 as a set of descriptors, grouped as follows: each of the first five equations includes a global descriptor and is tuned just with indicative structural descriptors; the regressions in the next two groups are developed with entering the local indicative descriptors and quantum descriptors calculated with the AM1 method (eq. 6–9) and DFT approach (eq. 10–13), respectively.

The set of regressions 1-5 developed for each stationary phase, displays good statistics ($R = 0.955–0.975$ for SE–30; $R = 0.931–0.947$ for OV–225 and $R = 0.925–0.940$ for NGA). Each of the checked global molecular indices (M, MR, α, W, CTI) can be successfully used for QSRR modeling as a descriptor with almost similar statistic accuracy. One of the main factors monitored in chromatographic laboratory practice is the value of Δ_{max}, which indicates the deviation between experimental and calculated retention data. The experimental interlaboratory uncertainty of retention data on polar phases is up to 25 index units [5]. Proceeding to these requirements, the Δ_{max} values corresponding to our equations were unsatisfactorily larger than the experimental error generally assumed, even though the statistic parameters for the equations 1–5 (Table 4) seem to be high: ($\Delta_{max} = 84–124$ i.u. for SE-30; $\Delta_{max} = 201–269$ i.u. for OV–225 and $\Delta_{max} = 249-299$ i.u. for NGA).

The addition of calculative descriptors into QSRRS improves their statistics. In the case of AM1 approach for QSRR modeling, the entering of the quantum descriptors E_{Homo} and Q_i (eq.6-9) rise the R value ($R = 0.974-0.983$ for SE-30; $R = 0.961-0.981$ for OV–225 and $R = 0.961–0.982$ for NGA).

The values of Δ_{max} change as follows for the equations 6-9 (Table 4): ($\Delta_{max} = 77–117$ i.u. for SE–30; $\Delta_{max} = 103–188$ i.u. for OV–225 and $\Delta_{max} = 89–186$ i.u. for NGA).

The entering of the quantum descriptors E_{total} and q_i calculated at DFT level (eq. 10–13, Table 4) was meaningful and led to an increase in R ($R=0.955–0.981$ for SE–30; $R= 0.965–0.975$ for OV–225 and $R= 0.944–0.974$ for NGA). The changes for Δ_{max} in the equations 10–13 are (Table 4): ($\Delta_{max} = 74–103$ i.u. for SE–30; $\Delta_{max} = 133–209$ i.u. for OV–225 and $\Delta_{max} = 121–189$ i.u. for NGA).

The retention modeling in both polar phases benefits from the addition of quantum descriptors, calculated with either AM1, or DFT approach. The entering of the E_{Homo} parameter into the models improves the statistics, particularly for the polar phases OV–225 and NGA (Table 4, eq.6). This descriptor E_{Homo} quantifies electron pair donor - electron pair acceptor (EPD–EPA) interactions and meaningfully parameterizes the polar intermolecular interactions with the stationary phase. The role of the energies E_{Homo} and E_{Lumo} as an expression of Lewis basicity and acidity, respectively, is known and accounted for [46].

The full forms of the equations 6 from Table 4 with descriptor E_{Homo} for the three phases are presented in Table 5–1. It seems interesting to track the influence of entering the index E_{Homo} to QSRRs for phases with different polarities. The numeric values of the regression coefficients for the E_{Homo} descriptor increase according to phase selectivity towards the EPD-EPA interactions: (104.5 ± 43.3) for SE–30; (286.6 ± 153.9) for OV–225 and (321.2 ± 143.4) for NGA.

Comparing the statistics for the equations from Table 4 derived with different calculation methods allows claiming that the accuracy in the case of semiempirical AM1 approach is sufficient and it seems pointless to execute DFT calculations for QSRR developing.

Table 3-2. The cross-correlation matrix (DFT)

	M	MR	α	CTI_{dft}	E_{tot}	E_{homo}	q_1	q_2	q_6	q_7	OH	NH_2	NO_2	X	OCH_3	R_{orto}	$R_{o\text{-}Cl}$	R_{aldh}	R_{keton}	R_{ester}
M	1																			
MR	0.70	1																		
α	0.72	0.99	1																	
CTI_{dft}	0.58	0.83	0.82	1																
E_{tot}	-0.63	-0.06	-0.08	0.15	1															
E_{homo}	0.27	0.28	0.27	0.22	-0.12	1														
q_1	0.04	-0.22	-0.17	-0.16	-0.28	-0.23	1													
q_2	0.29	0.66	0.62	0.69	0.22	0.08	-0.43	1												
q_6	0.40	0.55	0.55	0.57	0.05	0.16	-0.36	0.58	1											
q_7	-0.08	0.13	0.07	0.12	0.30	0.31	-0.96	0.28	0.20	1										
OH	-0.25	-0.34	-0.33	-0.22	0.09	0.06	-0.04	-0.24	-0.10	0.05	1									
NH_2	-0.33	-0.28	-0.32	-0.28	0.12	-0.61	-0.10	-0.04	-0.18	0.05	-0.06	1								
NO_2	-0.03	-0.09	-0.15	0.14	0.05	0.05	0.02	0.05	-0.04	0.10	-0.03	-0.04	1							
X	0.53	0.01	0.05	-0.12	-0.43	0.14	0.13	-0.28	-0.11	-0.06	-0.12	-0.14	-0.08	1						
OCH_3	0.34	0.50	0.53	0.65	0.14	0.00	-0.19	0.64	0.76	0.04	-0.12	-0.14	-0.08	-0.27	1					
R_{orto}	0.43	0.65	0.64	0.60	0.12	0.24	-0.43	0.70	0.72	0.33	-0.20	-0.25	0.06	0.10	0.50	1				
$R_{o\text{-}Cl}$	0.38	0.08	0.11	0.02	-0.16	0.07	-0.12	-0.12	-0.02	0.16	-0.07	-0.08	-0.05	0.77	-0.16	0.39	1			
R_{aldh}	0.04	0.07	0.03	0.20	0.04	0.04	-0.03	0.24	-0.05	0.08	-0.03	-0.04	-0.02	-0.08	0.16	0.06	-0.05	1		
R_{keton}	0.21	0.26	0.28	0.54	0.07	0.07	0.21	0.23	0.16	-0.21	-0.06	-0.08	-0.04	-0.14	0.29	0.11	-0.08	-0.04	1	
R_{ester}	0.04	0.03	0.03	0.19	0.04	0.03	0.01	-0.13	-0.05	0.06	-0.03	-0.04	-0.02	-0.08	-0.08	-0.14	-0.05	-0.02	-0.04	1

Table 3-2. The cross-correlation matrix (DFT)

	M	MR	α	CTI_{dft}	E_{tot}	E_{homo}	q_1	q_2	q_6	q_7	OH	NH_2	NO_2	X	OCH_3	R_{orto}	R_{o-Cl}	R_{aldh}	R_{keton}	R_{ester}
M	1																			
MR	0.70	1																		
α	0.72	0.99	1																	
CTI_{dft}	0.58	0.83	0.82	1																
E_{tot}	-0.63	-0.06	-0.08	0.15	1															
E_{homo}	0.27	0.28	0.27	0.22	-0.12	1														
q_1	0.04	-0.22	-0.17	-0.16	-0.28	-0.23	1													
q_2	0.29	0.66	0.62	0.69	0.22	0.08	-0.43	1												
q_6	0.40	0.55	0.55	0.57	0.05	0.16	-0.36	0.58	1											
q_7	-0.08	0.13	0.07	0.12	0.30	0.31	-0.96	0.28	0.20	1										
OH	-0.25	-0.34	-0.33	-0.22	0.09	0.06	-0.04	-0.24	-0.10	0.05	1									
NH_2	-0.33	-0.28	-0.32	-0.28	0.12	-0.61	-0.10	-0.04	-0.18	0.05	-0.06	1								
NO_2	-0.03	-0.09	-0.15	0.14	0.05	0.05	0.02	0.05	-0.04	0.10	-0.03	-0.04	1							
X	0.53	0.01	0.05	-0.12	-0.43	0.14	0.13	-0.28	-0.11	-0.06	-0.12	-0.14	-0.08	1						
OCH_3	0.34	0.50	0.53	0.65	0.14	0.00	-0.19	0.64	0.76	0.04	-0.12	-0.14	-0.08	-0.27	1					
R_{orto}	0.43	0.65	0.64	0.60	0.12	0.24	-0.43	0.70	0.72	0.33	-0.20	-0.25	0.06	0.10	0.50	1				
R_{o-Cl}	0.38	0.08	0.11	0.02	-0.16	0.07	-0.12	-0.12	-0.02	0.16	-0.07	-0.08	-0.05	0.77	-0.16	0.39	1			
R_{aldh}	0.04	0.07	0.03	0.20	0.04	0.04	-0.03	0.24	-0.05	0.08	-0.03	-0.04	-0.02	-0.08	0.16	0.06	-0.05	1		
R_{keton}	0.21	0.26	0.28	0.54	0.07	0.07	0.21	0.23	0.16	-0.21	-0.06	-0.08	-0.04	-0.14	0.29	0.11	-0.08	-0.04	1	
R_{ester}	0.04	0.03	0.03	0.19	0.04	0.03	0.01	-0.13	-0.05	0.06	-0.03	-0.04	-0.02	-0.08	-0.08	-0.14	-0.05	-0.02	-0.04	1

Table 4. QSRR models derived for a set of substituted phenols (n=42) in GC and statistics: the correlation coefficient **R**; its square **R^2**; the standard deviation **s**; Fisher ratio value **F**; maximal residual value of deviation between the experimental and calculated retention data for corresp.solute, **Δmax$_i$ (i.u.)**.

	Calc. Method	Descriptors	R	R^2	s	F	Δmax$_i$
		I phase=SE-30					
1		CTI, OH, X, Cl, Br, NH$_2$, NO$_2$, R$_{o-Cl}$, R$_{ketone}$	0.971	0.942	45.3	58	115$_{32}$
2		CTI, OH, X, Cl, NH$_2$, NO$_2$, alk, R$_{o-Cl}$, R$_{o-Me}$, R$_{ketone}$, R$_{ester}$, R$_{o-NH2}$	0.975	0.950	44.0	46	91$_{32}$
3		α, OH, X, Cl, NH$_2$, R$_{o-Cl}$, R$_{o-Me}$, R$_{ketone}$, R$_{ester}$, R$_{aldeh}$	0.952	0.907	58.5	30	124$_{31}$
4		MR , OH, X, NH$_2$, OCH$_3$, R$_{orto}$, R$_{ketone}$, R$_{ald}$, R$_{ester}$	0.962	0.926	51.5	44	84$_{39}$
5		M, OH, X, Cl, NH$_2$, OCH$_3$, R$_{orto}$, R$_{ald}$, R$_{ketone}$,R$_{estr}$	0.961	0.923	53.2	37	92$_{26,.32}$
6	AM1	MR, E$_{homo}$,OH, X, Cl, NH$_2$, OCH$_3$, R$_{orto}$, R$_{ketone}$, R$_{ester}$,R$_{aldeh}$, R$_{o-Me}$	0.974	0.949	44.8	45	117$_{38}$
7	AM1	CTI $_{AM1}$, E$_{hydrat}$, OH, X, Cl, NH$_2$, NO$_2$, R$_{o-Cl}$, Q$_1$, Q$_2$, Q$_6$, Q$_7$	0.983	0.967	36.1	71	77$_{27}$
8	AM	CTI $_{AM1}$,OH, X, Cl, NH$_2$, R$_{o-Cl}$, R$_{o-NO2}$, Q$_1$, Q$_2$, Q$_6$, Q$_7$	0.980	0.960	38.9	66	78$_{27}$
9	AM1	CTI $_{AM1}$, OH, X, Cl, NH$_2$, R$_{o-Cl}$, R$_{o-NO2}$, R$_{vic}$, Q$_1$,Q$_2$,Q$_6$,Q$_7$	0.982	0.964	37.7	64	77$_{27}$
10$_1$	DFT	CTI$_{DFT}$,OH, NH$_2$, NO$_2$, R$_{o-Cl}$, E$_{tot}$, q$_2$	0.973	0.946	42.3	86	103$_{41}$
10$_2$	DFT	CTI$_{DFT}$,OH, NH$_2$, NO$_2$, R$_{o-Cl}$, E$_{tot}$, q$_2$	0.955	0.912	54.5	50	105$_{42}$
10$_3$	DFT	CTI$_{DFT}$, E$_{tot}$, OH, NH$_2$, NO$_2$, R$_{o-Cl}$, R$_{ketone}$, q$_1$,q$_2$, q$_6$,	0.968	0.937	48.2	46	97$_{16}$
11	DFT	MR, E$_{tot}$, OH, X, NH$_2$, OCH$_3$, R$_{orto}$, R$_{ketone}$, R$_{ald}$, R$_{ester}$, q$_2$, q$_6$, q$_7$	0.981	0.963	39.1	56	74$_{33}$
12	DFT	M, E$_{tot}$, OH, X, NH$_2$, OCH$_3$, R$_{orto}$, R$_{ketone}$, R$_{ald}$, R$_{ester}$, q$_2$, q$_6$,	0.973	0.947	45.6	43	101$_{26}$
13	DFT	α,OH,X,OCH$_3$,NH$_2$,R$_{orto}$, R$_{ketone}$,R$_{ester}$,R$_{aldeh}$,q$_6$	0.967	0.936	48.5	45	102$_{33}$
		II phase=OV-225					
1		CTI,OH, X, Cl, Br, NH$_2$, NO$_2$, R$_{o-Cl}$, R$_{o-Me}$, R$_{keton}$, R$_{ester}$,	0.947	0.898	105	24	261$_{32}$
2		CTI, OH, X, Cl, NH$_2$, NO$_2$, R$_{o-Cl}$, R$_{o-Me}$, R$_{keton}$, R$_{ester}$,	0.944	0.892	107	26	261$_{32}$
3		α, OH, X, Cl, NH$_2$, NO$_2$, R$_{o-Cl}$, R$_{o-Me}$, R$_{keton}$, R$_{ester}$, R$_{aldeh}$	0.934	0.873	118	18	201$_{16}$
4		MR,OH, X, NH$_2$, OCH$_3$, R$_{orto}$, R$_{keton}$, R$_{ester}$, R$_{aldeh}$,	0.931	0.867	117	23	229$_{35}$
5		M, OCH$_3$, X, OH, Cl, NH$_2$, R$_{orto}$, R$_{ald}$, R$_{keton}$, R$_{estr}$	0.943	0.889	108	25	237$_{32}$
6	AM1	MR,E$_{homo}$,OH,X,Cl,NH$_2$, NO$_2$,OCH$_3$, R$_{orto}$, R$_{ketone}$,R$_{ester}$, R$_{aldeh}$, R$_{o-Me}$	0.961	0.923	95	26	188$_{35}$
7	AM1	CTI $_{AM1}$, E$_{hydrat}$, OH, X, Cl, NH$_2$, NO$_2$, R$_{o-Cl}$, Q$_1$, Q$_2$, Q$_6$, Q$_7$	0.964	0.930	89	32	145$_{24}$
8	AM1	CTI $_{AM1}$, E$_{homo}$, OH, X, Cl, NH$_2$, NO$_2$, R$_{o-Cl}$, R$_{aldeh}$, Q$_1$, Q$_2$, Q$_6$, Q$_7$	0.980	0.960	68	52	104$_{27}$
9	AM1	CTI $_{AM1}$,E$_{homo}$,OH,X,Cl,NH$_2$,NO$_2$, alk, R$_{o-Cl}$, R$_{aldeh}$, Q$_1$, Q$_2$, Q$_6$, Q$_7$	0.981	0.962	67	49	103$_{27}$
10$_1$	DFT	CTI$_{DFT}$,OH, NH$_2$, NO$_2$, R$_{o-Cl}$, R$_{keton}$, E$_{tot}$, q$_1$, q$_2$, q$_6$, q$_7$	0.969	0.939	81	42	149$_{24}$
10$_2$	DFT	CTI$_{DFT}$, OH, NH$_2$, NO$_2$, R$_{o-Cl}$, R$_{keton}$, E$_{tot}$, q$_1$, q$_2$, q$_6$, q$_7$	0.940	0.883	112	21	209$_{13}$
11	DFT	MR,OH, X, NH$_2$, OCH$_3$, R$_{orto}$, R$_{keton}$, R$_{ald}$, R$_{ester}$, E$_{tot}$, q$_2$, q$_6$, q$_7$	0.975	0.951	75	42	185$_{10}$
12	DFT	M,OH, NH$_2$, R$_{orto}$, R$_{keton}$, R$_{ald}$, R$_{ester}$, E$_{tot}$, q$_2$, q$_6$,	0.965	0.931	85	42	200$_{10}$
13	DFT	α, OH, X, OCH$_3$, NH$_2$, R$_{orto}$, R$_{keton}$, R$_{ester}$, R$_{aldeh}$, E$_{tot}$, q$_2$, q$_6$, q$_7$	0.974	0.948	78	39	133$_{17}$
		III phase=NGA					
1		CTI,OH,X,Cl,Br,NH$_2$,NO$_2$, R$_{o-Cl}$,R$_{o-Me}$, R$_{keton}$,R$_{ester}$,	0.940	0.884	104	21	299$_{32}$
2		CTI,OH,X,Cl,NH$_2$,NO$_2$,alk,R$_{o-Cl}$,R$_{o-Me}$, R$_{keton}$,R$_{ester}$,R$_{o-alk,}$ R$_{o-NH2}$	0.940	0.884	108	16	285$_{32}$
3		α, OH, X, Cl,NH$_2$, NO$_2$, R$_{o-Cl}$, R$_{o-Me}$, R$_{keton}$, R$_{ester}$, R$_{ald}$	0.935	0.875	109	19	249$_{32}$
4		MR,OH, X, NH$_2$, R$_{orto}$,O-CH$_3$, R$_{keton}$, R$_{ester}$, R$_{aldeh}$	0.925	0.855	113	21	255$_{32}$
5		M, OH, X, Cl, NH$_2$, OCH$_3$, R$_{orto}$, R$_{ald}$, R$_{keton}$,R$_{estr}$	0.938	0.88	104	23	262$_{32}$
6	AM1	MR,E$_{homo}$,OH,X,Cl,NH$_2$, NO$_2$,OCH$_3$, R$_{orto}$, R$_{keton}$, R$_{ester}$, R$_{ald}$, R$_{o-Me}$	0.961	0.923	88	26	186$_{35}$
7	AM1	CTI$_{AM1}$, E$_{hydrat}$, OH, X, Cl, NH$_2$, NO$_2$, R$_{o-Cl}$, Q$_1$, Q$_2$, Q$_6$, Q$_7$	0.967	0.935	78	35	141$_{24}$
8	AM1	CTI$_{AM1}$, E$_{homo}$, OH, X, Cl, NH$_2$, NO$_2$, R$_{o-Cl}$, R$_{aldeh}$, Q$_1$, Q$_2$, Q$_6$, Q$_7$	0.982	0.965	59	60	89$_{27}$
9	AM1	CTI$_{AM1}$,E$_{homo}$, OH, X, Cl, NH$_2$, R$_{o-NO2}$, R$_{o-Cl}$, R$_{aldeh}$, Q$_1$, Q$_2$, Q$_6$, Q$_7$	0.982	0.965	59	60	115$_{10}$
10$_1$	DFT	CTI$_{DFT}$, E$_{tot}$, OH, NH$_2$, NO$_2$, R$_{o-Cl}$, R$_{keton}$, q$_1$, q$_2$, q$_6$, q$_7$	0.968	0.938	77	41	128$_{24}$
10$_2$	DFT	CTI$_{DFT}$, E$_{tot}$, OH, NH$_2$, NO$_2$, R$_{o-Cl}$, R$_{keton}$, q$_1$, q$_2$, q$_6$, q$_7$	0.944	0.892	101	22	186$_4$
11	DFT	MR, E$_{tot}$, OH, X, NH$_2$, OCH$_3$, R$_{orto}$, R$_{keton}$, R$_{aldeh}$, R$_{ester}$, q$_2$, q$_6$, q$_7$	0.973	0.948	73	39	121$_{3,17}$
12	DFT	M, E$_{tot}$, OH, NH$_2$, R$_{orto}$, R$_{keton}$, R$_{ald}$, R$_{ester}$, q$_2$, q$_6$,	0.964	0.930	80	40	189$_{26}$
13	DFT	α, E$_{tot}$, OH, X, OCH$_3$, NH$_2$, R$_{orto}$, R$_{keton}$, R$_{ester}$, R$_{aldeh}$, q$_2$, q$_6$, q$_7$	0.972	0.945	75	37	161$_{10}$

The pool of regressions with CTI index as a global descriptor was derived for the three phases and in the majority cases these regressions exhibit the best (equal) statistics. This was the reason to mainly list the models with the CTI index (AM1 calculations) in Table 4.

19

The set of equations (1–5) from Table 4 can be easily developed because it needs the simplest molecular parameterization just with additive global molecular indices (M, MR, etc.) and adding of structural substituents. The QSRRs of this type have good statistics and provide interesting information about stationary phase selectivity.

The full form for the QSRR equations № 4 from Table 4 with MR global descriptor can be seen in Table 5–2. The numeric values of the regression coefficients for the indicative structural descriptors in the similar equations from Table 5–2 valid for the three phases are graphically compared on Fig. 2. It is clearly seen on Fig. 2 that the contribution to the retention on the unipolar phase SE–30 is certainly smaller than that on polar phases for all structural substituents. The McReynolds Y′ and H′ indices are used to quantitate the phase selectivity towards the presence of alcohol, acidic and amide fragments in solute structures. The distribution of the values of McReynolds Y′ and H′ indices and their dependence on phase polarity on Figure 3 has the similar profile on varying the sets of regression coefficients for –OH, –NH$_2$ and –R$_{o–OH}$ descriptors from Figure 2.
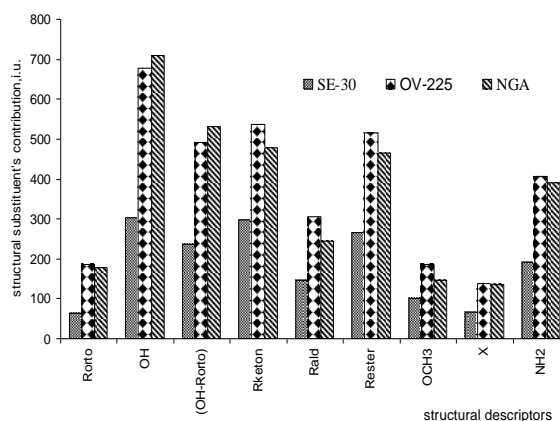
Figure 2. The contribution to the retention of structural substituents in QSRR models (equations 4, Table 5) developed for GC separation of substituted phenols on SE-30, OV-225 and NGA stationary phases.

Table 5-1. The QSRR models for a set of substituted phenols (n = 42) and statistics

St. Phase	Equations 6 (Table 4)	Statistics
SE-30	RI = -546.2 (±427.1) + (21.2±2.1)**MR** - (104.5±43.3)**E$_{Homo}$** - ----(85.2±20.3)**R$_{orto}$**+ (261.7±34.3)**R$_{keton}$** + (123.0±48.2)**R$_{ald}$** + (218.4 ±53.7)**R$_{ester}$** + (137.9±21.3)**OCH$_3$** + (110.5±31.4)**X** + (348.7±38.5)**OH**+ (305.0±50.4)**NH$_2$** - (52.5±30.3)**Cl** + (48.6±24.6)**R$_{o-Me}$**	R = 0.97 R^2 = 0.95 F = 44.9 S = 44.8 Δmax$_i$ = 117$_{38}$
OV-225	RI = -1673.3 (±1439.8) + (23.7±4.4)**MR** - (286.6±153.9)**E$_{Homo}$** - (230.7±44.6)**R$_{orto}$**+ (433.5±91.6)**R$_{keton}$** + (237.5±111.5)**R$_{ald}$** + (385.6 ±138.6)**R$_{ester}$** + (282.8±45.1)**OCH$_3$** + (262.0±45.1)**X** + (788.4±81.9)**OH**+ (706.6±143.1)**NH$_2$** - (149.6±65.4)**Cl** + (137.2±52.5)**R$_{o-Me}$** - (211.8±184.8)**NO$_2$**	R = 0.96 R^2 = 0.92 F = 25.9 S = 94.6 Δmax$_i$ = 188$_{35}$
NGA	RI = -1749.3 (±1341.6) + (21.2±4.1)**MR** - (321.2±143.4)**E$_{Homo}$** - (224.6±441.6)**R$_{orto}$**+ (360.1±85.4)**R$_{keton}$** + (165.0±103.9)**R$_{ald}$** + (314.1 ±129.1)**R$_{ester}$** + (246.7±42.0)**OCH$_3$** + (242.0±74.1)**X** + (826.1±76.3)**OH**+ (718.9±133.4)**NH$_2$** - (139.9±60.9)**Cl** + (142.4±48.9)**R$_{o-Me}$** - (250.9±172.2)**NO$_2$**	R = 0.96 R^2 = 0.92 F = 25.9 S = 88.1 Δmax$_i$ = 186$_{35}$

Table 5-2. The QSRR models for a set of substituted phenols (n = 42) and statistics

St. Phase	Equations 4 (Table 4)	Statistics
SE-30	RI = 487.5(±74.1) + (19.0±2.1)**MR** - (65.0±14.8)**R$_{orto}$**+ (298.9±33.2)**R$_{keton}$** + (146.8±53.2)**R$_{ald}$** + (264.5 ±53.9)**R$_{ester}$** + (100.6±16.4)**OCH$_3$** + (65.3±10.8) **X** + (302.7±40.8)**OH** + (191.6 ±33.4)**NH$_2$**	R = 0.96 R^2 = 0.93 F = 44.2 S = 51.5 Δmax$_i$ = 84$_{39}$
OV-225	RI = 1109.2(±167.8) + (19.2±4.7)**MR** -(185.4±33.5)**R$_{orto}$**+ (535.6±75.1)**R$_{keton}$** + (306.1±120.5)**R$_{ald}$** + (514.3± 122.2)**R$_{ester}$** + (186.9±37.1)**OCH$_3$** + (138.8±24.48) **X** + (677.1±92.5)**OH** + (406.5±75.5)**NH$_2$**	R = 0.93 R^2 = 0.87 F = 23.1 S = 116.7 Δmax$_i$ = 229$_{35}$
NGA	RI = 1358.3(±162.8) + (16.2±4.5)**MR** – (176.8±32.7)**R$_{orto}$** + (477.7 ± 72.9)**R$_{keton}$**+ (245.7±116.9)**R$_{ald}$** + (465.1 ±118.6)**R$_{ester}$** +(145.4±36.0)**OCH$_3$** + (134.8±23.7) **X** + (709.1±89.7)**OH** +(389.9±73.3)**NH$_2$**	R = 0.92, R^2 = 0.85 F = 20.9 S = 113.2 Δmax$_i$ = 255$_{32}$

The variation of McReynolds parameters for the same stationary phases and the dependence of these contributions on the polarity of the stationary phase are presented on Figure 3.

The third McReynolds index Z′ is used for phase selectivity evaluation towards ketone, aldehyde, amine and ester fragments in solute structures. In the case of our models from Table 5-2, the ketone, aldehyde, OCH$_3$, -NH$_2$ and ester fragments are included as separate descriptors, but for all these descriptors the similar profile of retention contribution is created from QSRRs regression coefficients values.

The phase selectivity towards the halogen substitutes is quantified with McReynolds seventh I′ index. The character of the changes in the I′ index on Figure 3 and our descriptor (X) on Figure 2 is similar. The maximum values for the retention contribution of iodine–containing structures are typical for a OV–225 phase.
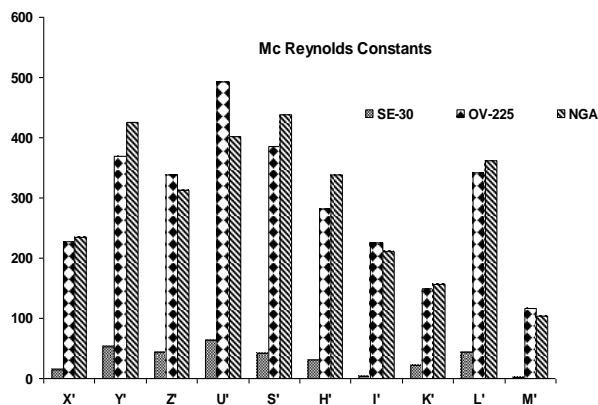
Figure 3. The *McReynolds* constants for SE-30, OV-225 and NGA stationary phases.

The tendency in contribution of structural indicative descriptors to the retention expressed by McReynolds indices and the variation in regression coefficients values derived from the QSRR models depends on stationary phase polarity and seems to be influenced in the similar way. The comparison of the parametric (numeric) values of the regression coefficients for structural substituents used as indicative descriptors in similar QSRR models derived for different stationary phases provide information about the polarity of the phases used in the case, similar to McReynolds constants.

Apparently in the case when the MLR form for QSRR modeling is preferred to quantify the retention behavior for a set of diverse noncongeneric solutes, separation on stationary phases with different polarities, the parametric values for these indicative descriptors reveal the stationary phase polarity in a similar way as McReynolds constants.

4. CONCLUSIONS

QSRR approach was applied for gas chromatographic retention modeling for a set of phenol derivates (n = 42) separated on three stationary phases with different polarity. The molecular indices, used as descriptors in MLRs were calculated at AM1 and DFT level. The charge–related topological index CTI, probed as a global descriptor for QSRRs deriving, revealed its ability to provide models with good statistics.

It was shown that the descriptors contribution analyses can be used to reveal the intermolecular solute – phase interactions. The numeric values of

the regression coefficients were compared with McReynolds constants. The comparison of the regression coefficient contribution of the structural descriptors in similar QSRR models for different stationary phases revealed the stationary phase selectivity.

REFERENCES

1. Sampling and Analysis Procedures for Screening of Industrial Effluents for Priority Pollutants, USEPA., Envir. Monitoring and Support Labor., Cincinnati, (1977).
2. WHO, World Health Organization Environmental Health Criteria, Geneva, No.202, 1998.
3. B.K. Chen, Cs. Horvath, *J. Chromatogr.,* 171 (1979), 15.
4. R. Kaliszan, *Chem. Rev.*, 107, 3212 (2007).
5. K. Heberger, *J. Chromatogr.* A, 1158, 273 (2007).
6. R. Kaliszan, QSRR: Quantitative Structure-Chromatographic Retention Relationships, Willey, New Jork, 1987.
7. R. Kaliszan, Structure, Retention in Chromatography. A Chemometric Approach, Harwood Academic, Amsterdam, 1997.
8. S. Eric, M. Pavlovic, G. Popovic, D. Agbaba, *J. Chromatogr. Sci.*, 45, 140 (2007).
9. W.L. Fitch, M. McGregor, A.R. Katritzky, A. Lomaka, R. Petruhin, M. Karelson, *J. Chem. Inf. Comput. Sci.,* 42, 830 (2002).
10. A.R. Katritzky, R. Petruhin, D. Tatham, S. Basak, E. Benfenati, M. Karelson, U. Maran, *J. Chem. Inf. Comput. Sci.,* 41, 675 (2001).
11. P. Gramatica, P. Pilutti, E. Papa, *SAR QSAR Environ. Res.* 13, 743 (2002).
12. M.R. Hadjmohammadi, M.H. Fatemi, K. Kamel, *J. Chromatogr.Sci.*, 45, 400 (2007).
13. C.K. Roy, I. Sanyal, P.P. Roy, *SAR QSAR Environ. Res.* 17, 563 (2006).
14. D.K. Tuppurainen, S.P.Korhonen, J. Ruuskanen, *SAR QSAR Environ. Res.* 17, 549 (2006).
15. V. Vapnik, Statistical Learning Theory, Wiley, New York, 1998.
16. R. Burbidge, M. Buxton, S. Holden, *Comput. Chem.* 26, 5 (2001).
17. R. Cherminski, A. Yasri, D. Hartsourgt, *Quant. Struct.-Act.Relat.* 20, 227 (2001).
18. V.C. Viterbo, J.P. Braga, A.P. Braga, M.B. de Almeida, *J. Chem. Inf. Comput. Sci,* 41, 309 (2001).
19. G.A. Bakken, P.C. Jurs, *J. Med. Chem.*, 43, 4534 (2000).
20. J. Sorich, J.O. Miners, R.A. McKinnon, D.A. Winkler, F.R. Burden, P.A. Smith, *J.Chem. Inf. Comput.Sci.* 43, 2019 (2003).
21. A.R. Katritzky, R. Petruhin, R. Jain, M. Karelson, *J. Chem. Inf. Comput. Sci,* 41, 1521 (2001).
22. S. Dietmann, C.Frőmmel, *Bioinformatics,* 18, 167 (2002).
23. S. Sremac, B. Skrbic, A. Onjia, *J. Serb. Chem. Soc.,* 70, 1291 (2005).
24. S. Sremac, A. Popovic, Z. Todorovic, D. Cokesa, A. Onjia, *Talanta*, 76, 66 (2008).
25. H.F. Chen, *Anal. Chim. Acta,* 609, 24 (2008).
26. W.O. McReynolds, *J. Chromatogr. Sci.* 8, 685 (1970).
27. L. Rohrschneider, *J. Chromatogr.* 48, 728 (1998).
28. M.H. Abraham, C.F. Poole, S.K. Poole, *J. Chromatogr.* A, 842, 79, (1999).
29. C.F. Poole, S.K. Poole, *J. Chromatogr.* A, 1184, 254,(2008).
30. C.F. Poole, The Essence of Chromatography, Elsevier, Amsterdam, 2003.
31. S.K. Poole, B.R. Kersten, C.F. Poole, *J. Chromatogr.,* 471 (1989), 91.
32. C.F. Poole, S.K. Poole, *Chem. Rev.*, 89, 377 (1989).
33. L. Rohrschneider, *J. Sep. Sci.* 24, 3 (2001).
34. L. Rohrschneider, *J. Chromatogr.* 17, 1 (1965).
35. L. Rohrschneider, *J. Chromatogr.* 22, 6 (1966).
36. H. Rotzsche, Stationary Phases in Gas Chromatography, Elsevier, Amsterdam, 1991.
37. J. Grzibowski, H. Lamparczyk, A. Nasal, A. Radecki, *J. Chromatogr.*, 196, 217 (1980).
38. I.P. Bangov, *J. Chem. Inf. Comput. Sci.*, 30, 277 (1990).
39. P.A. Demirev, A.S. Dyulgerov, I.P. Bangov, *J. Math. Chem.,* 8, 367 (1991).
40. I.P. Bangov, M. Moskovkina, A. Patleeva, *Bulg. Chem. Commun.*, 42 (4), 338 (2010).
41. MS Excel, Version 2003, Microsoft Corp., Redmond, WA, 2003.
42. Alex A. Granovsky, PC GAMESS version 7.1(Tornado), http://classic.chem.msu.su/gran/gamess/index.htm
43. M.W.Schmidt, K.K. Baldridge, J.A. Boatz, S.T. Elbert, M.S. Gordon, J.H. Jensen, S. Koseki, N. Matsunaga, K.A. Nguyen, S. Su, T.L. Windus, M. Dupuis, J.A. Montgomery. *J.Comput. Chem.* 14, 1347 (1993).
44. M. Charton, S.Clementi, S.Ehrenson, O.Exner, J. Shorter and S.Wold, *Quant. Struct. Act. Relat.*, 4, 29 (1985).
45. R. Kaliszan, *CRC Critical Reviews in Analytical Chemistry*, 16(4), 323 (2005).
46. G.R. Faminy, L. I. Wilson, *Rev. Comp. Chem.*, 211 (2002).

МОДЕЛИРАНЕ НА ГАЗХРОМАТОГРАФСКО ЗАДЪРЖАНЕ С ПОМОЩТА НА ХЕМОМЕТРИЧЕН ПОДХОД

М.Н. Московкина, И.П. Бангов, А.Ж. Патлеева

Катедра „Обща химия", Факултет по природни науки, Шуменски Университет „Еп. К. Преславски", Шумен,, 9712, ул. Университетска 115, България

(Резюме)

Хемометричният подход за установяване на количествени връзки от типа „структура-ретентно хроматографско свойство" (QSRR) е приложен за група от заместени феноли с цел създаване на модели за задържането им в газхроматографска колона. Експерименталните данни за група от 42 заместени фенола, включваща и приоритетни природни замърсители, разделени в три колони с различна хроматографска полярност (неполярна фаза SE–30 и полярни фази OV–225 и NGA), са взети от литературата. За създаването на моделите е използван статистическия метод на многопараметричната линейна регресия (MLR). Тополого-електронният индекс CTI, създаден от един от авторите (И.Б.) е проверен и оценен като глобален дескриптор. Хемометричния анализ на създадените модели ясно показва факторите, описващи междумолекулните взаимодействия (ММВ) с неподвижната фаза и обуславящи разделянето в хроматографската колона. Сравнението на приносите на отделните дескриптори в регресионните уравнения за различни неподвижни фази, показва, че те корелират добре с константите на МакРейнолдс за фазова селективност.

Characterization of the structure, electronic conjugation and vibrational spectra of the radical anions of p- and m-dinitrobenzene: a quantum chemical study

D. Y. Yancheva

Department of Structural Organic Analysis, Institute of Organic Chemistry, Bulgarian Academy of Sciences, Acad. G. Bonchev St., Block 9, 1113 Sofia, Bulgaria

The structure, charge distribution and electronic coupling between the functional groups, caused by the conversion of two main nitrobenzenes (p- and m-dinitrobenzene) into radical anions was studied at B3LYP/6-311++G** level. The vibrational spectra of the neutral compounds and the radical anions, which are closely related to the structural and electronic changes, were also studied and discussed. The enhanced vibrational coupling between the nitro groups in the radical anion species was described on the basis of force field analysis and frequency reduction upon radicalization. The electronic density analysis showed that in both cases the nitro groups bear equal parts of the additional electron: 0.36 e⁻ for the p-compound and 0.29 e⁻ for the m-isomer. The radical anion species are characterized by quinoid-like structures as well as a larger and stronger conjugated system than the corresponding neutral forms.

Keywords*:* Nitrobenzenes; Radical anions; Electronic structure; IR spectra; DFT

INTRODUCTION

The radical anions of nitro compounds currently receive much attention as important intermediates in the metabolic pathways of antibacterial, antiprotozoal and anticancer agents [1–5]. Several nitro compounds and some of their metal complexes [6–9] are used in the medicine as radio-sensitizers in the anti-tumor therapy, and the efficiency of the drugs is also related to the one-electron reduction potential of these compounds [6]. Some radical anions of nitroaromatic compounds present an environmental concern as metabolites of synthetic intermediates, dyes, pesticides, and explosives [10–12]. The nitro radical anions are extensively studied in view of the intramolecular electron-transfer dynamics as well [13–15].

Therefore, an understanding of the structure, the electronic charge distribution and the changes related to the chemical transformation of the nitro compounds into radical anions is very important from both fundamental and practical points of view. On the other hand, radical anion species are difficult to isolate and study due to their high reactivity. So far, the properties and reactivity of the nitro radical anions have been explored mainly by pulse radiolysis [16] and cyclic voltammetry [17,18]. The IR spectral studies also provide valuable information on the structure and formation of organic aromatic anions (radical-anions, carbanions, dianions, etc.) [19–21], and particularly on the formation of nitro radical anions [22]. Optical spectra measurements combined with computational methods present another relevant investigation approach [23]. Hence, the experimental spectral techniques complemented with computational methods are a reasonable choice of analytical tools to monitor the changes occurring when neutral molecules are converted into radical anions and to explain the observed effects from a theoretical point of view.

The present contribution is focused on p- and m-dinitrobenzene as simple model compounds describing the interaction of two nitro groups through an aromatic spacer. The effect of the relative positions of the nitro groups (para *vs*. meta) during conversion of the dinitrobenzenes into radical anions was analysed by DFT calculations. The essential changes in the structure, charge distribution and electronic coupling between the functional groups, caused by the conversion, are reported. Since the electronic structure and the nature of the aromatic substitution have a profound effect on the bioactivity, toxicity and redox properties of the nitroaromatic compounds, special emphasis is put on the discussion of the different electronic interactions characterizing the radical anion species. The vibrational spectra of the neutral compounds and the radical anions, which are

---

closely related to the structural and electronic changes, are also studied and discussed.

COMPUTATIONAL DETAILS

All theoretical calculations were performed using the Gaussian 09 package [24] of programs. The molecular geometry of the neutral compounds and the radical anions was optimized at B3LYP/6–311++G** level. The optimized structures were confirmed to be the local minima by frequency calculation (no imaginary frequency). Spin densities were computed using the Mulliken population analysis. For a better correspondence between experimental and calculated IR frequencies, the results were modified using the empirical scaling factor of 0.9688, reported by Merrick and Radom [25]. The theoretical vibrational spectra were analyzed in terms of potential energy distributions (PEDs) by using the VEDA 4 program [26]. For the plots of simulated IR spectra, pure Lorentzian band shapes were used with a bandwidth of 10 cm^{-1}.

RESULTS AND DISCUSSION

The conversion of p-dinitrobenzene (**1a**) and m-dinitrobenzene (**2a**) into radical anions (**1b** and **2b**, Scheme 1) could be done electrochemically in DMSO solution [22]. The negative radical formation is accompanied by color change and new spectral behavior reflecting the structure, electronic coupling and interactions established in the anionic species. The changes are related to those observed for monosubstituted nitrobenzene, but due to the interactions between the two electron acceptor groups attached to the phenyl ring their nature is more complex and subtle.
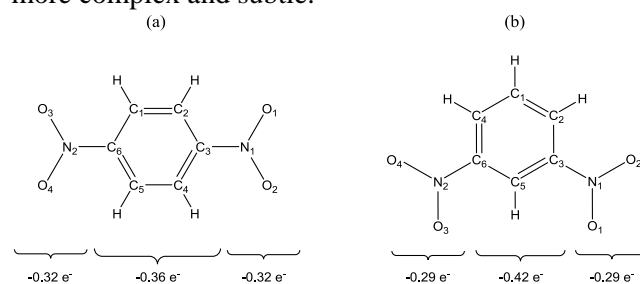
Scheme 1. Atomic numbering and spin density for: (a) **1b** and (b) **2b.**

Structural Analysis

The nitro groups in the free molecules of p- and m-dinitrobenzene are expected to be coplanar with the phenyl ring. Taking this into account, we maintained the symmetry of **1a**, as well as of the corresponding RA **1b**, during geometry optimization as D_{2h}, while this of the m-derivatives **2a** and **2b** was fixed as C_{2v}.

The calculated bond lengths included in Table 1 are denoted according to the atomic numbering presented in Scheme 1. For simplicity, in Table 1 the bond length duplicates resulting from the molecular symmetry are omitted. According to the DFT calculations, m- and p-dinitrobenzene in neutral form have comparable N-O and C-N bond lengths, very close to the values reported for nitrobenzene [27]. The data are also in excellent agreement with the bond lengths found by crystallographic studies on **1a** and **2a** [28,29].

Table 1. Bond lengths R (in Å) in **1a**, **2a** and their RAs **1b** and **2b.**

Species	Neutral molecules	RAs	ΔR^a
p-Dinitrobenzene	**1a**	**1b**	
$R(C^1-C^2)$	1.390	1.377	-0.013
$R(C^2-C^3)$	1.391	1.414	0.023
$R(C^1-C^6)$	1.391	1.414	0.023
$R(C^3-N^1)$	1.486	1.413	-0.073
$R(N^1-O^1)$	1.222	1.258	0.033
$R(N^1-O^2)$	1.222	1.258	0.033
m-Dinitrobenzene	**2a**	**2b**	
$R(C^1-C^2)$	1.392	1.392	0.00
$R(C^2-C^3)$	1.393	1.420	0.027
$R(C^3-C^5)$	1.392	1.392	0.00
$R(C^3-N^1)$	1.485	1.431	-0.054
$R(N^1-O^1)$	1.222	1.253	0.031
$R(N^1-O^2)$	1.223	1.254	0.031

^{a} $\Delta R = R_{RA} - R_{molecule}$ (Å)

The conversion into RAs leads to simultaneous shortening of the C-N bond and lengthening of the N-O bonds (Table 1). The differentiation is greater concerning the C-N bond length – in the p-substituted compound **1b** the C-N bond is much shorter than in **2b**. Compared to nitrobenzene, the C-N bond lengths decrease in the following order: **2b** (1.431 Å) > **1b** (1.413 Å) > $NO_2C_6H_5^-$ (1.395 Å).

As it can be seen from Table 1, the N-O bonds in both RAs are in the range 1.254–1.258 Å – by approximately 0.03 Å shorter than the N-O bonds in the RA of nitrobenzene. The geometry of the phenyl ring is also affected as a result of the conversion into RAs. In **1b** and **2b** the phenylene bond lengths are no longer identical, but altered in such a manner that their values are much closer to the C-N bond lengths and they form a quinoid-like structure influenced by the position of the NO_2 substituents. Hence, the structural changes reveal that the mesomeric interaction between the NO_2 groups and the phenyl ring is strongly enhanced in comparison to the neutral form and the electronic conjugation is extended over the whole RA species.

Important information for the distribution of the odd electron upon negative radical formation could be derived from atomic spin population analysis of **1b** and **2b**. Based on experimental and computational FTIR studies, it was found that the lowering of the stretching vibrations of the main functional groups of aromatic compounds accompanying their conversion into RAs is mainly related to the localization of spin density within the corresponding functional groups [30]. The spin population over the functional groups correlates to the experimentally observed lowering of the stretching vibrations and thus provides a reliable approach to predict and explain the spectral changes caused by the radicalization. The distribution of the odd electron over the fragments in **1b** and **2b** is illustrated in Scheme 1.

In both RAs, the two NO_2 groups bear equal parts of the odd electron: 0.36 e$^-$ in the case of **1b** and 0.29 e$^-$ in the case of **2b**. In comparison to the RA of nitrobenzene, where the corresponding value is 0.64 e$^-$ [27], the spin density over the NO_2 groups of **1b** and **2b** is about twice lower. As a consequence, the changes in the bond lengths characterizing the conversion of **1a** and **2a** into RAs are smaller than in the case of nitrobenzene. Furthermore, this should also result in smaller frequency shifting of the N-O stretching vibrations upon radicalization. However, concerning the differences between the two species studied here, we could conclude that the electronic conjugation

between the nitro groups of the p-isomer is more effective, as evidenced by the greater spin density over them and the shorter C-N distances in **1b**.

Force Field Analysis

The distribution of the odd electron in RAs may be further characterized by investigating the force field in these systems. For this purpose we computed the diagonal and coupling force constants with respect to the natural internal coordinates and used them to assist the analysis of the electronic and spectral changes resulting from the conversion. The shift of the frequencies of the characteristic groups is of particular interest since the participation of a small number of bonds in the vibration allows comparison of the frequencies with certain parameters describing the electronic structure of the RAs. Selected diagonal and coupling constants for the species studied are listed in Table 2.

In accordance with the structural changes upon radicalization, the corresponding diagonal force constants are larger for the C-N bonds and smaller for the N-O bonds for both RAs. The ΔK values of transitions **1a → 1b** and **2a → 2b** are smaller in comparison to nitrobenzene and its RA (ΔK_{C-N} = 2.03 and ΔK_{C-N} = −3.18), but they show the same tendency as found by the atomic spin density. A considerable frequency shifting of the N-O and C-N stretching vibrations should be expected for **1b** and **2b**.

It is known that the coupling constants of distant functional groups in p- and m-disubstituted aromatic nitriles increase substantially when the corresponding RAs are formed, thus indicating an enhanced electron coupling between the vibrating groups [27]. As it could be seen from the values of the coupling constants presented in Table 2, this relation also holds in case of the dinitrobenzene RAs investigated by us. The coupling constants of the N-O bonds increase up to two orders of magnitude with the negative radical formation. The force constants describing the interaction of the C-N bonds also indicate enhanced coupling in the RAs.

IR Spectral analysis

The described electronic and structural changes accompanying the formation of the RAs of p- and m-dinitrobenzene are related to the essential changes occurring in the IR spectral behavior of the studied species. The altered bond lengths and the enhanced electronic coupling between the nitro

Table 2. Selected diagonal and coupling force constants K (in mdyn.Å^{-1}) for **1a**, **2a** and their RAs **1b** and **2b.**

Species	Neutral molecules	RAs	ΔK^a
p-Dinitrobenzene	**1a**	**1b**	
Diagonal Force Constants			
$K(C^3-N^1)$	4.02	5.51	1.49
$K(N^1-O^1)$	10.31	7.97	-2.33
$K(N^1-O^2)$	10.31	7.97	-2.33
Interaction Force Constants			
$K(C^3-N^1)/(C^6-N^2)$	0.02	0.05	0.03
$K(N^1-O^1)/(N^2-O^3)$	0.01	0.33	0.32
$K(N^1-O^1)/(N^2-O^4)$	0.00	0.30	0.30
m-Dinitrobenzene	**2a**	**2b**	
Diagonal Force Constants			
$K(C^3-N^1)$	4.04	4.93	0.88
$K(N^1-O^1)$	10.34	7.88	-2.46
$K(N^1-O^2)$	10.26	7.90	-2.36
Interaction Force Constants			
$K(C^3-N^1)/(C^6-N^2)$	0.00	0.20	0.20
$K(N^1-O^1)/(N^2-O^3)$	0.03	0.64	0.61
$K(N^1-O^2)/(N^2-O^4)$	0.02	0.55	0.53
$K(N^1-O^1)/(N^2-O^4)$	0.00	0.56	0.56

^{a} $\Delta K = K_{RA} - K_{molecule}$ (mdyn Å^{-1})

groups in the RAs would lead to considerable shifting of the IR band positions and the character of the vibrational modes. Having in mind the above described differences between **1b** and **2b**, the spectral changes should be expected to be larger in the case of **1b**. In order to check this assumption, we studied the IR spectra of the neutral compounds and the corresponding anion species and compared them to experimental data in solid state and DMSO-d$_6$ solution obtained earlier by Juchnovski and Andreev [22,32,33].

The IR spectra (1600-800 cm^{-1}) of **1a** and **1b** and those of **2a** and **2b** are shown in Fig. 1. The most important vibrations of the nitro groups in the neutral dinitrobenzenes and their RAs arise from the stretching of the N-O bonds and the C-N bonds. Table 3 summarizes those vibrations and the proposed assignments based on the contribution of a given mode to the corresponding normal vibration according to the PED matrix.

Assignments of the nitro vibrations in 1b

Similarly to the neutral p-dinitrobenzene, RA **1b** belongs to the point group D$_{2h}$. As a result of the electronic coupling, the two nitro groups vibrate coherently which leads to the formation of four N-O stretching modes - two antisymmetric: in-phase v^{as}_{NO2} *(ip)* and out-of-phase v^{as}_{NO2} *(op)*, and two symmetric: in-phase v^{s}_{NO2} *(ip)* and out-of-phase v^{s}_{NO2} *(op)* vibrations. According to the analysis of

the theoretical IR frequencies of **1b**, only two of them, v^{as}_{NO2} *(ip)* and v^{s}_{NO2} *(op)*, are IR active – Fig. 1a.

The band of v^{as}_{NO2} *(ip)* is predicted to appear at 1397 cm^{-1}, which agrees well with the experimentally found value – 1417 cm^{-1} and the assignment suggested earlier by Juchnovski and Andreev [22]. On the other hand, according to the calculations, v^{s}_{NO2} *(op)* is expected at a much lower frequency – 1096 cm^{-1}, than suggested in Ref. [22]. However, this theoretical value could not be compared to an experimental one since no IR data below 1100 cm^{-1} were reported in [22] due to the limitations of the spectral technique used. The band assigned as v^{s}_{NO2} in [22] is registered at 1212 cm^{-1}. It is the most intensive band in the IR spectrum of **1b** and based on the theoretical calculations should be attributed to a mixed $v_{C-N}+\delta_{NO2}$ *(op)* vibration.

Assignments of the nitro vibrations in 2b

In the m-dinitrobenzene **2a** and its AR **2b**, point group C$_{2v}$, all four N-O stretching modes should be IR active. Nevertheless, in the case of the neutral m-dinitrobenzene **2a** only two bands could be identified in the theoretical IR spectrum – Fig. 1b. This is a result of the small splitting between the in-phase and out-of-phase components of v^{as}_{NO2} and v^{s}_{NO2} and the higher intensity of the out-of-phase components.
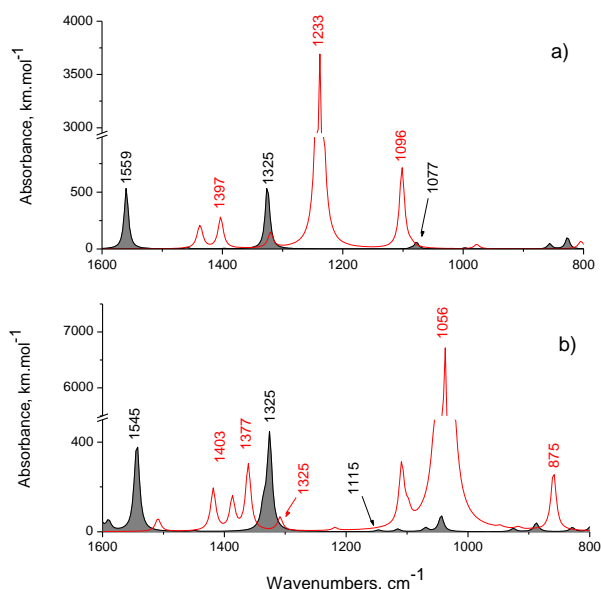
Fig. 1. Theoretical (B3LYP/6-311++G**) IR spectra of: a) **1a** (shaded) and **1b**; b) **2a** (shaded) and **2b**.

Our calculations show that among the N-O stretching vibrations of **2b**, ν^{as}_{NO2} (op) absorbs at the highest frequency: 1403 cm^{-1}. ν^{as}_{NO2} (ip) participates in a mixed $\nu_{CC} + \nu^{as}_{NO2}$ (ip) mode and gives rise to a band at 1377 cm^{-1}. The in-phase symmetric N-O stretching vibration ν^{s}_{NO2} (ip) has similar character and position to this of **1b**: mixed mode $\nu_{CN} + \nu^{s}_{NO2}$ (ip) at 1325 cm^{-1}. On the other hand, in the case of **2b** the out-of-phase component ν^{s}_{NO2} (op) is mixed with δ_{NO2} and the corresponding band is the strongest band in the whole spectrum. In the RA of m-dinitrobenzene the coordinate ν_{CN} also participates in a lower-frequency mixed vibration: $\nu^{as}+\delta_{CCC}+\nu_{C-N}$ (op) appearing at 878 cm^{-1}. These findings support in general the assignments made in [22], but the experimental values measured for some of these vibrations are much higher: 1516 cm^{-1} for ν^{as}_{NO2} (op) and 1274 cm^{-1} for ν^{s}_{NO2} (op). The discrepancy must be due to the great complexity of the nitro vibrational modes revealed by the theoretical data reported here. As a result of the strong conjugation of the nitro groups and the benzene ring, all characteristic nitro vibrations in the RA **1b** and **2b** show mixed character. On the other hand, the benzene ring vibrations are also affected and appear at new positions and with enhanced intensity – Fig. 1. Further IR studies of the p- and m-dinitrobenzene anions isolated in solid argon might be decisive for the accurate vibrational assignment.

IR spectral changes upon conversion into RAs

The spectral changes concerning the most important nitro vibrations could be best described if the average ν^{as}_{NO2} and ν^{s}_{NO2} are calculated [$\nu^{as}_{NO2} = (\nu^{as}_{NO2}(ip) + \nu^{as}_{NO2}(op)) / 2$ and $\nu^{s}_{NO2} = (\nu^{s}_{NO2}(ip) + \nu^{s}_{NO2}(op)) / 2$]. The changes are summarized below:

1) Decrease of ν^{as}_{NO2} by 162 cm^{-1} for **1b** and 154 cm^{-1} for **2b**, respectively.

2) Decrease of ν^{s}_{NO2} by 170 cm^{-1} for **1b** and 140 cm^{-1} for **2b**, respectively.

3) Increase of ν_{CN} by 156 cm^{-1} for **1b** and 220 cm^{-1} for **2b**, respectively. In the case of **1b** the coordinate ν_{CN} is delocalized over two vibrations: $\nu_{CN} + \nu^{s}_{NO2}(ip)$ and $\nu_{CN} + \delta_{NO2}(op)$ (see Table 3).

4) Strong enhancement of the *intensity of one main band* upon radicalization:

The IR spectra of the RAs studied are dominated by one extremely intensive band. In the spectrum of **1b**, this band originates from $\nu_{CN} + \delta_{NO2}$ vibration and absorbs about 60 times stronger than in the neutral compounds. In the IR spectrum of **2b** the intensity of the band is even higher, but corresponds to a mixed vibration $\nu^{s}_{NO2}(op) + \delta_{NO2}$, without contribution of ν_{CN}. Taking into account the assignments in both cases, one could conclude that a great migration of π-electron density in the conjugated system is connected to the δ_{NO2} motion and it is contributing at the largest extent to the very high intensities of these bands.

5) The uniform distribution of the odd electron upon both nitro groups accounts for the smaller reduction in frequency in the studied RAs as compared with those of nitrobenzene RA. In the case of nitrobenzene, ν^{as}_{NO2} and ν^{s}_{NO2} are shifted downwards with 278-275 cm^{-1} (B3LYP/6-311++G**) [27]. The reported experimental values in DMSO-d$_6$ solution are 285-289 cm^{-1} [34].

Table 3. Experimental and theoretical (B3LYP/6-311++G**) vibrational frequencies (ν in cm^{-1}) and IR intensities (A in km.mol^{-1}, in parentheses), and approximate assignments of the bands for the neutral p-dinitrobenzenes **1a** and **2a**, and the corresponding radical anions **1b** and **2b**

Species	Neutral molecules					RAs				
p-Dinitrobenzene	**1a**					**1b**				
Assignment	$\nu^{as}_{NO2}(ip)$	$\nu^{as}_{NO2}(op)$	$\nu^{s}_{NO2}(ip)$	$\nu^{s}_{NO2}(op)$	$\nu_{CN}+\delta_{CCC}$	$\nu_{CC}+\nu^{as}_{NO2}(ip)$	$\nu^{as}_{NO2}(op)$	$\nu_{CN}+\nu^{s}_{NO2}(ip)$	$\nu_{CN}+\delta_{NO2}(op)$	$\delta_{CCC}+\nu^{s}_{NO2}(op)$
IR [a]	1556	-	-	1339	1106	-	-	-	-	-
Raman [a]	-	1535	1358	-	-	-	-	-	-	-
DMSO-d$_6$ [b]	1552	-	-	1343	-	1417	-	-	1212	-
Calc. [c]	1559 (535.7)	1535 (0)	1336 (0)	1325 (540.2)	1077 (60.7)	1397 (274.4)	1373 (0)	1334 (0)	1233 (3710.9)	1096 (710.6)
m-Dinitrobenzene	**2a**					**2b**				
Assignment	$\nu^{as}_{NO2}(ip)$	$\nu^{as}_{NO2}(op)$	$\nu^{s}_{NO2}(ip)$	$\nu^{s}_{NO2}(op)$	$\nu_{NC}+\delta_{CCC}$	$\nu^{as}_{NO2}(op)$	$\nu_{CC}+\nu^{as}_{NO2}(ip)$	$\nu_{CN}+\nu^{s}_{NO2}(ip)$	$\nu^{s}_{NO2}+\delta_{NO2}(op)$	$\nu_{CN}+\delta_{CCC}+\nu^{as}_{NO2}(op)$
IR [d]	1540	1529	1352	1348	1147	-	-	-	-	-
Raman [d]	1538	1528	1353	1348	1147	-	-	-	-	-
DMSO-d$_6$ [b]	1540	-	-	1349	-	-	1360	1336	1274	-
Calc. [c]	1543 (95.2)	1545 (320.3)	1335 (96.4)	1325 (427.8)	1115 (11.87)	1403 (145.5)	1377 (296.0)	1325 (58.1)	1056 (6862.4)	878 (263.1)

[a] Experimental IR and Raman spectra in solid state [32] [b] Experimental IR spectra in DMSO-d$_6$ solution [22] [c] Calculated frequencies - B3LYP/6-311++G**, scaling factor – 0.9688; [d] Experimental IR and Raman spectra in solid state [33]

CONCLUSIONS

We show in this work that the conversion of p- and m-dinitrobenzene into RAs causes very essential structural, electronic and spectral changes. The two RAs studied exhibit uniform distribution of the odd electron over the two nitro groups, and quinoid-like structure with shorter C-N bonds and longer N-O bonds. The RA species are characterized by a larger and stronger conjugated system than the neutral form. The analysis of the N-O and C-N vibrations allows concluding that the formation of the RAs leads to a considerable increase of the electronic and vibrational interaction between the distant nitro groups. This conclusion is confirmed by the quantum chemical evaluation of the coupling force constants of the two nitro groups in the investigated neutral molecules and corresponding RAs.

REFERENCES:

1. D. I. Edwards, in: *Comprehensive Medicinal Chemistry*, 5th ed., C. Hansch (ed.), Pergamon Press, New York, 1990, Vol. 2, p. 725.
2. D. Greenwood, *Antimicrobial Chemotherapy*, 13th ed., Oxford University Press, Oxford, 1995.
3. J. Rodríguez, A. Gerpe, G. Aguirre, U. Kemmerling, O. E. Piro, V. J. Arán, J. D. Maya, C. Olea-Azar, M. González, H. Cerecetto, *Eur. J. Med. Chem.*, **44**, 1545 (2009).
4. M. A. La-Scalea, G. H. G. Trossini, C. M. S. Menezes, M. C. Chung, E. I. Ferreira, *J. Electrochem. Soc.*, **156**, F93 (2009).
5. H. R. Nasiri, R. Panisch, M. G. Madej, J. W. Bats, C. R. D. Lancaster, H. Schwalbe, *Biochim. Bioph. Acta*, **1787**, 601 (2009).
6. A.M. Rauth, T. Melo, V. Misra, *Int. J. Rad. Oncol. Biol. Phys.*, 42, 755(1998).
7. 7R. J. Mascarenhas, I. N. Namboothiri, B. S. Sherigara, V. K. Reddy, *J. Chem. Sci.*, **118**, 275 (2006).
8. A. Chandor, S. Dijols, B. Ramassamy, Y. Frapart, D. Mansuy, D. Stuehr, Nuala Helsby, J.-L. Boucher, *Chem. Res. Toxicol.*, 21, 836 (2008).
9. A. Ray, P. C. Mandal, A. D. Jana, W. S. Sheldrick, S. Mondal, M. Mukherjee, M. Ali, *Polyhedron*, **27**, 3112 (2008).
10. O. Isayev, B. Rasulev, L. Gorb, J. Leszczynski, *Mol. Divers.*, **10**, 233(2006).
11. A.-C. Schmidt, R. Herzschuh, F.-M. Matysik, W. Engewald, *Rapid Comm. Mass Spectrom.*, **20**, 2293 (2006).
12. A. E. Hartenbach, T. B. Hofstetter, M. Aeschbacher, M. Sander, D. Kim, T. J. Strathmann, W. A. Arnold, C. J. Cramer, R. P. Schwarzenbach, *Environm. Sci. Techn.*, **42**, 8352 (2008).
13. C. Frontana, I. González, F.J. González, *ECS Transactions*, **13**, 37 (2008).
14. D. Zigah, J. Ghilane, C. Lagrost, P. Hapiot, *J. Phys. Chem. B*, **112**, 14952 (2008).
15. J. P. Telo, S.F. Nelsen, Y. Zhao, *J. Phys. Chem. A*, **113**, 7730 (2009).
16. R.P. Mason, in: W.A. Pryor (Ed.), Free Radicals in Biology, vol. V, Academic Press, New York, 1982, p. 161.
17. J. H. Tocher, D. I. Edwards, *Free Radical Res. Commun.*, **16**, 19 (1992).
18. J. Carbajo, S. Bollo, L.J. Núñez-Vergara, A. Campero, J.A. Squella, *J. Electroanal. Chem.*, **531**, 187 (2002).
19. D. J. Cram, *Fundamentals of Carbanion Chemistry*, Academic Press, New York, 1965.
20. J. Corset, in: *Comprehensive Carbanion Chemistry*, E. Buncel, T. Durst, (eds.), Elsevier, Amsterdam, 1980, Part A.
21. I. N. Juchnovski, I. G. Binev, in: *Chemistry of Functional Groups*, *Suppl. C*, S. Patai, Z. Rappoport (eds.), Wiley, New York, 1983, Chapt. 4, p. 107-135 (and references therein).
22. I. Juchnovski, G. Andreev, *Compt. Rend. Acad. Bulg. Sci.*, **36**, 911 (1983).
23. S.F. Nelsen, M.N. Weaver, J.I. Zink, J.P. Telo, *J. Am. Chem. Soc.*, **127**, 10611 (2005).
24. M. J. Frisch, G. W. Trucks, H. B. Schlegel, G. E. Scuseria, M. A. Robb, J. R. Cheeseman, G. Scalmani, V. Barone, B. Mennucci, G. A. Petersson, H. Nakatsuji, M. Caricato, X. Li, H. P. Hratchian, A. F. Izmaylov, J. Bloino, G. Zheng, J. L. Sonnenberg, M. Hada, M. Ehara, K. Toyota, R. Fukuda, J. Hasegawa, M. Ishida, T. Nakajima, Y. Honda, O. Kitao, H. Nakai, T. Vreven, J. A. Montgomery, Jr., J. E. Peralta, F. Ogliaro, M. Bearpark, J. J. Heyd, E. Brothers, K. N. Kudin, V. N. Staroverov, R. Kobayashi, J. Normand, K. Raghavachari, A. Rendell, J. C. Burant, S. S. Iyengar, J. Tomasi, M. Cossi, N. Rega, J. M. Millam, M. Klene, J. E. Knox, J. B. Cross, V. Bakken, C. Adamo, J. Jaramillo, R. Gomperts, R. E. Stratmann, O. Yazyev, A. J. Austin, R. Cammi, C. Pomelli, J. W. Ochterski, R. L. Martin, K. Morokuma, V. G. Zakrzewski, G. A. Voth, P. Salvador, J. J. Dannenberg, S. Dapprich, A. D. Daniels, O. Farkas, J. B. Foresman, J. V. Ortiz, J. Cioslowski, and D. J. Fox, Gaussian 09, Revision A.1, Gaussian Inc., Wallingford CT, 2009.
25. J. Merrick, D. Moran, L. Radom, *J. Phys. Chem. A*, **111**, 11683 (2007).
26. M. H. Jamróz, Vibrational Energy Distribution Analysis VEDA 4, Drug Institute, Warsaw, 2004.

27. R. Ma, D. Yuan, M. Chen, M. Zhou, *J. Phys. Chem. A*, **113**, 1250 (2009).
28. M. Tonogaki, T. Kawata, S. Ohba, Y. Iwata, I. Shibuya, *Acta Cryst. B*, **49**, 1031 (1993).
29. J. Trotter, C. S. Williston, *Acta Cryst.*, **21**, 285 (1966).
30. B. Stamboliyska, *Bulg. Chem. Commun.*, **37**, 289 (2005).
31. I. N. Juchnovski, I. Binev, *Chem. Phys. Lett.*, **12**, 40 (1971).
32. G. Andreev, B. Stamboliyska, P. Penchev, *Spectrchim. Acta A*, **53**, 811 (1997).
33. G. Andreev, B. Schrader, H. Takahashi, D. Bougeard, I. Juchnovski, *Can. J. Spectrosc.*, **29**, 139 (1997).
34. I. Juchnovski, G. Andreev, *Compt. Rend. Acad. Bulg. Sci.*, **30**, 1021 (1977).

ОХАРАКТЕРИЗИРАНЕ НА СТРУКТУРАТА, ЕЛЕКТРОННОТО СПРЕЖЕНИЕ И ВИБРАЦИОННИТЕ СПЕКТРИ НА РАДИКАЛ-АНИОНИТЕ НА p- И m-ДИНИТРОБЕНЗЕН: ТЕОРЕТИЧНО ИЗСЛЕДВАНЕ

Д. Я. Янчева

Лаборатория „Структурен органичен анализ“, Институт по органична химия с център по фитохимия, Българска академия на науките, ул. „Акад. Г. Бончев“, бл. 9, 1113 София

(Резюме)

Структурата, разпределението на заряда и електронното спрежение между функционалните групи, съпътстващи превръщането на два основни нитробензена (p- и m-динитробензен) в съответните радикал-аниони, бяха изследвани чрез B3LYP/6-311++G** пресмятания. Вибрационните спектри на неутралните съединения и радикал-анионите, които са тясно свързани с промените в пространствената и електронната структура, също бяха изследвани и дискутирани. Засиленото вибрационно взаимодействие между нитро групите в радикал-анионните производни беше описано въз основа на анализ на силовото поле и понижение на ИЧ честотите при превръщането в радикали. Анализът на електронната плътност показа, че и в двата случая нитро групите носят равни части от допълнителния електрон: 0.36 e⁻ при p-динитробензена и 0.29 e⁻ при m-изомера. Радикал-анионите се характеризират с хиноидна структура, както и с по-силно електронното спрежение от неутралните съединения, което обхваща по-голяма част от молекулата.

Some limitations using optical sensors for determination of dissolved oxygen in wine

J. Ts. Zaharieva, M. M. Milanova, D. S. Todorovsky[*]

Faculty of Chemistry, University of Sofia, 1, J. Bourchier Blvd., Sofia 1164, Bulgaria

Ru(II)-tris (4,7-diphenyl-1,10-phenanthroline) dichloride immobilized in matrices from sol-gel produced SiO_2, SiO_2-citric acid/ethylene glycol polyester hybrid or poly (methylmetacrylate) is explored as a sensor for determination of dissolved oxygen in white and red wines. The significant overlapping of the 612 nm spectral bands of the oxygen-sensitive chromophore with the analyzed products band imposes the necessity of accounting for the impact of the latter in the analysis. The SiO_2-based composite is rather sensitive to the prolonged action of wine causing a disturbance of the linearity of the Stren-Volmer dependence and significant decrease of the respective constant.

Key words: optical oxygen sensors, wine, Ru(II) complexes, immobilization matrices, Stern-Volmer constant, fluorescence microscopy.

INTRODUCTION

The control of the dissolved oxygen content is of primary importance for optimal processing of a number of fermentation processes in food industry. Few parameters responsible for beer quality (alcohol concentration, colloid stability, taste) as well as technological losses are determined by the oxygen content during and after fermentation. What is more, both low and high concentrations of oxygen are damaging. Optical oxygen sensors based on the quenching of the luminescence of Ru(II)-tris (4,7-diphenyl-1,10-phenanthroline) dichloride (Rudpp) immobilized in sol-gel prepared SiO_2 can be successfully used for monitoring oxygen concentration in the product [1].

Oxygen content is of crucial importance for the quality of wine. It has to be minimal and constant. In the excess of oxygen, color darkening, microflora propagation, flavor loss, and accelerated aging are observed. In the same time, especially red wine needs some amount of oxygen in the course of the fermentation. The increased oxygen content is necessary when H_2S is formed in the new wine and at appearance of an unsavoury tannin taste immediately after fermentation. In such a case, however, the oxygen concentration must not increase after bottling. The oxygen content has to be known for the precise dosage of the necessary H_2SO_3.

It is accepted that the optimal oxygen content in the wine at the moment of bottling has to be 0.2–0.6 or, at least, <1 mg/l, ensuring complete and optimal fermentation, good stability and optimal "fragrance profile" of the white and rose wines, stable color of the red ones, low content of the antioxidant H_2SO_3 [2]. A review of the role of the dissolved oxygen in wine production is presented in [3].

Along with the electrochemical sensors, optical sensors for determination of the oxygen content in wine are already commercially available [4, 5] due to their advantages: no calibration and spare parts are need, no polarization (specific for the electrochemical devices) takes place [2]. The interval of determination is 0.00–20.0 mg/l at a resolution of 0.01 or 0.1 mg/l; precision is ±1 % of the full scale.

Optical oxygen sensing is usually based on collision quenching by molecular oxygen of a fluorophore embedded in a support matrix. The quenching process is described by the Stern-Volmer equation $I_0/I = 1 + K[O_2]$, where I_0 and I are the emission intensities in the absence and presence of oxygen, respectively, $[O_2]$ is the concentration of O_2 and K – the Stern-Volmer quenching constant. Rudpp is, so far, the most often used chromophore due to the sensitivity of its red emission intensity (when irradiated with blue light) to the O_2 – content. The immobilization matrix has to satisfy two contradictory requirements – to ensure strong enough entrapping of the dye and, in the same time, to allow the smaller analyte species to diffuse into the matrix and to interact with the fluorophore. So, the matrix properties are of crucial importance for sensor sensibility, detection limit, calibration stability, areas of application and exploitation life.

* To whom all correspondence should be sent:
E-mail: *nhdt@wmail.chem.uni-sofia.bg*

Apart from some technical data given in the production lists of the respective firms-manufacturers, literature data on the peculiarities of optical oxygen sensing in wines are rather limited. It is reported that Ru- [4] and Pt- [6] compounds are used as oxygen sensitive dyes. HIOXY type of sensor [5] with not-disclosed type of coating is recommended for monitoring oxygen in non-aqueous vapors and solutions. The sensor coating chemistry is described as ideal for use with oils, alcohols and hydrocarbon-based vapors and liquids. Polymerized sol gel coating is used in [6].

The applicability of the optical sensors to such an analytical object as wine is determined, besides the principal requirements to this type of sensors (sensitivity of the signal to the oxygen content, linearity of the Stern-Volmer dependence), by few peculiarities of the system: possible overlapping of the emission of the wine with the fluorescence signal of the optically active dye, rather low optical transparency of the red wines, stability of the complex doped matrix to the action of the analyzed medium. The present paper is a step in elucidating the influence of these factors on the optical measurement of dissolved oxygen in wines.

EXPERIMENTAL

Bottled dry red and white wines were analyzed immediately after the bottle opening.

The analysis were performed with films (deposited by dip-coating) containing Rudpp, immobilized in three types of matrices, consisting of sol-gel produced SiO_2, inorganic-organic hybrid (prepared by the simultaneous hydrolysis of tetraethoxysilane, esterification of the hydrolysed product with citric acid and esterification between the latter and ethylene glycol) and of poly(methylmetacrilate). Methods for production of the films are described in [7-9].

The photoluminescent response of the fabricated films to oxygen in liquids was measured by a Cary Eclipse (Varian) device. Due to the significant optical density of the red wines the spectral measurements were done in 1 mm-cuvette.

The relative mean square deviation of the photoluminescent signal intensity (determined by measuring of 5 parallel water samples containing $7.3.10^{-4}$ % O_2) is 0.5 %. The oxygen-free liquids were prepared by bubbling high-purity N_2 for 90 min through the pre-boiled water put in a closed vessel with a hydraulic gate, and fully oxygenated ones – by bubbling O_2 for 50 min through ice-cold liquid put in the same vessel.

The effect of the soaking of the SiO_2-based films in wine or other aggressive medium was evaluated by their performance in oxygen content measurement in gaseous phase. The photoluminescence response to oxygen was measured by the equipment described in [7] under illumination by blue LEDs with maximum of the spectral output band at 450 nm.

RESULTS AND DISCUSSION

1. Influence of the analyzed sample emission on the spectrum of the sensor film

The spectra of the films made from the above mentioned types of matrices and immersed in the analyzed wines are compared with the spectra of the analyzed samples (Fig. 1) in the spectral region of interest around the maximum in the Rudpp emission spectrum (612 nm).

Table 1. Ratios of the areas of the spectral bands at 612 nm of the wine and of the chromophore immersed in the same wine

Matrix	Wine	Ratio, %
SiO_2	red	13.4
	white	2.2
Hybrid	red	15.8
	white	8.0
PMMA	red	14.1
	white	12.2

Table 1 presents the ratios of the areas of the spectral bands at 612 nm of the wine and of the chromophore immersed in the same wine. The integration is performed in the wavelength interval 550-800 nm. It is seen that the overlapping is lowest for the SiO_2-based matrix due to the higher photoluminescence intensity obtained applying this matrix. The difference with other matrices for the analyzed red wines is <18 %. As can be expected the overlap for white wine is smaller but the differences between the different matrices are much stronger expressed.

2. Some peculiarities of O_2-sensitive films performance in wines

Influence of the film thickness on the fluorescence intensity. Table 2 presents data for the intensity of the main emission band (around 612 nm) of Rudpp immobilized in SiO_2 in few wine samples (with different oxygen content) in dependence of the film withdrawal rate in the course of its preparation. It is seen that with the increase of the film thickness a slight (approx. 5-6 % for samples 1-3) decrease of the fluorescence
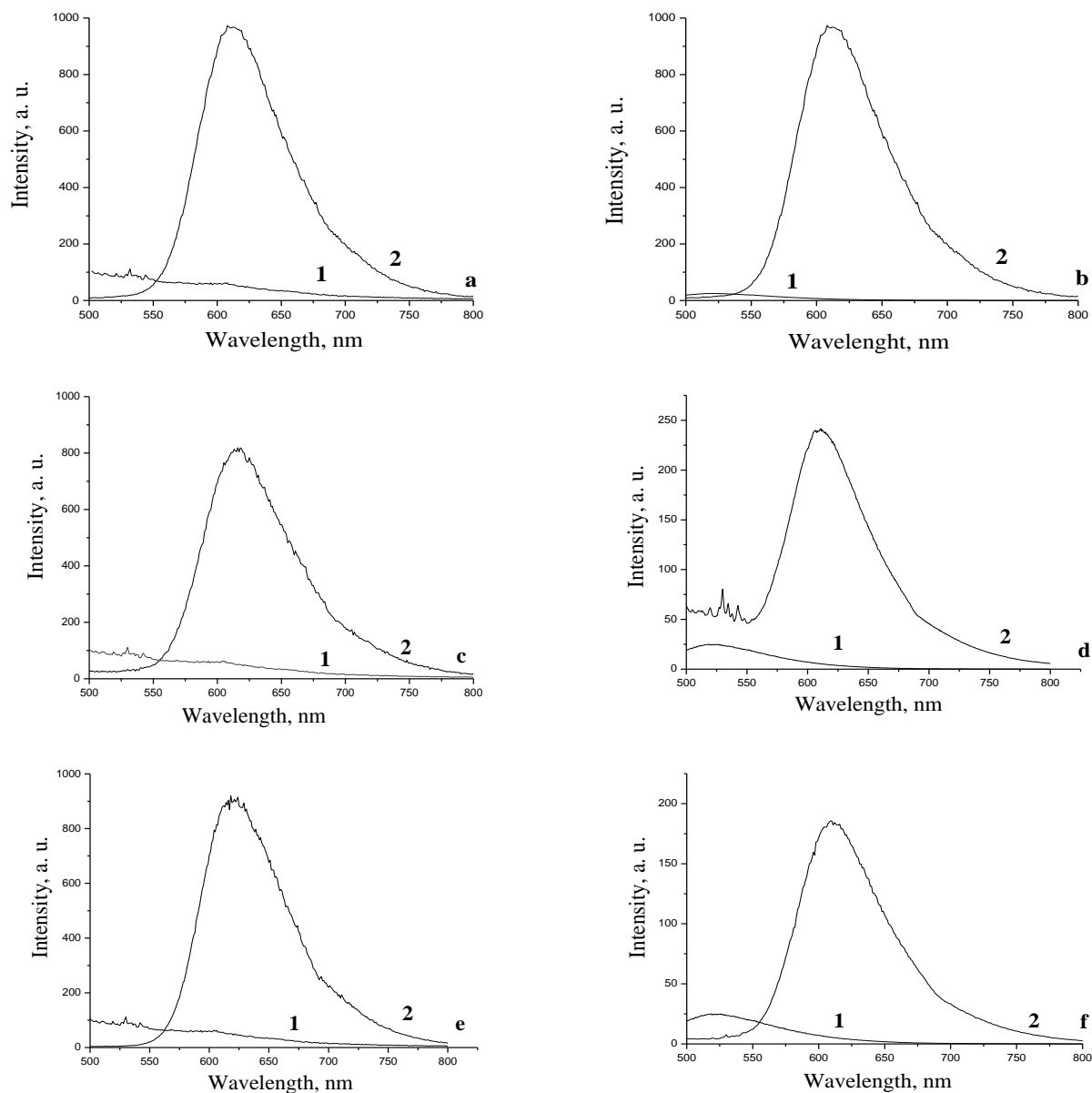
Fig. 1. Emission spectra of analyzed wines (1) and of Rudpp (2) in matrices from SiO_2 (a, b), hybrid (c, d) and from PMMA (e, f) immersed in red (a, c, e) and white (b, d, f) wine.

Table 2. Dependence of intensity (I) of the fluorescence at 612 nm of red wine samples with different oxygen content on the film thickness.

Film withdrawn rate, mm/s	I (arb. units), sample			
	1	2	3	4
0,015	79.5	84.4	95.5	111.5
0,75	76.0	78.8	91.8	99.1
[I(0,015)-I(0,75)]/I(0,015), %	4.4	6.6	5.3	11.1

intensity is registered. In some cases (sample 4) the effect is significant. It has to be mentioned that the data are related to films with rather great difference in the thickness, not commonly occurring in the practice. The typical withdrawal rate used for such films preparation (as well as in the present work) is 0.4 mm/s leading to a thickness of about 300 nm.

In a thicker layer, more chromophore molecules are available. Accounting for the high surface porosity of the dip-coated films (observed in the morphological study [11]) it can be expected that they can be reached by the analyte molecules and the quenching effect will be more pronounced.

(1)   (2)
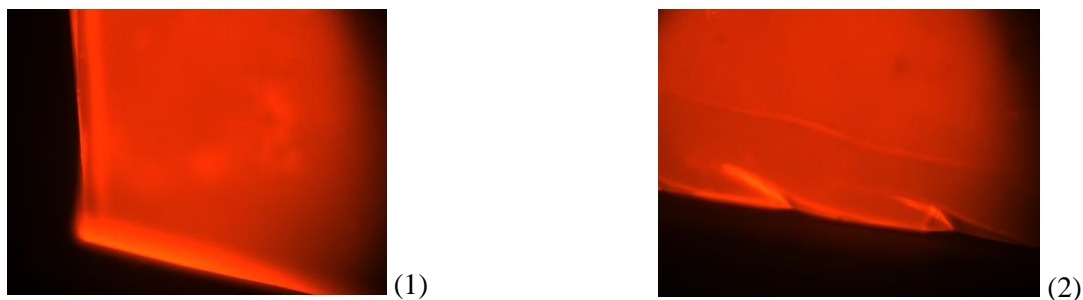
Fig. 2. Fluorescence microscopic images (x160) of Rudpp-SiO$_2$ after 330 h storage at 0 ^{o}C in white (1) and red (2) wine.

Table 3. Stern-Volmer constant (for hybrid matrix) and dissolved oxygen content in wine and distilled water

Sample	Dissolved oxygen content, ppm			Stern-Volmer constant	
	Without treatment	After bubbling with		Value, n.10^{-3} ppm^{-1}	Correlation coefficient*
		O$_2$	N$_2$		
Water	2.24	10.88	1.60	20 [8]	0.982
White wine	2.01	5.87	1.65	15	0.982
Red wine	2.04	5.56	1.46	22	0.979

* Linear fit.

Stern-Volmer relation. The data in Table 3 show that no significant difference exists in the linearity of Stern-Volmer dependence for distilled water and wines and in the values of the Stern-Volmer constant as determined by the O$_2$-sensitive film based on hybrid matrix [8]. So, it can be expected that the sensitivity of the determination of O$_2$ dissolved in wines will be of the same order as in distilled water.

Content of dissolved oxygen in wine. The data from the analysis of the oxygen content in red and white wine (as supplied or after bubbling for 1 h with O$_2$ or N$_2$) are compared with parallel analysis of distilled water treated in the same way (Table 3). The measurements are performed by the hybrid-based matrix [8]. The results show oxygen concentration in the analyzed samples (~2 mg/kg), approx. 2 times higher than the admissible one. As far as no special precautions are taken, the increased content may be due to the oxygen enrichment of the sample during the measurement. It is found that bubbling with N$_2$ leads to an oxygen concentration decrease with ~25 %. It seems that oxygen saturation of the studied wine samples at ambient temperature is reached at 5.5-6 mg/kg, i.e. the oxygen solubility in these types of wine is approximately twice lower than in water at the same temperature. It could be supposed that salting out action of species dissolved in wine is (at least, partially) responsible for this effect.

3. Stability of the Rudpp-SiO$_2$ composite on the wine action

The test was carried out by soaking of the studied films in red and white wine, stored at ~5 ºC (to avoid fermentation) for 384 h and compared with the effect of dilute HCl. The effect is evaluated through the influence on the value of the Stern-Volmer quenching constant Ksv. The value of Ksv determines the sensitivity and the detection limit of the analytical method. The data in Table 4 (see also [10]) show that the effect of the wine is much stronger than that of a hydrochloric solution with similar pH at higher temperature (the difference between the later and the value for fresh film is within the errors limit). The reasons for this strong effect are to be elucidated.

Table 4. Influence of the storage (384 h) in acidic media on the Stern-Volmer constant (Ksv, gaseous phase) of Rudpp-SiO$_2$ films

Aggressive medium	Correlation coefficient	Ksv.10^{-3} %$^{-1}$
Fresh film	0.994	28.3
HCl, pH 4.0, 21 ºC	0.914	30.9
Red wine, pH 3.6, ~5 ºC	0.982	2.5
White wine, pH 3.6, ~5 ºC	0.994	2.4

The fluorescence microscopy reveals some disruption of the sensor membranes surface after soaking in wine. The spots with paler color (Fig. 2) suggest some leakage of the chromophore. Such defects can explain the disturbance of the linearity of the Stern-Volmer dependence seen on Fig. 3 and the decrease of the correlation coefficients for linear fit of the experimental data (Table 4). It is known that surface non-homogeneity of the optically active film is one of the main reasons for the non-linearity of the dependence and the low value of the Stern-Volmer constant [7].
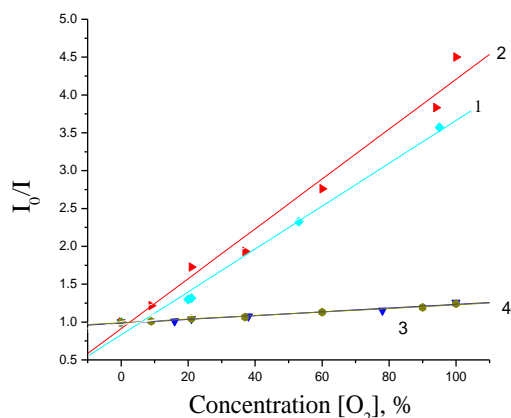
Fig.3. Stern-Volmer dependence (gaseous phase) of Rudpp-SiO$_2$ films: initial film (1), the same after storage for 384 h in HCl, pH=4, 21 ^{0}C (2), red (3) and white (4) wine (~5 ^{o}C).

CONCLUSION

The reported results lead to the following conclusions:

Microcomposites based on Ru(II)-tris(4,7-diphenyl-1,10-phenantroline) immobilized in matrices of sol-gel produced SiO$_2$, SiO$_2$-citric acid/ethylene glycol polyester and poly(methylmetacrylate) can be used for determination of oxygen dissolved in white and red wines. The significant overlapping of the spectral bands of the analyzed product and of the oxygen-sensitive chromophore imposes the necessity of accounting for the impact of the sample own emission in the analysis, i.e., the calibration of the sensor should be made in the same wine with controllable oxygen content. The use of SiO$_2$-based matrix is advantageous from this point of view because of smaller overlapping.

The value of the Stern-Volmer constant for the hybrid film immersed in wine is of the same order as for distilled water.

The SiO$_2$-based microcomposite described in this work is not suitable for continued measurement of oxygen in wine due to the relatively fast worsening of its functional properties under the action of the analyzed medium. Further evaluation of the applicability of the hybrid matrix from this point of view has to be done.

REFERENCES

1 S. Anastasova, M. Milanova, D. Todorovsky, *J. Biochem. Biophys. Methods*, **70,** 1292 (2008).
2 P. Pütz, http://www.aguaafrica.co.za/PDF/ HQd. pdf.
3 W. J. du Toit, J. Marais, I. S. Pretorius, M. S. du Toit, *Afr. J. Enol. Vitic.* **27,** 76 (2006).
4 http://www.shop.spectrecology.com.
5 http://www.aguaafrica.co.za/PDF/HQd.pdf.
6 M. R. Shahriari, Method and composition for a platinum embedded sol gel optical chemical sensor with improved sensitivity and chemical stability. Publication date 08/21/2008 Patent application number: 20080199360.
7 S. Anastasova,. M. Milanova, S. Rangelov, D. Todorovsky, *J. Non-Crystalline Solids,* **354**, 4909 (2008).
8 J. Zaharieva, M. Milanova, D. Todorovsky, *J. Mater. Chem.* **21**, 4893 (2011).
9 J. Zaharieva, M. Milanova, D. Todorovsky, *Appl. Surface Sci.* **257**, 6858 (2011).
10 S. Anastasova, M. Milanova, J. Zaharieva, D. Todorovsky, *Bulg. Chem. Ind*. **80**, 28 (2009).
11 S. Anastasova, M. Milanova, E. Kashchieva, H. Funakubo, T. Kamo, N. Grozev, P. Stefanov, D.Todorovsky, *Appl. Surf. Sci*. **254**, 1545 (2008).

НЯКОИ ОГРАНИЧЕНИЯ ПРИ ИЗПОЛЗВАНЕ НА ОПТИЧНИ СЕНЗОРИ ЗА ОПРЕДЕЛЯНЕ НА РАЗТВОРЕН ВЪВ ВИНО КИСЛОРОД

Й. Цв. Захариева, М. М. Миланова, Д. Ст. Тодоровски

*Факултет по химия и фармация, Софийски университет, бул. Дж Баучер 1,
София 1164, България*

(Резюме)

Ru(II)-трис(4,7-дифенил-1,10-фенантролин) дихрорид, имобилизиран в матрици от SiO$_2$, хибрид, състоящ се от SiO$_2$ и полиестер на лимонена киселина с етилен гликол или от поли(метилметакрилат) е изследван като сензор за определяне на кислород, разтворен в бели и червени вина. Значителното припокриване на спектралната ивица при 612 nm на кислородно-чувствителния хромофор със собствената ивица на анализирания продукт налага необходимост от отчитане на влиянието на последната при анализа. Композитът, базиран на SiO$_2$ е твърде чувствителен към продължително действие на виното, което води до нарушаване на линейността на зависимостта на Stren-Volmer и значително намаляване на стойността на константата на Stren-Volmer.

Reverse phase extraction chromatography of rhodium(III) with N-n-octylaniline

S. J. Kokate, S.R. Kuchekar*

P. G. Department of Analytical Chemistry, A. C. S. College, Satral, At Satral, Tal. Rahuri, Dist. Ahmednagar,

MS, India, 413 711

Novel separation methods are developed for the extraction of rhodium(III) from aqueous chloride media with N-n-octylaniline (liquid anion exchanger) coated on silica gel. Rhodium(III) was quantitatively extracted from 0.1 mol/L hydrochloric acid, eluted with 1.0 mol/L hydrochloric acid and determined by spectrophotometrically. Different parameters, *viz.* effect of hydrochloric acid concentrations, N-n-octylaniline concentrations and flow rates of mobile phase were studied. The method was applied for separation of rhodium(III) from synthetic mixtures corresponding to alloys. It was free from interferences from a number of cations and anions. A separation scheme was developed for the mutual separation of rhodium(III), platinum(IV) and gold(III). The nature of the extracted species, ascertained by the log-log plot of N-n-octylaniline concentration *versus* distribution ratio, indicates that the probable extracted species is $[(RR'NH_2^+)_3 . RhCl_6^{3-}]$.

Key words: Extraction chromatography, rhodium(III), separation, alloys

1. INTRODUCTION

The abundance of rhodium in the earth crust is only 0.001 ppb [1]. It has a wide range of applications in the production of alloys, optical instruments and jewelry. Recently it has been employed in automobile catalytic converters as a monitor to control NO_x emission [2]. Rhodium has a low abundance, high price and wide range of applications; hence the development of an innovative method for its separation would be of analytical merit.

Rhodium was separated from palladium by a reverse phase extraction chromatographic method using Bu_3PO_4 as a stationary phase [3], however, this method requires high concentration of mineral acid for the extraction. A column packed with silica treated with tri-n-octylammonium salt [4] was used for separation of platinum(IV), palladium(II), iridium(IV) and rhodium(IV) using hydrochloric and nitric acid media. The method requires high concentrations of mineral acids for the extraction and elution of the metals and it takes 2 hr. Extraction chromatography of platinum metals was carried out using Bu_3PO_4 coated on VAPEX [5]; the method requires high concentrations of mineral acids for the extraction. An alkylated 8-hydroxyquinoline extractant (Kelex 100) [6] was used for separation of rhodium chlorocomplexes by the supported liquid membrane technique. Rhodium

was extracted as rhodium chloride and was separated from palladium and platinum with trioctylamine or aliquat 336 in toluene [7]. The metal was stripped with concentrated hydrochloric acid. N, N'-dimethyl-N, N'-diphenyltetradecyl-malonamide [8] was used for the solvent extraction of rhodium. The metal was stripped by a mixture of 4.0 mol/L hydrochloric acid in presence of 0.05 mol/L sodium hypochlorite. Alamine 336 in kerosene was used for the selective separation of iridium(III), ruthenium(III) and rhodium(III) from chloride media [9]. Cyanex 923 [10] was used for the extraction separation of iridium(III) and rhodium(III) from 5.0 to 8.0 mol/L hydrochloric acid media; the method was applied to the metal recovery from a synthetic solution corresponding to a spent catalyst. Rhodium(III) was extracted in acidic medium with bis-(2-ethylhexyl) phosphoric acid [11]; the method was used for the separation of some noble metals but it requires 4.0 mol/L hydrochloric acid for stripping. N-n-octylaniline and n-octylaniline were used for the extraction separation of zinc(II), cadmium(II), mercury(II) [12], copper(II), silver(I), gold(III) [13], gallium(III), indium(III), and thallium(III) [14]. N-octylaniline was also used for the extraction column chromatographic separation of gallium(III), indium(III) and thallium(III) [15]. Recently methods were developed for the extraction chromatographic separation of platinum(IV) [16], palladium(II) [17], ruthenium(III) [18], iridium(III) [19], molybdenum(VI) [20], manganese(II) [21],

---

* To whom all correspondence should be sent:
 e-mail: shashi17@gmail.com

copper(II) [22], bismuth(III) [23], and gold(III) [24] using N-n-octylaniline as a stationary phase.

The present work deals with the extraction chromatographic separation of rhodium(III) from aqueous chloride media with N-n-octylaniline (liquid anion exchanger) coated on silica gel. Rhodium(III) was quantitatively extracted from 0.10 mol/L hydrochloric acid, eluted with 1.0 mol/L hydrochloric acid and was determined spectrophotometrically [25]. The method was applied to the separation of rhodium(III) from binary mixtures and synthetic mixtures corresponding to alloys. Mutual separation scheme was developed for separation of rhodium(III), platinum(IV) and gold(III).

2. EXPERIMENTAL

Apparatus

An Elico digital spectrophotometer model SL-159 with 1-cm quartz cells was used for the absorbance measurements. The pH measurements were carried out on an Elico digital pH meter model LI-120.

Reagents

Rhodium(III) solution. A standard stock solution of rhodium(III) was prepared by dissolving 1.0 g of rhodium trichloride (Loba Chemie) in 1.0 mol/L hydrochloric acid and diluting to 250 mL with distilled water. The solution was standardized gravimetrically [26]. A working solution containing 25 μg of rhodium(III) was made by diluting the stock solution with distilled water. The N-n-octylaniline solution was prepared using a method reported by Gardlund [27]. The stock solution of N-n-octylaniline was prepared in chloroform. Standard solutions of different metal ions were prepared by dissolving the corresponding salt with distilled water and dilute hydrochloric acid. All other chemicals used were of A.R. grade.

Preparation of anion exchange material

The preparation of silaned silica gel was described earlier [16]. A portion (5.0 g) of silaned silica gel was soaked in 5.0% (v/v) N-n-octylaniline previously equilibrated with hydrochloric acid (0.10 mol/L) for 10 min. The solvent was evaporated almost to dryness. The slurry of N-n-octylaniline coated silica gel was prepared in distilled water by centrifugation at 2000 r/min. This slurry was packed in the chromatographic column to give a bed height of 6.0 cm. The bed was covered with a glass wool plug.

General procedure for extraction of rhodium(III)

An aliquot of a solution containing 25.0 μg of rhodium(III) was made up to 25.0 mL by adjusting the concentration of hydrochloric acid to 0.10 mol/L. This solution was passed through the column containing silica coated with 5.0% (v/v) N-n-octylaniline with a flow rate of 0.5 mL/min. After extraction, rhodium(III) was eluted with 25.0 mL of 1.0 mol/L hydrochloric acid. The solution was evaporated to a moist residue. The latter was dissolved in a minimum amount of 1.0 mol/L hydrochloric acid and rhodium(III) was determined by a spectrophotometric method [25].

3. RESULTS AND DISCUSSION

Effect of hydrochloric acid concentration

An amount of 25 μg of rhodium(III) in 25 mL aqueous solution was extracted by varying the acid concentration from 0.05 to 0.25 mol/L hydrochloric acid with 5.0% N-n-octylaniline on silica gel as the stationary phase. The percent extraction of rhodium(III) initially increases, becomes quantitative at 0.1 mol/L hydrochloric acid and then it decreases (Fig. 1).
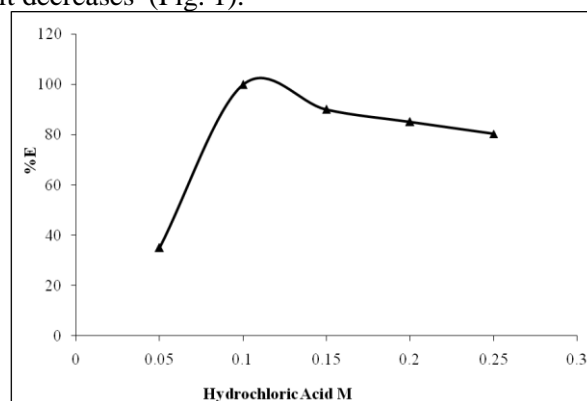
Fig .1. Extraction behavior of rhodium(III) as a function of hydrochloric acid concentration.

Effect of flow rate

The effect of flow rate on the percent extraction of rhodium(III) was studied in the range from 0.5 mL/min to 3.0 mL/min. It was observed that the increase in flow rate was inversely proportional to the percent extraction. Optimum extraction was observed at flow rates from 0.5 to 1.0 mL/min.

Effect of N-n-octylaniline concentration

The effect of different concentrations (1.0 to 5.0%) of N-n-octylaniline on the extraction of rhodium(III) over hydrochloric acid concentrations in the range from 0.05 to 0.25 mol/L was studied. Extraction of rhodium(III) was quantitative with

5.0% of N-n-octylaniline in 0.10 mol/L hydrochloric acid medium. The extraction of rhodium(III) increases with an increase in the concentration of N-n-octylaniline. The nature of the extracted species was determined by a log-log plot of the distribution coefficient *versus* N-n-octylaniline concentration at 0.05 and 0.15 mol/L hydrochloric acid, which gave a slope of 2.58 and 2.67, respectively (Fig. 2). This indicated that the metal-to-amine ratio in the extracted species is 1:3 and the probable extracted species is $[(RR'NH_2^+)_3 . RhCl^{3-}_6]$. The extraction mechanism can be explained as follows:

$$[RR'NH]_{org} + HCl_{aq} \rightleftharpoons [RR'NH_2^+ . Cl^-]_{org} \quad (1)$$

$$3[RR'NH_2^+ . Cl^-]_{org} + RhCl^{3-}_6 \rightleftharpoons$$
$$[(RR'NH_2^+)_3 . RhCl^{3-}_6] + 3Cl^- \quad (2)$$
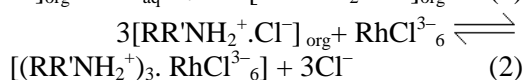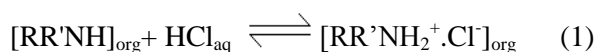
where R= $-C_6H_5$ R'= $-CH_2(CH_2)_6CH_3$.

Effect of the eluting agent

It was evident from the data that all acid eluents employed in the present investigation were effective and the optimum elution of rhodium(III) was in the concentration range 1.0 to 4.0 mol/L (hydrochloric, nitric, sulphuric, hydrobromic and perchloric acids), Table 1. Water elutes only 45% of rhodium(III). In the actual process 1.0 mol/L hydrochloric acid was used for elution of rhodium(III).

Fig. 2. Log-log plot of the distribution ratio *versus* N-n-octylaniline concentration at 0.05 mol/L and 0.15 mol/L hydrochloric acid.

Effect of foreign ions

The extraction of rhodium(III) in presence of cations and anions was carried out according to the recommended procedure to examine the interferences. The tolerance limit was set at the amount required to cause $\pm$ 2% error in the recovery of rhodium(III), Table 2. Interferences only from thiocyanate and tartrate anions are registered.

Table 1. Effect of eluting agents: rhodium(III) 25 µg; stationary phase 5.0% N-n-octylaniline.

Molarity (mol/L)	HCl Recovery (%)	HNO$_3$ Recovery (%)	H$_2$SO$_4$ Recovery (%)	HBr Recovery (%)	HClO$_4$ Recovery (%)
0.5	89.0	91.0	87.0	90.2	92.0
1.0	99.8	99.7	99.8	99.7	99.8
2.0	99.8	99.7	99.8	99.7	99.8
3.0	99.8	99.7	99.8	99.6	99.8
4.0	99.8	99.7	99.8	99.6	99.8

Statistical analysis of the results for rhodium(III)

Statistical analysis was carried out for interpretation of the results. The magnitudes of mean, median, average deviation, average deviation of mean, standard deviation, standard deviation of mean and coefficient of variation were determined. The values obtained indicated that the proposed method offers reproducible results, Table 3.

4. APPLICATIONS

Analysis of synthetic mixtures corresponding to alloys and to a catalyst

The validity of the method was verified by applying the proposed method for extraction of rhodium(III) from synthetic mixtures corresponding to alloys and to a catalyst. The compositions were laboratory-prepared for iridium alloy, jewelry alloy, neuyanskite alloy, osmiridium alloy, platinum-rhodium thermocouple wire and platinum-palladium-rhodium catalyst and were

Table 2. Effect of foreign ions: rhodium(III) 25 μg; stationary phase 5.0% N-n-octylaniline; mobile phase 1.0 mol/L HCl

Foreign Ion	Added as	Tolerance limit, μg	Foreign Ion	Added as	Tolerance limit, μg
Mo(VI)	$(NH_4)_6 MO_2O_{24}$	200	Iodide	KI	1000
Cr(VI)	$K_2Cr_2O_7$	200	Fluoride	NaF	1000
Al(III)	$AlCl_3$	200	Bromide	KBr	1000
Cd(II)	$CdCl_2. 2H_2O$	100	Malonate	$CH_2(COONa)_2$	1000
Sn(II)	$SnCl_2.2H_2O$	100	Succinate	$(CH_2COONa)_2.6H_2O$	1000
Zn(II)	$ZnSO_4.7H_2O$	100	Persulfate	$K_2S_2O_8$	1000
V(V)	V_2O_5	100	Oxalate	$(COOH)_2.2H_2O$	1000
U(VI)	$UO_2(NO_3)_2.6H_2O$	100	Salicylate	HOC_6H_4COONa	1000
Ca(II)	$CaCl_2.2H_2O$	250	Au(III)	$HAuClO_4.H_2O$	100
Ni(II)	$NiCl_2.6H_2O$	200	Ag(I)	$AgNO_3$	50
Ti(IV)	TiO_2	200	Ir(III)	$IrCl_3.xH_2O$	100
Mg(II)	$MgCl_2.6H_2O$	400	Ru(III)	$RuCl_3.xH_2O$	100
Cu(II)	$CuSO_4.5H_2O$	400	Pt(IV)	H_2PtCl_6	100
Pb(II)	$Pb(NO_3)_2$	400	Os(VIII)	OSO_4	100
Fe(II)	$FeSO_4.7H_2O$	400	Pd(II)	$PdCl_2.xH_2O$	100
Hg(II)	$HgCl_2$	50			

Table 3. Statistical analysis of the results: rhodium(III) added 25.0 μg

Amount Found [μg]	Difference	(Difference)^2	Results
25.02	0.00	0.0000	M = 25.02
25.06	0.04	0.0016	M =25.02
24.98	-0.04	0.0016	d =0.0014
24.97	-0.05	0.0025	D =0.0005
25.11	0.09	0.0081	s =0.0508
24.98	-0.04	0.0016	S =0.019
25.03	0.01	0.0001	C.V =0.20%

analyzed by the proposed method. The results of the analysis reveal the good agreement between the added and the found values, Table 4.

Mutual separation of rhodium(III), platinum(IV) and gold(III)

The separation of rhodium(III), platinum(IV) and gold(III) from one another was carried out by quantitatively extracting platinum(IV) from 0.015 mol/L ascorbic acid, pH 1.0 using 1.5% N-n-octylaniline coated on silica gel. Rhodium (III) and gold (III) remained in the aqueous phase. The extracted platinum (IV) was eluted with a 20 mL portion of distilled water from the column and was determined by a spectrophotometric method [25]. The aqueous phase containing rhodium(III) and gold(III) was evaporated almost to dryness; after addition of water the solution was adjusted to 0.10 mol/L hydrochloric acid and was passed through the column containing silica coated with 5.0% N-n-octylaniline at a flow rate of 0.5 mL/min. After extraction, rhodium(III) was eluted with 25.0 mL of 1.0 mol/L hydrochloric acid. The eluted fraction was evaporated almost to dryness and rhodium(III) was determined using a spectrophotometric method. The aqueous phase containing gold(III) was evaporated almost to dryness and gold(III) was determined by a spectrophotometric method [25]. The results of the analysis are presented in Table 5.

Table 4. Analysis of synthetic mixtures corresponding to alloys and catalyst: stationary phase 5.0% N-n-octylaniline; mobile phase 1.0 mol/L HCl. *Average of three determinations.

Alloy composition (μg)	Rhodium added equivalent to(μg)	Rhodium found (μg)*	E (%)	Relative error (%)
Iridium alloy [Rh 7.0; Pd 3.5; Cu 8.01; Pt 55.51; Fe 3.51; Ir 28.01]	100	99.6	99.6	0.40
Jewelry alloy [Rh 1.0; Ru 4.0; Pd 95.0]	50	49.9	99.8	0.20
Neuyanskite alloy [Rh 100; Os 650; Pt, 400; Ru 50; Ir 3100]	100	99.6	99.6	0.40
Osmiridium alloy [Rh 110; Os 325; Pt 100, Ru 80; Ir 450; Au 10]	100	99.7	99.7	0.30
Pt-Rh wire [Rh 13; Pt 87]	50	49.9	99.8	0.20
Pt-Pd-Rh catalyst [Rh 0.005-0.05; Pd 0.03-0.15; Pt 0.03-0.20]	25	24.9	99.7	0.30

Table 5. Mutual separation of rhodium(III), platinum(IV) and gold(III).

Metal ion	Amount added (μg)	Amount found[*] (μg)	Chromogenic ligand	E (%)	RSD[**] (%)
Pt(IV)	50	49.90	$SnCl_2$	99.8	0.20
Rh(III)	25	24.92	$SnCl_2$+KI	99.7	0.30
Au(III)	100	99.80	$SnCl_2$	99.8	0.20

*Average of three determinations.

**RSD (%) = (amount added – amount found/ amount added) × 100.

4. CONCLUSIONS

The method permits the mutual separation of rhodium(III), platinum(IV) and gold(III). The reliability of the method is verified by analyzing a synthetic mixture corresponding to various alloys and a catalyst. The method is free from interference by a large number of cations and anions. It is simple, rapid and reproducible.

REFERENCES

1 C. A. Hampel, Rare Metals Handbook, Robert E. Krieger Publishing Co Inc, Huntington, NY, 2nd Ed. 1971, 305.

2 http://en.wikipedia.org/wiki/Rhodium

3 C. Pohlandt, T. W. Steele, *Talanta*, **19,** 839 (1971).

4 S. Przeszlakowski, A. Flieger, *Talanta*, **28,** 557 (1981).

5 V. Frantisk, V. Alena, *Analytica Chemie*, **10,** 67 (1974).

6 S.N. Ashrafizadeh, G. P. George, *Sep. Sci. Technol.*, **31,** 895 (1996).

7 G. Levitin, G. Schmuckler, *Reactive and Functional Polymers*, **54,** 149 (2003).

8 P. Malik, A. Paiva, *Solvent Extr. Ion Exch.,* **26,** 25 (2008).

9 E. Goralska, M. T. Coll, A. Fortuny, C. S. Kedari, A. M. Sastre, *Solvent Extr. Ion Exch.*, **25,** 65 (2007).

10 D.V. Chavan, P. M. Dhadke, *J. Chem. Technol. Biotech.*, **77,** 925 (2002).

11 V. Sherikar, P.M. Dhadke, *Rhodium Express,* **15,** 4 (1996).

12 H.R. Aher, S.R. Kuchekar, *Asian J. Chem.*, **16,** 695 (2004).

13 H.R. Aher, S.R. Kuchekar, *Intern. J. Chem.*, **4,** 157 (2006).

14 H.R. Aher, S.R. Kuchekar, *Chem. Envi. Research*, **15,** 161 (2006).

15 H.R. Aher, S.R. Kuchekar, *Ind. J. Chem. Technol.*, **15,** 403 (2008).

16 S.J. Kokate, S.R. Kuchekar, *Chinese J. Chromatogr.*, **27,** 809 (2009) 809.

17 S.J. Kokate, H.R. Aher, S.R. Kuchekar, *Bulg. Chem. Comm.*, **41,** 272 (2009).

18 S.J. Kokate, H.R. Aher, S.R. Kuchekar, *J. Saudi Chem. Soc.*, **14,** 41 (2010).

19 S.J. Kokate, H.R. Aher, S.R. Kuchekar, *Anal. Chem. An Indian J.*, **8,** 575 (2009).

20 S.J. Kokate, A.A. Gavande, V.K. Vikhe, H.R. Aher, S.R. Kuchekar, *Ind. J. Chem. Technol.*, **17,** 154 (2010).

21 S.R. Phule, Y.S. Shelar, S.R. Kuchekar, *Anal. Chem. An Indian J.*, **9,** 260 (2010).

22 S. R. Phule, S. J. Kokate, S. R. Kuchekar, *J. Saudi Chem. Soc.*, **15,** 209 (2011).

23 S.R. Phule, H.R. Aher, S.P. Lawande, S.R. Kuchekar, *Chemistry for Sustainable Development, Springer,* 209 (2012).

24 S. Kokate, H. Aher, S. Kuchekar, *Bulg. Chem. Comm.*, **43,** 406 (2011).

25 E.B. Sandell, Colorimetric Determination of Traces of Metals. B. L. Clarke, P. J. Elving, I. M Kolthoff, Interscience Publishers, New York 3rd Ed., 1965.

26 F.E. Beamish, J.C. Van Loon, Analysis of Noble Metals: Overview and Selected Methods, Academic Press, London, (1977) 142.

27 Z.C. Gardlund, R.J. Curtis, G.W. Smith, *Liquid Crystals and Ordered Fluids*, **2,** 541 (1973).

ОБРАТНОФАЗОВА ЕКСТРАКЦИОННА ХРОМАТОГРАФИЯ НА РОДИЙ(III) С N-N-ОКТИЛАНИЛИН

С. Дж. Кокате, С. Р. Кучекар

Департамент "Аналитична химия", П.В.П. Колеж, Праваранагар, Лони, Рахата, окр. Ахмеднагар, МС, 413 713 Индия

(Резюме)

Предложен е нов метод за екстракционно разделяне на родий(III) от солнокисели разтвори с N-n-октиламин (течен йонообменник), нанесен върху силициев оксид. Родий(III) се екстрахира количествено из 0.1 mol/L солна киселина, елуира се с 1.0 mol/L солна киселина и се определя спектрофотометрично. Изследвано е влиянието на концентрацията на солната киселина и N-n-октиламина, както и скоростта на мобилната фаза. Методът е приложен за разделяне на родий(III) от синтетични смеси, съответстващи на различни сплави. Установено е, че голям брой катиони и аниони не пречат. Разработена е схема за разделянето на родий(III), платина(IV) и злато(III) един от друг. От двойнологаритмичната зависимост между концентрацията на N-n-октиламина и коефициента на разпределение е установено, че вероятният състав на екстрахираната форма е $[(RR'NH_2^+)_3 . RhCl_6^{3-}]$.

Properties of nickel (II) doped silica xerogels

N. Avramova[a] and I. Avramov*[b]

[a] *University of Sofia, Faculty of Chemistry, Department of Applied Organic Chemistry, 1166 Sofia, Bulgaria*
[b] *Institute of Physical Chemistry, Bulgarian Academy of Science, 1113 Sofia, Bulgaria,*

Silica xerogels doped with varying content of Ni^{2+} are prepared using a sol–gel method based on acid-catalyzed hydrolyzation of tetraethylorthosilicate (TEOS) and gelation at 50 ^{o}C. The samples are investigated by differential scanning calorimetry, DSC, thermo gravimetry, TG and X-ray diffraction. Detailed thermal analyses up to 500 ^{o}C demonstrate a strong effect of the Ni content on the crystallization behavior of doped xerogels. A sharp endotherm of dehydration is observed in the vicinity of 150 ^{o}C. The activation energy related to this endotherm is evaluated to $E_a = 80$ [kJ/mol]. Additional two endotherms are observed depending on both Ni amount and heating rate.

INTRODUCTION

Nanostructured materials are of increasing interest because of their physical properties and technological applications. Mechanical, thermal, optical, electrical, magnetic and catalytic properties are size-dependent and diverse for nano and bulk materials [1–3]. A number of works is focused on new methods of synthesis of NiO nanoparticles [4–7]. They have been prepared by decomposition of nickel hydroxide [2,5], by decomposition of nickel acetate [6], or by oxidation of Ni nanoparticles [7]. Crystalline NiO is obtained by decomposition of nickel (II) nitrate hexahydrate through pyrolysis of its aerosol nitrate [8].

The sol-gel process is a method for synthesizing new materials [9-17]. Sol-gel chemistry offers possibility for preparation of transparent ceramic materials like xerogels. The sol-gel incorporation of high amounts of rare-earth ions using tetraethoxysilan (TEOS) and nitrate solutions of rare earth ions was recently described [9–20]. The monoliths obtained in our recent papers display interesting optical properties [17,18]. In our previous paper [21] we described for the first time, in detail, the thermal behaviour of Sm^{3+} doped silica xerogels. Strong influence of Sm content on the thermal properties of xerogels was demonstrated. Two different activation energies related to dehydration and chemical decomposition of $Sm(NO_3)_3 \cdot 6H_2O$ were evaluated: $E_a = 38$ kJ/mol, and $E_a = 210$ kJ/mol [18]. The aim of this study is to investigate thermal behavior of nickel (II) doped silica xerogels.

EXPERIMENTAL

Xerogels doped with Ni(II) were prepared at room temperature by acid-catalyzed hydrolyzation of tetraethylorthosilicate (TEOS), dissolved in ethanol (EtOH) and hydrolyzed with HCl at *pH=2*. It was followed by gelation and subsequent drying at 50 ºC (Boeco dry block). Prior to hydrolysis a 0.55 M $Ni(NO_3)_2$ solution was added to the TEOS / EtOH solution. The initial molar composition for all samples was TEOS / H_2O = 1/4, with Ni/Si contents of 0, 0.01, 0.03, 0.05, 0.1, 0.2 and 0.45, respectively, and a starting amount of 5 ml TEOS. The duration of the different sol-gel steps was 1 h for room - temperature hydrolysis, 48 h for gelation in closed glass containers and 100 h for drying at 50ºC in open glass containers.

Nickel doped silica xerogels were characterized by X-ray diffraction and thermal analysis. A standard powder diffractometer Philips PW 1050 was applied for this study.

The thermal properties of nickel doped silica xerogels were studied systematically by differential scanning calorimetry (DSC) and thermogravimetry (TG) using a Mettler TA 3000 system. All experiments were performed in aluminum pans, in the temperature range from 25 to 500ºC with samples of about 10 mg. The heating rates applied for the DSC study were: 3, 5, 10, 15, 20, 25, 30, and 40 K/min. The weight losses and corresponding temperature maxima were estimated from TG curves.

* To whom all correspondence should be sent:
E-mail: avramov@ipc.bas.bg

RESULTS AND DISCUSSION

Solid grains with typical sizes bellow 1 cm were formed during drying. The undoped gels, as well as samples with low nickel content were transparent while the Ni containing samples were slightly translucent due to the dispersed microcrystallines. This is in line with the structural model discussed in our previous publications, according to which the nitrate complexes are distributed between the SiO_4 tetrahedra [17,19–23].

The DSC study of nickel doped sol-gel samples showed a strong influence of the concentration of Ni^{2+} on the type and shape of the curves. The influence of the heating rate was studied at constant composition. Data from the DSC study were compared with the results of TG analysis and the results are summarized in Table 1.

All Ni-doped xerogels are characterized by three peaks of weight losses (see Fig.1): a first one in the vicinity of 150 ºC, a second one at about 300 ºC and a third one at about 400ºC. The first peak position depends on the concentration of nickel, as well as on the scan rate. On Table 1 data for a heating rate $q = 20$ [K/min] are given.

Table 1 The dependence of the temperatures and enthalpies of the three peaks on the Ni content. The first and the third peak of weight losses are marked with subscripts 1 and 3, respectively. The second DSC peak is too weak.

Ni %	T_1 , ºC	H_1 , J/g	T_3 , ºC	H_3 , J/g
1	147,4	154,8	352.0	63,6
3	145,5	131,8	374,1	31.0
5	190,1	222,3	375,7	184,1
10	175,4	237,5	398,3	198.0
20	158,5	389,0	341,8	323,6
45	173,5	170.0	325,6	360.0

Similar peaks were observed in all DSC curves. Their temperatures and enthalpies depend on the concentration of Ni^{2+}, and on the scanning rate. Typical DSC and differential TG curves of 0.10 Ni/Si doped xerogel are shown in Fig. 2. The heating rate was 20 [K/min]. The derivative *dm/dT* of the TG curve is a measure of the rate of the weight loss. The temperature of the first DSC endothermic peak coincides with the temperature T_1 of the TG peak of weight losses. It is logical to suggest that the effect is caused by dehydration. In order to estimate the activation energy of this process samples with 5% Ni were scanned with heating rates varying between 3 and 40 K/min. The results are treated by the method of Qzawa (see [24–26]). Dependence of the logarithm of the heating rate $q = dT/dt$ against the reciprocal of the
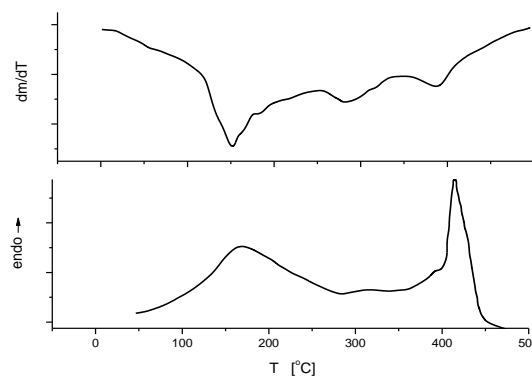
Fig. 1. Results of TG and DSC studies of the samples with 10 % Ni content at heating rates of 20 [K/min]. The top of the figure is the mass derivative as a function of temperature. The bottom presents the DSC scan.
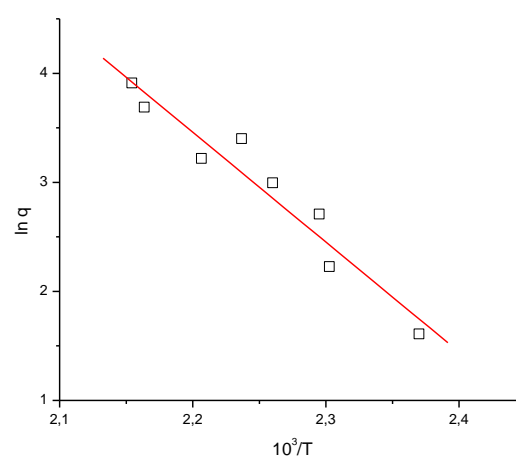
Fig.2. Arrhenius plot of the dependence of temperature of the reciprocal of the maximum of the first endothermic peak, T_{max} [K], on the heating rate, *q*.

maximum of temperature (in [K]) (Arrhenius coordinates) gives a straight line, the slope of which determines the corresponding activation energy, E_a. The dependence of the temperature of the maximum of the peak on the heating rate in Arrhenius coordinates leads to the value for $E_a = 80$ [kJ/mo]l (Fig. 2).

The heat treatment leads to two different processes - dehydration and chemical decomposition of the nitrate microcrystals. When heated to 500 ºC, samples change from transparent, light green, to opaque and black. It is known that after heating over 480 ºC, nickel nitrate transforms to fully crystalline NiO [8]. Taking into account the results of the TG analysis, it follows that the high-temperature peak reflects the decomposition of dehydrated $Ni(NO_3)_2$. Unfortunately, the process is rather turbulent, resulting in noise in the high temperature peak. Therefore, in this case, analyses in Arrhenius coordinates were not reliable. The non-doped SiO_2 does not display such peak.

4. CONCLUSIONS

Nickel doped silica xerogels were prepared by sol–gel chemistry, including acid hydrolyzation, gelation and drying at 50ºC. From nickel contents about 5% and higher a microcrystalline phase of pure $Ni(NO_3)_2\cdot4H_2O$ co-existing with the amorphous SiO_2 gel was obtained. The TG analysis demonstrates presence of two volatile products at heating: water and nitrogen oxides. For the first time detailed DSC and TG analyses of Ni^{2+} doped xerogels is presented. The thermal properties of these gels depend strongly on the Ni content. The heating rate significantly affects the peaks registered by DSC and TG. Two different processes take place at heating: dehydration of xerogels and chemical decomposition of $Ni(NO_3)_2$.

REFERENCES

1 S. L. Lai, J.Y. Guo, V. Petrova, G. Ramanath, L. H. Allen, *Phys. Rev. Lett.*, 77, 99 (1996)

2 J. M. Boyer, B. Repetti, R. Garrigos, M. Meyer, A. Bee, *J. Metast. Nanocryst. Mat., e-volume,* 29 (2001)

3 H. Amekura, Y. Fudamoto, Y. Takeda, N. Kishimoto, *Phys. Rev. B,* 71, 17, 2404 (2005)

4 F. Porta, S. Recchia, C. Bianchi, F. Confalonieri, G. Scari, *Colloids and surfaces A: Physicochemical and engineering aspects,* 155, 395 (1999)

5 J. T. Richardson, D. I. Yiagas, B. Turk, K. Forster, M.V. Twigg, *J. Appl. Phys.,* 70, 6977 (1991)

6 W. Xiong, J. Song, L. Gao, J. Jin, H. Zheng, Z. Zhang, *Nanotechnology,* 16, 37 (2005)

7 M. Ghosh, K. Biswas, A. Sundaresan, C. N. R. Rao, *J. Mater. Chem.*, 16, 106 (2006)

8 M. Gadalla and Hsuan -Fu Yu, *J. Thermal Analysis and Calorimetry,* 37, 319 (1991)

9 G. Clavel, M.-G. Willinger, D. Zitoun, N. Pinna, *Eur. J. Inorg. Chem*. No. 6, 863 (2008).

10 12. A. Pucci, G. Clavel, M.-G. Willinger, D. Zitoun, N. Pinna, *J. Phys. Chem. C* 113, no. 28, 12048 (2009)

11 T. Brezesinski, J. Wang, S. H. Tolbert, B. Dunn, *J. Sol-Gel Sci. Technol.* 57, 330 (2011)

12 T. R. Bryans, V. L. Brawner, E. L. Quitevis, *J. Sol-Gel Sci. Technol.* 17, 211 (2000)

13 P. Mallick, S. Sahu, *Nanoscience and Nanotechnology,* 2(3),: 71-74 ,(2012)

14 A. Gatelyte, D. Jasaitis, A. Beganskiene, A. Kareiva, *Materials Science* 17, 1392 (2011)

15 M. Bredol, Th. Jüstel, S. Gutzov, *Opt. Mater.* 18, 337 (2001).

16 S. Gutzov, C. Berger, M. Bredol, C. L. Lengauer, *J. Mater. Sci. Letters* 21, 1105, (2002).

17 M. Bredol, S. Gutzov, *Opt. Mater.* 20, 233 (2002).

18 M. Bredol, S. Gutzov, Th. Jüstel., *J. Non-Cryst. Solids*, 321, 225 (2003).

19 S. Gutzov, M. Bredol, *J. Mat. Sci. Letters* 41, 1835 (2006)

20 S.Gutzov, G.Ahmed, N. Petkova, E. Füglein, I. Petkov, *J. Non-Cryst. Solids* 354, 3438 (2008).

21 N. Avramova, S. Gutzov, E. Fuglein and I. Avramov, *J. Non-Cryst. Solids* 356, 422 (2010)

22 R. Reisfeld, Y. Kalisky, *Nature*, 283 281 (1980).

23 M. Ebelmen, *Ann. Chimie Phys.*, 16 129 (1846)

24 T. Ozawa, *Polymer* 12, 150 (1971).

25 H. Yinnon, D. Uhlmann, *J. Non-Cryst. Solids* 54, 253 (1983).

26 J. Malek, E. Cernoskova, J. Svejka, J. Sestak, G. Van der Plaats, T*hermochim. Acta,* 280/281, 353 (1996).

СВОЙСТВА НА НИКЕЛ (II) ДОТИРАНИ КСЕРОГЕЛИ

Н. Аврамова[1], И. Аврамов[2]

1)Химически факултет, СУ „Св. Климент Охридски“, 1166 София
2)Институт по физикохимия, Българска академия на науките, 1113 София

(Резюме)

Силициеви ксерогели, легирани с различно съдържание на Ni^{2+} са подготвени с помощта на зол-гел метод, основан на киселинно катализиран хидролиз на тетраетилортосиликат (TEOS) и желиране при 50 ° C. Пробите са изследвани чрез диференциална сканираща калориметрия, DSC, термо гравиметрия, TG и рентгенова дифракция. Подробни термични анализи до 500 ° C показват силно влияние на съдържанието на Ni на кристализация поведението на легираните ксерогели. Остър ендотермен пик на дехидратация се наблюдава около 150 ° C. Активиращата енергия, свързани с този пик се оценява на $E_A = 80$ [кДж / мол]. Два допълнителни ендотермни пика са забелязани като те зависят както от съдържанието на Ni така и от скоростта на нагряване.

Reduction of the impact of peak emissions of pollutants from multipurpose batch chemical and biochemical plants

N. Gr. Vaklieva-Bancheva, E. G. Kirilova*

Institute of Chemical Engineering, Bulgarian Academy of Sciences, Acad. G. Bonchev Str., Bl. №103, 1113 Sofia, Bulgaria

The study presents a system-oriented approach for reduction of the impact of peak emissions of pollutants from batch chemical or biochemical plants through appropriate managing of the manufacturing starting times of the respective products. It deals with the problem by proposing novel assessments of the environmental impact of the peaks that account only for these instantaneous values of the pollutant emission strengths that exceed a given limit level and allow the pollutants to be unified by the medium of their emission. Using these assessments an optimization criterion and optimization problem are formulated. As a result, the most appropriate shifting of the starting times of manufacturing for one or more of the products within the time horizon is determined. The efficiency of the approach is illustrated on a case study of dairy industry.

Keywords: Batch plants, environmental impact peaks reduction, peaks assessments, shifting of production starting times, dairy industry

INTRODUCTION

Reduction of the impact of peak emissions from batch chemical or biochemical plants is crucial not only for the environment but also for the associated waste treatment facilities. This requires an identification of the waste emissions inventories that have peak impacts on the environment and quantification of these impacts via proper metrics for air and water pollution evaluation. The latter motivates the development of various systematic approaches which direct the research from the end-of-pipe treatment to waste minimization at the source. This is actual in the context of the constantly rising costs of waste processing, raw materials and energy needed for the batch processes. Many of these approaches manage to eliminate or reduce these pollutions by substituting raw materials, recipes, solvents and by replacing or modifying process equipment. For this purpose, Hall and Camm [1] have developed a structured approach for identification of emissions of volatile organic pollutants produced in batch processes which have peak environmental impacts, by their minimization through direct replacement of raw materials, solvents and equipment used for the processes. The research is based on analysis of the profile of each one of the generated pollutants associated with the production processes.

In many cases the peak environmental impacts are caused by overloaded utility systems, as energy, steam, solvent recovering, etc., associated with the main processes. There are many approaches which manage to reduce the overloaded utility system peaks through appropriate planning or scheduling of the production systems. In most cases this leads to the formulation of multipurpose optimization problems that should satisfy environmental along with production and economical criteria and this requires the application of specific methods and techniques for their solution.

For example, Lee and Malone [2] have created an approach for planning of a batch distillation system together with the solvent recovery system. It results in formulation of a multipurpose optimization problem aiming at maximizing the overall productivity of the system by simultaneously minimizing the costs of disposed solvent, solvent distillation and recovery. The problem is solved by simulated annealing optimization technique coupled with discrete event simulation. As a result, installation of intermediate storage units for solvent deposit and increasing the distillation system capacity are proposed as feasible solutions.

When the load of utility systems associated to the main processes varies within a broad range and considerably exceeds the average demands in short time intervals, an approach developing optimal

---

* To whom all correspondence should be sent:
E-mail: eshopova@mail.bg

production system schedules should be applied. Moreover, the efficiency of this approach is greatly improved by including additional measures as better standardization of the equipment, choice of an optimized production schedule and control of the level of utilities consumption. To this purpose a methodology based on combination of computer simulation and analytically based approach of modeling and optimizing brew houses for steam consumption from an industrial brewery is developed [3]. As a result of the optimization, 55% reduction in peak load of the steam system is achieved.

On the other hand, the reduction of the peak utility load in batch processes, especially as regards electricity consumption, has a purely environmental and significant economical impact. The latter consists in the motivation of highly energy-intensive industries to work with TOU (Time Of Use) tariffs of electricity consumption, by imposing strict financial penalties for loading of the production systems above the permissible limit of consumption level. On this base, a mathematical model of energy consumption management for batch loaded systems applicable to any type of process industry is developed in [4]. The model is coupled with an optimization formulation using integer programming for minimization of the total electricity cost for production, subject to process flows and storage constraints for different tariff structures. Application of the proposed methodology for a steel plant resulting in optimal load schedules shows that significant reductions in peak loads (about 50%) and electricity cost (about 5.7%) are achievable. Analogous optimal scheduling problems have been formulated in [5] in the case study of the high-energy process of electrolysis in caustic soda and chlorine production. As a result, the curve of energy load is flattened through shifting the peak loads in the time and reductions of 19% in peak-period demand and 3.9% in electricity cost satisfying TOU tariffs are achieved.

One can see that many of the developed methodologies and approaches for reduction of environmental peak impacts result in formulation of multi-objective scheduling problems. However, the optimal environmental schedules obtained in such a way can also cause peak impacts on the environment. In most cases this is due to simultaneous generation of multiple pollutants as a result of process units operation under zero wait (ZW) policy in processing tasks implementation.

When production tasks are in the same time sources of pollutants, they could be divided in routine and non-routine. Routine waste sources are expected in products manufacturing. The mass of generated pollutants depends on the chosen production recipes, the composition of used raw materials (concentration of key compounds in the raw materials) as well as on the routes for products manufacturing. Key compounds are these components of the raw materials, the composition of which can be controlled within admissible boundaries. On the other hand, the appearance of non-routine sources is due to incorrect implementation of the technological processes, breakdowns of the equipment, transportation network and others.

However, the reduction of the routine waste source impact is complicated by the discreetness of the processing tasks and cyclic products manufacturing, as well as by the existence of process/units assignments resulting in multiple production routes with different batch sizes. The latter requires application of special approaches for their modeling.

The goal of this study is to propose an alternative system-oriented approach for environmentally benign management and reduction of the impact of the peak emissions of individual or combined pollutions from batch chemical plants, supposing that the production system operates under the most acceptable operational conditions.

Further the article is structured as follows: chapter 2 presents a mathematical model describing the emission strength from batch routine sources, based on the application of Fourier transform. Its application to the management of peak releases is shown. In chapter 3, the developed mathematical model is used for special environmental impact peaks assessments accounting for only these of the instantaneous values of the emission strengths of the pollutant that exceed a given limit level and allowing pollutants to be unified by the medium of their emission. In chapter 4 an optimization problem for reduction of the impact of peak emissions is formulated. Chapter 5 shows the implementation of the proposed approach on a case study from the dairy industry

.

MATHEMATICAL MODELING OF THE STRENGTH OF POLLUTANT EMISSIONS FROM ROUTINE WASTE SOURCES

Let's assume that some batch processing task l of product i is carried out cyclically (with a cycle time TC_i), being at the same time a routine waste source of pollutant w and the mass rate of this pollutant is constant during the processing time T_{il}. Then the generation of pollutant w from such batch routine waste source within the time horizon is presented on Figure 1. Having in mind these assumptions we have proposed a mathematical model of the strength of pollutant emission from a routine waste source within time horizon on the base of application of Fourier transform for presenting the discrete cyclic function of waste mass rate as a continuous one.
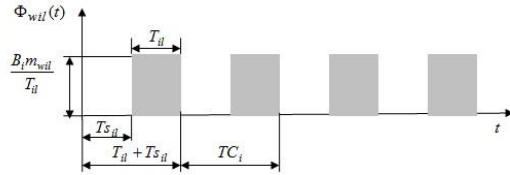
Fig.1. Cyclic generation of pollutant w from batch waste routine source within time horizon.

Then, the discontinuous and periodic function $\Phi_{wil}(t)$ of the emission strength of pollutant w from the discussed routine source l is defined as follows:

$$\Phi(t)_{wil} = \begin{cases} 0 & за \ 0 \leq t \leq Ts_{il} \\ \dfrac{B_i m_{wil}}{T_{il}} & за \ Ts_{il} \leq t \leq Ts_{il} + T_{il} \\ 0 & за \ Ts_{il} + T_{il} \leq t \leq TC_i \end{cases}, \ 0 \leq t \leq TC_i, \quad (1)$$

where:

Ts_{il} [s] is the time of appearance of the waste routine source l related to the beginning of the cycle duration; TC_i [s],

$\dfrac{B_i m_{wil}}{T_{il_i}} [kg/s]$ is the mass rate of a pollutant w (or

emission strength), evaluated by the batch size B_i [kg] and Pollution Index m_{wil} [kg/kg], [6, 7] which is the mass of the pollutant w processed from the production task l per 1 kg target product.

Function $\Phi_{wil}(t)$ is discontinuous and periodic with a period $TC_i > 0$ and can be approximated in Fourier series as follows, [8]:

$$F(t)_{wil} = B_i m_{wil} \begin{bmatrix} \dfrac{1}{TC_i} + \\ \sum_k \dfrac{1}{k\varphi_i T_{il}} [[cos(k\varphi_i Ts_{il})(1 - cos(k\varphi_i T_{il})) + sin(k\varphi_i Ts_{il})sin(k\varphi_i T_{il})]sin(k\varphi_i t) \\ + [sin(k\varphi_i Ts_{il})(cos(k\varphi_i T_{il}) - 1) + cos(k\varphi_i Ts_{il})sin(k\varphi_i T_{il})]cos(k\varphi_i t)]] \end{bmatrix}$$

$$\text{for } 0 \leq t \leq H, \quad (2)$$

where $\dfrac{2\pi}{TC_i} = \varphi_i$

The obtained continuous function $F(t)_{wil}$ (2) represents the mathematical model describing the emission strength of pollutant w from routine source l of product i, appearing cyclically in the time horizon H. It gives information for the mass rate of the "generated" pollutant in each moment t [kg pollutant w/s] and includes the general features of batch plants as batch size, cycle time, processing time. Pollution Index m_{wil} accounts for the mass of generated pollutant depending on the composition of some main key compounds in the raw materials.

The integral of mathematical model (2) allows assessing the whole amount M_{wil} of pollutant w emitted by processing task l of product i within the horizon:

$$Mass_{wil} = \int_0^H F(t)_{wil} dt. \quad (3)$$

Additionally, the sums by both l and i provide the total amount of pollutant w in manufacturing of the product i,

$$Mass_{wi} = \sum_l Mass_{wil} = \sum_l \int_0^H F(t)_{wil} dt, \quad (4)$$

and the total amount of pollutant w in case of compatible manufacturing of a group of products

$$Mass_w = \sum_i \sum_l Mass_{wil} = \sum_i \sum_l \int_0^H F(t)_{wil} dt. \quad (5)$$

This model provides an opportunity to follow for distribution of the emission strength of pollutant w within the time horizon H from all routine sources of a single product manufacturing:

$$F(t)_{wi} = \sum_l F(t)_{wil}, \forall l \in L. \quad (6)$$

or in compatible manufacturing of a group of products:

$$F(t)_w = \sum_i \sum_l F(t)_{wil}, \forall l \in L, \forall i \in I. \quad (7)$$

The function (7) is also a Fourier series. It contains information for the peak releases of pollutants due to the simultaneous appearance of

routine sources belonging to different products manufacturing, Fig. 2a.

Appropriate shifting of the manufacture starting times of one or several products rearranges the routine sources in the time horizon and could reduce the peak emissions making the function (7) relatively smoother. The latter provides an opportunity for management of the peak releases, see Fig. 2b.
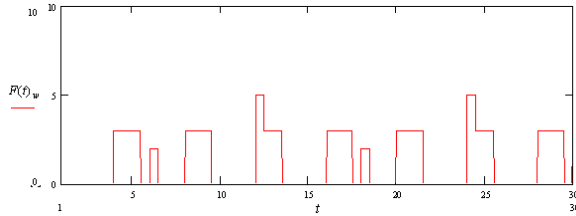
Fig. 2a. Without shifting of manufacture starting time.
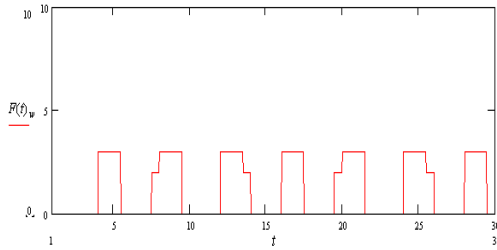
Fig. 2b. With shifting of manufacture starting time.

Fig. 2. Strength of emissions of pollutant w within the time horizon H in case of compatible manufacturing of two products.

For this purpose the model (7) should be transformed as follows:

$$F(\tau_i, t)_{wil} = B_i m_{wil} \begin{bmatrix} \frac{1}{TC_i} + \\ \sum_k \frac{1}{k\varphi_i T_{il}} \big[[cos(k\varphi_i Ts_{il})(1 - cos(k\varphi_i T_{il})) + sin(k\varphi_i Ts_{il}) sin(k\varphi_i T_{il})] sin(k\varphi_i)(t - \tau_i) \\ + [sin(k\varphi_i Ts_{il})(cos(k\varphi_i T_{il}) - 1) + cos(k\varphi_i Ts_{il}) sin(k\varphi_i T_{il})] cos(k\varphi_i)(t - \tau_i)] \big] \end{bmatrix}$$

$$\text{for } 0 \le t \le H \text{ and } \frac{2\pi}{TC_i} = \varphi_i. \qquad (8)$$

Thus, determination of the proper values of the starting times τ_i for each one of the products results in rearrangement of the waste routine sources within the time horizon H.

Based on the proposed mathematical model suitable quantitative assessments can be made which can be used as optimization criteria in the problems for reduction of peak environmental impact from batch chemical or biochemical plants.

PEAK ENVIRONMENTAL IMPACT ASSESSMENTS OF BATCH PLANTS

We proposed suitable *Local* and *Global Assessments* for quantification of the *Peak Environmental Impact* like the Local and Global Environmental Impact Assessments developed in [9–11] by means of *Peak Environmental Impact Indices* formulated in a proper way. The latter account only for these of the instantaneous values of the emission strengths of pollutant w that exceed the strength of the *Environmental Impact Limit Index*. The *Peak Environmental Impact Indices* unify pollutants of different types through the medium of their emission - air, water, etc. and provide information for the mass rate of the carrier, needed in each moment of time t for the pollutant w to be kept in the standard limit value for a given medium.

The *Environmental Impact Limit Index* of pollutant w $LIM_{wi}(t)$ is defined on the base of the determined minimum quantity of pollutant w, assuming that the compatible manufacturing of the products realized in "continuous" mode within the horizon H and $LIM_{wi}(t)$ has a constant value over the horizon, Fig. 3.
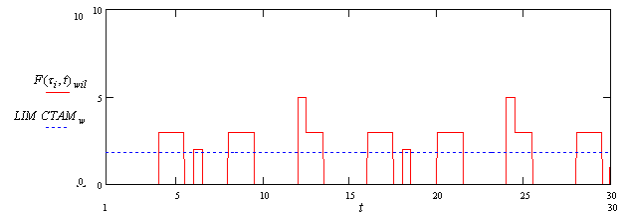
Fig. 3. Emissions strength of pollutant w into the time horizon H in compatible manufacturing of two products and corresponding Environmental Impact Limit Index.

Thus the Environmental Impact Limit Index for a given pollutant w generated from a waste routine source in products manufacturing or compatible production of a group of products will have a constant value for each time t and it is determined as follows (an example for the air):

$$LIM\,CTAM_{wil} = \frac{1}{\mu a_w} \frac{Q_i.m^*_{wil}}{H}, \qquad (9\,a)$$

$$LIM\,CTAM_{wi} = \frac{1}{\mu a_w} \sum_l \frac{Q_i.m^*_{wil}}{H}, \qquad (9\,b)$$

$$LIM\,CTAM_{w} = \frac{1}{\mu a_w} \sum_i \sum_l \frac{Q_i.m^*_{wil}}{H}, \qquad (9\,c)$$

where m_{wil}^* represents Pollutant Indices obtained as minima from a theoretical point of view of Local and Global Environmental Impact Assessments.

Then, for the air the *Peak Environmental Impact Index* using (9 c) is defined as follows:

$$P\,CTAM_w = signum\ (\bullet)[CTAM_w - LIM\ CTAM_w],\ (10)$$

where $signum(\bullet)$ is a sign function determined as follows:

$$signum(\bullet) = \begin{cases} 1 & if \quad CTAM_w \geq LIM\ CTAM_w \\ 0 & otherwise \end{cases}.\ (11)$$

Using (8) *Peak Environmental Impact Indices*, shown for the example of the air is:

$$P\,CTAM_w = signum(\bullet)\left(\frac{1}{\mu a_w}\sum_i\sum_l F(\tau_i,t)_{wil} - \frac{1}{\mu a_w}\sum_i\sum_l \frac{Q_i.m_{wil}^*}{H}\right),$$

$$for\ 0 \leq t \leq H,\quad (12)$$

where $signum(\bullet)$ is:

$$signum(\bullet) = \begin{cases} 1 & if \quad \frac{1}{\mu_w}\sum_i\sum_l F(\tau_i,t)_{wil} \geq \frac{1}{\mu a_w}\sum_i\sum_l \frac{Q_i.m_{wil}^*}{H} \\ 0 & otherwise \end{cases}.\ (13)$$

Integrating *Peak Environmental Impact Indices* within the time horizon results in determination of the *Local* (for a given pollutant) and *Global* (for a group of pollutants) *Peak Environmental Impact Assessments* in a similar way as the *Local* and *Global Environmental Impact Assessments*, as is shown on an example for *Peaks Critical Air Mass*.

$$PCTAM_w\big|^H = \int_0^H signum(\bullet)\left(\frac{1}{\mu_w}\sum_i\sum_l F(\tau_i,t)_{wil} - \frac{1}{\mu a_w}\sum_i\sum_l \frac{Q_i.m_{wil}^*}{H}\right)dt$$

$$(14)$$

$$PEI_w\big|^H = \left[PCTAM_w\big|^H, PCTWM_w\big|^H, PSDM_w\big|^H,....\right],\ (15)$$

$$GPEI\big|^H = \sum_w PEI_w\big|^H.\ (16)$$

(15) and (16) can be used as optimization criteria in the problem for reduction of the peak environmental impact of batch chemical and biochemical plants.

MATHEMATICAL FORMULATION OF THE PROBLEM FOR PEAK ENVIRONMENTAL IMPACT REDUCTION

Based on already defined *Local* and *Global Peak Environmental Impact Assessments* the problem of peak environmental impact reduction can be formulated.

After establishing the conditions at which the production system has minimal environmental impact, the problem of peak environmental impact reduction is solved [12–14]. This means that the concentrations of the key compounds for products manufacturing, the recipes, the size and number of produced batches in a given production horizon, i.e. the chosen production routes are known. The peak environmental impact reduction is usually realized with respect to a single or a group of pollutants w', $w' \in W'$, ($W' \in W$), which simultaneously appear within the time horizon as a result of the discrete nature of the processes and they are subject to a joint treatment of the gas, water or other facilities.

As noted above, the purpose of peak management is to rearrange the waste routine sources within the time horizon through shifting the starting times of products manufacturing. Thus the curve of their real environmental impact should be flattened as much as possible within the horizon so as to approximate it to the *Environmental Impact Limit Index* of the pollutant.

4.1. Control variables

To control the starting times of products manufacturing we introduce a vector **T** of variables τ_i, defined for each product i, determining the moment of its beginning with respect to the beginning of the time horizon:

$$T = (\tau_1, \tau_2,...,\tau_i,...,\tau_I),\ \forall i,\ i \in I.\quad (17)$$

Each variable τ_i should be controlled in the admissible to its time tolerance TH_i:

$$0 \leq \tau_i \leq TH_i,\quad \forall i,\ i \in I.\quad (18)$$

The time tolerance TH_i, used for the management of the starting times of products manufacturing is determined as follows:

$$TH_i = H - Nb_i.TC_i + (\sum_{l=1}^L T_{il} - TC_i),\forall i,\ i \in I.\ (19)$$

The starting times for products manufacturing can be shifted for those products i only, for which a time tolerance TH_i exists:

$$TH_i > 0 \quad (20)$$

If there is no time tolerance for any of the products i, the management of peak environmental impact is impossible.

4.2. Objective functions

As objective functions the *Local* and *Global Peak Environmental Impact Assessments* (15) and (16) to some pollutants w' are used as follows:

$$PEI_{w'}\big|^H = \left[PCTAM_{w'}\big|^H, PCTWM_{w'}\big|^H, PSDM_{w'}\big|^H, \ldots\right],$$
$$w' \in W' \qquad (21)$$

or

$$GPEI\big|^H = \sum_{w'} PEI_{w'}\big|^H . \quad (22)$$

They are obtained on the base of the integrated for the time horizon H *Peak Environmental Impact Indices* as it is shown on the example of the air:

$$PCTAM_{w'}\big|^H = \int_0^H signum(\bullet)\left(\frac{1}{\mu_w}\sum_i\sum_l F(\tau_i, t)_{w'il} - \frac{1}{\mu a_{w'}}\sum_i\sum_l \frac{Q_i.m_{w'il}^*}{H}\right)dt$$
$$. \quad (23)$$

Each of the assessments (21) or (22) can be used as an optimization criterion in formulating the problem of peak environmental impact reduction and it is a subject of minimization:

$$\Psi = \min_T PEI_{w'}\big|^H . \qquad (24)$$

or

$$\Psi = \min_T GPEI\big|^H . \qquad (25)$$

The statement proposed above represents the mathematical model of peak environmental impact minimization due to the simultaneous appearance of relevant waste routine sources within the planned horizon. It incorporates an objective function (21) or (22) and relations (23) required for its solution. Moreover, it introduces a set of continuous variables (17) for shifting the starting times of products manufacturing, as well as a set of constraints (18) keeping corresponding shifting to be within the admissible time tolerances (19) and (20) for the products. In general, the problem formulated in such a way is a multipurpose one.

From a practical point of view, however, it is more relevant that the reduction of the environmental impact peak be implemented only in one medium, for example air or water, which transforms the problem into a single objective one. The most environmentally benign reduction of peak impacts is achieved at these values of shifting times τ_i at which the chosen objective function has a minimal value.

A CASE STUDY

To illustrate the efficiency of the proposed approach we have used a case study from the dairy industry. In particular, the multipurpose production system for realization of the compatible manufacturing of two types of curds is considered: product 1 with 0.3% fat content and product 2 with 1% fat content, (Table 1). The products are manufactured within a time horizon of 400 h fulfilling a demand of 7000 kg for each product. Curd production is associated with the release of a large amount of waste water containing significant amounts of proteins, milk fat, lactose and other organic matters. The Biochemical Oxygen Demand – BOD is a measure of the effluent strength of waste water in terms of the amount of dissolved oxygen utilized by microorganisms during the oxidation of organic components. Some of these pollutants come as a result of dairy processing such as pasteurization, acidification and draining while the rest are due to losses of raw materials, by-products and products, for example spilled and leaked milk or whey, coagulated milk, butter, curd particles to the unit walls.

Based on the waste routine analysis of the chosen production recipe of curd production, the processing tasks "Pasteurization" and "Draining" were identified as waste routine sources from which peak impacts on the environment can be expected [15]. The preliminary optimal production schedule (Table 2) has a Global BOD assessment equal to _238.45_ [kg O₂], [15].

Table 1. Type and size of dairy unites used for curds processing.

Type	Vessels of dilution				Pasteurizers				Vats			Drainers		
№	1	2	3	4	5	6	7	8	9	10	11	12	13	14	15
[m³]	0.4	0.35	0.3	0.4	0.3	0.25	0.15	0.1	0.3	0.4	0.25	0.08	0.06	0.06	0.01

Table 2. Values of the control variables corresponding to the optimal solution.

Product	Milk fat content, %	Production routes - units	Batch size, [kg]	Number of batches	Production demand, [kg]	Production horizon, [h]
Solution (H=400h), GBOD=238.45 [kg O$_2$]						
1	0.083	6,7,9,15	75.29	93	7002	373.5
2	0.255	5,8,10,12	72.73	97	7055	389.5

The corresponding value of environmental impact peak assessment is obtained when all starting times for products manufacturing are at the beginning of the time horizon, i.e. $\tau_i = 0,\ \forall i$ is PBOD=187.43[$kg\ O_2$]. On Fig. 4 the distribution of the environmental impact peak during the first 40 hours of the time horizon is shown. In the graphic notes the *Environmental Impact Limit Index LIM BOD* is shown. *PBOD* is determined from the amount of generated BOD exceeding at certain periods of time *LIM BOD* due to the simultaneous appearance in the time horizon of the processing tasks "Pasteurization" and "Draining" in both productions.
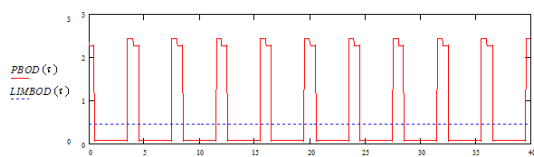
Fig. 4. Distribution of the peaks' environmental impact in the curd production at $\tau_i = 0,\ \forall i$.

As a result of the solution of the optimization problem formulated in the previous chapter, the value of *PBOD* is reduced to 99.32 [$kg\ O_2$]. This result is obtained by applying the optimization technique described in [16] and solving 10 times the problem. Values of the control variables for 8 equally optimal solutions are as follows:

A) $\tau_1 = 0$ a $1 \leq \tau_2 \leq 2$ (5 solutions);

B) $\tau_1 = 0$ a $1 \leq \tau_1 \leq 2$ (3 solutions).

The distribution of peaks releases leading to reduction of its environmental impact assessment to 99.32 [$kg\ O_2$] obtained at $\tau_1 = 0$ and τ_2=1.599 h is shown on Figure 5.
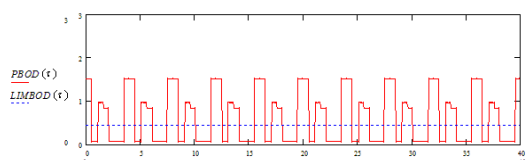
Fig. 5. Distribution of peaks' environmental impact in curd production at $r_1 = 0$, and $r_2 = 1.599$

Once again we note that the reduction of the environmental impact peak does not change the global environmenthal impact assessment *GBOD* of 238.45 $kg\ O_2$ determined for this particular case.

The change in the starting times of the products manufacturing results in rearrangement of the waste routine sources within the time horizon so that the production generates more frequently but smaller amounts of waste water during the equipment washing after production of each batch.

CONCLUSION

In this study we have proposed a systematic approach for the reduction of environmental impact peaks which could emerge by the simultaneous appearance of a group of waste routine sources. The approach is applicable to the case of already obtained environmentally benign production schedules of operation of multipurpose batch chemical or biochemical production systems. It allows rearrangement of the waste routine sources by suitable shifting of the manufacture starting times of one or more of the products within the time horizon. In order to manage these peak releases a mathematical model describing the emissions strength of batch routine sources is proposed by means of Fourier transform of the discrete batch function of the pollutant into a continuous one. Based on this model special environmental impact peak assessments are performed. They account only for these of the instantaneous values of the emissions strengths of pollutant exceeding a given limit level and allow unifying of the pollutants by the medium of their emission. They are involved as optimization criteria in the problem of reduction of environmental impact peaks.

The efficiency of the proposed approach is illustrated on example of the compatible production of two types of curds. It is found that shifting of the starting time of one of the product manufacturing by 1 to 2 hours leads to the best rearrangement of the waste routine sources - processing tasks "Pasteurization" and "Draining" within the time horizon at minimum environmental impact peaks.

REFERENCES

1 S. Hall, R. Camm, *Environmental Protection Bulletin*, **63,** 3 (1999).
2 Y. G. Lee, M. F. Malone, *Ind. Eng. Chem. Res.*, **39(6),** 2035 (2000).
3 D. Mignon, J. Hermia, *Comput. Chem. Eng.*, **20(3)**, 249 (1996).
4 S. Ashok, *Appl. Energ.*, **83**, 413 (2005).
5 C. A. Babu, S. Ashok, *IEEE Trans. Power Syst.*, **23(2),** 399 (2008).
6 A. K. Hilaly, S. K. Sikdar, *J. Air Waste Manag. Assoc.*, **44**, 1303 (1994).
7 A. K. Hilaly, S. K. Sikdar, *Ind. Eng. Chem.*, **34**, 2051 (1995).
8 N. G. Vaklieva-Bancheva, E. G. Shopova, B. B. Ivanov, *Hung. J. Ind. Chem.*, **30**, 199 (2002).
9 E. N. Pistikopoulos, S.K., Stefanis, A. G. Livingston, *AIChemE Symposium Series, Volume on pollution prevention via process and product modifications*, **90(303)**, 139 (1994).
10 S. K. Stefanis, A. G. Livingston, E. N. Pistikopoulos, *Comput. Chem. Eng.*, **19**, S39-S44 (1995).
11 S. K. Stefanis, A. G. Livingston, E. N. Pistikopoulos, *Comput. Chem. Eng.*, **21(10)**, 1073 (1997).
12 E. G. Shopova, N. G. Vaklieva-Bancheva, *J. U. Chem. Technol. and Metall., XXXVIII,* **3**, 779 (2003).
13 N. G. Vaklieva-Bancheva, E. G. Shopova, B. B. Ivanov, *Bulg. Chem. Commun.,* **36(4)**, 253 (2004).
14 N. G. Vaklieva-Bancheva, E. G. Kirilova, *J. Clean. Prod.*, **18(13)**, 1300 (2010).
15 E. G. Kirilova, PhD Thesis, IChE-BAS, Sofia, 2011.
16 E. G. Shopova & N. G. Vaklieva-Bancheva, *Comput. Chem. Eng.*, **30(8)**, 1293 (2006).

РЕДУЦИРАНЕ НА ПИКОВИТЕ ВЪЗДЕЙСТВИЯ ОТ ЗАМЪРСИТЕЛИ ВЪРХУ ОКОЛНАТА СРЕДА ЗА МНОГОЦЕЛЕВИ ПЕРИОДИЧНИ ХИМИЧНИ И БИОХИМИЧНИ ПРОИЗВОДСТВА

Н. Гр. Ваклиева-Банчева, Е. Г. Кирилова

Институт по инженерна химия, Българска академия на науките, ул.”Акад. Г. Бончев”, бл. 103, София 1113, България

(Резюме)

    Това изследване представя един системно-ориентиран подход за редуциране на пиковите въздействия от замърсители върху околната среда за периодични химични и биохимични производства чрез подходящо управление на стартовите времена за производство на продуктите в производствените системи. Този подход въвежда оригинални екологични оценки за въздействие на пиковете, които отчитат само тези от моментните стойности на въздействие, които надвишават определено гранично ниво и позволяват обединяването на различни типове замърсители чрез средата, в която се излъчват. Тези оценки са използвани като оптимизационни критерии във формулираната задача за редуциране на пиковите въздействия върху околната среда от периодични химични и биохимични производствени системи. В резултат на нейното решаване са определени най-подходящите стартови времена за производство на продуктите в даден времеви хоризонт. Ефективността на подхода е показана на пример от млечната индустрия.

Biomimetic oxidative dehydrogenation of 1,4-dihydropyridines with m-chloroperoxybenzoic acid (m-CPBA) in the presence of tetraphenylporphyrinatoiron(III) chloride [Fe(TPP)Cl]

G. Karimipour[*1], T. Mousavinejad[2]

[1]*Department of Chemistry, Yasouj University, Yasouj 75918-74831, Iran; fax: (+98) 741 3342172*
[2]*Department of Coating Research Center, Industrial & Environmental Protection Division, Research Institute of Petroleum Industry (RIPI), P.O.BOX 14665-137, Tehran, Iran.*

A simple and efficient methodology for the oxidative dehydrogenation of Hantzsch 1,4-dihydropyridines (1,4-DHPs) to their corresponding pyridine derivatives with m-chloroperoxybenzoic acid (m-CPBA) in the presence of tetraphenylporphyrinatoiron(III) chloride [Fe(TPP)Cl] was described. Product formation takes place within just a few minutes with ~100% selectivity in 95-100% yield. This method may provide valuable information for evaluating the oxidation path of 1,4-DHPs by cytochrome P-450 in the human body.

Keywords: Decarboxylation; m-Chloroperoxybenzoic Acid (m-CPBA); 1,4-Dihydropyridine (1,4-DHP) ; Tetraphenylporphyrinatoiron(III) chloride [Fe(TPP)Cl].

INTRODUCTION

The analogies manifested between Hantzsch 1,4-dihydropyridines (1,4-DHPs) and NADH coenzymes make 1,4-DHPs an important class of drugs (amlodipine besylate and nifedipine) and define their application in organic synthesis as fine starting materials [1]. For example, various novel dihydroindolizine-based were synthesized using 2-formyl-1,4-DHP by the Michael addition/intramolecular amino-nitrile cyclization method [2].

Recently, a great number of reagents and procedures (i. e., ferric nitrate on a solid support [3] ceric ammonium nitrate [4], Claycop [5], pyridinium chlorochromate [6], nitric acid [7], nitric oxide and N-methyl-N-nitrosotoluene-P-sulfonamide [8]) has been applied for the oxidation of 1,4-DHPs. However, in most cases, researchers have to deal with problems such as harsh reaction conditions, long reaction time, tedious workup and low yields and selectivities. On the other hand, Hantzsch 1,4-DHPs are oxidized to pyridine derivatives by the action of cytochrome P-450 in the liver [9].

So, based on the resemblance between porphyrins and P-450 enzymes, Moqhadam published some papers about the application of metalloporphyrins in catalytic dehydrogenation of 1,4-DHPs [10-13]. In this work, mimicking cytchrome P-450, we introduced tetraphenyl-porphyrinatoiron(III) chloride [Fe(TPP)Cl] as a catalyst and imidazole (Im) as a co-catalyst for oxidative dehydrogenation of 1,4-DHPs by m-chloroperoxybenzoic acid (m-CPBA) to improve the yield and selectivity (Scheme 1).

Fe(TPP)Cl

Scheme 1
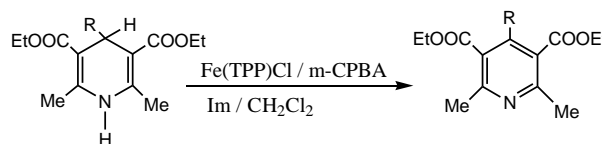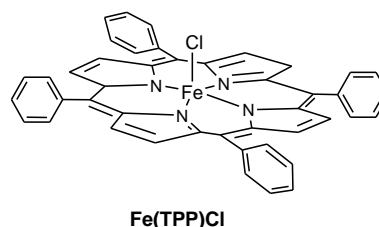
EXPERIMENTAL

Chemicals were purchased from Fluka, Merck and Aldrich chemical companies. Tetraphenylporphyrin (H_2TPP) was prepared and metallated according to the procedure used by Adler [14]. All

---

* To whom all correspondence should be sent:
E-mail: ghkar@mail.yu.ac.ir

Hantzsch 1,4-dihydropyridines were synthesized by the reported procedures [15].

All reactions were performed at room temperature in a 25 mL flask equipped with a magnetic stirring bar. To a solution of Hantzsch 1,4-dihydropyridine (0.15 mmol), Fe(TPP)Cl (0.003 mmol) and imidazole (Im) (0.045 mmol) in CH_2Cl_2 (2 mL) m-chloroperoxybenzoic acid (m-CPBA) (0.18 mmol) was added. The progress of the reactions was monitored by TLC and GC (Agilent 6890N) and HPLC (Agilent 1100). After the reaction was completed, the product was purified using a silica gel plate or a silica gel column (eluent: CCl_4–Et_2O) and was analyzed by spectroscopic methods.

RESULTS AND DISCUSSION

The structural analogy between synthetic metalloporphyrins and natural enzymes like cytochrome P-450 provides a valuable pathway for organic and inorganic chemists to construct transition metal-porphyrin complexes with catalytic, optoelectronic and photodynamic properties. Organic compounds could be effectively and highly selectively oxidized by oxygen donors such as PhIO, ClO^-, H_2O_2, ROOH or IO_4^- in the presence of metalloporphyrins [16].

In continuation of our earlier work on the oxidative dehydrogenation of 1,4-dihydropyridins by Tryp–Mn/n–Bu_4NIO_4 [17], we report here a facile and efficient procedure for conversion of various 1,4-DHPs into the respective pyridine derivatives by Fe(TPP)Cl and m-CPBA with 95–100% yields in a few minutes at ambient conditions (Scheme 1).

In the initial experiment, 4-methyl substituted DHP was oxidized by m-CPBA in CH_2Cl_2 at room temperature. We found that the oxidation does not efficiently proceed in the absence of catalyst (<15% yield). Moreover, simple Fe(II) and Fe(III) salts have not enough capability to improve the oxidation.

In the further experiments, different molar ratios of reagents and catalyst were examined to attain the optimum conditions for oxidation of 1,4-DHPs. The maximum yield with the starting 1,4-DHP was obtained at a molar ratio of Fe(TPP)Cl: Im: 1,4-DHP: m-CPBA = 1: 15 :50 : 60 (see Experimental).
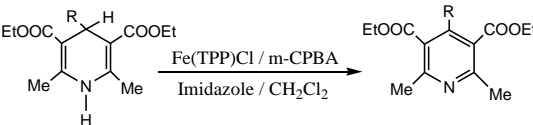
It is notable that the catalytic activity of Fe(TPP)Cl increased during the reactions. It seems that the produced pyridine derivatives act as axial ligands for the catalyst, accelerating the oxidation during the course of the reactions. This hypothesis was confirmed by adding a nitrogenous donor such as imidazole into the reaction mixture. In this case the oxidation rate was 4.5 times higher than without imidazole. Nitrogenous ligands such as imidazoles and pyridines are reported to improve selectivity, reactivity and turnover number of metalloporphyrin-mediated reactions, by weakening of the M–O bond in the oxidized form of the porphyrin catalysts by donating electron density into the M–O antibonding orbitals [18].
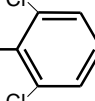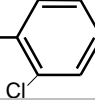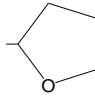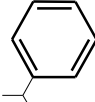
Scheme 2
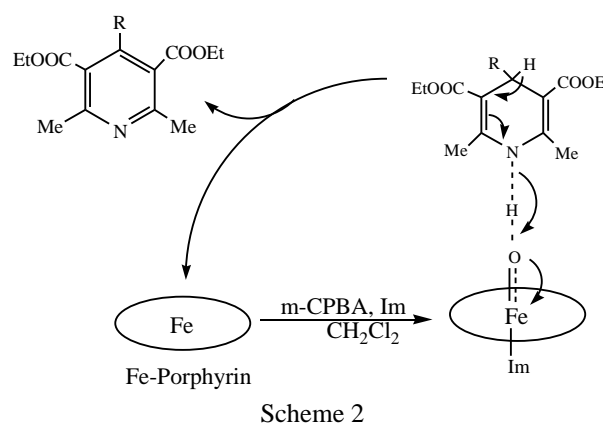
The coordinated nitrogenous bases (*i.e.* imidazole and/or the produced pyridines) assist the possible electronic changes in the Fe centre and lead to the facile formation of a metal-oxo intermediate [19]. Also, the nitrogenous bases facilitate the transfer of oxygen atom from the metal-oxo intermediate to the substrates. It is plausible to assume that the oxidations occurs by an electrophilic attack of oxo iron porphyrin [19] to the N–H hydrogen atom, followed by concomitant elimination of the hydrogen atom on the 4-position of the 1,4-DHPs, as shown in Scheme 2. It may be assumed that the metabolism of 1,4–DHPs in the liver may take place by a similar pathway in the presence of cytochrome P–450.

The iron(III) porphyrin/m-CPBA catalytic system can be used for oxidizing a wide variety of 1,4-dihydropyridine derivatives bearing an alkyl or an aryl group to their corresponding pyridine derivatives in excellent yields at room temperature in the presence of imidazole as axial ligand. The results are summarized in Table 1. The formation of the products is very rapid, so it is not possible to evaluate the effect of structural parameters (i. e. steric and electronic) on the reaction mechanism and rate.

Table 1. Oxidative dehydrogenation of Hantzsch 1,4-dihydropyridines with m-CPBA catalyzed by Fe(TPP)Cl/m-CPBA-Im in CH_2Cl_2

Entry	R	Time (min)	Yield (%)
1	H	1	100
2	-CH_3	1	100
3	-CH-CH_3	2	98
4	-CH-CH_2-CH_3	2	96
5	-OCH_3	1	100
6		2	100
7	(NO_2)	1	100
8	(NO_2)	1	100
9	(Cl, Cl)	6	95
10	(Cl)	2	100
11	(Cl)	5	98
12		4	98
13	(CH_3)	5	100

[a]All products were identified by comparison with authentic samples (IR, 1H NMR, m.p.).

CONCLUSIONS

This paper describes a convenient and efficient process for oxidative decarboxylation of 1,4-dihydropyridines to the corresponding pyridine derivatives with m-CPBA by a biomimetic Fe(TPP)Cl catalyst. This biomimetic catalytic methodology offers very attractive features such as mild reaction conditions, high efficiency of the catalyst and 95–100% yield with ~100% selectivity in less than 5 minutes. Therefore, the present method could be used in organic synthesis.

REFERENCES

1 (a) L. Navidpour, R. Miri, A. Shafiee. F, *Arzneimittel Drug Res*., **54**, 499 (2004); (b) J. Striessnig, *Cell. Physiol. Biochem*., **9**, 242 (**1999**).
2 S. Marchalin, B. Baumlova, P. Baran, H. Oulyadi, A. Daich, *J. Org. Chem.,* **71**, 9114 (2006).
3 M. Balogh, I. Hermecz, Z. Meszaros, P. Laszlo, *Helv. Chim. Acta.,* **67**, 2270 (1984).
4 Pfister J. R, *Synthesis,* 689 (1990).
5 A. Maquestiau, A. Mayence, J. J. V. Eynde, *Tetrahedron Lett.,* **32**, 3839 (1991).
6 J. J. V. Eynde, A. Mayence, A. Maquestiau, *Tetrahedron.,* **48**, 463 (1992).
7 R. H. Bouchr, D. F. Guengerich, *J. Med. Chem.,* **29**, 1596 (1986).
8 X. Q. Zhu, B. J. Zhao, J. P. Chang, *J. Org. Chem*., **65**, 8158 (2000).
9 F. P. Guengerich, W. R. Brian, M. Iwasaki, M. A. Sari, C. Baernhielm, P. Berntsson, *J. Med. Chem*., **34**, 1838 (1991).
10 M. Nasr-Esfahani, M. Moghadam, S. Tangestaninejad, V. Mirkhani, A. R. Momeni, *Bioorg. Med. Chem*., **14**, 2720 (2006).
11 M. Moghadam, M. Nasr-Esfahani, S. Tangestaninejad, V. Mirkhani, *Bioorg. Med. Chem. Lett*., **16**, 2026 (2006).
12 M. Moghadam, M. Nasr-Esfahani, S. Tangestaninejad, V. Mirkhani, M. A. Zolfigol, *Can. J. Chem*., **84**, 1 (2006).
13 M. Nasr-Esfahani, M. Moghadam, S. Tangestaninejad, V. Mirkhani, *Bioorg. Med. Chem. Lett*., **15**, 3276 (2005).
14 A. D. Adler, F. R. Long, J. D. Finarellii, J. Goldmacher, J. Assour, L. Korsakoff, *J. Org. Chem.,* **32**, 476 (1967).
15 M. A. Zolfigol, M. Safaiee, *Synlett*., 827 (2004).
16 D. Mohajer, G. R. Karimipour, M. Bagherzadeh, *New J. Chem*., **28**, 740 (2004).
17 G. R. Karimipour, M. Nasr-Esfahani, G. Valipour, *J. Chem. Res. (S)*., 605 (2006).
18 (a) J. Y. Liu, X. F. Li, Y. Z. Li, W. B. Chang, A. J. Huang, *J. Mol. Catal. A.*, **187**, 163 (2002); (b) E. Baciocchi, T. Boschi, C. Galli, A. Lapi, P. Tagliatesta, *Tetrahedron*., **53**, 4497 (1997); (c) K. Konishi, K. Oda, K. Nishida, T. Aida, S. Inoue, *J. Am. Chem. Soc*., **114**, 1313 (1992); (d) R. L. Halterman, S. T. Jan, *J. Org. Chem*., **56**, 5253 (1991); (e) J. P. Battioni, D. Dupre, D. Mansuy, *J. Organomet. Chem*., **328**, 173 (1987); (f) D. Mansuy., *Pure. Appl. Chem*., **59**, 759 (1987); (g) E. Guilmet, B. Meunier, *Tetrahedron Lett*., **23**, 2449 (1982); (h) E. Guilmet, B. Meunier, *Nouv. J. Chim*., **6**, 511 (1982).
19 P. R. Ortiz de Montellano, *Chem. Rev.,* **110**, 932 (2010), and references therein.

БИОМИМЕТИЧНО ОКСИДАТИВНО ДЕХИДРОГЕНИРАНЕ НА 1,4-ДИХИДРОПИРИДИНИ С М-ХЛОРПЕРОКСИБЕНЗОЕНОВА КИСЕЛИНА (M-CPBA) В ПРИСЪСТВИЕ НА ЖЕЛЕЗЕН(III)ТЕТРАФЕНИЛПОРФИРИНАТ ХЛОРИД [FE(TPP)CL]

Г. Каримипур[1], Т. Мусавинеджад[2]

[1]*Катедра по химия, Университет Иасудж, Иасудж 75918-74831, Иран; факс: (+98) 741 3342172*

[2]*Катедра по изследване на покрития, Подразделение по индустрия и опазване на околната среда, Изследователски институт по нефтопреработване (RIPI), P.O.BOX 14665-137, Техеран, Иран*

(Резюме)

Представена е проста и ефективна методология за оксидативно дехидрогениране на Hantzsch на 1,4-дихидропиридини (1,4-DHP) до техните съответни производни на пиридин с *m*-хлорпероксибензоенова киселина (m-CPBA) в присъствието на железен(III)тетрафенилпорфиринат хлорид [Fe(TPP)Cl]. Получаването на продуктите става в рамките на само няколко минути с ~100% селективност при 95-100% добив. Методът може да предостави полезна информация за оценка на окислителната пътека на 1,4-DHP с цитохром Р-450 в човешкото тяло.

An efficient catalytic synthesis of 1,2-dihydro-1-aryl-3*H*-naphth[1,2-*e*][1,3]oxazin-3-one derivatives using silica supported Preyssler heteropolyacid, $H_{14}[NaP_5W_{30}O_{110}]/SiO_2$ (50%) as a heterogeneous catalyst

Ali Gharib [1,2]*, Bibi Robabeh Hashemipour Khorasani [2], Manouchehr Jahangir [1], Mina Roshani[1]

[1]Department of Chemistry, Islamic Azad University, Mashhad, IRAN
[2]Agricultural Researches and Services Center, Mashhad, IRAN

Silica supported Preyssler type heteropolyacids are found to be efficient catalysts for the synthesis of 1,2-dihydro-1-aryl-3*H*-naphth[1,2-*e*][1,3]oxazin-3-one derivatives in good yields in a convenient, efficient and green reaction by condensation of *β*–naphtol, aromatic aldehydes, urea, and ethanol under reflux conditions. The catalyst is recycled and reused several times.

Keywords: Preyssler; heteropolyacid; naphtho-oxazine; aromatic aldehyde; catalyst.

INTRODUCTION

Naphthalene-condensed 1,3-oxazin-2-ones have been reported to act as antibacterial agents [1]. They have been used as precursors in the preparation of phosphinic ligands for asymmetric catalysis [2]. Sodium hydrogen sulphate (NaHSO₄), n-tetrabutylammonium bromide (TBAB) as a phase transfer catalyst (PTC) in water, and 1-butyl-3-methyl imidazolium hydrogen sulphate ([bmim]HSO₄) as ionic liquid (IL) have been used as mild reaction promoters for the cyclocondensation of formaline, *β*-naphthol and aromatic amines to afford the respective 2,3-dihydro-2-phenyl-1H-naphtho-[1,2–e] [1,3] oxazine derivatives [3]. 1,2-Dihydro-1-arylnaphtho[1,2-e][1,3]oxazine-3-one derivatives were synthesized in high yields using a facile one-pot condensation of 2-naphthol, aromatic aldehydes and urea catalyzed by perchloric acid supported on silica under thermal solvent-free conditions [4]. 1,2-Dihydro-1-phenyl-naphtho [1,2–e] [1,3] oxazin-3-one derivatives were prepared in good yields using a novel one-pot reaction involving *β*-naphthol, urea and aromatic aldehydes under solvent-free conditions [5]. Hitherto, only few reports for the synthesis of naphthalene-condensed oxazinone derivatives have been documented in the literature. Aromatic oxazines were first synthesized in 1944 by Holly and Cope through Mannich reactions from phenols, formaldehyde, and amines [6]. From the

1950s to the 1960s, many benzoxazines and naphthoxazines were synthesized by Burke and co-workers [7]. Fulop *et al*. reported the condensation of amino alkylnaphthols as precursors with phosgene in the presence of triethylamine giving naphthalene - condensed 1,3 - oxazin - 2 - one derivatives in moderate yields [8]. Cimarelli and co-workers used carbonyl di-imidazole instead of phosgene for the synthesis of these compounds [9]. Polyoxometalates (POMs) are attracting much attention as building blocks for functional composite materials because of their interesting nanosized structures [10–12]. This interest has resulted in the development of numerous protocols for the synthesis of nanostructured materials over a range of sizes. However, in spite of the extensive investigations on the synthesis and characterization of Keggin-type nanocatalysts [13–14], the synthesis of sodium 30-tungstopentaphosphate nanocatalysts has been largely overlooked.

In our attempt to use POMs as catalysts in organic reactions, we reported that Preyssler-type heteropolyacid $[NaP_5W_{30}O_{110}]^{14-}$ shows good catalytic reactivity [15–21]. We were encouraged by our recent success in working with POMs as green catalysts, and by the research in the field of nanotechnology [22–23]. In the last decades, heteropolyacids (HPAs) and related polyoxometalate compounds have attracted much attention as economically and environmentally friendly catalysts [24–32]. HPAs have very strong Brønsted acidity, approaching the superacid range; moreover, they are efficient oxidants. HPAs are very soluble in polar solvents such as water,

* To whom all correspondence should be sent:
E-mail: : *aligharib5@yahoo.com*

alcohols, ketones, *etc.* Therefore, HPAs are employed in homogeneous systems as acid and oxidation catalysts and, particularly, they show higher catalytic activity than mineral acids [22, 26, 29]. On the other hand, HPAs are non-toxic and mildly to non-corrosive, so they are generally recognized as clean and safe catalysts.

EXPERIMENTAL

Materials

All chemicals were purchased from Merck Company. Melting points were measured by the capillary tube method with an Electrothermal 9200 apparatus. All reactions were followed using Kieselgel 60 F256 TLC.

INSTRUMENTS

^{1}H NMR spectra were recorded on a Bruker AQS AVANCE-300 MHz spectrometer using TMS as an internal standard (DMSO solution). IR spectra were recorded in KBr disks on the FT-IR Bruker Tensor 27. Mass spectra were recorded using a MS 5973 Network Mass Selective detector. All products were characterized by ^{1}H NMR, FTIR, mass spectra and melting point.

Preparation of the silica supported Preyssler heteropolyacid catalyst, $H_{14}[NaP_5W_{30}O_{110}]/SiO_2$, ($H_{14}$–$P_5/SiO_2$), (50% catalyst loading):

$H_{14}[NaP_5W_{30}O_{110}]$, ($H_{14}$–$P_5$) was prepared by passing a solution of the potassium salt in water through a column (50 cm × 1 cm) of Dowex 50W×8 in the H^+ form and evaporating the eluate to dryness under vacuum. The supported heteropolyacid catalyst was synthesized according to our previous report [18] by impregnating the support (SiO_2 powder) with an aqueous solution of $H_{14}[NaP_5W_{30}O_{110}]$, ($H_{14}$–$P_5$). After stirring the mixture, the solvent was evaporated, dried at 120 ºC and was calcined at 250 ºC in a furnace prior to use.

GENERAL EXPERIMENTAL PROCEDURE

A mixture of an appropriate *β*-naphthol (2 mmol), aldehyde (2 mmol), urea (0.03 mol), silica supported Preyssler heteropolyacid, $H_{14}[NaP_5W_{30}O_{110}]/SiO_2$ (50% catalyst loading) as a catalyst (0.07 g) and C_2H_5OH (10 mL) was heated under reflux for a properiate time. The progress of the reaction was monitored by TLC. Then the

reaction mixture was filtered for separating the heterogeneous heteropolyacid catalyst and the reaction mixture was poured onto crushed ice, extracted with ethyl acetate and washed with water. The ethyl acetate extract was dried over anhydrous sodium sulphate and concentrated under reduced pressure. The crude product was re-crystallized from CH_2Cl_2.

SPECTRAL DATA:

1-phenyl-1*H*-naphtho[1,2-e][1,3]oxazin-3(2*H*)-one *(5a):*

m.p. 216–218ºC, IR (KBr, cm^{-1}) v_{max}: 3295, 1730, 1517; ^{1}H NMR (300 MHz, DMSO-d_6) δ_H: 6.17 (d, 1H, J = 2.1 Hz, CH), 7.76 (m, 11H, Arom.), 8.85 (s, 1H, NH); ^{13}C NMR (100 MHz, DMSO-d$_6$) δ_C: 54.22, 114.50, 117.30, 123.54, 125.53, 127.42, 127.81, 128.47, 129.08, 129.30, 129.41, 130.68, 130.86, 143.32, 147.85, 149.77; MS (m/z, %): 275 (M$^+$, 7), 231 (100), 202 (35). Anal. calcd for $C_{18}H_{13}NO_2$: C, 78.53; H, 4.76; N, 5.09. Found: C, 78.57; H, 4.71; N, 5.14.

1,2-Dihydro-l-(4-chlorolphenyl)-3*H*-naphth[1,2–e][1,3]oxazin-3-one *(5b):*

m.p. 209–210ºC, IR (KBr, cm^{-1}) v_{max}: 3222, 3145, 1734; ^{1}H NMR (300 MHz, DMSO-d_6) δ_H: 6.22 (1H, s, CH), 7.79 (10H, m, Arom.), 8.90 (1H, s, NH); ^{13}C NMR (100 MHz, DMSO-d6) δ_C: 53.40, 114.01, 117.32, 123.50, 125.60, 127.92, 128.06, 129.13, 129.23, 129.37, 129.42, 130.85, 133.06, 142.20, 147.90, 149.60; MS (m/z, %): 309 (M$^+$, 5), 265(60), 231(100), 202(27). Anal. calcd for $C_{18}H_{12}NO_2Cl$: C, 69.80; H, 3.90; N, 4.52. Found: C, 69.86; H, 3.84; N, 4.48.

1-(4-fluorophenyl)-1*H*-naphtho[1,2–e][1,3]oxazin-3(2*H*)-one *(5c):*

m.p. 201–203ºC, IR (KBr, cm^{-1}) v_{max}: 3134, 2952, 1755; ^{1}H NMR (300 MHz, DMSO-d_6) δ_H: 5.96 (1H, d, J = 3 Hz, CH), 7.71 (m, 10H, Arom.), 8.61 (d, 1H, J = 2.7 Hz, NH); ^{13}C NMR (100 MHz, DMSO-d$_6$) δ_C: 53.37, 114.28, 116.05, 116.35, 117.33, 123.50, 125.58, 127.86, 129.11, 129.56, 130.83, 139.58, 147.86, 149.69, 160.40, 163.65; MS (m/z, %): 294 (M$^+$+1, 15), 249 (100), 231(10), 220 (25). Anal. calcd for $C_{18}H_{12}FNO_2$: C, 73.71; H, 4.12; N, 4.78. Found: C, 73.75; H, 4.07; N, 4.72.

1-(4-bromophenyl)-1*H*-naphtho[1,2-e][1,3]oxazin-3(2*H*)-one *(5d):*

m.p. 218–220°C, IR (KBr, cm^{-1}) ν_{max}: 3145, 1732; ^{1}H NMR (300 MHz, DMSO-d_6) δ_H: 6.24 (s, 1H, CH), 7.79 (m, 10H, Arom.), 8.90 (s, 1H, NH); ^{13}C NMR (100 MHz, DMSO-d_6) δ_C: 53.55, 113.93, 117.32, 121.65, 123.47, 125.61, 127.90, 129.12, 129.22, 129.68, 130.86, 132.34, 142.60, 147.90, 149.60; MS (m/z, %): 353 (M$^+$, 25), 309 (100), 230 (100), 200 (100). Anal. calcd for C$_{18}$H$_{12}$NO$_2$Br: C, 61.04; H, 3.41; N, 3.95. Found: C, 61.07; H, 3.44; N, 3.91.

1-(2-chlorophenyl)-1*H*-naphtho[1,2-e][1,3]oxazin-3(2*H*)-one *(5e):*

m.p. 250–252°C, IR (KBr, cm^{-1}) ν_{max}: 3219, 3140, 1728; ^{1}H NMR (300 MHz, DMSO–d_6) δ: 6.51 (1H, s, CH), 7.67 (m, 10H, Arom.), 8.90 (s, 1H, NH); ^{13}C NMR (100 MHz, DMSO-d_6) δ_C: 52.15, 112.96, 117.30, 122.72, 125.58, 128.09, 128.80, 129.25, 129.32, 130.28, 130.51, 130.87, 131.10, 132.15, 139.95, 148.27, 149.13; MS (m/z, %): 309 (M$^+$, 9), 283(17), 231(100). Anal. calcd for C$_{18}$H$_{12}$NO$_2$Cl: C, 69.80; H, 3.90; N, 4.52. Found: C, 69.76; H, 3.85; N, 4.50.

1-(3-bromophenyl)-1*H*-naphtho[1,2-e][1,3]oxazin-3(2*H*)-one *(5f):*

m.p. 225–227°C, IR (KBr, cm^{-1}) ν_{max}: 3140, 1730; ^{1}H NMR (300 MHz, DMSO-d_6) δ_H: 6.25 (1H, s, CH), 7.89 (m, 10H, Arom.), 8.93 (s, 1H, NH); ^{13}C NMR (100 MHz, DMSO–d_6) δ_C: 53.47, 113.75, 117.36, 122.47, 123.48, 125.68, 126.30, 128.0, 129.15, 129.24, 130.39, 130.87, 131.01, 131.43, 131.77, 145.77, 148.01, 149.63; MS (m/z, %): 353 (M$^+$, 18), 310 (63), 231 (100). Anal. calcd for C$_{18}$H$_{12}$NO$_2$Br: C, 61.04; H, 3.41; N, 3.95. Found: C, 61.07; H, 3.45; N, 3.98.

RESULTS AND DISCUSSION

A convenient, efficient and green method for the synthesis of 1,2-dihydro-1-aryl-3*H*-naphth[1,2–*e*][1,3]oxazin-3-ones is reported (Scheme **1**).
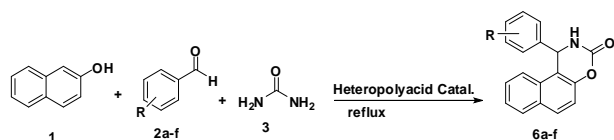
Scheme 1. Synthesis of 1,2-dihydro-1-aryl-3*H*-naphth[1,2–*e*][1,3]oxazin-3-ones using a H$_{14}$[NaP$_5$W$_{30}$O$_{110}$]/SiO$_2$ catalyst (50% catalyst loading).

The reaction of *β*-naphthol, benzaldehyde and urea in the presence of silica supported Preyssler heteropolyacid catalyst was investigated at properiate times under reflux conditions (Table **1**). We found that the reaction proceeds efficiently and with good yields with the aldehydes (**1**–**5**) having electron-withdrawing substituents, but the reaction yields were lower when the aldehydes (**6**–**7**) having electron-donating substituents (benzaldehydes) were used (Table **1**). According to the proposed mechanism, this reaction was considered to proceed through the acyliumin intermediate (**4**) (formed by reaction of the aldehyde (**2**) with urea (**3**) and H$^+$ of the Preyssler heteropolyacid catalyst) and the subsequent reaction of the *β*-naphtol (**1**) with the acyliumin (**4**), affording the product (**5**). At a high temperature, the product (**5**) underwent cyclization to afford the products (**5a–f**) (Scheme **2**).

Table 1. Results of the synthesis of 1,2-dihydro-1-aryl-3*H*-naphth[1,2-*e*][1,3]oxazin-3-ones using H$_{14}$[NaP$_5$W$_{30}$O$_{110}$]/SiO$_2$ (50% catalyst loading) under reflux conditions

Entry	Aldehyde	Time (min)	[a]Yield (%)
1		31	85
2		35	92
3		40	80
4		45	82
5		55	80
6		130	70.5
7		120	72
8		60	91

[a]Isolated yield.

The work-up procedure of this reaction is very simple. After completion of the reaction, the mixture was filtered off to separate the catalyst and the solvent was evaporated to dryness under reduced pressure. The pure products were obtained by re-crystallization from CH_2Cl_2.

Scheme 2. Mechanism of the synthesis of 1,2-dihydro-1-aryl-3*H*-naphth[1,2-*e*][1,3]oxazin-3-ones
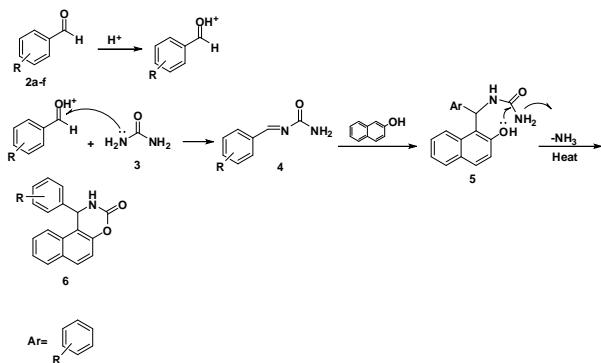
REUSABILITY OF THE CATALYST

At the end of the reaction, the catalyst could be recovered by simple filtration. The recovered catalyst was washed with dichloromethane and dried at 130 ºC for 1 h. The recycled catalyst was used for other reactions without appreciable loss in its catalytic activities (Table **2**). In addition, as a non-hygroscopic, non-corrosive and water stable solid acid, this catalyst is easily handled and suitable for large-scale operation. The reaction appears to be heterogeneously catalyzed. High yields, relatively short reaction times, simplicity of operation and easy work-up procedure are some other advantages of this protocol.

Table 2. Reusability of silica supported Preyssler heteropolyacid catalyst, $H_{14}[NaP_5W_{30}O_{110}]/SiO_2$ (50% catalyst loading) in the synthesis of 1-phenyl-1*H*-naphtho[1,2-*e*][1,3]oxazin-3(2*H*)-one (Table **1**, entry **8**).

Entry	Number of recycles	Time (min)	[a]Yield (%)
1	1	60	90
2	2	60	89
3	3	60	87
4	4	60	84

[a]Isolated yield

CONCLUSIONS

In conclusion, we have described a very simple and convenient procedure for the synthesis of 1,2-dihydro-1-aryl-3*H*-naphth[1,2–*e*][1,3]oxazin-3-one

derivatives catalyzed by the non-corrosive, and environmentally benign (green) Preyssler type heteropolyacid. Also, the catalyst is recyclable and could be reused without significant loss of activity. Even after four reaction runs, the catalytic activity of $H_{14}[NaP_5W_{30}O_{110}]/SiO_2$ (50% catalyst loading) was almost the same as that of the freshly used catalyst.

REFERENCES

1 N. Latif, N. Mishriky, F. M. Assad, *Aust. J. Chem.*, **35**, 1037 (1982).
2 Y. Wang, X. Li, K. Ding, *Tetrahedron Asym.*, **13**, 1291 (2002).
3 S. B. Sapkal, K. F. Shelke, B. B. Shingate, M. S. Shingare, *J. Korean. Chem. Soc.*, **54**, 437 (2010).
4 H. A. Ahangara, G. H. Mahdaviniab, K. Marjania, A. Hafeziana, *J. Iran. Chem. Soc.,* **7**, 770 (2010).
5 S. S. Kottawar, S. A. Siddiqui, S. R. Bhusare, Rasayan. *J. Chem.*, **3**, 646 (2010).
6 F. W. Holly, A. C. Cope, *J. Am. Chem. Soc.*, **66**, 1875 (1944).
7 W. J. Burke, *J. Am. Chem. Soc.*, **71**, 609 (1949).
8 I. Szatmari, A. Hetenyi, L. Lazar, F. Fulop, *J. Heterocyc. Chem.*, **41**, 367 (2004).
9 C. Cimarelh, G. Palmieri, E. Volpini, *Can. J. Chem.*, **82**, 1314 (2004).
10 Y. Mago, M. Lu, V. Wraback, H. Shen, *Journal of Applied Physics.*, **85**, 2595 (1999).
11 J. Zhang, R. M. Dickson, *J. Physics Review Letters.*, **93**, 077402 (2004).
12 B. Ding, J. Gong, J. Kim, S. Shiratori, *Nanotechnology.*, **16**, 785 (2005).
13 D. P. Sawant, A. Vinu, N. E. Jacob, F. Lefebvre, S. B. Halligudi, *Journal of Catalysis.*, **235** (2), 341 (2005).
14 Uchida, S., Mizuno, N. "Design and syntheses of nano-structured ionic crystals with selective sorption properties*", Coordination Chemistry Reviews.*, 251(21-24): 2537-2546 (2007).
15 F. F. Bamoharram, M. M. Heravi, M. Roshani, M. Akbarpour, *Journal of Molecular Catalysis A: Chemical.*, **255** (1-2), 193 (2006).
16 F. F. Bamoharram, M. M. Heravi, M. Roshani, M. Jahangir, A. Gharib, *Journal of Molecular Catalysis A: Chemical.*, 271 (1-2), 126 (2007).
17 F. F. Bamoharram, M. M. Heravi, M. Roshani, N. Tavakoli, *Journal of Molecular Catalysis A: Chemical.*, **252** (1-2), 219 (2006).
18 F. F. Bamoharram, M. M. Heravi, M. Roshani, M. Jahangir, A. Gharib, *Applied Catalysis A: General.*, **302** (1), 42 (2006).
19 F. F. Bamoharram, M. Roshani, M. H. Alizadeh, H. Razavi, M. Moghayadi, *Journal of The Brazilian Chemical Society.*, **17** (3), 505 (2006).

20 F. F. Bamoharram, M. M. Heravi, M. Roshani, A. Gharib, *Journal of the Chinese Chemical Society*., **54**, 1017 (2007).

21 F. F. Bamoharram, M. M. Heravi, M. Heravi, M. Dehghan, *Metal-Organic, and Nano-Metal Chemistry*., **39**, 394 (2009).

22 F. F. Bamoharram, K. D. Hosseini, A. Golmakani, *International Journal of Nanomanufacturing*., In Press (2009).

23 F. F. Bamoharram, M. M. Heravi, M. M. Heravi, M. Meraji, *International Journal of Green Nanotechnology: Physics and Chemistry*., **1**, 26 (2009).

24 I. V. Kozhevnikov, *Russ. Chem. Rev*., **56**, 811 (1987).

25 I. V. Kozhevnikov, *Catal. Rev. Sci. Eng*., **37**, 311 (1995).

26 M. Misono, *Catal. Rev. Sci. Eng*., **29**, 269 (1987).

27 M. Misono, *Stud. Surf. Sci. Catal*., **75**, 69 (1993).

28 M. Misono, N. Nojiri, *Appl. Catal*., **64**, 1 (1990).

29 T. Okuhara, N. Mizuno, M. Misono, *Adv. Catal*., **41**, 113 (1996).

30 I. V. Kozhevnikov, *Appl. Catal. A: Gen*., **256**, 3 (2003).

31 I. V. Kozhevnikov, *Chem. Rev*., **98**, 171 (1998).

32 I. V. Kozhevnikov, K. I. Matveev, *Appl. Catal*., **5**, 135 (1983).

ЕФЕКТИВЕН КАТАЛИТИЧЕН СИНТЕЗ НА 1,2- ДИХИДРО-1-АРИЛ-3Н-НАФТ[1,2-*E*][1,3]ОКСАЗИН-3-ОН ПРОИЗВОДНИ ПРИ ИЗПОЛЗВАНЕ НА ХЕТЕРОПОЛИКИСЕЛИНА НА НОСИТЕЛ СИЛИЦИЕВ ДИОКСИД $H_{14}[NAP_5W_{30}O_{110}]/SIO_2$ (50%) КАТО PREYSSLER ХЕТЕРОГЕНЕН КАТАЛИЗАТОР

А. Гариб [1,2], Б. Р.Х .Кхорасани[2], М. Джахангир[1], М. Рошани[1]

[1]*Катедра по химия, Ислямски университет Азад, Машхад, Иран*

[2]*Център по селскостопански изследвания и услуги, Машхад, Иран*

(Резюме)

Установено е, че хетерополикиселини тип Preyssler върху силициев диоксид са ефективен катализатор при синтеза на 1,2- дихидро-1-арил-3Н-нафт[1,2-е][1,3]оксазин-3-он производни с добър добив чрез удобна, ефективна и зелена реакция при кондензация на β– нафтол ароматни алдехиди, уреа и етанол при условия на отвеждане. Катализаторът се рециклира и използва отново няколко пъти.

A convenient catalytic synthesis of 2*H*-indazolo[2,1-*b*]phthalazine-triones on reusable silica supported Preyssler heteropolyacid

Ali Gharib [1,2]*, Bibi Robabeh Hashemipour Khorasani [2], Manouchehr Jahangir [1], J. (Hans) W. Scheeren [3]

[1]*Department of Chemistry, Islamic Azad University, Mashhad, IRAN*
[2]*Agricultural Researches and Services Center, Mashhad, IRAN*
[3]*Cluster for Molecular Chemistry, Department of Organic Chemistry, Radboud University Nijmegen, The Netherlands*

Efficient synthesis of 2*H*-indazolo[2,1-*b*]phthalazine-1,6,11(13*H*)-trione derivatives was achieved by one-pot three-component condensation reaction of phthalhydrazide, dimedone, and aromatic aldehydes under solvent-free conditions. Good to excellent yields were obtained at short reaction times on the reusable silica supported Preyssler heteropolyacid catalyst.

Keywords: Indazolo[2,1-*b*]phthalazine-trione, Phthalhydrazide, Dimedone, Preyssler, Heteropolyacid

INTRODUCTION

In the past few decades, the synthesis of new heterocyclic compounds has been a subject of great interest due to their wide applicability. Heterocyclic compounds widely occur in the nature and are essential to life. Among the large variety of heterocyclic compounds, heterocycles containing the phthalazine moiety are of interest because of their pharmacological and biological activities [1]. Phthalazine derivatives were reported to possess vasorelaxant [2], cardiotonic [3] and anticonvulsant [4] properties. A number of methods have been reported in the literature for the synthesis of phthalazine derivatives [5,6]. In recent decades, heteropolyacids (HPAs) have been used as catalysts for fine organic synthetic processes, thus being important for industries related with fine chemicals [7], including flavors, pharmaceuticals and food industries [8]. Heteropolyacids are more active catalysts than conventional inorganic and organic acids for various reactions in solutions [9]. They are used as industrial catalysts for several liquid phase reactions [10–13]. Among heteropolyacids, polytungstic acids are the most widely used catalysts owing to their high acid strengths, thermal stabilities, and low reducibilities. Catalysts based on heteropolyacids as Brønsted acids have many advantages over liquid acid catalysts. They are non-corrosive and environmentally benign, presenting fewer disposal problems. Solid heteropolyacids have attracted much attention in organic synthesis owing to easy work-up procedures, easy filtration, and minimization of cost and waste generation due to recycling and reuse of the catalysts [14-16]. Supported heteropolyacid on silica gel has been used as an effective catalyst for Diels Alder [17] and Fries rearrangement [18], as well as for Friedel-Crafts reactions [19]. In recent years, heterogeneous catalysts have gained importance due to economic and environmental considerations [1,3,20]. Among the various heterogeneous catalysts, particularly, heteropolyacids supported on silica gel have the advantages of low cost, ease of preparation, and catalyst recycling. These catalysts are generally less expensive, eco-friendly, highly reactive, easy to handle and recoverable.

EXPERIMENTAL

Materials

All chemicals were obtained from Merck and were used as received.

Instruments

^{1}H NMR spectra were recorded on a FT NMR Bruker 400 MHz spectrometer at 298 K. Melting points were recorded on an Electrothermal type 9100 apparatus and were uncorrected. Chemical shifts were reported in ppm (δ-scale) relative to the internal standard TMS (0.00 ppm); the solvent was

---

used as a reference. IR spectra were recorded on a Buck 500 scientific spectrometer (KBr pellets). The products were identified by comparison of their m.p., IR and NMR spectra with those of authentic samples.

Preparation of silica supported Preyssler heteropolyacid catalyst, $H_{14}[NaP_5W_{30}O_{110}]/SiO_2$ (50%)

$H_{14}[NaP_5W_{30}O_{110}]$, ($H_{14}$–$P_5$) was prepared by passing a solution of the potassium salt in water through a column (50 cm × 1 cm) of Dowex 50W×8 in the H$^+$ form and evaporating the eluate to dryness under vacuum. Supported heteropolyacid catalyst was obtained according to our previous report [21–24] by impregnating the support (SiO$_2$ powder) with an aqueous solution of $H_{14}[NaP_5W_{30}O_{110}]$, ($H_{14}$–$P_5$). After stirring the mixture, the solvent was evaporated, the product was dried at 120 ºC and was calcined at 250 ºC in a furnace prior to use.

General Procedure for the synthesis of 2H-indazolo[2,1-b]phthalazine-1,6,11(13H)-trione derivatives

A mixture of dimeone (1 mmol), aldehydes (1.5 mmol), phthalhydrazide (1 mmol) and silica supported Preyssler heteropolyacid catalyst (0.07 g) was heated under reflux conditions for the appropriate time (Table **2**). The reaction was monitored by TLC. After completion, the reaction mass was cooled to room temperature and was washed with water, then the solid residue was isolated and dissolved in CH$_2$Cl$_2$. The catalyst was filtered; the solvent was evaporated from the reaction mixture. The solid product was purified by re-crystallization from aqueous C$_2$H$_5$OH (25%). The products were characterized by comparison of their physical data with those of known compounds.

The spectral data of some representative 2H-indazolo[1,2–b]phthalazine-1,6,11(13H)-triones are given below.

3,4-Dihydro-3,3-dimethyl-13-phenyl-2H-indazolo[2,1-b]phthalazine-1,6,11(13H)-trione **(4a)** [25]:

Yellow powder. M.p. 203–205 °C; IR (KBr) v_{max}/cm^{-1}: 2953, 1564, 1572; ^{1}H NMR (CDCl$_3$, 400 MHz) δ: 8.31 (m, 2H), 7.85 (d, 2H, *J* = 3.2, 7.6 Hz), 7.43 (d, 2H, *J* = 7.2 Hz), 7.32 (m, 3H), 6.46 (s, 1H), 3.44 (d, 1H, *J* = 18.8 Hz), 3.26 (d, 1H, *J* = 2.4, 18.8 Hz), 2.36 (s, 2H), 1.23 (s, 6H); ^{13}CNMR (CDCl$_3$, 100 MHz) δ: 192.0, 156.0, 154.4, 150.8, 136.3, 134.5, 133.5, 129.0, 128.6, 128.0, 127.5, 127.1, 118.6, 65.1, 50.7, 38.0, 34.5. 28.7, 28.4; MS, *m/z* (%): 372 (M+, 15), 295 (100), 104 (84), 76 (67). Anal. calcd for C$_{23}$H$_{20}$N$_2$O$_3$: C 74.18, H 5.41, N 7.52; found: C 74.26, H 5.36, N 7.49.

3,4-Dihydro-3,3-dimethyl-13-(4-chlorophenyl)-2H-indazolo[2,1-b]phthalazine-1,6,11(13H)-trione **(4b)** [25]:

Yellow powder. M.p. 261–263 ºC; IR (KBr) v_{max}/cm^{-1}: 2950, 1651, 1628; ^{1}H NMR (CDCl$_3$, 400 MHz) δ: 8.31 (m, 2H), 7.86 (m, 2H), 7.35 (d, 2H, *J* = 8.4 Hz), 7.31 (d, 2H, *J* = 8.4 Hz), 6.43 (s, 1H), 3.40 (d, 1H, *J* = 18.8 Hz), 3.25 (dd, 1H, *J* = 2.0, 18.8 Hz), 2.36 (s, 2H), 1.24 (m, 6H); ^{13}C NMR (CDCl$_3$, 100 MHz) δ: 192.0, 156.0, 154.3, 151.0, 134.9, 134.6, 134.5, 133.5, 129.0, 128.9, 128.5, 128.0, 127.6, 118.0, 64.2, 50.9, 38.0, 34.6, 28.7, 28.4; Anal. calcd for C$_{23}$H$_{19}$ClN$_2$O$_3$: C 67.90, H 4.71, N 6.89; found: C 67.96, H 4.80, N 6.77.

3,4-Dihydro-3,3-dimethyl-13-(4-bromophenyl)-2Hindazolo[2,1-b]phthalazine-1,6,11(13H)-trione **(4c)** [25]:

White powder. M.p. 265–267 ºC; IR (KBr) v_{max}/cm^{-1}: 2956, 1655, 1623; ^{1}H NMR (CDCl$_3$, 400 MHz) δ: 1.20 (s, 3H, CH$_3$), 1.22 (s, 3H, CH$_3$), 2.35 (s, 2H, CH$_2$CO), 3.39 (d, *J*= 19.1 Hz, 2H), 6.40 (s, 1H, CHN), 8.32 (m, 8H, Ph); ^{13}C NMR (CDCl$_3$, 100 MHz) δ: 28.5, 28.7, 34.6, 38.1, 50.7, 64.5, 118.0, 122.7, 127.6, 128.1, 128.8, 128.9, 129.1, 131.9, 133.6, 134.7, 135.4, 151.1, 154.3, 156.0, 192.2; MS, m/z (%): 451 (Mþ, 7), 295 (100), 104 (28), 76 (34). Anal. calcd for C$_{23}$H$_{19}$BrN$_2$O$_3$: C, 61.21; H, 4.24; N, 6.21%. Found: C, 61.12; H, 4.16; N, 6.31%.

3,4-Dihydro-3,3-dimethyl-13-(4-methylphenyl)-2Hindazolo[2,1-b]phthalazine-1,6,11(13H)-trione **(4d)** [25]:

Yellow powder. M.p.: 226–228 ºC; IR (KBr) v_{max}/cm^{-1}: 2955, 1660, 1628, 1466, 1357, 1313, 1270, 1144, 1076, 1025, 826, 793, 699. ^{1}H NMR (CDCl$_3$, 400 MHz) δ: 8.29 (m, 2H), 7.84 (m, 2H), 7.30 (d, 2H, *J* = 8.0 Hz), 7.15 (d, 2H, *J* = 7.6 Hz), 6.44 (s, 1H), 3.42 (d, 1H, *J* = 18.8 Hz), 3.25 (dd, 1H, *J* = 2.0, 18.8 Hz), 2.32 (s, 2H), 2.31 (s, 3H), 1.21 (s, 6H); ^{13}C NMR (CDCl$_3$, 100 MHz) δ: 192.1, 156.0, 154.1, 150.6, 138.5, 134.7, 133.3, 133.5, 129.4, 129.2, 127.9, 127.7, 118.7, 64.7, 51.0, 38.0, 34.6, 28.7, 28.4, 21.0; Anal. calcd for C$_{24}$H$_{22}$N$_2$O$_3$: C 74.59, H 5.74, N 7.25; found: C 74.60, H 5.68, N 7.38.

3,4-Dihydro-3,3-dimethyl-13-(4-nitrophenyl)-2H-indazolo[2,1-b]phthalazine-1,6,11(13H)-trione **(4e)** [25]:

Yellow powder. M.p.: 217–219 ºC; IR (KBr) ν_{max}/cm^{-1}: 3075, 2957, 1693, 1660, 1616, 1520, 1365, 1275, 1143, 1100, 1018, 857, 793, 720. ^{1}H NMR (CDCl$_3$, 400 MHz) δ: 88.34 (m, 2H), 8.20 (d, 2H, J = 8.8 Hz), 7.90 (d, 2H, J = 1.6, 5.6 Hz), 7.65 (d, 2H, J = 8.8 Hz), 6.50 (s, 1H), 3.41 (d, 1H, J = 19.2 Hz), 3.26 (d, 1H, J = 2.0, 19.2 Hz), 2.33 (s, 2H), 1.23 (s, 6H); ^{13}C NMR (CDCl$_3$, 100 MHz) δ: 192.0, 155.8, 154.5, 151.5, 147.8, 143.5, 134.7, 133.8, 128.7, 128.5, 128.1, 128.0, 127.7, 124.0, 117.2, 64.0, 50.8, 38.0, 34.8, 28.9, 28.4; Anal. calcd for C$_{23}$H$_{19}$N$_3$O$_5$: C 66.18, H 4.59, N 10.07; found: C 66.23, H 4.50, N 10.02.

3,4-Dihydro-3,3-dimethyl-13-(3-nitrophenyl)-2*H*-indazolo[2,1-*b*]phthalazine-1,6,11(13*H*)-trione (**4f**) [26]:

Yellow powder. M.p.: 270–272 ºC; IR (KBr) ν_{max}/cm^{-1}: 3075, 2954, 1670, 1657, 1612, 1358, 1270, 1147, 1105, 1050, 720. ^{1}H NMR (CDCl$_3$, 400 MHz) δ: 8.33 (m, 2H), 8.17 (d, 2H, J = 7.2 Hz), 7.90 (m, 3H), 7.58 (t, 1H, J = 7.2 Hz), 6.53 (s, 1H), 3.45 (d, 1H, J = 19.6 Hz), 3.28 (d, 1H, J = 2.0, 19.6 Hz), 2.37 (s, 2H), 1.23 (s, 6H); ^{13}C NMR (CDCl$_3$, 100 MHz) δ: 192.0, 156.0, 154., 151.8, 148.5, 138.6, 134.2, 133.9, 129.6, 129.0, 128.5, 128.2, 127.7, 123.7, 121.4, 117.3, 64.0, 50.8, 38.0, 34.6, 28.7, 28.3; Anal. calcd for C$_{23}$H$_{19}$N$_3$O$_5$: C 66.18, H 4.59, N 10.07; found: C 66.19, H 4.66, N 10.03.

3,4-Dihydro-3,3-dimethyl-13-(4-fluorophenyl)-2*H*-indazolo[2,1-*b*]phthalazine-1,6,11(13*H*)-trione (**4g**) [25]:

Yellow powder. M.p. 218–220 ºC; IR (KBr) ν_{max}/cm^{-1}: 2950, 1668, 1660; ^{1}H NMR (CDCl$_3$, 400 MHz) δ: 8.30 (m, 2H), 7.85 (m, 2H), 7.40 (m, 2H), 7.03 (t, 2H, J = 8.8 Hz), 6.45 (s, 1H), 3.40 (d, 1H, J = 18.8 Hz), 3.25 (d, 1H, J = 2.4, 18.8 Hz), 2.36 (s, 2H), 1.23 (s, 6H); ^{13}C NMR (CDCl$_3$, 100 MHz) δ: 192.0, 163.9, 161.5, 156.0, 154.4, 151.0, 134.6, 133.6, 132.0, 129.0, 128.8, 128.0, 127.7, 118.1, 115.7, 115.6, 64.2, 50.9, 38.1, 34.5, 28.7, 28.4; Anal. calcd for C$_{23}$H$_{19}$FN$_2$O$_3$: C 70.76, H 4.91, N 7.18; found: C 70.83, H 4.84, N 7.26.

3,4-Dihydro-3,3-dimethyl-13-(2-chlorophenyl)-2*H*-indazolo[2,1-*b*]phthalazine-1,6,11(13*H*)-trione (**4h**) [26]:

Yellow powder. M.p.: 264–266 ºC, IR (KBr) ν_{max}/cm^{-1}: 3056, 2958, 2893, 1660, 1630, 1600, 1466, 1358, 1269, 1150, 1105, 1053, 757, 700. ^{1}H NMR (CDCl$_3$, 400 MHz) δ: 8.29 (m, 2H), 7.86 (m, 2H), 7.47 (d, 1H, J = 6.8Hz), 7.30 (m, 3H), 6.69 (s, 1H), 3.40 (d, 1H, J = 18.8 Hz), 3.25 (d, 1H, J = 2.0, 18.8 Hz), 2.32 (s, 2H), 1.24 (m, 6H); ^{13}C NMR (CDCl$_3$, 100 MHz) δ: 192.0, 156.3, 154.1, 151.9, 134.6, 133.5, 133.0, 132.5, 130.6, 129.7, 129.0,

128.7, 128.0, 127.7, 127.3, 64.1, 50.8, 38.1, 34.6, 28.9, 28.4; Anal. calcd for C$_{23}$H$_{19}$ClN$_2$O$_3$: C 67.90, H 4.71, N 6.89; found: C 70.01, H 4.67, N 6.94.

13-(3-chlorophenyl)-3,3-dimethyl-3,4-dihydro-2*H*-indazolo[1,2-*b*]phthalazine-1,6,11(13*H*)-trione (**4i**) [26]:

Yellow powder. M.p.: 204–206 ºC; IR (KBr) ν_{max}/cm^{-1}: 3067, 2959, 2870, 1656, 1626, 1578, 1465, 1360, 1312, 1269, 1145, 789, 700, 677; ^{1}H NMR (400 MHz, CDCl$_3$): δ 1.20 (s, 6H), 2.35 (s, 2H), 3.20 (d, 1H , J 19.1 Hz), 3. 42 (d, 1H, J 19.1 Hz), 6.40 (s, 1H), 7.30 (m, 4H), 7.85 (d, 2H, J 3.3, 5.7 Hz), 8.29 (m, 2H) ppm; ^{13}C NMR (100 MHz, CDCl$_3$): δ 28.5, 28.6, 34.6, 38.0, 50.8, 64.1, 117.8, 125.8, 127.0, 127.5, 128.1, 128.9, 129.0, 130.0, 133.6, 134.5, 138.5, 151.2, 154.4, 156.0, 192.1 ppm; MS: m/z (%) = 406 (M$^+$, 30), 296 (48), 295 (100), 239 (11), 149 (7), 130 (7), 104 (21), 76 (19), 55 (8), 43 (7). MS: m/z (%) = 406 (M+, 30), 296 (48), 295 (100), 239 (11), 149 (7), 130 (7), 104 (21), 76 (19), 55 (8), 43 (7). Anal. calcd for C$_{24}$H$_{22}$N$_2$O$_3$: C, 67.90; H, 4.71; N, 6.89; found: C, 67.98; H, 4.78; N, 6.94.

3,4-Dihydro-3,3-dimethyl-13-(3,4-dichlorophenyl)-2*H*indazolo[2,1-*b*]phthalazine-1,6,11(13*H*)-trione (**4j**) [26]:

Yellow powder. M.p.: 219–221 ºC ; IR (KBr) ν_{max}/cm^{-1}: 2965, 1660, 1627, 1469, 1390, 1352, 1314, 1265, 1145, 1100, 830, 701; ^{1}H NMR (CDCl$_3$, 400 MHz) δ: 8.31 (m, 2H), 7.88 (m, 2H), 7.44 (m, 2H), 7.31 (d, 1H, J = 2.0, 7.6 Hz), 6.38 (s, 1H), 3.40 (d, 1H, J = 19.2 Hz), 3.26 (d, 1H, J = 1.6, 19.2 Hz), 2.35 (s, 2H), 1.24 (s, 6H); ^{13}CNMR (CDCl$_3$, 100 MHz) δ: 192.0, 155.8, 154.6, 151.5, 136.7, 134.6, 133.8, 133.1, 132.8, 130.6, 128.9, 128.7, 128.1, 127.6, 126.8, 117.4, 63.8, 50.5, 38.0, 34.6, 28.6, 28.5; MS: m/z (%) = 440 (14), 405 (19), 383 (11), 296 (31), 295 (100), 104 (22), 76 (20), 55 (6); Anal. calcd for C$_{23}$H$_{18}$Cl$_2$N$_2$O$_3$: C 62.60, H 4.11, N 6.35; found: C 62.65, H 4.23, N 6.30.

3,4-Dihydro-3,3-dimethyl-13-(3,4,5-trimethoxyl)-2*H*indazolo[2,1-*b*]phthalazine-1,6,11(13*H*)-trione (**4k**):

Yellow powder. M.p.: 232–234 ºC; IR (KBr) ν_{max}/cm^{-1}: 2960, 1655, 1627, 1595, 1506, 1465, 1425, 1363, 1311, 1265, 1125, 1000, 700; ^{1}H NMR (CDCl$_3$, 400 MHz) δ: 8.32 (m, 2H), 7.81 (m, 2H), 6.63 (s, 2H), 6.40 (s, 1H), 3.82 (m, 9H), 3.45 (d, 1H, J = 18.8 Hz), 3.22 (d, 1H, J = 2.0, 18.8 Hz), 2.37 (s, 2H), 1.25 (s, 6H); ^{13}CNMR (CDCl$_3$, 100 MHz) δ: 192.1, 156.2, 154.5, 153.3, 150.5, 138.1, 134.5, 133.6, 131.7, 129.0, 128.8, 128.0, 127.8, 118.2, 104.5, 65.0, 60.8, 56.1, 50.9, 38.2, 34.7,

29.7, 28.8, 28.1; MS: m/z (%) = 462 (M$^+$, 38), 296 (22), 295 (100), 239 (7), 104 (10), 76 (8). Anal. calcd for $C_{26}H_{26}N_2O_6$: C 67.52, H 5.67, N 6.06; found: C 67.61, H 5.74, N 6.02.

3,3-dimethyl-13-o-tolyl-3,4-dihydro-2*H*-indazolo[1,2-*b*]phthalazine-1,6,11(13*H*)-trione (**4l**):

Yellow powder. M.p.: 241–243 ºC; IR (KBr) v_{max}/cm^{-1}: 3045, 2959, 1663, 1600, 1467, 1359, 1314, 1275, 1145, 1103, 1082, 797, 764, 701; ^{1}H NMR (400 MHz, CDCl$_3$): δ 1.20 (s, 3H), 1.21 (s, 3H), 2.30 (s, 2H), 2.77 (s, 3H), 3.26 (d, 1H, *J* 1.9, 19.1 Hz), 3.45 (d, 1H, *J* 19.0 Hz), 6.62 (s, 1H), 7.11 (m, 4H), 7.82 (m, 2H), 8.20 (d, 1H, *J* 3.2, 5.8 Hz), 8.36 (d, 1H, *J* 3.2, 5.9 Hz) ppm; ^{13}C NMR (CDCl$_3$, 100 MHz): δ 19.4, 28.3, 28.7, 34.7, 38.0, 50.8, 61.4, 119.8, 125.2, 126.4, 127.5, 128.0, 128.4, 129.1, 129.3, 130.8, 133.5, 134.6, 135.2, 137.0, 150.6, 154.0, 156.0, 192.2 ppm; MS: m/z (%) = 386 (M+, 4), 295 (27), 279 (32), 167 (73), 149 (100), 113 (21), 104 (13), 83 (13), 71 (35), 70 (29), 57 (48), 43 (27), 41 (24); Anal. calcd for $C_{24}H_{22}N_2O_3$: C, 74.59; H, 5.74; N, 7.25; found: C, 74.65; H, 5.80; N, 7.31.

13-(4-hydroxy-3-methoxyphenyl)-3,3-dimethyl-3,4-dihydro-2*H*-indazolo[1,2-*b*]phthalazine-1,6,11(13*H*)-trione (**4m**):

Yellow powder. M.p.: 250–252 ºC; IR (KBr) v_{max}/cm^{-1}: 3406, 2957, 1660, 1600, 1495, 1360, 1270, 1235, 1135, 1030, 791, 627; ^{1}H NMR (400 MHz, CDCl$_3$): δ 1.24 (s, 6H), 2.35 (s, 2H), 3.24 (d, 1H, *J* 19.0 Hz), 3. 45 (d, 1H, *J* 18.9 Hz), 3.90 (s, 3H), 5.31 (br, 1H), 6.40 (s, 1H), 6.79 (m, 2H), 7.08 (s, 1H), 7.29 (s, 1H), 7.86 (s, 2H), 8.30 (m, 2H) ppm; ^{13}C NMR (100 MHz, CDCl$_3$): δ 192.3, 156.2, 150.7, 146.5, 146.0, 134.5, 133.4, 129.3, 129.0, 128.1, 128.0, 127.6, 119.2, 118.5, 114.7, 111.0, 64.7, 56.0, 51.0, 38.2, 34.5, 28.7, 28.5 ppm; MS: m/z (%) = 418 (M+, 11), 415 (12), 295 (76), 231 (14), 162 (100), 132 (23), 104 (81), 77 (22), 76 (29), 51 (13), 50 (13); Anal. calcd for $C_{24}H_{22}N_2O_3$: C, 68.89; H, 5.30; N, 6.69; found: C, 68.95; H, 5.38; N, 6.76

RESULTS AND DISCUSSION

In continuation of our work on the catalytic properties of heteropolyacids [22–24], herein, we report a suitable method for the use of silica supported Preyssler heteropolyacid (50%) as a catalyst for the synthesis of 2,2-dimethyl-13-phenyl-2,3-dihydro-1*H*indazolo[2,1-*b*]phthalazine-4,6,11(13*H*)-trione (Scheme **1**).
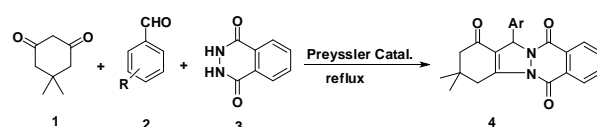
Scheme **1**

Dimedone **1**, phthalhydrazide **3**, and aromatic aldehydes **2a-m** in the presence of silica supported Preyssler heteropolyacid (50%) undergo a fast reaction under reflux at solvent-free conditions for several minutes to produce 2*H*-indazolo[2,1–*b*]phthalazine-1,6,11(13*H*)-triones **4a-m** (Table **1**). At these optimized reaction conditions, the scope and the efficiency of the procedures were explored for the synthesis of a wide variety of substituted 2*H*-indazolo[2,1-*b*]phthalazine-triones. The results are summarized in Table **1**. As shown in Table **1**, the direct three-component reactions worked well with a variety of aryl aldehydes including those bearing electron-withdrawing and electron-donating groups such as Me, OMe, Cl, F, Br and NO$_2$, and the desired compounds were obtained in high to excellent yields. This methodology offers significant improvements with regard to the scope of transformation, simplicity of operation, and green aspects avoiding expensive or corrosive catalysts. The structures of the products were established from their spectral properties (^{1}H NMR, ^{13}C NMR), elemental analysis and by comparison with available literature data. The formation of products **4a-4i** can be rationalized by initial formation of heterodiene **5** (Scheme **2**) using the standard Knoevenagel condensation of dimedone with aromatic aldehyde in the presence of a catalytic amount of silica supported Preyssler heteropolyacid (50%). Subsequent Michael-type addition of phthalhydrazide to the heterodienes followed by cyclization and dehydration afford the corresponding products **4a-4i** (Scheme **2**, Table **1**).

A possible mechanism for the formation of entries **4a–g**, **4h–k** in Table **1** is proposed in Scheme **2**. It is reasonable to assume that entries **4a–g**, **4h–k** in Table **1** result from the initial formation of the heterodiene **5** by standard Knoevenagel condensation of dimedone **1** and aldehyde **2**. Then, the subsequent Michael-type addition of the phthalhydrazide **3** to the heterodyne **5** followed by cyclization affords the corresponding products (Table **1**, entries **4a-g**, **4h-k**) and Scheme **2**.

Table 1. Synthesis of 2*H*-indazolo[2,1-*b*] phthalazine-1,6,11(13*H*)-trione derivatives in the presence of silica supported Preyssler heteropolyacid (50%) under reflux conditions

Entry	Compound	Aldehyde	Time (min)	[a]Yield (%)
1	4a	CHO (benzaldehyde)	8	94
2	4b	CHO, F (4-fluoro)	6	85
3	4c	CHO, Cl (4-chloro)	7	87.5
4	4d	CHO, Br (4-bromo)	6	92
5	4e	CHO, Cl (2-chloro)	7.5	88
6	4f	CHO, Cl (3-chloro)	10	91.5
7	4g	CHO, Cl, Cl (2,4-dichloro)	7	93.5
8	4h	CHO, O_2N (4-nitro)	11	89
9	4i	CHO, NO_2 (3-nitro)	15	80.5
10	4j	CHO, H_3C (4-methyl)	6.5	89
11	4k	CHO, CH_3 (2-methyl)	7	89.5
12	4l	H_3CO, CHO, HO	14	82.5
13	4m	H_3CO, CHO, H_3CO, OCH_3	9	84.5

[a] Isolated yield.

Scheme **2**

To recognize the capability of the present method in comparison with reported methods for the preparation of 2*H*-indazolo[2,1–*b*]phthalazine-1,6,11(13*H*)-trione derivatives from dimedone, aromatic aldehydes and phthalhydrazide, the model reaction of dimedone, benzaldehyde and phthalhydrazide was described. The reusability of the catalyst was tested in the synthesis of 3,3-dimethyl-13-phenyl-3,4-dihydro-1*H*-indazolo[1,2–*b*]phthalazine-1,6,11(2*H*,13*H*)-trione. HPA on silica is relatively inert toward HPAs, at least above a certain loading level, although some chemical interactions take place between HPA and SiO_2, the interaction involving the hydroxyl groups of silan and the acidic protons of heteropolyacids. The results show a decrease in the acidity of the silica supported Preyssler heteropolyacid in the following way: 10 %< 20 %< 30 %< 40% <50%. (Table 2).

Table 2. Synthesis of 3,3-dimethyl-13-phenyl-3,4-dihydro-1*H*-indazolo[1,2-*b*]phthalazine-1,6,11(2*H*,13*H*)-trione (**4a**) in the presence of silica supported Preyssler heteropolyacid under reflux conditions

[a]Yield (%)	Catalyst	Entry
28	$H_{14}[NaP_5W_{30}O_{110}]/SiO_2$ (10%)	1
43	$H_{14}[NaP_5W_{30}O_{110}]/SiO_2$ (20%)	2
60	$H_{14}[NaP_5W_{30}O_{110}]/SiO_2$ (30%)	3
72	$H_{14}[NaP_5W_{30}O_{110}]/SiO_2$ (40%)	4
94	$H_{14}[NaP_5W_{30}O_{110}]/SiO_2$ (50%)	5

[a] Isolated yield.

The catalyst was recovered after each run, washed with CH_2Cl_2, dried in an oven at 90 °C for 50 min prior to use and tested for its activity in the subsequent run. The catalyst was tested for 5 runs and it displayed very good reusability. The whole amount of the product could be isolated from the reaction mixture simply by CH_2Cl_2 extraction, and the catalyst system could be recovered and recharged with fresh substrates. Screening the system for five subsequent runs, the product was obtained in 93 %, 91%, 90%, 88% and 88% yields, respectively (Table **3**).

Table 3. Recycling of a silica supported Preyssler heteropolyacid catalyst $H_{14}[NaP_5W_{30}O_{110}]/SiO_2$ (50%) in the synthesis of 3,3-dimethyl-13-phenyl-3,4-dihydro-1*H*-indazolo[1,2-*b*]phthalazine-1,6,11(2*H*,13*H*)-trione (**4a**) under reflux conditions

Run	[a]Yield (%)
1	93
2	91
3	90
4	88
5	88

[a]Isolated yields and yields obtained in the first, second, third, fourth and fifth reuse of the catalyst.

CONCLUSIONS

A very simple and convenient procedure was described for the synthesis of 2*H*-indazolo[2,1-*b*]phthalazine-1,6,11(13*H*)-trione catalyzed by a three-component condensation reaction of dimedone, aromatic aldehydes and phthalhydrazide using the non-corrosive, and environmentally benign (green) silica supported Preyssler type heteropolyacid $H_{14}[NaP_5W_{30}O_{110}]/SiO_2$ (50%) under solvent-free conditions. In addition, it is possible to apply the tenets of green chemistry to the generation of biologically interesting products in solvent-free media, which is less expensive and less toxic than using organic solvents. Also, the catalyst is recyclable and could be reused without significant loss of activity. Even after three reaction runs, the catalytic activity of silica supported Preyssler heteropolyacid, $H_{14}[NaP_5W_{30}O_{110}]/SiO_2$ (50%), was almost the same as that of the freshly used catalyst.

REFERENCES

1 R. W. Carling, K. W. Moore, L. J. Street, D. Wild, C. Isted, P. D. Leeson, S. Thomas, D. O'Conner, R. M. McKernan, K. Quirk, S. M. Cook, J. R. Atack, K. A. Wafford, S. A. Thompson, G. R. Dawson, P. Ferris, J. L. Castro, *J. Med. Chem*., **47**, 1807 (2004).

2 S. Grasso, G. DeSarro, N. Micale, M. Zappala, G. Puia, M. Baraldi, C. Demicheli, *J. Med. Chem*., **43**(15), 2851 (2000).

3 Y. Nomoto, H. Obase, H. Takai, M. Teranishi, J. Nakamura, K. Kubo, *Chem. Pharm. Bull. (Tokyo)*, **38**, 2179 (1990).

4 N. Watanabe, Y. Kabasawa, Y. Takase, M. Matsukura, K. Miyazaki, H. Ishihara, K. Kodama, H. Adachi, *J. Med. Chem.,* **41**(18), 3367 (1998).

5 T. Sheradsky, R. Moshenberg, *J. Org. Chem.,* **51**(16), 3123 (1986).

6 H. W. Heine, L. M. Baclawski, S. M.; Bonser, G. D. Wachob, *J. Org. Chem.,* **41**(20), 3229 (1976).

7 I. V. Kozhevnikov, In: Derouane, E.; Ed., *Catalysts for Fine Chemical Synthesis, Catalysis by Polyoxometalates 2;* Wiley, New York, 2002.

8 T. Okuhara, N. Mizuno, M. Misono, *Adv. Catal.*, **41**, 113 (1996).

9 R. S. Drago, J. A. Dias, T. Maier, *J. Am. Chem. Soc*., **119**(33), 7702 (1997).

10 Y. Ono, J. M. Thomas, K. I. Zamaraev, Eds., *Perspectives in Catalysis*; Blackwell, London, (1992) p. 341.

11 I. V. Kozhevnikov, K. I Matveev, *Appl. Catal.,* **5** (2), 135 (1983).

12 Y. Izumi, K. Urabe, A. Onaka, Zeolite, *Clay and Heteropolyacids in Organic Chemistry*; Kodansha/VCH, Tokyo/Weinheim, (1992) p. 99.

13 I. V. Kozhevnikov, *Catal. Rev. Sci. Eng*., **37**, 311 (1995).

14 M. A. Schwegler, H. Bekkum, N. Munck, *Appl. Catal*. A., **74**, 191 (1991).

15 R. Fazaeli, S. Tangestaninejad, H. Aliyan, *Can. J. Chem.*, **84,** 812 (2006)

16 G. Meuzelaar, L. Maat, R. Sheldon, I. V. Kozhevnikov, *Catal. Lett*. **45**, 249 (1997).

17 E. F. Kozhevnikova, E. Rafiee, I. V. Kozhevnikov, *Appl. Catal. A*., **260**, 25 (2004).

18 Y. Isumi, K. Hisano, T. Hida, Appl. Catal. A., **181**, 277 (1999).

19 J. Mao, T. Nakajo, T. Okuhara, *Chem. Lett.* **11**, 1104 (2002).

20 S. Grasso, G. DeSarro, N. Micale, M. Zappala, G. Puia, M. Baraldi, C. Demicheli, *J. Med. Chem.*, **43**, 2851 (2000).

21 F. F. Bamoharram, M. M. Heravi, M. Roshani, M. Jahangir, A. Gharib, *Appl. Catal. A,* **302** (1), 42 (2006).

22 A. Gharib, J. (Hans) W. Scheeren, F. F. Bamoharram, M. Roshani, M. Jahangir. Polish *Journal of Chemical Technology.,* **11** (2), 31 (2009).

23 F. F. Bamoharram, M. M. Heravi, M. Roshani, A. Gharib, M. Jahangir, *Journal of the Chinese Chemical Society*., **54**, 1017 (2007).

24 A. Gharib, M. Jahangir, M. Roshani, Magazine of the Royal *Australian Chemical Institute In*c., **76**(2), 12 (2009).

25 H. A. Shaterian, M. Ghashang, M. Feyzi, *Appl. Catal. A.,* **345**, 128 (2008).

26 M. Sayyafi, M. Seyyedhamzeh, H. R. Khavasi, A. Bazgir, *Tetrahedron*, **64**, 2375 (2008).

УДОБЕН КАТАЛИТИЧЕН СИНТЕЗ НА 2H- ИНДАЗОЛО[2,1-B]ФТАЛАЗИН-ТРИ-ОНИ ВЪРХУ ВЪЗОБНОВЯЕМА ХЕТЕРОПОЛИКИСЕЛИНА ТИП PREYSSLER ВЪРХУ СИЛИЦИЕВ ДИОКСИД

А. Гариб [1,2], Б. Р. Х. Кхорасани [2], М. Джахангир [1], Ю.(Ханс) В. Шаарен [3]

[1] *Катедра по химия, Ислямски университет Азад, Машхад, Иран*

[2] *Център по селскостопански изследвания и услуги, Машхад, Иран*

[3] *Клъстер Молекулна химия, Катедра по органична химия, Университет Радбуд, Неймехен, Холандия*

(Резюме)

Ефективен метод за синтез на 2H- индазоло[2,1-b]фталазин-три-он производни е осъществен чрез едностъпкова три компонентна кондензация на фталов хидразид, димедон и ароматни алдехиди при условия без разтворител. Получени са добри до отлични добиви за кратко реакционно време върху възобновяема хетерополикиселина тип Preyssler като катализатор при използване на носител силициев диоксид.

Design and Synthesis of *N*-[2- (2,3-dimethoxy-strychnidin-10-ylidenamino)-ethyl]-succinamic acid 4-allyl-2-methoxy-phenyl ester

[1]L. Figueroa-Valverde[*], [2]F. Díaz-Cedillo, [1]E. García-Cervera, [1]E. Pool-Gómez, [1]M. López-Ramos

[1]*Laboratorio de Farmacoquímica de la Facultad de Ciencias Químico-Biológicas de la Universidad Autónoma de Campeche, Av. Agustín Melgar, Col Buenavista C.P.24039, Campeche Cam., México.*
[2]*Escuela Nacional de Ciencias Biológicas del Instituto Politécnico Nacional. Prol. Carpio y Plan de Ayala s/n Col. Santo Tomas, México, D.F. C.P. 11340.*

In this study a brucine derivative was synthesized using several strategies. In the first stage the compound 4-(4-allyl-2-methoxy-phenoxy)-4-oxobutanoic acid (**3**) was obtained by the reaction of 4-allyl-2-methoxyphenol with succinic acid using N,N'-diciclohexylcarbodiimide/*p*-toluensulfonic acid as a catalyst. The second stage was achieved by the reaction of **3** with ethylenediamine to form 4-allyl-2-methoxyphenyl 4-[(2-aminoethyl)amino]-4-oxobutanoate (**5**) in presence of a carbodiimide derivative. Finally, the compound *N*-[2-(2,3-dimethoxy-strychnidin-10-ylidenamino)-ethyl]-succinamic acid 4-allyl-2-methoxy-phenyl ester (**7**) was prepared by the reaction of **3** with N[1]-(2,3-dimethoxystrychnidin-10-yliden)-ethane-1,2-diamine using as a catalyst a carbodiimide derivative. The compound **7** was also synthesized by the reaction between **5** and brucine using boric acid as a catalyst.

Keywords. Brucine, ethylenediamine, succinic acid, carbodiimide.

INTRODUCTION

Since several years ago, some derivatives of brucine have been developed for use in different biological and analytical methods1[1-4]. For example, there are studies which show the synthesis of N-chloromethylbrucine chloride by the reaction of brucine with dichloromethane [5]. Other studies have shown the preparation of a brucine derivative (brucidine) by electrolytic reduction of brucine [6]. In addition, there are reports of the synthesis of N-(5-carboxypentyl)brucinium bromide via N-alkylation of brucine with 6-bromohexanoic acid [7]. Other experimental data showed the preparation of the compounds brucinium hydrogen (S)-malate pentahydrate and anhydrous brucinium hydrogen (2R,3R)-tartrate by the reaction between brucine and D-L-malic acid or L-tartaric acid in ethanol-water medium [8]. Additionally, porphyrin-brucine conjugates were synthesized by N-alkylation of brucine with alkylbromotetraphenylporphyrin derivatives [9].

Recently, a brucine derivative (N[1]-(2,3-dimethoxystrychnidin-10-yliden)-ethane-1,2-diamine) was synthesized by the reaction of brucine and ethylenediamine using boric acid as a catalyst. Another brucine derivative (11-[(2-amino-ethylamino)-methyl]-2,3-dime-thoxystrychnidin-10-one) was prepared by the reaction of brucine with ethylenediamine in presence of formaldehyde [10]. Another study described the synthesis of a brucine-dihydropyrimidine derivative using the multi-component system (brucine, benzaldehyde and thiourea) [11]. All these experimental data reveal that several procedures for synthesis of brucine derivatives are available; however, expensive reagents and special conditions are required. Therefore, in this study a new brucine derivative (*N*-[2-(2,3-dimethoxy-strychnidin-10-ylidenamino)-ethyl]-succinamic acid 4-ally-2-methoxy-phenyl ester) was synthetized using several chemical methods.

EXPERIMENTAL

General methods

N[1]-(2,3-dimethoxystrychnidin-10-yliden)-ethane-1,2-diamine (**6**) was prepared according to a previously reported method by Figueroa [10]. The other compounds used in this study were purchased from Sigma-Aldrich Co., Ltd. The melting points for the different compounds were determined on an Electrothermal (900 model) device. Infrared spectra (IR) were recorded in KBr pellets on a Perkin Elmer Lambda 40 spectrometer. ^{1}H and ^{13}C NMR spectra were recorded on a Varian VXR-300/5 FT

---

* To whom all correspondence should be sent:
E-mail: lauro_1999@yahoo.com

NMR spectrometer at 300 and 75.4 MHz in CDCl₃ using TMS as internal standard. EIMS spectra were obtained with a Finnigan Trace GCPolaris Q. spectrometer. Elemental analysis data were acquired from a Perkin Elmer Ser. II CHNS/0 2400 elemental analyzer.

4-(4-allyl-2-methoxyphenoxy)-4-oxobutanoic acid (3)

A solution of 4-allyl-2-methoxyphenol (100 mg, 0.61 mmol), succinic acid (144 mg, 1.22 mmol), N,N'-dicyclohexylcarbodiimide (190 mg, 0.92 mmol) and *p*-toluenesulfonic acid anhydrous
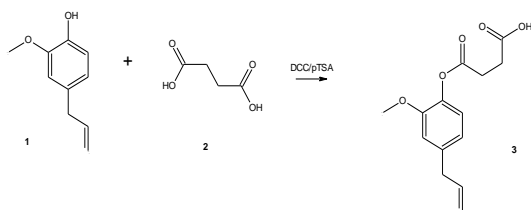
Fig. 1. Synthesis of 4-(4-allyl-2-methoxy- phenoxy)-4-oxobutanoic acid (**3**). Reaction between 4-allyl-2-methoxyphenol (**1**) and succinic acid (**2**) using N,N'-dicyclohexylcarbodiimide/*p*-toluenesulfonic acid (DCC/p-TSA) as a catalyst.

(110 mg, 0.64 mmol) in 10 mL of methanol was stirred for 72 h at room temperature. The reaction mixture was evaporated to a smaller volume. Then the mixture was diluted with water and extracted with chloroform. The organic phase was evaporated to dryness under reduced pressure, the residue was purified by crystallization from methanol:water (3:1) yielding 62 % of product, m.p. 190–194 ºC; IR (V$_{max}$, cm^{-1}): 1734, 1720 and 1624; ^{1}H NMR (300 MHz, CDCl₃) δ$_H$: 2.60 (t, 2H, $J = 6.00$ Hz), 2.90 (t, 2H, $J = 6.00$ Hz), 3.32 (m, 2H), 3.76 (s, 3H), 5.03 (d, d, 1H, $J = 1.76$ Hz, 16.07), 5.10 (d, d, 1H, $J = 1.76$ Hz, 11.05), 5.97 (m, 1H), 6.74 (d, 2H, $J = 8.13$), 7.05 (d, 1H, $J = 8.13$), 8.60 (s, 1H) ppm. ^{13}C NMR (75.4 Hz, CDCl₃) δ$_C$: 29.31(**C**-16), 29.63 (**C**-15), 39.35 (**C**–12), 55.80 (**C**-8), 113.24 (**C**-6), 115.52 (**C**-14), 122.14 (**C**–3), 122.43 (**C**–4), 137.70 (**C**-13), 139.43 (**C**–5), 151.98 (**C**-2), 171.39 (**C**–10), 174.10 (**C**–17) ppm. MS (70 ev): $m/z = 234.10$ (M$^+$). Anal. calcd. for C$_{14}$H$_{16}$O$_5$: C, 63.63; H, 6.10; O, 30.27. Found: C, 63.60; H, 6.12.

4-allyl-2-methoxyphenyl 4-[(2-aminoethyl)amino]-4-oxobutanoate (5)

A solution of **3** (100 mg, 0.38 mmol), ethylenediamine (144 mg, 1.22 mmol) and N-(3-

dimethylaminopropyl)-N'-ethylcarbodiimide (90 mg, 0.58 mmol) in 10 mL of methanol was stirred for 72 h at room temperature. The reaction mixture was evaporated to a smaller volume. Then the mixture was diluted with water and extracted with chloroform. The organic phase was evaporated to dryness under reduced pressure, the residue was purified by crystallization from methanol:water (3:1) yielding 45 % of product, m.p. 198–200 ºC; IR (V$_{max}$, cm^{-1}): 3382, 1730, 1680 and 1622; ^{1}H NMR (300 MHz, CDCl₃) δ$_H$: 2.44 (t, 2H, $J = 6.20$ Hz), 2.74 (t, 2H, $J = 6.20$ Hz), 2.98 (t, 2H, $J = 6.00$ Hz), 3.28 (m, 2H), 3.33 (t, 2H, $J = 6.00$ Hz), 3.80 (s, 3H), 4.86 (broad), 5.02 (d, d, 1H, $J = 1.76$ Hz, 16.07), 5.10 (d, d, 1H, $J = 1.76$ Hz, 16.07), 5.97 (m, 1H), 6.78 (d, d, 1H, $J = 1.76$ Hz, 16.07), 6.90 (d, d, 1H, $J = 1.76$ Hz, 16.07) ppm. ^{13}C NMR (75.4 Hz, CDCl₃) δ$_C$: 29.58 (**C**–15), 30.42 (**C**–16), 39.35 (**C**-12), 41.99 (**C**-21), 42.68 (**C**-20), 55.80 (**C**–8), 112.86 (**C**–6), 115.51 (**C**–14), 121.51 (**C**–3), 129.41 (**C**–4), 137.70 (**C**–13), 139.45 (**C**–2, **C**–5), 151.60 (**C**–1), 169.56 (**C**–10), 172.71 (**C**-17) ppm. MS (70 ev): $m/z = 306.20$ (M$^+$). Anal. calcd. for C$_{16}$H$_{22}$N$_2$O$_4$: C, 62.73; H, 7.24; N, 9.14; O, 20.89. Found: C, 62.70; H, 7.20; N, 9.10.

N-[2-(2,3-dimethoxy-strychnidin-10-ylidenamino)-ethyl]-succinamic acid 4-allyl-2-methoxy-phenyl ester (7).
Method A.

A solution of **3** (100 mg, 0.38 mmol) and **6** (170 mg, 0.39 mmol), N-(3-dimethylaminopropyl)-N'-ethylcarbodiimide (110 mg, 0.70 mmol) in 10 mL of methanol was stirred for 48 h at room temperature. The reaction mixture was evaporated to a smaller volume. Then the mixture was diluted with water and extracted with chloroform. The organic phase was evaporated to dryness under reduced pressure, the residue was purified by crystallization from methanol:water (4:1) yielding 72 % of product, m.p. 164–166 ºC; IR (V$_{max}$, cm^{-1}): 2812, 1738, 1678, 1628; ^{1}H NMR (300 MHz, CDCl₃) δ$_H$: 1.40–1.46 (m, 2H), 1.64–1.72 (m, 3H), 1.80-1.89 (m, 3H), 2.23–2.37 (m, 2H), 2.49 (t, 2H, $J = 6.3$ Hz), 2-52-2.66 (m, 2H), 2.69-2.71 (m, 2H), 2.72 (t, 2H, $J = 6.3$ Hz), 2.75 (m, 1H), 2.92 (m, 1H), 3.22 (m, 2H,), 3.33 (t, 2H, $J = 6.3$ Hz), 3.52-3.58 (m, 2H), 3.60–3.64 (m, 2H), 3.73 (t, 2H, $J = 6.3$ Hz), 3.80 (s, 6H), 3.94 (s, 3H), 4.70 (m, 1H), 5.03 (d, d, 1H, $J = 1.75$ Hz, 16.03), 5.10 (d, d, 1H, $J = 1.75$ Hz, 11.05), 5.83 (s, 1H), 5.97 (m, 1H), 6.71–6.79 (d, 2H, $J = 8.50$ Hz), 6.95 (d, 2H, $J = 8.50$ Hz), 7.55 (s, 1H), 8.12 (broad) ppm. ^{13} C NMR (75.4 Hz, CDCl₃) δ$_C$: 28.12 (**C**-13), 29.22 (**C**-

36), 29.58 (**C**–4), 30.43 (**C**-17), 38.79 (**C**–8), 39.35 (**C**-48), 40.72 (**C**-27), 45.65 (**C**-9), 51.6 (**C**-26), 52.24 (**C**-7), 55.80 (**C**-47), 56.01 (**C**–34), 56.29 (**C**-32), 59.92 (**C**–5), 64.62 (**C**-18), 65.06 (**C**–10), 66.82 (**C**-2), 79.27 (**C**-27), 98.33 (**C**–21), 105.71 (**C**–24), 113.22 (**C**-41), 115.53 (**C**–50), 121.51 (**C**–44), 122.87 (**C**-43), 129.27 (**C**–19), 137.76 (**C**–49), 138.80 (**C**–20), 139.15 (**C**–42), 139.45 (**C**–39), 143.26 (**C**-23), 147.76 (**C**-22), 147.82 (**C**-12), 151.61 (**C**–40), 169.56 (**C**–37), 172.73 (**C**–29) ppm. MS (70 ev): *m/z* = 684.30 (M$^+$). Anal. calcd. for C$_{39}$H$_{48}$ N$_4$O$_7$: C, 68.40; H, 7.06; N, 8.18; O, 16.35. Found: C, 68.38; H, 7.02; N, 8.06.

Method B.

A solution of **5** (100 mg, 0.32 mmol), brucine (127 mg, 0.32 mmol) and boric acid (60 mg, 0.80 mmol) in 10 mL of methanol was stirred for 72 h at room temperature. The reaction mixture was evaporated to a smaller volume. Then the mixture was diluted with water and extracted with chloroform. The organic phase was evaporated to dryness under reduced pressure, the residue was purified by crystallization from methanol:water (4:1) yielding 38 % of product. The ^{1}H NMR and ^{13}C NMR data of the product were similar to those of the product obtained by method A.

RESULTS AND DISCUSSION

It should be mentioned that some procedures for obtaining of brucine derivatives are available in the literature. Nevertheless, these procedures suffer from several drawbacks: some reagents are of limited stability; preparation can be dangerous[6–8]. Therefore, in this study we report a route for synthesis of a new brucine derivative (**7**) using several strategies. The first step involves the esterification of the hydroxyl group of compound **1** to form **3**. The synthesis of **3** has been reported previously [12]; nevertheless in this study a new strategy for its development was used. Although there are diverse reagents available to produce ester derivatives [13, 14], most of the conventional methods are of limited use for some compounds. Therefore, in this study the method reported by Erlanger and co-workers [15] for esterification of other compounds was used. Thus, compound **3** was synthesized by the reaction of compound **1** with succinic acid using 1,3-dicyclohexylcarbodiimide (DCC) as coupling reagent. When DCC is used alone as a condensing agent in ester synthesis, the yield of esters is often unsatisfactory due to formation of an N-acylurea by-product. Some reports showed that addition of a catalytic amount

of a strong acid to the esterification reaction in the presence of DCC considerably increases the yield of esters and decreases the formation of N-acylurea [16]. Therefore, *p*-toluenesulfonic acid was used to increase the yield of **3** in the esterification of **1** with succinic acid in the presence of DCC.

On the other hand, in the ^{1}H NMR spectrum of **3** there are signals at 2.60–2.90 ppm for methylenes bound to carboxyl group, at 3.32 ppm for methylene bound to phenyl group; at 3.76 ppm for methoxy group; 5.03–5.97 ppm for protons involved in the alkene group; at 6.74–7.05 ppm for hydrogens of phenyl group. Finally, a signal at 8.60 ppm for carboxyl group was found. The ^{13}C NMR spectrum contains peaks at chemical shifts of 29.31–29.63 ppm for protons involved in the methylenes bound to carboxyl group. Other signals at 39.35 ppm for methylene bound to phenyl group; at 55.80 ppm for methoxy group; at 113.24, 122.14 and 139.43–171.39 ppm for phenyl group were found. Finally, signals at 115.52 and 137.70 ppm for alkene group; at 174.10 ppm for carboxyl group were displayed. The presence of **3** was further confirmed from the mass spectrum which showed a molecular ion at m/z 264.10.
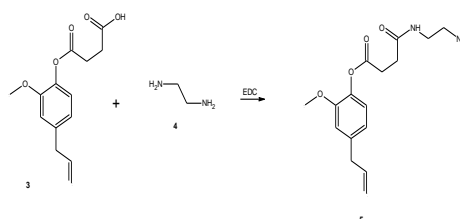
Fig.2. Synthesis of 4-allyl-2-methoxyphenyl 4-[(2-aminoethyl)amino]-4-oxobutanoate (**5**). Reaction between 4-(4-allyl-2-methoxy-phenoxy)-4-oxobutanoic acid (**3**) with ethylenediamine (**4**) in presence of N-(3-Dimethylaminopropyl)-N'-ethylcarbodiimide (EDC) to form **5**.

The second step was achieved by the reaction of **3** with ethylenediamine (**4**) to form an amide group involved in compound **5** (Figure 2). Although many procedures for the formation of amides are known in the literature, the most widely used one employs carboxylic acid chlorides as electrophiles which react with the amino group in the presence of an acid scavenger [17]. Despite its wide scope, this protocol suffers from several drawbacks: limited stability of many acid chlorides and hazardous reagents needed for their preparation (e.g., thionyl chloride) [18]. Therefore, in this study N-(3-dimethylaminopropyl)-N'-ethylcarbodiimide (EDC) [19] was used to form compound **5**.
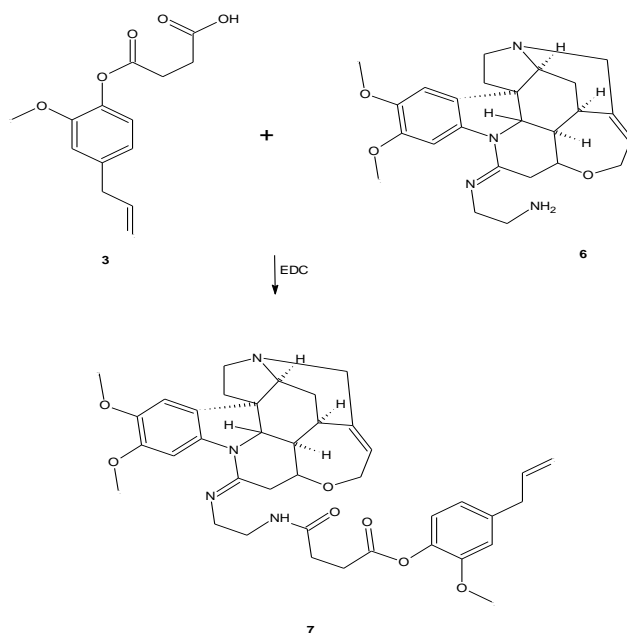
Fig. 3. Synthesis of *N*-[2-(2,3-dimethoxy-strychnidin-10-ylidenamino)-ethyl]-succinamic acid 4-ally-2-methoxy-phenyl ester (**7**). Reaction of 4-(4-allyl-2-methoxy- phenoxy)-4-oxobutanoic acid (**3**) with *N¹-(2,3-dimethoxystrychnidin-10-yliden)-ethane-1,2-diamine* (**6**) to form **7** using N-(3-Dimethylaminopropyl)-N'-ethylcarbodiimide (EDC) as catalyst.
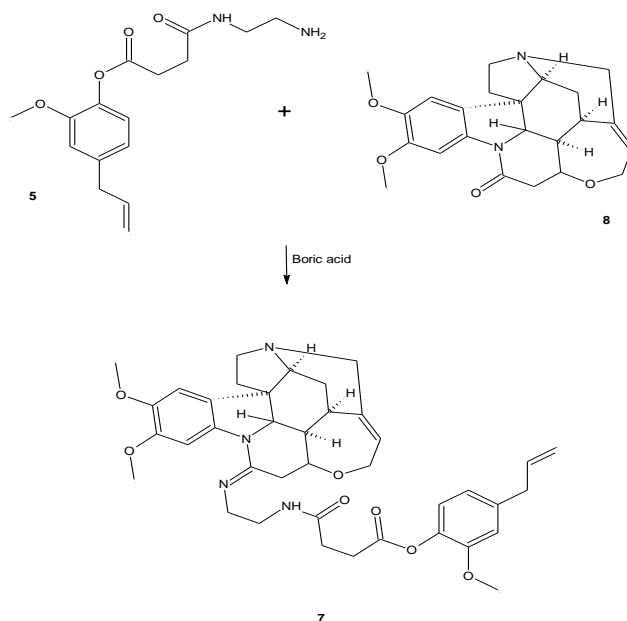
Figure 4. Synthesis of *N*-[2-(2,3-dimethoxy-strychnidin-10-ylidenamino)-ethyl]-succinamic acid 4-allyl-2-methoxy-phenyl ester (**7**). Reaction between 4-allyl-2-methoxyphenyl 4-[(2-aminoethyl)amino]-4-oxobutanoate (**5**) and brucine (**8**) to form **7** using boric acid as a catalyst.

The ¹H NMR spectrum of **5** shows signals at 2.44–2.74 ppm for methylenes bound to both amide and ester groups; at 2.98–3.28 ppm for methylenes bound to both amide and amine groups; at 3.33 ppm for methylene bound to phenyl group. Finally, other signals at 3.80 ppm for methoxy group; at 4.86 ppm for both amide and amine groups; at 5.02-

5.97 ppm for protons involved in the alkene group; at 6.78-6.90 ppm phenyl group were found. It should be mentioned that the ¹H NMR spectra of the secondary amides are usually more complex than the primary amides due to the presence of a substituent bound to the amide nitrogen atom. These substituents produce a much wider range of

chemical shifts for the amide proton which may, in addition, display coupling to aliphatic groups bound to it. The chemical shifts of aliphatic groups bound to the carbonyl group are similar to those observed for the primary amides, while those groups bound to the nitrogen resonate at slightly lower field than the corresponding amines [20].

On the other hand, the ^{13}C NMR spectrum of **5** contains peaks at chemical shifts of 29.58–30.42 ppm for methylenes bound to both amide and ester groups; at 39.35 ppm for methylene bound to phenyl group; at 41.99–42.68 ppm for methylenes bound to both amide and amine groups; at 55.80 ppm for methoxy group; at 112.86, 121.51–129.41, 139.45–151.60 ppm for carbons of phenyl group. Finally, other signals at 115.51 and 137.70 ppm for alkene group; at 169.56 ppm for ester group; at 172.71 ppm for both amide and amine groups were found. The presence of **5** was further confirmed from the mass spectrum which showed a molecular ion at m/z 306.20.

On the other hand, the compounds **3** and **5** were bound to the brucine nucleus; in the first case, **3** reacted with **6** to form **7** using a carbodiimide derivative as a catalyst (method A). The ^{1}H NMR spectrum of **7** shows signals at 140–2.37, 2.52–2.71, 2.75–2.92, 3.52–3.64, 4.70, 5.83 and 7.55 ppm for the brucine nucleus; at 3.22 ppm for methylene bound to phenyl group; at 3.33 and 3.73 ppm for methylenes bound to both amide and imino groups; at 3.80–3.94 ppm for methoxy groups. Finally, other signals at 5.03–5.10 and 5.97 ppm for alkene group; at 6.71–6.95 ppm for phenyl group; at 8.12 ppm for amide group were found. The ^{13}C NMR spectrum of **7** contains peaks at chemical shifts of 28.12, 29.58–30.43, 32.08–38.79, 40.38, 45.65, 52.24, 59.92–105.71, 179.27, 138.80 and 143.26-147.82 ppm for the brucine nucleus; 29.12 and 31.70 ppm for methylenes bound to both ester and amide groups; at 39.35 ppm for methylene bound to phenyl group; at 40.72 and 51.60 ppm for methylenes bound to both amide and imino groups; at 55.80, 56.01 and 56.29 ppm for methoxy groups; at 113.22, 121.51, 122.87, 139.15, 139.45 and 151.61 ppm for phenyl group. Finally, other signals at 115.53 and 137.76 ppm for carbons involved in the alkene group; at 169.56 ppm for ester group; at 172.73 ppm for amide group were found. The presence of **7** was further confirmed from the mass spectrum which showed a molecular ion at m/z 684.30.

In the search of another way to synthesize **7,** in this study the compound **5** was bound to the brucine nucleus (**8**) to form an imino group involved in compound **7** (method B) (Figure 4). There are several procedures for the synthesis of imino groups which are described in the literature [21-23]; nevertheless, in this study boric acid was used as a catalyst, because it is not an expensive reagent and no special conditions for its use are required[10]. Similar ^{1}H NMR and ^{13}C NMR data were obtained compared to those of method A product. Following this pathway, however, a lower yield was obtained, most probably due to the insufficient time of the reaction.

In conclusion, a facile procedure for the formation of a brucine-derivative (**7**) was developed in this study.

REFERENCES

1 K. Zahn, N. Eckstein, C. Tränkle, W. Sadée, K. Mohr. J. Pharm. Exp. Ter., 301, 2720 (2002).

2 A. Black, P. Vogel. Helv. Chim. Acta, 67, 1612 (1984).

3 H. Young Kim, Hui-Ju Shih, W. E. Knabe, Kyungsoo Oh. Angew. Chem., 121, 7556 (2009).

4 J. Show, T. Hooker. Can. J. Chem., 56, 1222 (1978).

5 N. Birdsall, T. Farries, P. Gharagozloo, S. Kobayashi, S. Lazareno, M. Sugimoto. Mol. Pharm., 55, 778 (1999).

6 S. Findlay. J. Am. Chem. Soc., 73, 3008 (1951).

7 K. Záruba, V. Král. Tet. Asym., 13, 2567 (2002).

8 S. Graham, U. Wemuth, J. White. Acta Cryst., C62, o353 (2006).

9 K. Záruba, J. Králová, Pa. Řezanka, P. Poučková, L. Veverková, V. Král. Org. Biomol. Chem., 8, 3202 (2010).

10 L. Figueroa-Valverde, F. Díaz-Cedillo, M. López-Ramos, .García-Cervera, E. Pool Gómez, Asian J. Chem., 24, 2173 (2012).

11 L. Figueroa-Valverde, F. Díaz-Cedillo, M. López-Ramos, E. García-Cervera, E. Pool Gómez, R. Torres-Cutz. Asian J. Chem., 24, 2321 (2012).

12 C. Ghisalberti. Eur. Patent., WO03082233-A1 (2003).

13 R. Crossland, K, Servis., J. Org. Chem., 35:3195 (1970).

14 H. Zhu, F. Yang, J. Tang, M. He. Green Chem., 5, 38 (2003).

15 F. Erlanger, F. Borek F, M. Beiser, S. Lieberman. J. Biol. Chem., 228.713 (1957).

16 K. Holmberg, B. Hansen. Acta Chem. Scand., B33, 410 (1979).

17 A. Medvedeva, M. M. Andreev, L. Safronova, G. Sarapulova. Arkivok., 9, 143 (2001).

18 D. Levin. Org. Process Res. Dev., 1, 182 (1997).

19 N. De Silva. Am. J. Respir. Cell. Mol. Biol., 29, 757 (2003).

20 L. Figueroa-Valverde, F. Díaz-Cedillo, L. Tolosa, G. Maldonado, G. Ceballos-Reyes. J. Mex. Chem. Soc., 50, 42 (2006).

21 A. Shirayev, I. Moiseev, S. Karpeev. Arkivok., 4, 199 (2005).

22 D. Uppiah, M. Bhowon, S. Jhaumeer. E-J. Chem., 6, 195 (2009).

23 M. Hania. E- J. Chem., 6, 629 (2009).

ДИЗАЙН И СИНТЕЗ НА 4-АЛИЛ-2-МЕТОКСИ-ФЕНИЛ ЕСТЕР НА N-[2-(2,3-ДИМЕТОКСИ-СТРИХНИН-10-ИЛИДЕ АМИНО)ЕТИЛ] АМИНОЯНТЪРНА КИСЕЛИНА

[1]Л. Фигероа-Валверде, [2]Ф. Диаз-Седийо, [1]Е. Гарсия-Цервера, [1]Е. Пуул-Гомез, [1]М. Лопез-Рамос

[1] *Лаборатория по фармацевтична химия, факултет по химико-биологични науки в Автономния университет в Кампече, ул. Агустин Мелгар, полк. Буенависта СР24039, Кампече Кам, Мексико.*
[2] *Национално училище по биологични науки, Национален политехнически институт,Прол. Карпио и План де Аяла С/Н, полк. Санто Томас, Мексико, DF С.Р. 11340*

(Резюме)

В настоящото изследване е синтезирано производно на бруцина чрез няколко стратегии. През първия етап е получено съединението 4-(4-алил-2-метокси-фенокси)-4-оксобутанова киселина (3) е получено чрез реакцията на 4-алил-2-метоксифенол с янтарна киселина, използвайки N,N'-дициклохексилкарбодиимид/р-толуенсулфонова киселина като катализатор. Вторият етап е достигнат чрез реакцията на (3) с етилендиамин, за да се получи 4-алил-2-метоксифенил 4-[(2-аминоетил) амино]-4-оксобутаноат (5) в присъствие на производно на карбодиимид. Накрая съединението 4-алил-2-метокси-фенил естер на N-[2-(2,3-диметокси-стрихнидин-10-илиденамино) етил]-аминоянтърна киселина (7) бе получено от реакцията на 3 с N[1]-(2,3-диметоксистрихнидин-10-илидин) етан-1 ,2-диамин използвайки карбодиимидно производно като катализатор. Съединението 7 беше синтезирно също и чрез реакцията между 5 и бруцин, използвайки борна киселина като катализатор.

A comparative study of inclusion complexes of substituted indole derivatives with β-cyclodextrin

S. Panda*, J. Krushna Tripathy

PG Department of Chemistry Berhampur University, Bhanja Bihar-760007, Odisha, India

Some [arylidenamino]-1,3,4-thiadiazino[6,5-b] indoles were synthesized starting from indole-2,3-dione, thiosemicarbazide and aromatic aldehydes with activating and deactivating groups. Inclusion complexes of these compounds were prepared with β-cyclodextrin to increase their solubility and bioaccessibility. Thermodynamic properties like change in free energy, change in enthalpy, change in entropy and stability constant of the inclusion complexes were determined in order to elucidate whether the inclusion complex formation is thermodynamically allowed or not. The compounds and their inclusion complexes were screened against *S. aureus* and *E. coli.* It was found that the antibacterial activities of the compounds significantly increase after inclusion complex formation.

Keywords: Substituted indole, β-cyclodextrin, inclusion complex, antimicrobial activity

INTRODUCTION

Indole and its derivatives are very good pharmacophores exhibiting a wide spectrum of pharmacological activities such as antidepressive, antiinflammatory, fungicidal, bactericidal and tuberculostatic activities [1–4]. Azedinones and thiazolidinones also show excellent antimicrobial activities [5–8]. There are reports that compounds containing indole or substituted indole coupled with azedinone or thiazolidinone units are acting as drugs for treating a number of diseases [7,8]. Since the bioaccessibility of drugs depends upon their solubility, the poor solubility of these compounds in polar medium (water) may be a limiting factor reducing pharmacological activities. The solubility and bioaccessibility of these compounds can be significantly enhanced by forming inclusion complexes with cyclodextrins, non-toxic oligosaccharides [9]. Out of all known cyclodextrins, β-cyclodextrin is usually considered for inclusion complex formation because it is cheap, easily available and highly stable towards heat and oxidation [10, 12].

In the present work an attempt was made to synthesize some 2-[arylidenamino]-1,3,4-thiadiazino[6,5–b]indoles in their purest forms starting from indole-2,3-dione and using aryl aldehydes with activating (p-bromobenzaldehyde) and deactivating (p-nitrobenzaldehyde) groups. The inclusion complexes of the compounds were prepared with β-cyclodextrin as to enhance their solubility in polar medium which may increase the bio-accessibility of the compounds. The formation of compounds and their inclusion complexes were ascertained from elemental analysis data, melting point data and study of spectral characteristics. Thermodynamic properties of the inclusion complexes were also studied to determine the thermodynamic stability of the inclusion complexes and the type of host-guest interaction. The antimicrobial susceptibility of these compounds and their inclusion complexes were also studied.

EXPERIMENTAL

Apparatus and Materials

All chemicals of acceptable purity grade were procured from the local market. Double distilled water used as a solvent was prepared in the laboratory. Electronic spectra were recorded on a Shimadzu UV–1700 spectrophotometer and IR spectra were recorded in KBr pellets on a Shimadzu 8400 FTIR spectrophotometer. Melting points were recorded by the open capillary method.

Synthesis of 2-[arylidenamino]-1, 3, 4-thiadiazino [6,5-b] indoles

Three different 2-[arylidenamino]-1,3,4-thiadiazino [6,5–b] indoles were synthesized starting from indole-2,3-dione (according to Scheme I) through the following intermediate steps [8]:

* To whom all correspondence should be sent:
E-mail: Sunakar_bu@yahoo.co.in

i)Synthesis of 3-thiosemicarbazideindole-2-one: a mixture of 2 g of indole-2,3-dione and 1.23 g of thiosemicarbazide in 50 ml of methanol was refluxed for one hour. The completion of the reaction was checked by TLC. The excess of methanol was distilled off. The content was cooled and poured into ice-cold water. It was filtered, washed with water, dried and recrystallised from ethanol to obtain 3-thiosemicarbazideindole-2-one [8].

ii) Synthesis of 2-amino-1,3,4-thiadiazino [6,5–b] indole: 3 g of 3-thiosemicarbazideindole-2-one was mixed with a small quantity of cold concentrated H_2SO_4. The reaction mixture was left at room temperature for 16 hours. The reaction mixture was then poured into ice-cold water and neutralized with liquid NH_3 to obtain a solid mass. The latter was filtered through Whatman-42 filter paper. It was washed with water, dried and recrystallised from ethanol to yield 2-amino-1,3,4-thiadiazino [6,5–b] indole.

a) Synthesis of benzylidenamino-1,3,4-thiadiazino [6,5–b] indole (compound I): 1.06 g of benzaldehyde and 2.02 g of 2-amino-1,3,4-thiadiazino [6,5–b] indole were taken in 50 ml of methanol. The mixture was refluxed for 6 hours in presence of glacial acetic acid. The completion of the reaction was checked by TLC and the excess of methanol was distilled off. The refluxed mixture was poured into ice-cold water, filtered, washed with water and dried. The dried mass was recrystallized from ethanol.

b) Synthesis of 2-[4-nitrobenzylidenamino]–1,3,4-thiadiazino [6,5–b] indole (compound II): 1.51 g of p-nitrobenzaldehyde and 2.02 g of 2-amino-1,3,4-thiadiazino [6,5–b] indole were taken in 50 ml of methanol. The mixture was refluxed for 6 hours in presence of glacial acetic acid. The completion of the reaction was checked by TLC and the excess of methanol was distilled off. The refluxed mixture was poured into ice-cold water, filtered, washed with water and dried. The dried mass was crystallized from ethanol.

c) Synthesis of 2-[4-bromobenzylidenamino]-1,3,4-thiadiazino [6,5–b] indole (compound III): 1.87 g of p-bromobenzaldehyde and 2.02 g of 2-Amino-1, 3, 4-thiadiazino [6, 5–b] indole were taken in 50 ml of ethanol. The mixture was refluxed for 6 hours in presence of glacial acetic acid. The completion of the reaction was checked by TLC and the excess of methanol was distilled off. The refluxed mixture was poured into ice-cold water, filtered, washed with water and dried. The dried mass was crystallized from ethanol.

Scheme-I

R= H, p-NO_2 ,p-Br
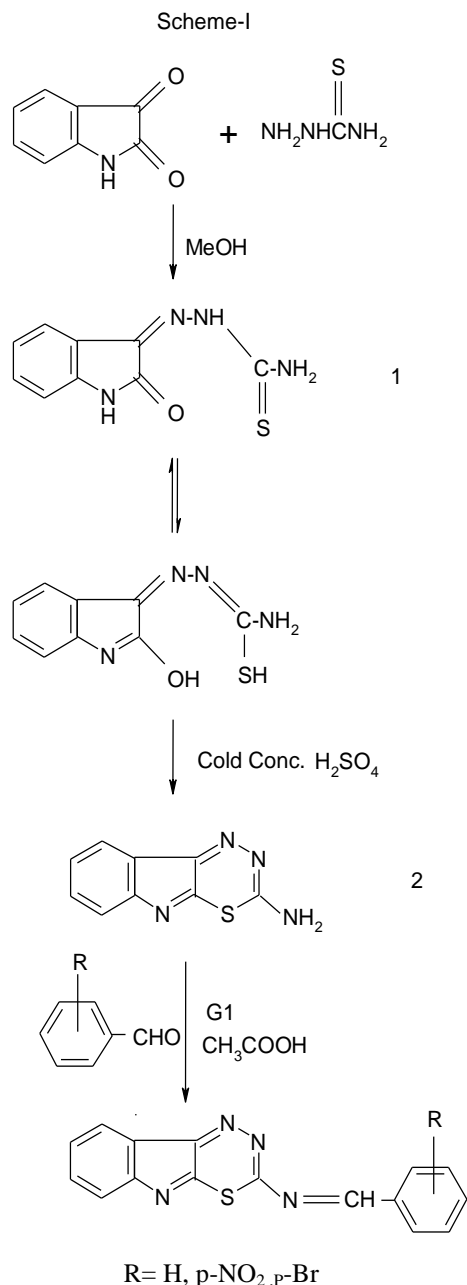
Phase solubility measurements

The solubility of the compounds at various concentrations in the aqueous phase was checked.

β-cyclodextrin (0–10 mM) was studied by the Higuchi-Corner method [13]. Accurately weighed samples of these compounds were shaken in a rotary flask shaker at room temperature in a series of conical flasks for a period of 48 hours till the attainment of equilibrium. The solutions were filtered through Whatman-42 filter paper and were analyzed in a UV-visible spectrophotometer. The absorbance values at λmax were plotted against different concentrations of β-cyclodextrin.

Synthesis of inclusion complexes

The inclusion complexes of the compounds (I, II and III) with β-cyclodextrin were prepared by the co-precipitation method [14]. Solutions of these compounds of the required concentrations were added dropwise to a β-cyclodextrin solution of the required concentration. The mixtures were stirred for 48 hours and filtered. The filtrate was cooled for 24 hours in a refrigerator. The precipitate obtained was filtered through a G-4 crucible filter, washed with water and dried in air for 24 hours.

Study of thermodynamic properties

The thermodynamic stability constant of the complexes was calculated using the Benesi-Hildebrand relation [15]. The dependence of the stability constant K of each complex on the temperature was calculated. From the slope of the linear plot of ln K *vs.* 1/T, ΔH was obtained. Then ΔS was calculated from van't Hoff's equation

$$\ln K = \Delta H/RT - \Delta S/R$$

The value of ΔG was calculated at 298 K using the equation:

$$\Delta G = -RT \ln K$$

Antibacterial study

The antibacterial activity of the compounds was studied by the cup-plate method. Solutions of the test compounds 500 µg/ml in dimethylsulfoxide (DMSO) were prepared. The bacterial strains were inoculated into 100 ml of the sterile nutrient broth and incubated at 37 ± 1 °C for 24 hours. The density of the bacterial suspension was standardized by the McFarland method. Wells of uniform diameter (6 mm) were made on agar plates, after separate aseptic inoculation with the test organisms. The standard drug and the test compounds were introduced using micropipettes and the plates were placed in a refrigerator at 8–10ºC for proper diffusion of the drug into the media. After two hours of cold incubation, the petri plates were transferred to the incubator and were maintained at 37 ± 2ºC for 18–24 hours. Then the zone of inhibition in the petri plates was determined using a vernier scale and was compared to that obtained with the standard drug tetracycline. The results were presented as the mean value (mm) of the zone of inhibition of three sets of experiments.

RESULTS AND DISCUSSION

The synthesis of compound I (benzylidenamino-1,3,4 -thiadiazino[6,5–b] indole),
compound II (2-[4-nitrobenzylidenamino]-1,3,4-thiadiazino[6,5–b] indole) and
compound III (2-[4-bromobenzylidenamino]-1,3,4-thiadiazino[6,5–b]indole) were confirmed by elemental analysis and spectral data, as shown in Table 1.

The elemental composition matches the theoretical data. The IR data of compound I show characteristic absorption at 672,1296,1611,1682 and 3141 cm^{-1} indicating the presence of C–S, C–C, N–N, C=N and benzene ring in the compound, as expected. The IR data of compound II show characteristic absorptions at 719, 1301, 1462, 1581, 1701 and 3146 cm^{-1} indicating the presence of C$^-$S, C–C, C–N, N–N, C=N and benzene ring in the compound, as expected. Similarly, the IR data of compound III show characteristic absorptions at 561,719,1527,1591,3022,3051 cm^{-1} indicating the presence of C-Br, C-S, C=N ,N-N, =C-H and benzene ring in the compound. The IR data of the complex I show characteristic absorption at 670,1290,1605,1679 and 3130 cm^{-1} indicating the presence of C-S, C-C, N-N, C=N and benzene ring in the complex. The IR data of the complex II show characteristic absorptions at 712, 1294, 1456, 1573, 1692 and 3135 cm^{-1} indicating the presence of C-S, C-C, C-N, N-N, C=N and benzene ring in the complex. Similarly, the IR data of the complex III show characteristic absorptions at 560,716,1300,1524,1588 and 3048 cm^{-1} indicating the presence of C-Br, C–S, C–C, N–N, C=N and benzene ring in the complex.

The synthesis of inclusion complexes of compound I (benzylidenamino-1,3,4-thiadiazino[6,5-b]indole), compound II (2-[4-nitrobenzylidenamino]-1,3,4-thiadiazino[6,5-b]indole) and compound III (2-[4-bromobenzylidenamino]-1,3,4-thiadiazino[6,5-b]indole) were confirmed by the changes in melting point, colour and spectral characteristics(UV-Vis and IR). The melting points of compounds I, II and III are found to be 224º C, 245º C and 246 º C, respectively, and the melting points of their inclusion complexes are 228º C, 255º C and 249º C (Table 1). The colour of the compounds I, II and III is yellow, while their inclusion complexes are pale yellow, pale yellow and reddish yellow, respectively.

Table 1. Analytical data of compounds with and without inclusion complex

S.No.	Compound/ Complex	Melting Point	Colour	Elemental Analysis (First line - found value, second line - calculated value)					λ max (A⁰)	IR (KBr) cm–¹
				C	H	N	S	O		
1	Compound I	224	Yellow	66.4	3.45	19.4	1.0		3550	672(C-S) 1296(C-C) 1611(N-N)
				66.2	3.44	19.3	1.03			1682(–C=N) 3141(Ring)
2	Compound I- β- CD	228	Pale Yellow	–	–	–	–	–	3542	670(C-S) 1290(C-C) 1605(N-N) 1679(C=N) 3130()Ring)
3	Compound II	245	Yellow	57.5	2.7	20.9	9.56	9.55	3548	719 (C-S) 1301(C-C)
				57.3	2.69	20.9	9.55	9.55		1462 (C-N) 1581(N-N) 1701(–C=N) 3146(Ring)
4	Compound II- β- CD	255	Pale Yellow	–	–	–	–	–	3540	712 (C-S) 1294(C-C) 1456(C-N) 1573(N-N) 1692(-C=N) 3135(Ring)
5	Compound III	246	Yellow	62.8	3.3	18.4	10.5	5.0	3552	561(C-Br) 719(C-S)
				62.7	3.26	18.3	10.4	5.2		1301(C-C) 1527(N-N) 1591(C=N) 3051(Ring)
6	Compound III -β- CD	249	Reddish Yellow	–	–	–	–	–	3548	560(C-Br) 716 (C-S) 1300(C-C) 1524(N-N) 1588(C=N) 3418(Ring)

Compound I: benzylidenamino-1,3,4-thiadiazino[6,5-b]indole; Compound II: 2-[4-nitrobenzylidenamino]-1,3,4-thiadiazino[6,5-b]indole; Compound III: 2-[4-bromobenzylidenamino]-1,3,4-thiadiazino[6,5-b]indole.

The absorption maxima of the compounds I, II and III are found at 3550, 3548 and 3552 Aº, while their inclusion complexes have absorption maxima at 3542, 3540 and 3548 Aº, respectively. The higher melting points of the inclusion complexes of the compounds are due to the fact that extra amount of thermal energy is required for the latter to bring it out of the β-cyclodextrin cavity.

It is quite interesting to note that the absorption maxima are shifted towards lower wavelengths after formation of the inclusion complex (Table I). This may be attributed to the transfer of the compound from a more protic environment to a less protic environment in the cavity of β-cyclodextrin, which may be further supported by IR data. The IR stretching frequencies due to different bonds are shifted downward towards low energy and the peaks become broader, weaker and smoother. Such changes in spectral characteristics due to inclusion complex formation may be due to weak interactions like hydrogen bonding, van der Waal's forces, hydrophobic interactions, etc. ,between the guest compound and the host β-cyclodextrin [16–19].

The phase solubility plots of the compounds in β-cyclodextrin solution are shown in Fig. 1. In all cases there is a linear increase in solubility of these compounds with increasing concentration of β-cyclodextrin. Since the slopes of all plots are less than unity, the stoichiometry of these complexes may be written as 1:1[20].
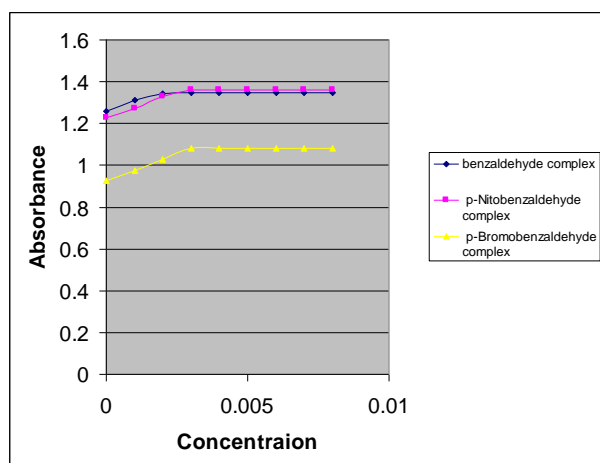
Fig. 1. Phase solubility plot of substituted indole derivatives.
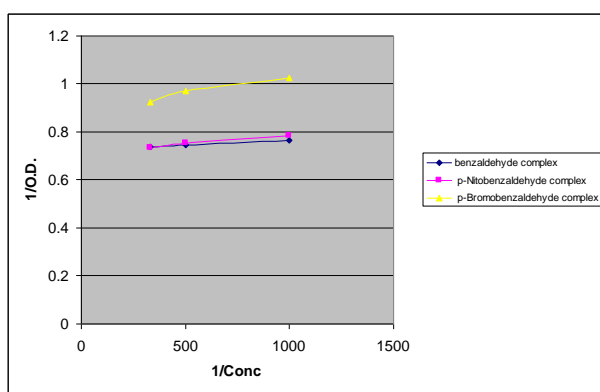
Fig. 2. Plot of 1/ O.D. *vs.* concentration of substituted indole derivatives.

The thermodynamic stability constants (K_T) of the inclusion complexes are determined using the Benesi-Hildebrand relation [15] Good linear correlations are obtained for a plot of $1/\Delta A$ *vs.* [β-CD]$_o$ for the compounds I, II and III (Fig. 2) The values of K_T for all complexes are calculated using the relation

K_T = Intercept/Slope

The K_T values of the inclusion complexes of compounds I, II and III with

β-cyclodextrin are found to be 421, 387 and 413 M^{-1}, respectively (Table 2). The data obtained are within $100 - 1000$ M^{-1} (ideal values) indicating appreciable stabilities for the inclusion complexes [20]. The lower values of the stability constants for compounds II and III than for compound I may be related to steric factors (due to the nitro group in compound II and the bromo group in compound III).

The thermodynamic parameters associated with the interaction of the compounds with β-cyclodextrin for 1:1 stochiometry were also calculated by determining the stability constants (K-values) at different temperatures. The K-values

were found to decrease with the rise in temperature, as expected for an exothermic process (deencapsulation) [21,22]. The dependence of ln K *vs.* inverse absolute temperature produced linear plots (Fig. 3). From the slopes of the curves, van't Hoff reaction isotherm and van't Hoff equation, the values of ΔG (change in free energy), ΔH (change in enthalpy) and ΔS (change in entropy) were calculated at 298 K (Table 2). As Table 2 shows, ΔG values are negative for all inclusion complexes. These data clearly demonstrate that formation of inclusion complexes of compounds I, II and III with β-cyclodextrin is a spontaneous process. Further it was found that for all three inclusion complexes ΔH values are negative and ΔS values are positive(cf. Table 2). The negative value of the enthalpy
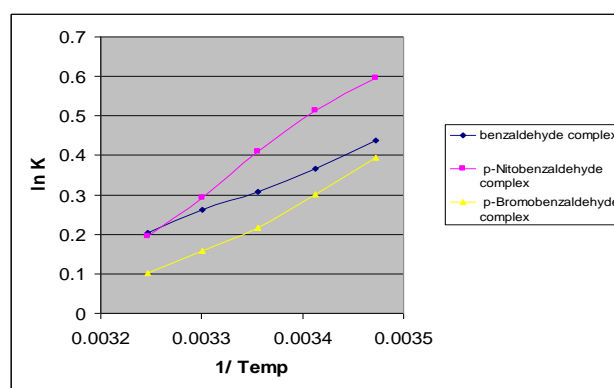
Fig. 3. Plot of ln K vs. 1/T of substituted indole derivatives.

change (ΔH) and the positive value of the entropy change (ΔS) indicate that all three processes of inclusion complex formation are energy allowed and entropy allowed. The smaller value of ΔS for the inclusion complex of compound II may be related to a steric

Table 2: Thermodynamic data of inclusion complexes at 298 K.

Complexes	K M^{-1}	ΔG kJ/mole	ΔH kJ/mole	ΔS J/mole
Compound I- β- CD	421	-14.98	-12.105	9.65
Compound II- β- CD	387	-14.736	-14.934	0.665
Compound III- β- CD	413	-14.932	-13.346	5.321

Compound I: benzylidenamino-1,3,4-thiadiazino[6,5-b]indole. Compound II: 2-[4-nitrobenzylidenamino]-1,3,4-thiadiazino[6,5-b]indole. Compound III: 2-[4-bromobenzylidenamino]-1,3,4-thiadiazino[6,5-b]indole.

factor, which correlates with its lower thermodynamic stability constant (Table 2). The antibacterial activities of the compounds and of their inclusion complexes against *S. aureus* and *E.coli* are shown in Figs. 4A and 4B. Both the compounds and their inclusion complexes are susceptible to the bacteria. However, the inclusion
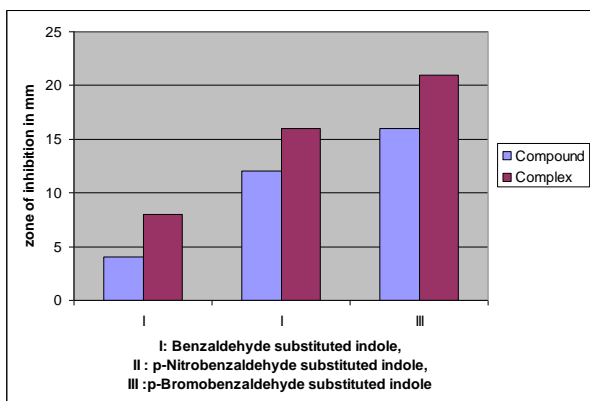
Fig. 4A. Antimicrobial susceptibility test against *S. aureus.*
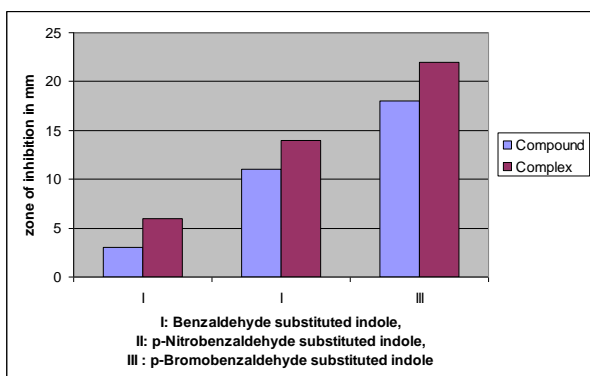
Fig. 4B. Antimicrobial susceptibility test against *E.coli.*

complexes display significantly higher antibacterial activity as compared to their corresponding compounds. This may be attributed to the enhanced solubility of the compounds in the inclusion complexes formed, so that they become more available to specific tissues and display increased antibacterial activity, as earlier suggested [23-26].

CONCLUSION

From the above results and discussion, it is clear that the formation of inclusion complexes of compounds I, II and III is thermodynamically allowed. These complexes can be a very good analytical tool for enhancing the bioaccessibility of the drugs. The study further reveals that the formation of inclusion complexes leads to a significant increase in antibacterial activity.

REFERENCES

1. A. K. Sengupta, A. K. Pandey, H. N. Verma, M. W. A. Ali Khan, *J. Ind. Chem. Soc.*, **62**, 165 (1985). S. Biradar, *Indian J. Pharm. Sci.*, **63,** 299 (2001).
2. A.V. Astakhova and N. B. Demina, *Pharm. Chem. J.*, **38**, 105 (2004)
3. M. V. Shetty, P. Parimo, Y.M. Chopra, *European J. Med. Chem. Chin. Ther.*, 581 (1978).
4. H. Inlon, H. De Vogelaer, M. Descamps, J. Bauthier, M. Colot, J. Richard, R. Charlier, *Chem. Abstr.*, **88**, 601 (1978) .
5. M. Oimoni, M. Hamada, T. Hava, *J. Antibiot.*, **27**, 989 (1974)
6. B. S. Holla, K.V. Udupa, *J. Ind. Chem. Soc.*, **65**, 524 (1988).
7. S. Kapimoto, J. Nishie, *Japan. J. Tuber.*, **2**, 334 (1954**).**
8. H. Panwar, R.S. Verma, V.K. Srivastava, A. Kumar, *Ind. J. Chem.*, **45B**, 2099 (2006).
9. B. Pose-Vilarnovo, I. Predomo-Lopez, M. Echezarreta-Lopez., *J. Pharm. Sci.,* **13**, 325 (2001).
10. V.G. Belikov, E. V.Komapantseva, *Khim.-Farm. Zh.*, **24**, 19 (1990).
11. H. Yano, F. Hiramaya, H. Arima, *J. Pharm. Sci.*, **90**, 493 (2001).
12. C.F.H. Allen, G.H.W. Mekee, *Organic Synthesis Coll.*, **2**, 15 (1999).
13. T. Higuchi, K. Connors, *Adv. Anal. Chem. Instrum.*, **4**, 117 (1965).
14. S. Panda and S. S. Nayak, *Asian J. Res. Chem.*, **2(4)**, 539 (2009)
15. H.A. Benesi, J.H. Hilderband, *J. Am. Chem .Soc.*, **71**, 2703 (1999).
16. K.G. Mohammed, C.A. Moji, *Pharm. Dev. Tech.*, **6** , 315 (2001).
17. Q. Chen, D. Guowang, *Chem. J.*, **6**, 37 (2001).
18. S.S. Nayak, S. Panda, P.M. Panda, S. Padhy, *Bulg. Chem. Commun.*,**42,** 147 (2010).
19. A.P. Mukna, M.S. Nagarsenkar, *AAPS Pharm. Sci. Tech.*, **5**, 19 (2001).
20. Z. Szetli, *Molecular entrapment and release properties of drugs by cyclodextrins, Controlled Drug Bio-availibility,* Willey Interscience publications, **3**, 365 (1985).
21. S. Tommasini, D. Raneri, R. Ficarra, M.L. Calabro and R. Stancanelli., *J. Pharm. Biomed. Anal.*, **35**, 379 (2004) .
22. R.A Rajewski, V.J. Stella, *J. Pharm. Sci.*, **85**, 1142 (1996).
23. Y.L. Loukas., V. Vraka, G. Gregordias, *J. Pharm. Biomed. Anal.*,**16**, 263 (1997).
24. T. Stalin, P. Vasantharani, B. Shanti, A. Sekhar, N. Rajendra, *Ind. J. Chem., A*, **45,** 1113 (2006).
25. R. Cruickshank, J. P. Marmion, R. H. A. Swain, *Medicinal Microbiology*, 11, 91 (1975) 38, 105 (2004).
26. A.V. Astakhova, N.B. Demina, *Pharm. Chem. J.*, 38, 105 (2004)

СРАВНИТЕЛНО ИЗСЛЕДВАНЕ КОМПЛЕКСИ НА ВКЛЮЧВАНЕ НА ЗАМЕСТЕНИТЕ ИНДОЛ ДЕРИВАТИ С В-ЦИКЛОДЕКСТРИН

С. Панда, Дж. Крушна Трипати

ПГ Катедра по химия университет Бернампур, Бихар-760007, Одаша, Индия

(Резюме)

Някои [арилденамино] -1,3,4-ттиадиазино [6,5-b] индоли са синтезирани като се започне от индол-2,3-дион, тиосемикарбазид и ароматни алдехиди с активиране и деактивиране на групи. Комплекси на включване на тези съединения са получени с бета-циклодекстрин, за да се увеличи тяхната разтворимост и биологичнат им достъпност. Термодинамични свойства, като промяна в свободна енергия, промяна в енталпията, промяна на ентропията и стабилитетна константа на комплекси на включването са определени, за да се изясни дали формирането на комплекси на включване е термодинамично позволено или не. Съединенията и комплексите им на включване бяха проверени спрямо *S. Aureus* и *E. Coli*. Установено бе, че антибактериалниата активност на съединенията се увеличава значително след включването им в образуване на комплекси.

Crystallization behaviour and magnetic properties of sodium-silicate glasses containing iron and manganese oxide

[1][*]Ruzha Harizanova, [1]Ivailo Gugov, [2]Christian Rüssel

[1]*University of Chemical Technology and Metallurgy, 8 Kl. Ohridski Blvd., 1756 Sofia, Bulgaria*
[2]*Institut für Glaschemie "Otto-Schott-Institut", Friedrich-Schiller-Universität, Fraunhoferstr. 6, 07743 Jena, Germany*

Abstract. Oxide glasses and nanocrystalline glass-ceramics, containing large amounts of transition metal ions, exhibit novel and unusual electrical and magnetic properties and find various applications in magnetorheology, electronics, magnetic resonance imaging and sensor technology. The present work is dedicated to the study of the crystallization behaviour, phase formation and the resulting magnetic properties of the synthesized products in the system $Na_2O/MnO/SiO_2/Fe_2O_3$. Two glasses with 15 mol% Fe_2O_3-concentration and different MnO concentrations are prepared by melting under oxidizing or reducing conditions. Further, the glasses are annealed by applying different time/temperature programs in order to precipitate nano-scale magnetic crystals. The phase composition and microstructure of the glass-ceramics are studied by X-ray diffraction and electron microscopy. The obtained data are used to reveal the crystallization kinetics. The magnetic properties of the selected samples, measured on a vibrating sample magnetometer, vary from para- to superparamagnetic.

Keywords: iron oxide and manganese oxide, crystallization kinetics, nano-scale materials, magnetic properties.

1. INTRODUCTION

There are numerous reports on the synthesis and application of oxide glasses containing 3d-transition metal ions [1-14]. These glasses and the corresponding glass-ceramics have interesting and promising electrical and magnetic properties especially if nanocrystals are formed by appropriate heat treatment [15, 16] and find applications as components of ferrofluids in electronics, as solder materials or in magnetorheology. Depending on the phase composition, size and volume fraction of the magnetic particles, the obtained crystals can be used as components of contrast agents in magnetic resonance imaging and in biomagnetic sensors for the detection of different chemical and biochemical substances [17, 18]. Many authors report the synthesis of nanosized magnetic crystals by means of wet chemical routes, i.e. by precipitation of magnetite (Fe_3O_4) [19-22] but also of Co_3O_4 and $MnFe_2O_4$ [22, 23] from aqueous solutions. Another preparation route is the controlled crystallization of glasses containing relatively large amounts of transition metal ions which, however, results in higher tendency for spontaneous crystallization [2, 7, 24–28]. The spontaneous crystallization can be suppressed or even avoided by either adjusting the glass composition (decreasing the transition metal concentration) or increasing the cooling rate [10, 11, 25]. Thermal annealing of the obtained glasses enables the precipitation of nanosized ferrimagnetic or superparamagnetic particles with tailored size-distribution [10, 11]. In literature, the effect of iron oxides combined with a second transition metal oxide, on the phase composition and microstructure of glassy materials, synthesized by conventional melting techniques, is already reported [7, 25], but attempts to precipitate nanoscale crystals in such complex systems are scarcely performed.

This paper presents a study on the precipitation of nanosized spinel phases from glasses in the system $Na_2O/MnO/SiO_2/Fe_2O_3$ by using a conventional glass-melting technique and subsequent thermal annealing. Vibration magnetometry permits to determine the magnetic properties of the obtained glass-ceramic materials.

2. EXPERIMENTAL

Within the system $Na_2O/MnO/SiO_2/Fe_2O_3$ two glasses with the following compositions, given in mol%, were prepared:
- glass A: $13.6Na_2O/8.5MnO/62.9SiO_2/15.0Fe_2O_{3-\delta}$ (reduced by using $FeC_2O_4.2H_2O$ as raw material).
- glass B: $16Na_2O/10MnO/59SiO_2/15Fe_2O_3$ (Fe_2O_3 used as raw material).

The samples prepared using FeC_2O_4 as raw material are further denoted as "reduced", while

* To whom all correspondence should be sent:
 e-mail: ruza_harizanova@yahoo.com

samples melted using Fe_2O_3 are designated as "oxidized". Reagent grade raw materials: Na_2CO_3, $MnCO_3$, SiO_2, Fe_2O_3 or $FeC_2O_4.2H_2O$ are used for the preparation of the glasses. The batches (100 g) are homogenized and melted in SiO_2-crucibles using a $MoSi_2$-furnace at melting temperatures in the range from 1400 to 1450°C (kept for 1.5 h in air). The melts are cast into a pre-heated graphite mould, transferred to a muffle furnace and kept at 480°C for 10 min. Then, the furnace is switched off and the samples allowed to cool down to room temperature. Further, the glasses A and B are annealed at temperatures in the range from 510 to 700°C, according to the determined T_g-values, for times from 10 min to 100 h in order to precipitate in them nanocrystalline phase containing 3d-metals . The heating rate from room temperature to the desired annealing temperature was always 10K/min. The annealing temperatures were always clearly above the glass transition temperatures: $T_g = 490$ °C for glass A and $T_g = 494$ °C for glass B, [25]. The phase compositions are determined by X-ray diffraction (XRD: Siemens, D 5000), using $Cu_{K\alpha}$-radiation; the 2θ-values were in the range from 10 to 60° The obtained microstructures are studied by scanning electron microscopy (SEM: JEOL 7001F), the samples are cut, polished and coated with carbon. Secondary (SE), as well as backscattered electrons (BSE) are used for imaging. The magnetic measurements are performed on a vibrating sample magnetometer.

3. RESULTS AND DISCUSSION

3.1 Results

Information about the characteristic temperatures and microstructure of glasses A and B is already given in [25]. After annealing of glasses A and B, they are examined by X-ray diffraction and the results are shown in Fig. 1a for the crystallized samples A and in Fig. 1b – for the samples of type B. It is seen from the XRD patterns that the annealing at 550°C for times up to 24 h results in formation of only one crystalline phase in both glasses A and B. The X-ray reflexes of this phase are similar to the reflexes of the phases $(Mn_{0,6}, Fe_{0,4})(Mn_{0,4},Fe_{1,6})O_4$ (JCPDS 88–1965) and Fe_3O_4 (JCPDS 87–2334). However, the relatively broad peaks and the proximity of the main reflexes of the two phases (difference in main peak positions ~ 0.7°), do not allow an exact determination of the chemical composition of the formed crystals only by means of XRD. Possibly, the precipitated phase is a solid solution of a mixed spinel type $(Fe^{2+}, Mn^{2+})(Fe^{3+}, Mn^{3+})_2O_4$.
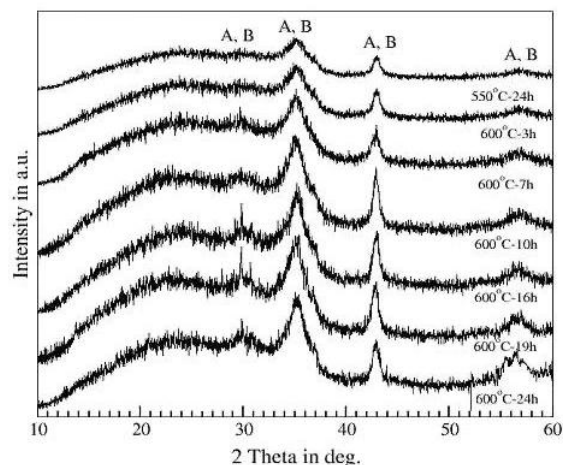
Fig. 1a XRD-patterns of samples A annealed at 550 and 600°C for different times- formation of mixed crystals $MnFe_2O_4$ (A) and Fe_3O_4 (B)
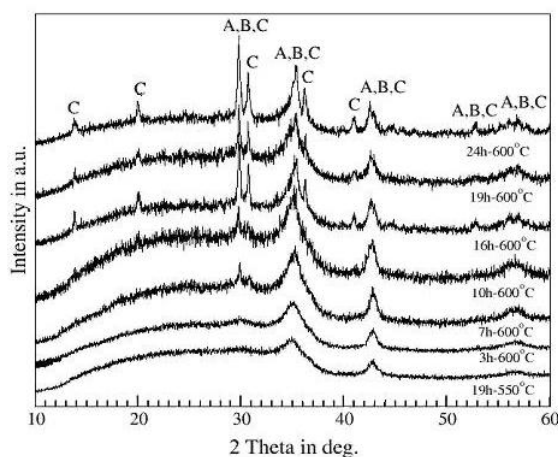
Fig. 1b XRD-patterns of samples B, annealed at 550 and 600°C for different times – formation of mixed crystals $MnFe_2O_4$ (A) and Fe_3O_4 (B), as well as of $NaFe(SiO_3)_2$ (C)

The observation of one morphological type of crystals is also done while examining the annealed at 550°C samples A by scanning electron microscopy – see Fig. 2a. The average size of the formed spinel crystals is about 50 nm for 3h annealing time, as shown in Fig. 2b (see insert). Similar results are obtained from the SEM micrographs (not shown) of glasses B heat treated at 550°C.

The heat treatment of glasses A and B at 600 °C leads to the formation of two types of crystals: nanosized spinel crystals and micron-sized elongated crystals. This is seen on Fig. 3 for sample A and on Figs. 4a and 4b for sample B. The second crystalline phase is attributed to aegirine, $NaFe(SiO_3)_2$ (JCPDS 34-0185), as shown in Fig. 1b. The average sizes of the formed nanocrystals for the glasses A, annealed at 550°C for times from 40 min to 24 h, are studied in order to investigate the kinetics of crystallization.

85
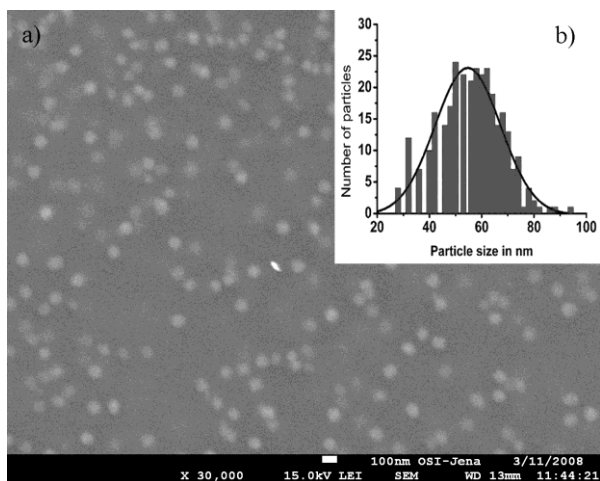
Fig. 2: (a) SEM (SE) image of C-covered sample A, annealed for 3 h at 550°C – uniform distribution of the nanosized (Fe, Mn)-based crystals; **(b)** Gauss-fitted chart with the size distribution of the nanocrystals, precipitated in sample A, annealed for 3 h at 550°C – maximum centred at about 54 ± 1 nm
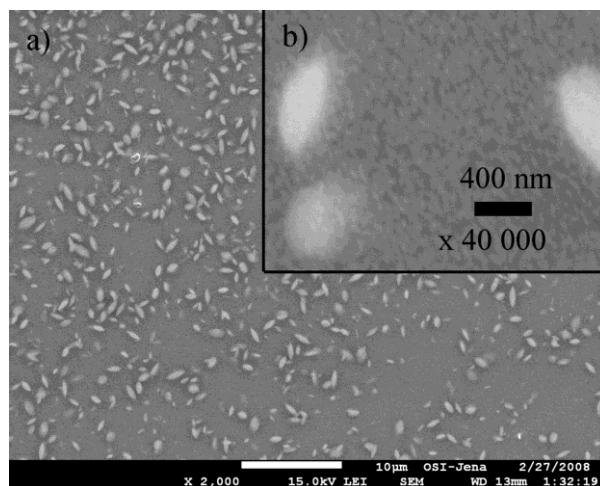

Fig. 4a and 4b SEM (SE) images of C-covered sample B, crystallized for 12 h at 600°C – two morphologically different types of crystals, the nanosized (Fe, Mn)-based crystals and elongated NaFe(SiO$_3$)$_2$, are present

Fig. 3 SEM (SE) image of C-covered sample A, annealed for 24 h at 600°C – uniform distribution of (Fe, Mn)-based nanocrystals and formation of a second crystalline phase which corresponds to the large ellipsoidal crystals
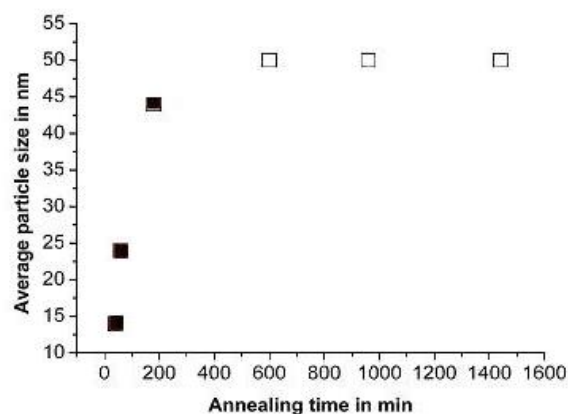
Fig. 5 Kinetics of crystallization of samples of type A, annealed at 550°C for different times – solid symbols represent ASAXS data taken from [29] and hollow ones are from processing of SEM images

The data are shown in Fig. 5. Here the hollow symbols represent data for the mean size obtained by SEM images processing. The solid square symbols are taken from [29] and are obtained by anomalous small-angle X-ray scattering (ASAXS) experiments. It is seen in Fig. 5 that the size of the crystals varies from about 14±0.5 nm, [29] to 50±1 nm for annealing times from 40 min to 24 h, respectively. After annealing for 3h at 550°C the size of the precipitated spinel nanocrystals does not change with further increase of the annealing time, i.e. the crystal growth may be supposed to be kinetically self-constrained.

The magnetic properties of selected bulk samples from type A annealed for different times at different temperatures above the glass transition temperature are measured on a vibrating sample magnetometer. As an example, Fig. 6 shows the magnetisation curve of glass A heat-treated for 24 h at 600°C. The nanosized spinel crystals found in this sample display superparamagnetic behavior while the larger aegirine crystals are paramagnetic at room temperature and do not influence the results of the magnetic measurements.
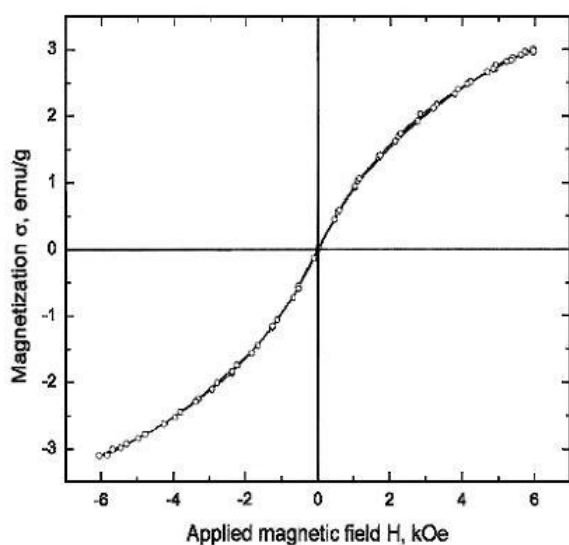
Fig. 6 Magnetization *versus* intensity of an external magnetic field for a sample A annealed for 24 h at 600°C – superparamagnetic-like behaviour observed

3.2 DISCUSSION

The different crystallization behaviour of the oxidized sample B and the reduced sample A could be attributed to the different incorporations of Fe^{2+} and Fe^{3+} ions in the glass-network, as observed for Fe_2O_3 concentrations ≤ 2 mol%, [30-40] and is already pointed out and discussed in [25, 29]. The ability to form glasses might also be affected by the redox ratio Fe^{2+}/Fe^{3+} which is supposed to be different in the oxidized and reduced samples. Sample A has a higher SiO_2 concentration and a lower alkali concentration and is thus assigned a higher acidity of the glass-matrix, according to the acidity-basicity concept, [32, 37]. At the same time, the oxidized sample B has a higher Na_2O concentration and a lower SiO_2 content, i.e. higher basicity. This determines the higher concentration of Fe^{3+} ions in comparison to the concentration of Fe^{2+} ones, as suggested by Duffy [32]. The latter implies that crystallization of phases containing mainly ferric ions should be easier in the annealed samples B, which is supported by Figs. 1a and 1b, where the aegirine phase appears at lower annealing times in sample B compared to sample A. For the formation of $MnFe_2O_4$ or rather a mixed spinel phase of the type $(Fe^{2+}, Mn^{2+})(Fe^{3+}, Mn^{3+})_2O_4$, (as already suggested in Ref. [19]), the valence state in which Mn occurs in the glass is of great importance. In the case of Mn containing oxide glasses, similar redox equilibrium to that described above for Fe is also formed and was already discussed in our previous work, [29]. Thus, the addition of both Mn and Fe oxides enables the

crystallization of a spinel phase from the type $(Fe^{2+}, Mn^{2+})(Fe^{3+}, Mn^{3+})_2O_4$. The data from Figs. 1 to 4 show that the addition of reducing agents does not change the type of the crystallizing spinel species. It, however, affects the crystallization of the $NaFe(SiO_3)_2$ (aegirine) phase. For the crystallized samples B, the formation of aegirine is observed in larger amounts and for smaller annealing times in comparison to the samples A. The latter can be explained by the higher concentration of Fe^{3+}-ions in the case of B. Actually, as shown in Figs. 3 and 4, in the sample B, annealed for 12 h at 600ºC, nanocrystals of the (Fe,Mn)-spinel and aegirine crystals of oval shape are present in notable quantities, while in the A type sample crystallized for 24 h at 600ºC the same phases but in smaller quantities are found. So, it may be suggested that in the annealed samples A, where the SiO_2 concentration and hence, the Fe^{2+}/Fe^{3+}-ratio is larger, the formation and the crystal growth of aegirine are suppressed for temperatures up to 600ºC and annealing times up to 16 h, (see Figs. 1, 3 and 4).

The average particle sizes, as recently determined from SEM images and SAXS [29] and seen here in Fig. 5, are in the range from 14 to 50 nm and do not change if the annealing time is longer than 3 h. It is suggested in [29] that only the volume fraction of the nano-sized crystalline phase increases while increasing the annealing temperature, which can further have impact on the magnetic properties of the annealed samples [10]. This type of crystallization kinetics shows that the growth of the spinel phase in the reduced samples A is kinetically self-constrained, cf. Fig. 5 and [10, 11, 41, 42]. As described in [29], during the annealing process, the concentration of Fe and Mn ions decreases in vicinity of the growing spinel crystal. So, a silica-rich shell with rapidly increasing viscosity is formed around the growing Fe, Mn-based crystals. When the glass transition temperature of this shell approaches the annealing temperature the crystal growth is decelerated and finally stops for kinetic reasons.

The magnetic measurements show paramagnetic behaviour and absence of hysteresis for the sample of type A, annealed for 3h at 540ºC, though in this sample nanocrystals are contained. The reason for this magnetic behaviour is not clear and needs further investigation. In contrast to the paramagnetic behaviour of the sample annealed for 3 h at 540ºC, the sample, crystallized for 24 h at 600ºC, possesses superparamagnetic properties at room temperature and no hysteresis – as seen in Fig. 6. The same is already observed in other glass-

ceramic systems containing nanosized spinel crystals [10, 15]. However, here, due to lower intensities of the applied external magnetic field as compared to the data in [10], we suppose that no saturation of the mass magnetization is reached. So, further investigation is needed in this direction in order to better elucidate the magnetic behaviour of the studied glass-ceramic materials.

4. CONCLUSION

Crystalline spinel phase of the type $(Mn^{2+}, Fe^{2+})(Fe^{3+}, Mn^{3+})_2O_4$ is precipitated in the two investigated compositions with 15 mol% Fe-oxide for temperatures up to 600^oC, while for longer annealing times at $600°C$ a second crystalline phase – aegirine, $NaFe(SiO_3)_2$ - is also formed. The precipitation of hematite is avoided in the whole temperature interval investigated for both reduced and oxidized compositions. For crystallization times from 40 min to 24 h and annealing temperature of 550^oC, kinetically self-constrained growth of the spinel nanocrystals is observed, with average crystallite sizes of about 50 nm which does not further increase for times longer than 3 h. The magnetic measurements on a sample annealed for 24h at $600°C$ show superparamagnetic behaviour at room temperature.

REFERENCES:

1 A.Karamanov, M.Pelino, *J. Non-Cryst. Sol.* **281** 139 (2001).

2 M.Romero, J.M.Rincon , *J. Am. Ceram. Soc.* **82** 1313 (1999).

3 J.D.Mackenzie, *J. Non-Cryst. Sol.* **2** 16 (1970).

4 L.Murawski, C.H.Chung, J.D.Mackenzie, *J. Non-Cryst. Sol.* **32** 91 (1979).

5 J.D.Mackenzie, *J. Am. Ceram. Soc.* **47** 211 (1964).

6 J.D.Mackenzie *in: Modern Aspects of the Vitreous State,* vol. 3, J.D. Mackenzie (Ed.), Butterworths, London, 1964, p. 126.

7 H.J.L. Trap, J.M.Stevels, *Phys. Chem. Glasses* **4** 193 (1963).

8 R.A.Anderson, R.K.MacCrone, *J. Non-Cryst. Sol.* **14** 112 (1974).

9 J.Allersma , J.D.Mackenzie, *J. Chem. Phys.* **47** 1406 (1967).

10 S.Woltz, R.Hiergeist, P.Görnert, C.Rüssel, *J. Magn. Magn. Mater.* **298** 7 (2006).

11 S.Woltz, C.Rüssel, *J. Non-Cryst. Sol.* **337** 226 (2004).

12 H.H.Qiu, M.Kudo, H.Sakata, *Mater. Chem. Phys.* **51** 233 (1997).

13 H.H.Qiu, H.Mori, H. Sakata, T.Hirayama, *J. Ceram. Soc. Jpn.* **103** 32 (1995).

14 S.Roy, D.Chakravorty, *J. Mater. Res.* **9** 2314 (1994).

15 S.Odenbach, *J. Phys: Condens. Matter.* **16** 1135 (2004).

16 G.Y.Zhou, Z.Y.Jiang, *Smart Mater. Struct.* **13** 309 (2004).

17 Y.Sakai, N.Abe, S.Takeuchi, F.Takahashi, *J. Ferment. Bioeng.* **80**: 300 (1995).

18 T.Aytur, J.Foley, M.Anwar, B.Boser, E.Harris, P.R.Beatty, *J. Immunol. Methods* **314** 21 (2006).

19 Z.J.Zhang, Z.L.Wang, B.C. Chakoumakos, J.S. Yin, *J. Am. Chem. Soc.* **120** 1800 (1998) .

20 X.Wang, Y.Li, *Chem. Commun.* 2901 (2007), DOI: 10.1039/b700183e.

21 H.Si, C.Zhou, H.Wang, S.Lou, S.Li, Z.Lu, L.S.Li, *J. Coll. Interf. Sci.* **327** 466 (2008).

22 W.Shi, N.Chopra, *J Nanopart. Res.* (2010), DOI: 10.1007/s11051-010-0086-0.

23 T.Herranz, S.Rojas, M.Ojeda, F.J.Perez-Alonso, P.Terreros, K.Pirota, J.L.G.Fierro, *Chem. Mater.* **18** 2364 (2006).

24 R.Harizanova, G.Völksch, C.Rüssel, *J. Mater. Sci.* **45** 1350 (2010).

25 R.Harizanova, G.Völksch, C.Rüssel, *Mater. Res. Bull.* (2010), doi:10.1016/j.materresbull.2010.09.036.

26 G.Völksch, R.Harizanova, C.Rüssel, S.Mitsche, P.Pölt, *Glastech. Ber. Glass Sci. Technol.* **77C** 438 (2004).

27 R.Harizanova, R.Keding, C.Rüssel, *J. Non-Cryst. Sol.* **354** 65 (2008).

28 R.Harizanova, R.Keding, G.Völksch, C.Rüssel, *Eur. J. Glass Sci. Technol. B* **49** 177 (2008).

29 R.Harizanova, I.Gugov, C.Rüssel, D.Tatchev, V.S.Raghuwanshi, A.Hoell, *J. Mater. Sci.* (2011), DOI 10.1007/s10853-011-5840-x.

30 C.Rüssel, A.Wiedenroth, *Chem. Geol.* **213** 125 (2004).

31 R.A.Levy, C.H.Lupis, P.A.Flinn, *Phys. Chem. Glasses* **17** 94 (1976).

32 A.Duffy, *Phys. Chem. Glasses* **40** 54 (1999).

33 A.Wiedenroth, C.Rüssel, *J. Non-Cryst. Sol.* **347** 180 (2004).

34 A.Wiedenroth, C.Rüssel, *J. Non-Cryst. Sol.* **297** 173 (2002).

35 G.Gravanis, C.Rüssel, *Glastech. Ber.* **62** 345 (1989).

36 P.A.Bingham, J.M.Parker, T.Searle, J.M.Williams, K.Fyles, *J. Non-Cryst. Sol.* **253** 203 (1999).

37 J.A.Duffy, M.D.Ingram, *J. Non-Cryst. Sol.* **21** 373 (1976).

38 L.D.Pye,   A.Montenero,   I.Joseph   (Eds.), *Properties of Glass-Forming Melts,* Taylor & Francis, Boca Raton, 2005, p. 27.

39 L.Kido, M.Müller, C.Rüssel, *Chem. Mater.* **17** 3929 (2005).

40 L.Kido, M.Müller, C.Rüssel, *J. Non-Cryst. Sol.* **351** 523 (2005).

41 C.Rüssel, *Chem.Mater.* **17** 5843 (2005).

42 C. Bocker, C.Rüssel, *J. Europ. Ceram. Soc.* **29** 1221 (2009).

КРИСТАЛИЗАЦИОННО ПОВЕДЕНИЕ И МАГНИТНИ СВОЙСТВА НА НАТРИЕВО-СИЛИКАТНИ СТЪКЛА, СЪДЪРЖАЩИ ОКСИДИ НА ЖЕЛЯЗОТО И МАНГАНА

[1]Р. Харизанова, [1]И.Гугов, [2]К. Рюсел

[1]*Химикотехнологичен и Металургичен университет, бул. "Кл. Охридски" № 8, 1756, София,България*
[2]*Ото Шот институт, Фридрих Шилер университет, ул. "Фраунхофер" №. 6, 07743, Йена, Германия*

(Резюме)

Оксидните стъкла и нанокристални стъклокерамики, съдържащи йони на преходните метали с висока концентрация, проявяват авангардни и необичайни електрични и магнитни свойства и намират разнообразни приложения в магнитореологията, електрониката, магниторезонансните изследвания и сензорните технологии. Настоящата работа е посветена на изучаването на кристализационното поведение, фазообразувнето и магнитните свойства на продуктите на синтез в системата $Na_2O/MnO/SiO_2/Fe_2O_3$. Синтезирани са две стъкла с 15 мол % Fe_2O_3 и различна концентрация на MnO, стопени при окислителни или редуциращи условия. Впоследствие стъклата са темперирани чрез прилагане на различни програми температура-време, целящи получаването на наноразмерни магнитни кристали. Фазовият състав и микроструктурата на стъклокерамиките са изучени с използване на рентгенова дифракция и електронна микроскопия. Получените данни са използвани за изследване на кинетиката на кристализация. Магнитните свойства на избрани проби, измерени с използване на вибрационна магнитометрия, варират от пара- до суперпарамагнитни.

A Simple Method for Synthesis of Cadmium Oxide Nanoparticles Using Polyethylene Glycol

M. Tabatabaee[a*], A. A. Mozafari[a], M. Ghassemzadeh[b], M. Reza Nateghi[a], I. Abedini[c]

[a]*Department of Chemistry, Yazd Branch, Islamic Azad University, Yazd, Iran*
[b]*Chemistry & Chemical Engineering Research Center of Iran, Tehran, Iran*
[c]*Department of Applied Chemistry, Malek-e-Ashtar University, Esfahan, Shahin Shahr, Iran*

Nano-sized cadmium oxide was synthesized by a simple method using $Cd(NO_3)_2.4H_2O$ as a reagent in the presence of polyethylene glycol (PEG 2000). X-ray diffraction (XRD), scanning electron microscopy (SEM), transmission electron microscopy (TEM), and energy dispersive spectrometry (EDS) were used to characterize the structure and morphology of the synthesized powder. The results showed that PEG played a significant role in the decomposition of cadmium nitrate to cadmium oxide nanoparticles. The CdO crystals were grown in face-centered cubes over the range (15-25 nm).

Keywords: Nanoparticles; Cadmium oxide, Polyethylene glycol

INTRODUCTION

In the past few years, much attention has been focused on the research field of nano-crystalline oxide materials both because of their fundamental importance and the wide range of potential technological applications [1–6]. CdO is a degenerate, n-type semiconductor used in optoelectronic applications such as photovoltaic cells [7], solar cells [8], phototransistors [9], IR reflectors [10], transparent electrodes [11], gas sensors [2, 12, 13] and a variety of other materials. These applications are based on its specific optical and electrical properties [14]. Polyethylene glycols (PEG) in aqueous solution are highly mobile molecules with a large exclusion volume, mostly free of charges, which can avoid the strong interaction between the constituents [15]. A number of studies have reported that PEG can modify or control the surface of the nanometer crystals; moreover it can act as a dispersing agent of the nanometer crystals in the process of synthesis [16, 17]. There are some reports on the synthesis of CdO nanoparticles for nanowires and nanofilms by chemical co-precipitation or sonochemical methods [2, 18–20], but to the best of our knowledge, there are no reports in the literature dealing with the use of polyethylene glycol for the synthesis of CdO. In this work, we report a new and simple method for the synthesis of nano-sized cadmium oxide by decomposition of cadmium nitrate in polyethylene glycol.

EXPERIMENTAL PROCEDURE

2 g of cadmium nitrate tetrahydrate, $Cd(NO_3)_2 \cdot 4H_2O$, with 99% purity were added to 30 g of polyethylene glycol (average molecular weight 2000, abbreviated as PEG2000). A transparent solution was obtained at 80ºC, which was refluxed for two hours at 250°C. 30 ml of deionized water were added to the resulting brown suspension. The precipitate was filtered off and washed three to four times using double distilled water and ethanol to remove polyethylene glycol and other impurities. The prepared CdO powder was dried at 200ºC for 5 min. The sample was characterized by powder X-ray diffraction (Bruker, Advance D8) with Cu Kα (λ=1.5406 Å) incident radiation. The size distribution and morphology of the sample was analyzed by scanning electron microscopy (SEM, Philips XL30) and transmission electron microscopy (TEM, Philips CM10). Energy dispersive spectrometry (EDS) attached to SEM was employed to perform the elemental analyses of the nanostructured materials.

RESULTS AND DISCUSSION

The XRD pattern of nano-sized CdO is shown in Fig.1. It shows the diffraction peaks at 2θ values of 33.0º, 38.3º, 55.3º, 65.9º and 65.9º, which are attributed to the formation of CdO.

* To whom all correspondence should be sent:
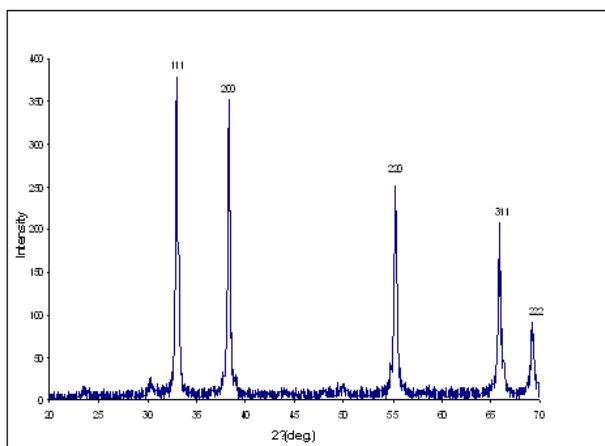E-mail: tabatabaee45m@yahoo.com

Fig. 1 XRD patterns of the synthesized CdO nanocrystallite.

No characteristic peaks from other impurities were detected. The crystal structure consists of face centered cubes and the entire d-line patterns match the reported values. The crystallite size was estimated from the broadening of CdO (111) diffraction peak (2θ = 32.2◦) using Debye-Scherrer's formula:

$$t = \frac{k\lambda}{B \cos\theta}$$

where t is the average size of the crystallite, assuming that the grains are spherical, k is 0.9, λ is the wavelength of X-ray radiation, B is the peak full width at half maximum (FWHM) and θ is the angle of diffraction. The crystallite size of nano-sized CdO is found to be ~25 nm. The TEM micrograph of the nano-sized powder along with the electron diffraction pattern is shown in Fig. 2.
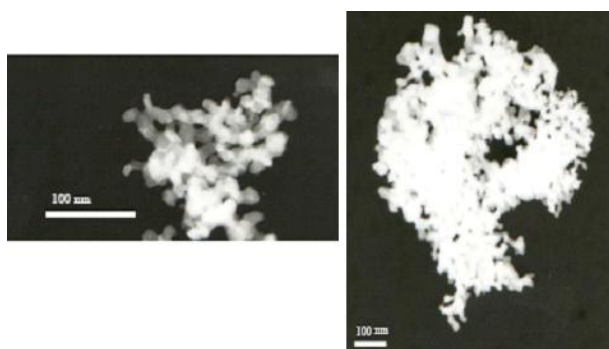
Fig. 2 TEM image of the synthesized CdO.

The TEM micrograph clearly shows that the particle size of nano-sized CdO is ~15–25 nm. This result is in good agreement with the crystallite size calculated using the XRD data. The morphology of the CdO nanocrystallites is shown in Fig. 3.
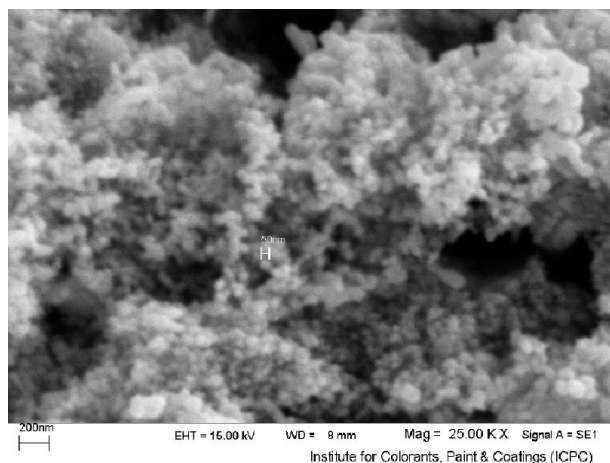
Fig. 3 Scanning electron micrographs of the synthesized CdO.

In the analysis of the cadmium oxide nanoparticles by energy dispersive spectroscopy (EDS), the presence of strong CdLa signals confirms the presence of CdO in the sample (Figure 4).
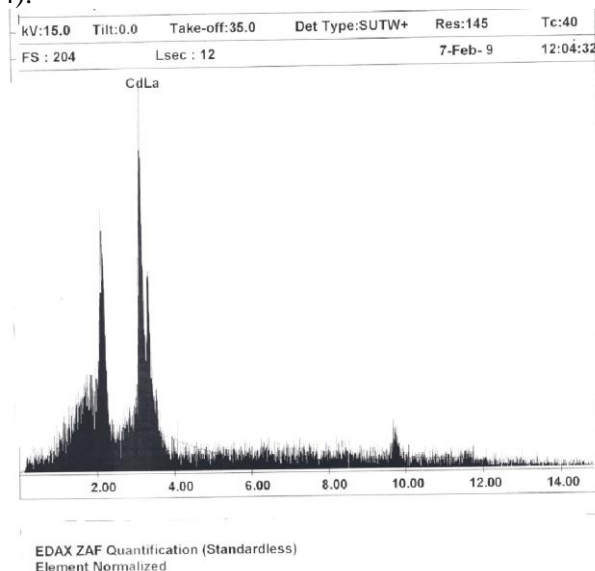
Fig 4. EDS image of the synthesized CdO.

The results showed that PEG played a significant role in the decomposition of cadmium nitrate to cadmium oxide nanoparticles. The CdO crystals were grown in face-centered cubes over the range (15-25 nm).

By the co-precipitation method used, $Cd(OH)_2$ was formed in a basic medium. The subsequent calcination of $Cd(OH)_2$ lead to the formation of CdO. In polyethylene glycol, decomposition of cadmium nitrate was assumed. This indicates that NO_2 was the main product during the decomposition. This observation is fully consistent with the following mechanism proposed for other anhydrous nitrates of divalent metals [21]:

$$M(NO_3)_{2(s)} \longrightarrow MO_{(g)} + 2NO_{2(g)} + 0.5O_2$$

followed by

$$MO_{(g)} \longrightarrow MO_{(s)}$$
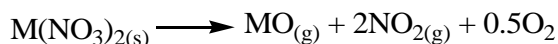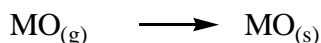
CONCLUSION

By the co-precipitation method used, $Cd(OH)_2$ was formed in a basic medium. The subsequent calcination of $Cd(OH)_2$ lead to the formation of CdO. In polyethylene glycol, $Cd(NO_3)_2 \cdot 4H_2O$ decomposed and nano-sized cadmium oxide was directly formed, without formation of $Cd(OH)_2$. The CdO crystals were grown as face-centered cubes over the range (15-25 nm).

REFERENCES

1 B. L. Cushing, V. L. Kolesnichenko, C. J. ÓConnor, *Chem. Rev*., **104**, 3893 (2004).
2 R.B. Waghulade P.P. Patil, Renu Pasricha, *Talanta*, **72**, 594 (2007).
3 G.N. Chaudhari, A.M. Bende, A.B. Bodade, S.S. Patil, V.S. Sapkal, *Sens. Actuators B*, **115** 297 (2006).
4 A. Srivastava,K. Jain, A.K. Rashmi, S.T. Srivastava, Lakshmikumar, *Mater. Chem. Phys*. **97**, 85 (2006).
5 G.N. Chaudhari, A.M. Bende, A.B. Bodade, S.S. Patil, S.V. Manorama, *Talanta*, **69,** 187, (2006).
6 C. Aifan, H. Xiaodong, T. Zhangfa, B. Shouli, L. Ruixian, L.C. Chiun, *Sens. Actuators B*, **115**, 316 (2006).
7 C.H. Champness, K. Ghoneim, J.K. Chen, *Can. J. Phys*., **63**, 767 (1985).
8 L. M. Su, N. Grote, F . Schmitt, *Electron. Lett*., **20**, 716 (1984).
9 L. M. Su, N. Grote, F. Schmitt, *Electron Lett*., **20**, 717 (1984).
10 I.M. Ocampo, A.M. Ferandez, P.J. Sabastian, *Semicond. Sci. Technol*., **8**, 750 (1993).
11 F.A. Benko, F.P. Koffyberg, *Solid State Commun*., **57**, 901 (1986).
12 K. Gurumugan, D. Mangalarag, SA. K. Narayandass, K. Sekar, C. P. Girija Vallabham, *Semicond. Sci. Tech*., **9**, 1827 (1994).
13 C. Xiangfeng, L. Xingqin, M. Guangyao, *Sens. Actuators B*, **65**, 64 (2000).
14 R.S. Mane, H.M. Pathan, C.D. Lokhande, S-H Han, *Solar Energy*, **80**, 185 (2006).
15 C. Qiu, X. Xiao, R. Liu, *Ceramics International*, **34**, 1747 (2008).
16 J.X. Duan, X.T. Huang, E. Wang, *Mater. Lett*., **60**, 1918 (2006).
17 M.A. Malmsten, K.B. Emoto, J.M. Van Alstine, *J. Colloid Interf. Sci*., 202, 507 (1998).
18 A. Askarinejad, A. Morsali, *Mater. Lett*., **62**, 478 (2008).
19 R.R. Salunkhe, V.R. Shinde, C.D. Lokhande, *Sens. Actuators B*, **133**, 296 (2008).
20 Y. W. Wang, C.H. Liang, G. Z. Wang, T. Gao, S. X. Wang, J. C. Fan, L. D. Zhang, *J. Mater. Sci. Let*t., **20**, 1687 (2001).
21 K.T. Wojciechowski, A. Małecki, *Thermochim. Acta*, **331**, 73 (1999).

ПРОСТ МЕТОД ЗА СИНТЕЗА НА НАНОЧАСТИЦИ ОТ КАДМИЕВ ОКСИД ПРИ ИЗПОЛЗВАНЕТО НА ПОЛИЕТИЛЕНГЛИКОЛ

М. Табатабаее[a], А.А. Мозафари[a], М. Гасемзаде[b], М. Реза Натеги[a], И. Абедини[c]

[a]Департамент по химия, Клон Язд, Ислямски университет „Азад“, Язд, Иран
[b]Ирански изследователски център по химия и химично инженерство, Техеран, Иран
[c] Департамент по приложна химия, Университет „Малек-е-Ащар“, Есфахан, Шахин Шахр, Иран

(Резюме)

Синтезирани са наноразмерни частици от кадмиев оксид по прост метод, използвайки $Cd(NO_3)_2.4H_2O$ в присъствие на полиетиленгликол (PEG 2000). Използвани са рентгенова дифракция, сканираща електронна микроскопия, трансмисионна електронна микроскопия и енерго-дисперсионна спектроскопия за охарактеризиране на структурата и морфологията на синтезираните прахове. Резултатите показват, че PEG играят значителна роля за разлагането на кадмиев нитрат до наночастици от кадмиев оксид. Кристалите от CdO израстват в лицево-центрирана кубична решетка с размери в интервала15-25 nm.

Gel chromatographic analysis of ficin under native and under denaturing conditions

N.A.A. Sidek, Z. Alias, S. Tayyab*

Biomolecular Research Group, Biochemistry Programme, Institute of Biological Sciences, Faculty of Science, University of Malaya, 50603 Kuala Lumpur, Malaysia

Abstract. The hydrodynamic behaviour of a commercial ficin preparation was studied by analytical gel chromatography on Sephacryl S-200 HR column under native and under denaturing (in presence of 9 M urea / 6 M guanidine hydrochloride, GdnHCl) conditions. The commercial ficin preparation was fractionated into seven distinct active components (I–VII) under native conditions. The elution of the components (I–III) as compared to α-chymotrypsinogen and the elution of the components (IV–VII) at a volume exceeding the total bed volume were suggestive of the interaction between the protein molecules and the gel. Treatment of ficin with denaturants (9 M urea / 6 M GdnHCl) resulted in its elution in the form of two peaks, indicating the presence of two classes of conformers differing in their stability towards denaturants. Analysis of the chromatographic data yielded the available Stokes radii of ficin (peak I fraction) as 9.2 Å (under native conditions), 25.8 Å (in presence of 9 M urea) and 40.9 Å (in presence of 6 M GdnHCl). A comparison of Stokes radii of ficin obtained under denaturing conditions suggested complete denaturation of ficin in 6 M GdnHCl compared to 9 M urea which produced significantly less conformational alteration.

Key words: ficin, gel chromatography, guanidine hydrochloride, Stokes radius, urea

INTRODUCTION

Denaturation of a protein by chemical denaturants like urea and guanidine hydrochloride (GdnHCl) usually results in the same unfolded state of proteins [1, 2]. However, this is not always true as some proteins, *e.g.* papain, cytochrome c_{551} and stem bromelain have shown different behaviour in these denaturants [3–5]. Ficin (E.C. 3.4.22.3) is a sulfhydryl protease belonging to the papain super family based on its many properties and structural similarity to papain [6]. The enzyme, which can be naturally obtained from the latex of fig trees, is known to consist of several active components [7–15]. Occurrence of multiple molecular forms of ficin has been suggested due to variation in the folding mechanisms producing different conformers [15]. The possibility of homologous replacements of an amino acid for another in the amino acid sequence to produce these multiple forms cannot be ruled out [15]. Results on the characterization of these multiple molecular forms of ficin have shown a mixed behaviour. While several reports have suggested similarities in these components based on their molecular properties [10–15], others have shown some differences [9, 13]. Despite extensive studies on the molecular

properties of these components [9–15], no attempt has been made so far to investigate the effect of denaturants (urea and GdnHCl) on their behaviour.

Both acid and chemical denaturation studies have been performed on the major ficin fraction [16, 17]. Recently, we have shown different denatured states of ficin produced by 9 M urea and 6 M GdnHCl [18]. We have also noticed differences in the denaturation behaviour of a commercial ficin preparation (consisting of several active components) when compared to that obtained with a major ficin fraction (unpublished results). This has prompted us to investigate the hydrodynamic behaviour of commercial ficin under native and under denaturing conditions using analytical gel chromatography. Here we report our data on the gel chromatographic analysis of a commercial ficin preparation both in the absence and presence of 9 M urea or 6 M GdnHCl.

EXPERIMENTAL

Materials

Ficin from fig tree latex, 2 × crystallized (Lot 058K7019), Sephacryl S-200 HR (Lot 116K0771), urea (SigmaUltra) (Lot 127K0106), GdnHCl (Lot 078K5425), blue dextran (Lot 066K1083), L-tyrosine (Lot 0001412611) and various marker proteins such as α-chymotrypsinogen A, type II

---

from bovine pancreas (Lot 029K7014), carbonic anhydrase from bovine erythrocytes (Lot 99H0669) and cytochrome c from horse heart (Lot 088K7000) were procured from Sigma-Aldrich Inc., USA. Conalbumin and ovalbumin were obtained from the Gel Filtration Calibration Kit HMW (Lot 375428) supplied by GE Healthcare, UK. All other chemicals used were of analytical grade purity.

Analytical procedures

Ficin concentration was determined spectrophotometrically using the specific extinction coefficient of 21.0 at 280 nm [6] on a Shimadzu double beam spectrophotometer, model UV-2450. Concentrations of urea and GdnHCl stock solutions were determined following the method suggested by Pace *et al.* [19] using the data of Warren and Gordon [20] and Nozaki [21], respectively.

Preparation of denatured protein solutions

Stock urea (10 M) and GdnHCl (6.67 M) solutions were made in 0.1 M sodium phosphate buffer, pH 7.0. To 0.5 ml stock protein sol mg/ml), 4.5 ml of stock denaturant soluti added in separate tubes in order to get the final urea and GdnHCl concentrations as 9 M and 6 M respectively. The final solution mixture (5.0 ml) was incubated for 6 h at 25°C prior to gel chromatography.

Analytical gel chromatography

Gel chromatography was performed using a Sephacryl S-200 HR column (Econo-Column, Bio-Rad Laboratories, USA) (1.5 × 16.6 cm) interfaced with AktaPrime Plus chromatographic system (GE Healthcare, UK). A 500 μl sample (2–2.5 mg protein/ml) was injected into a column pre-equilibrated with 0.1 M sodium phosphate buffer, pH 7.0 with or without 9 M urea / 6 M GdnHCl and the flow rate was maintained at 0.3 ml/min. The column was also calibrated with standard protein markers both under native and denaturing (in presence of 9 M urea / 6 M GdnHCl) conditions. The different marker proteins used with their known Stokes radii under native conditions and in presence of 9 M urea or 6 M GdnHCl were: conalbumin, ovalbumin, carbonic anhydrase, α-chymotrypsinogen A and cytochrome c [22–28]. Void volume, V_o of the column was determined by passing blue dextran, whereas the total volume, V_t was calculated using the formula, $\pi r^2 h$, where 'r' is the radius of the column (0.75 cm) and 'h' is the height of the gel bed in the column (16.6 cm). V_t was found to be 29.35 ml under native conditions,

as well as in presence of 9 M urea. Since the height of the gel bed increased from 16.6 cm to 16.8 cm in the presence of 6M GdnHCl, the value of V_t changed from 29.35 ml to 29.7 ml. Elution volumes were determined by passing each component at least twice through the same column. Values of the elution volume of different marker proteins, as well as of ficin, peak I fraction, obtained under both native and denaturing conditions were transformed into distribution coefficient, K_d and available distribution coefficient, K_{av}, in the same way as described earlier [29]. Stokes radii of native and denatured ficin peak I fraction were determined by treating the gel chromatographic data according to Laurent and Killander [30] and Ackers [31]. Theoretical calculations were also made to determine the Stokes radii of native and denatured ficins following the method suggested by Uversky [27]. A molecular weight value of 23,800 [8] was used for ficin in these calculations.

RESULTS AND DISCUSSION

Figure 1 shows elution profiles of a commercial ficin preparation under both native (A) and denaturing (B and C) conditions when chromatographed on a Sephacryl S-200 HR column (1.5 × 16.6 cm).
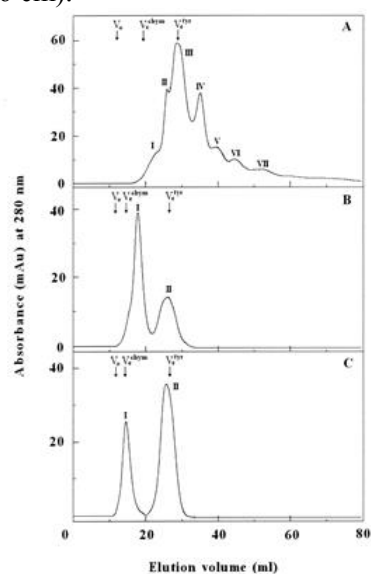

Fig. 1. Elution profiles of a commercial ficin preparation on Sephacryl S-200 HR column (1.5 × 16.6 cm) equilibrated with 0.1 M sodium phosphate buffer, pH 7.0 (A); 0.1 M sodium phosphate buffer containing 9 M urea (B) and 0.1 M sodium phosphate buffer containing 6 M GdnHCl (C). Elution volumes of blue dextran, α-chymotrypsinogen and L-tyrosine are shown by arrows marked by V_o, V_e^{chym} and V_e^{tyr}, respectively.

The values of the elution volume of blue dextran (void volume), α-chymotrypsinogen and L-tyrosine on the same column are marked in Fig. 1 as V_o,

94

V_e^{chym} and V_e^{tyr}, respectively. Under native conditions, the values of V_o, V_e^{chym} and V_e^{tyr} were found to be 11.97, 19.36 and 29.0 ml, respectively (Table 1). As can be seen from Fig. 1A, the commercial ficin preparation was fractionated into seven components (I–VII) with elution volumes of 22.4, 25.48, 28.93, 34.65, 39.59, 44.16 and 52.41 ml, respectively (Table 1).

Table 1. Values of elution volume, V_e of commercial ficin, α-chymotrypsinogen, L-tyrosine and blue dextran on Sephacryl S-200 HR column (1.5 × 16.6 cm) equilibrated with 0.1 M sodium phosphate buffer, pH 7.0 with or without 9 M urea or 6 M GdnHCl.

Protein/ Sample	Elution volume, V_e (ml)		
	0.1 M Sodium phosphate buffer, pH 7.0	0.1 M Sodium phosphate buffer, pH 7.0 containing 9 M urea	0.1 M Sodium phosphate buffer, pH 7.0 containing 6 M GdnHCl
Ficin Peak - I	22.40	17.79	14.54
- II	25.48	26.21	25.67
- III	28.93		
- IV	34.65		
- V	39.59		
- VI	44.16		
- VII	52.41		
α-Chymotrypsinogen	19.36	14.56	14.35
L-Tyrosine	29.00	26.62	26.68
Blue dextran	11.97	11.57	11.75

Interestingly, all these fractions were found active when checked for enzymatic activity. In view of this, all these components are believed to represent various isomeric forms of ficin. This was in accordance with previous reports [7–15] suggesting the presence of several components (conformers) in the ficin preparation. Four components, namely, IV, V, VI and VII, were eluted from the column with elution volumes higher than the total bed volume, V_t (29.35 ml) of the column (Table 1). Even the remaining three components (I, II and III) stayed longer in the column, as reflected by their elution volumes in relation to the total volume of the column (Table 1). This became more evident when the elution volumes of these three components were compared with the elution volume of α-chymotrypsinogen on the same column (19.36 ml). Being approximately similar in size (molecular weight = 25, 656), α-chymotrypsinogen was eluted much earlier than the three components of ficin (I, II and III). In fact, peak III had more or less the same elution volume as that obtained with L-tyrosine (Table 1). Emergence of peaks IV–VII after the total bed volume and higher elution volumes of peak I–III compared to similar sized protein, α-

chymotrypsinogen, clearly suggested an interaction between these protein components and the gel. It seems probable that ficin components reacted with the gel through non-polar interactions in the same way as adsorption of aromatic compounds takes place onto the Sephadex gel [32]. The unusual retention of ficin on Sephadex G-75 has been shown in a previous report [8], attributing it to the high content of aromatic residues. The role of both hydrophobic and ionic interactions has been suggested in the interaction of a few proteins with the gel due to the weak hydrophobic and ionic nature of gel filtration media [33]. Therefore, interaction of cationic ficin with Sephacryl gel may involve both hydrophobic and ionic interactions. A few other proteins such as lysozyme and *Bacillus licheniformis* α-amylase have also shown interaction with the gel media [34–35].

Treatment of a commercial ficin preparation with 9 M urea for 6 h at 25ºC and its chromatographic analysis on Sephacryl S-200 HR column (1.5 × 16.6 cm) equilibrated with 0.1 M sodium phosphate buffer, pH 7.0 containing 9 M urea showed the presence of two peaks, namely, I and II (Fig. 1B) with elution volumes of 17.79 and 26.21 ml, respectively (Table 1). Furthermore, the values of the elution volume of α-chymotrypsinogen (14.56 ml), L-tyrosine (26.62 ml) and blue dextran (11.57 ml) on the same column also changed compared to those obtained under native conditions (Table 1). Since 9 M urea denatures the globular conformation of a protein into a more extended random-coil conformation, the lower values of the elution volumes of peak I and II compared to those obtained under native conditions are understandable. However, the emergence of seven components of ficin (under native conditions) in the form of two peaks (I and II) in presence of 9 M urea suggested the presence of two different entities differing in their denatured conformations. It seems possible that the different conformers of ficin represented by peaks I–VII under native conditions might be grouped into two classes based on their conformational stability in presence of 9 M urea. Peak I (Fig. 1B) might incorporate two other isomers in a denatured form, which were eluted as peaks I, II and III under native conditions (Fig. 1A). Similarly, peak II (Fig. 1B) might represent those conformers in a denatured form, which were eluted as peaks IV –VII under native conditions (Fig. 1A). It is noteworthy that peak II obtained in 9 M urea had a similar elution volume to that of L-tyrosine (Table 1), suggesting

relatively more compact conformation than peak I molecules in 9 M urea.

Interestingly, when the commercial ficin preparation was treated with 6 M GdnHCl at 25°C for 6 h and chromatographed on Sephacryl S-200 HR column (1.5 × 16.8 cm) equilibrated with 0.1 M sodium phosphate buffer, pH 7.0 containing 6 M GdnHCl, the elution profile also showed the presence of two peaks (I and II) with elution volumes of 14.54 and 25.67 ml, respectively (Fig. 1C, Table 1). The values of V_o, V_e^{chym} and V_e^{tyr} changed in the same way as those obtained in presence of 9 M urea when compared to those found under native conditions (Table 1). These results further supported our hypothesis on the existence of two classes of conformers differing in structural stability against these chemical denaturants. Although peak II obtained in presence of 6 M GdnHCl showed a slight difference in elution volume when compared to that of peak II observed with 9 M urea, peak I showed a remarkable difference in elution volume under these two denaturing conditions (Table 1). Peak I obtained with 6 M GdnHCl-denatured ficin was eluted much earlier (14.54 ml) than peak I obtained with 9 M urea-treated ficin (17.79 ml) (Table 1). Such difference in the elution volumes of peak I obtained in 6 M GdnHCl as well as in 9 M urea suggested different denatured states of ficin peak I fraction, which was completely denatured in 6 M GdnHCl and partially denatured in 9 M urea. Similar denatured states of proteins have been observed after treating them with either 8 M urea or 6 M GdnHCl [1, 2]. This can be clearly seen from the elution volumes of α-chymotrypsinogen which were similar in 9 M urea and in 6 M GdnHCl (Table 1), suggesting a similar denatured conformation of the protein in these two denaturants. Interestingly, the elution volume of ficin peak I fraction in 6 M GdnHCl matched very well the elution volume of α-chymotrypsinogen in 9 M urea. This was suggestive of the completely denatured conformation of ficin peak I fraction in 6 M GdnHCl. On the other hand, a higher value of the elution volume (17.79 ml) obtained for ficin peak I fraction in 9 M urea clearly indicated the retention of some native elements in the urea-denatured state. In other words, 6 M GdnHCl was found to be the stronger denaturant compared to 9 M urea with respect to ficin peak I fraction denaturation. This agreed well with a previous report [18] in which we have shown completely different denatured states of ficin produced by 9 M urea and 6 M GdnHCl, ficin being completely denatured in 6 M GdnHCl.

In order to validate the different action of these two denaturants on ficin (peak I fraction) denaturation, we determined the Stokes radii of ficin under native and under denaturing conditions using analytical gel chromatography. The same column was calibrated by passing different marker proteins with known Stokes radii (see column 2 of Table 2), *i.e.* conalbumin, ovalbumin, carbonic anhydrase, α-chymotrypsinogen and cytochrome c under native conditions, as well as in presence of 9 M urea or 6 M GdnHCl. Table 2 shows the values of the elution volume of different marker proteins, as well as the ficin peak I fraction obtained under native and denaturing (in presence of 9 M urea / 6 M GdnHCl) conditions. Transformations of V_e into K_{av} and K_d were made as described in the 'Materials and Methods' section and these values along with their other transformations, $(-\log K_{av})^{1/2}$ and $erfc^{-1}K_d$ are also given in Table 2.

Figures 2A and B show standard plots of marker proteins under native and denaturing conditions after treating the gel chromatographic data according to Laurent and Killander [30] and Ackers [31], respectively, which yielded the following linear equations:

Under native conditions:

$$(-\log K_{av})^{1/2} = 0.0110 \text{ Stokes radius, Å} + 0.374 \quad (1)$$

$$\text{Stokes radius, Å} = 59.622 \, erfc^{-1}K_d - 11.689 \quad (2)$$

In presence of 9 M urea:

$$(-\log K_{av})^{1/2} = 0.0138 \text{ Stokes radius, Å} + 0.317 \quad (3)$$

$$\text{Stokes radius, Å} = 41.773 \, erfc^{-1}K_d + 3.1006 \quad (4)$$

In presence of 6 M GdnHCl:

$$(-\log K_{av})^{1/2} = 0.0117 \text{ Stokes radius, Å} + 0.4218 \quad (5)$$

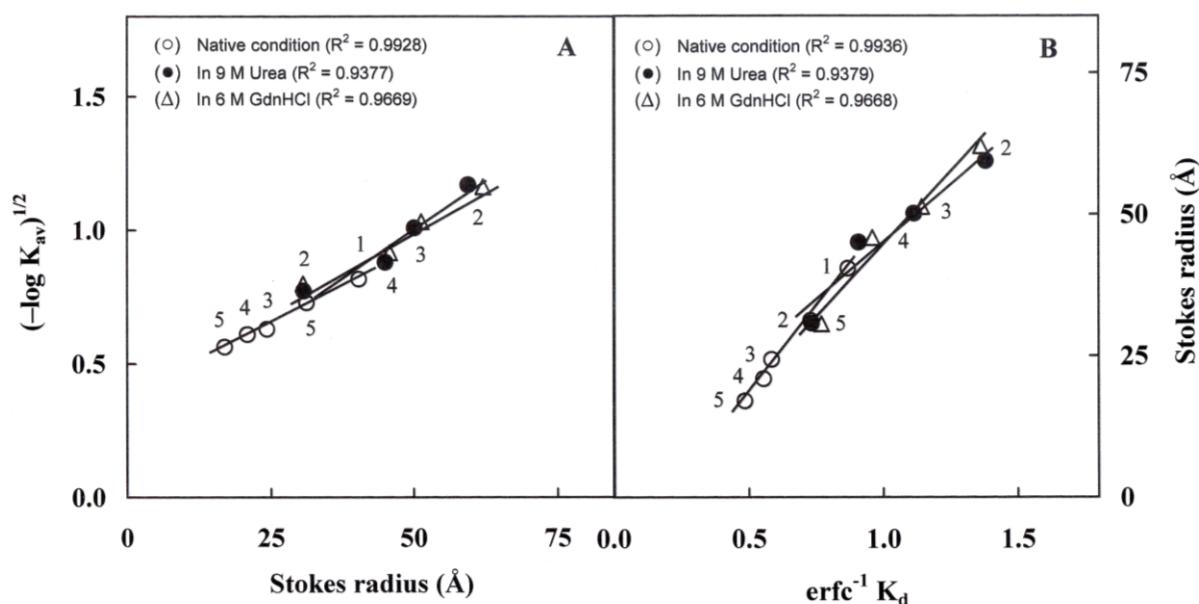$$\text{Stokes radius, Å} = 50.887 \, erfc^{-1}K_d - 6.4588 \quad (6)$$

Fig. 2. Treatment of gel chromatographic data of marker proteins in the absence (○) and presence of 9 M urea (●) or 6 M GdnHCl (Δ) according to (A) Laurent and Killander [30] and (B) Ackers [31] for the determination of Stokes radii of native, urea-denatured and GdnHCl-denatured ficins (peak I fractions).

Table 2. Analytical gel chromatographic data of marker proteins and ficin peak I fraction on Sephacryl S-200 HR column (1.5 × 16.6 cm) under native (0.1 M sodium phosphate buffer, pH 7.0) and denaturing conditions (buffer containing either 9 M urea or 6 M GdnHCl).

Proteins	Stokes radius (Å)	V_e (ml)	K_{av}	K_d	$(-\log K_{av})^{1/2}$	$erfc^{-1} K_d$
A. Under native conditions						
Conalbumin	40.4 [26]	15.71	0.2152	0.2196	0.8168	0.8697
Ovalbumin	31.2 [25]	17.09	0.2946	0.3006	0.7285	0.7311
Carbonic anhydrase	24.3 [23]	18.95	0.4016	0.4099	0.6294	0.5841
α-Chymotrypsinogen	20.9 [22]	19.36	0.4252	0.4339	0.6094	0.5544
Cytochrome c	17.0 [26]	20.36	0.4827	0.4927	0.5624	0.4851
Ficin Peak - I	–	22.40	0.6001	0.6124	0.4709	0.3578
B. In presence of 9 M Urea						
Ovalbumin	59.4 [27]	12.33	0.0427	0.0505	1.1701	1.3803
Carbonic anhydrase	50.1 [27]	13.28	0.0962	0.1136	1.0084	1.1130
α-Chymotrypsinogen	45.0 [27]	14.56	0.1682	0.1987	0.8799	0.9093
Cytochrome c	30.7 [27]	16.07	0.2531	0.2990	0.7725	0.7340
Ficin Peak - I	–	17.79	0.3498	0.4133	0.6754	0.5798
C. In presence of 6 M GdnHCl						
Ovalbumin	62.0 [24]	12.55	0.0446	0.0536	1.1623	1.3619
Carbonic anhydrase	51.3 [27]	13.30	0.0864	0.1038	1.0314	1.1427
α-Chymotrypsinogen	45.8 [28]	14.35	0.1448	0.1741	0.9160	0.9603
Cytochrome c	30.6 [27]	15.88	0.2301	0.2766	0.7988	0.7707
Ficin Peak - I	–	14.54	0.1554	0.1869	0.8991	0.9334

Substitution of $(-\log K_{av})^{1/2}$ and $erfc^{-1}K_d$ values of ficin peak I fraction obtained under native and denaturing conditions (Table 2) into equations 1–6 yielded the values of Stokes radii of native and denatured ficins. These values obtained from two different treatments along with their mean values are given in Table 3. It should be noted that under native conditions and in presence of 9 M urea, the elution volume of ficin peak I fraction falls outside the range of standard proteins used (Table 2) due to interaction of the protein molecules with the gel. Therefore, such experimentally determined Stokes radii of ficin are referred to as 'available Stokes radii'. Stokes radii of ficin under native and denaturing conditions were theoretically calculated as well by substituting the molecular weight of ficin (23, 800 Da [8]) into different equations as suggested by Uversky [27] and these values are also listed in the last column of Table 3.

97

Native ficin (peak I fraction) yielded an experimentally determined value of Stokes radius of 9.2 Å compared to 23.0 Å theoretically calculated using Uversky's equation [27] (Table 3). Such a low value of experimentally determined Stokes radius of ficin can be ascribed to the possible interaction of the protein with the gel, as this value was based on the elution volume of the protein on Sephacryl S-200 HR column. Treatment of ficin with either 9 M urea or 6 M GdnHCl led to an increase in its hydrodynamic volume as revealed by the increase in its Stokes radius from 9.2 Å to 25.8 Å in presence of 9 M urea and 40.9 Å in presence of 6 M GdnHCl (Table 3).

Table 3. Stokes radii of ficin under native and under denatured conditions as determined from analytical gel chromatographic data following the methods of Laurent and Killander [30] and Ackers [31], as well as using the theoretical method of Uversky [27].

Ficin (Peak - I)	Stokes radius (Å)			
	Laurent and Killander's method [30]	Ackers' method [31]	Mean	Uversky's method [27]
Native	8.8	9.6	9.2	23.0
In 9 M urea	24.9	26.6	25.8	43.3
In 6 M GdnHCl	40.8	41.0	40.9	45.1

Both 9 M urea and 6 M GdnHCl are known to remove all kinds of non-covalent interactions present in a protein's three-dimensional structure [34–38]. Theoretical calculations of Stokes radii of ficin in 9 M urea (43.3 Å) as well as in 6 M GdnHCl (45.1 Å) following Uversky's method [27] also supported this contention, as these values were found similar to each other and much higher than that of the native ficin (Table 3). This was further supported by the Stokes radii of α-chymotrypsinogen in 9 M urea or 6 M GdnHCl (Table 2) which were similar to the theoretically calculated value of ficin (Table 3). A significant difference was noticed between the experimentally determined values of Stokes radii of ficin obtained in presence of 9 M urea (25.8 Å) and 6 M GdnHCl (40.9 Å). Furthermore, the experimentally determined value of Stokes radius of ficin in 6 M GdnHCl is close to the theoretically determined value of denatured ficin (Table 3). Although the presence of 9 M urea produced a significant change in the hydrodynamic volume of ficin, this was significantly less than the change observed with 6 M GdnHCl. These results suggested a nearly complete denaturation of ficin in presence of 6 M

GdnHCl compared to 9 M urea which partially denatured it. All these results were found in agreement with our previously published report suggesting different denatured states of ficin produced in 6 M GdnHCl and in 9 M urea, being completely denatured in 6 M GdnHCl [18].

REFERENCES

1 .C. N. Pace, Crit. Rev. Biochem. Mol. Biol., **3**, 1 (1975).
2 C. Tanford, K. Kawahara, S. Lapanje, J. Am. Chem. Soc., **89**, 729 (1967).
3 B. Ahmad, T. A. Shamim, R. H. Khan, J. Biochem., **141**, 251 (2006).
4 S. Gianni, M. Brunori, C. Travaglini-Allocatelli, Protein Sci., **10**, 1685 (2001).
5 P. Zhuang, D. A. Butterfield, Biophys. J., **60**, 623 (1991).
6 I. E. Liener, B. Friedenson, Methods Enzymol., **19**, 261 (1970).
7 K. B. Devaraj, P. R. Kumar, V. Prakash, J. Agric. Food Chem., **56**, 11417 (2008).
8 . P. T. Englund, T. P. King, L. C. Craig, A. Walti, Biochemistry, **7**, 163 (1968).
9 I. K. Jones, A. N. Glazer, J. Biol. Chem., **245**, 2765 (1970).
10 A. A. Kortt, S. Hamilton, E. C. Webb, B. Zerner, Biochemistry, **13**, 2023 (1974).
11 D. E. Kramer, J. R. Whitaker, Plant Physiol., **44**, 1560 (1969).
12 J. P. G. Malthouse, K. Brocklehurst, Biochem. J., **159**, 221 (1976).
13 V. C. Sgarbieri, S. M. Gupte, D. E. Kramer, J. R. Whitaker, J. Biol. Chem., **78**, 751 (1964).
14 D. C. Williams, V. C. Sgarbieri, J. R. Whitaker, Plant Physiol., **43**, 1083 (1968).
15 D. C. Williams, J. R. Whitaker, Plant Physiol., **44**, 1574 (1969).
16 K. B. Devaraj, P. R. Kumar, V. Prakash, Int. J. Biol. Macromol., **45**, 248 (2009).
17 K. B. Devaraj, P. R. Kumar, V. Prakash, Process Biochem., **46**, 458 (2010).
18 N. A. A. Sidek, A. A. A. Halim, S. Tayyab, Turk. J. Biochem., **35**, 45 (2010).

19 C. N. Pace, B. A. Shirley, J. A. Thomson, Protein Structure: A Practical Approach, Oxford University Press, New York, 1989, p. 311.

20 J. R. Warren, J. A. Gordon, J. Phys. Chem., **70**, 297 (1966).

21 Y. Nozaki, Methods Enzymol., **26**, 43 (1972).

22 I. M. Cheeseman, C. Brew, M. Wolyniak, A. Desai, S. Anderson, N. Muster, J. R. Yates, T. C. Huffaker, D. G. Drubin, G. Barnes, J. Cell Biol., **24**, 1137 (2001).

23 J. D. Colbert, A. Plechanovová, C. Watts, Traffic, **10**, 425 (2009).

24 R. J. T. Corbett, R. S. Roche, Biochemistry, **23**, 1888 (1984).

25 S. C. Sanyal, D. Bhattacharyya, C. D. Gupta, Eur. J. Biochem., **269**, 3856 (2002).

26 W. M. Southerland, D. R. Winge, K. V. Rajagopalan, J. Biol. Chem., **253**, 8747 (1978).

27 V. N. Uversky, Biochemistry, **32**, 13288 (1993).

28 H. –X. Zhou, J. Phys. Chem., B., **106**, 5769 (2002).

29 S. Tayyab, S. Qamar, M. Islam, Biochem. Edu., **19**, 149 (1991).

30 T. C. Laurent, J. Killander, J. Chromatogr., **14**, 317 (1964).

31 G. K. Ackers, *J. Biol. Chem.*, **242**, 3237 (1967).

32 J. Porath, Adv. Protein Chem., **17**, 209 (1962).

33 N. P. Golovchenko, I. A. Kataeva, V.K. Akimenko, J. Chromatogr. A, **591**, 121 (1992).

34 H. N. Ong, B. Arumugam, S. Tayyab, J. Biochem., **146**, 895 (2009).

35 C. Y. Tan, R. N. Z. Rahman, H. A. Kadir, S. Tayyab, Acta Biochim. Pol., **58**, 405 (2011).

36 A. Caballero-Herrera, K. Nordstrand, K. D. Berndt, L. Nilsson, Biophys. J., **89**, 842 (2005).

37 L. J. Donald, V. M. Collado, J. J. Galka, J. D. O'Neil, H. W. Duckworth, P. C. Loewen, K. G. Standing, Rapid Commun. Mass Spectrom., **23**, 788 (2009).

38 O. D. Monera, C. M. Kay, R. S. Hodges, Protein Sci., **3**, 1984 (1994).

39 Y. Nozaki, C. Tanford, J. Biol. Chem., **238**, 4074 (1963).

40 D. B. Wetlaufer, S. K. Malik, L. Stoller, R. L. Coffin, J. Am. Chem. Soc., **86**, 508 (1964).

ГЕЛ -ХРОМАТОГРАФСКИ АНАЛИЗ НА ФИЦИН ПРИ ЕСТЕСТВЕНИ УСЛОВИЯ И ПРИ ДЕНАТУРИРАНЕ

Н. А. А. Сидек, З. Алиас, С. Таййаб

Група за биомолекулярни изследвания,Програма за биохимия, Институт по биологични науки, Научен факултет, Малайски университет, 50603 Куала Лумпур, Малайзия

(Резюме)

Изследвани са хидродинамичните отнасяния на търговски препарат от фицин с помощта на аналитична гел-хроматография на колона Sephacryl S-200 HR при нативни условия и при денуриране (с 9 M карбамид / 6 M гванидин хидрохлорид, GdnHCl). Търговският препарат от фицин е фракциониран на седем различни активни компоненти (I–VII) при нативниуслвия. Елуирането на компонентите (I–III), сравнени с α-хемотропсиноген и елуирането на компонентите (IV–VII) в обеми, превишаващи общия обем на колоната дават сведения за взаимодействията между протеиновите молекули и гела. Третирането на фицина с денатуранти (с 9 M карбамид / 6 M гванидин хидрохлорид, GdnHCl) води до елуирането като два пика, показващо съществуването на два класа конформери различаващи се по тяхната устойчивост спрямо денатуриращите агенти. Анализът на хроматографските данни дава Стоксовите радиуси на фицина (за фракцията по пик 1) 9.2 Å (при наивни условия), 25.8 Å (в присъствие на 9 M карбамид) и 40.9 Å (в присъствие на 6 M GdnHCl). Сравнението на Стоксовите радиуси на фицина, получени при условия на денатуриране говорят за пълно денатуриране в 6 M GdnHCl в сравнение на 9 M карбамид, което води до сначително по-малко конформационни изменения.

Synthesis, crystal structure and theoretical study of two isomeric poly-substituted derivatives of 1,4-dihydropyridine

Stefan Dochev,[1] Markus Ströbele,[2] Hans-Jürgen Meyer,[2] Ilia Manolov[3]

[1]Research Group Mihovilovic, Research Division of Organic Chemistry, Institute of Applied Synthetic Chemistry, Faculty of Technical Chemistry, Vienna University of Technology, A-1060 Vienna, Austria
[2]Abteilung für Festkörperchemie und Theoretische Anorganische Chemie, Institut für Anorganische Chemie, Universität Tübingen, Ob dem Himmelreich 7, D-72074 Tübingen, Deutschland
[3]Department of Pharmaceutical Chemistry, Faculty of Pharmacy, Medical University, Dunav 2 Str., BG-1000 Sofia, Bulgaria;

1,4-Dihydropyridines are well known as an important class of calcium-channel blockers with wide clinical usage as antihypertensive agents. They have very interesting spectral and chemical properties, which are investigated experimentally and theoretically. Two isomeric poly-substituted 1,4-dihydropyrid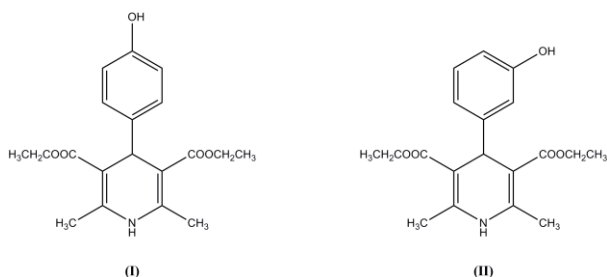ines were synthesized by three different one-step synthetic schemes. The structures of diethyl 4-(4-hydroxyphenyl)-2,6-dimethyl-1,4-dihydropyridine-3,5-dicarboxylate (**I**) and diethyl 4-(3-hydroxyphenyl)-2,6-dimethyl-1,4-dihydropyridine-3,5-dicarboxylate (**II**) were characterized by melting point, elemental analysis, IR and UV-Vis spectroscopy. Their structures were confirmed by X-Ray crystallography. The compound (**I**) crystallizes in a monoclinic system, space group $P2_1/c$, $a = 739.1(1)$, $b = 2769.5(3)$, $c = 880.9(1)$ Å, $\alpha = 104.24(2)$ º, $\beta = \gamma = 90$º, $Z = 4$, $V = 1.7476(4)$ Å^3. The compound (**II**) crystallizes triclinic, space group $P\bar{1}$, $a = 742.8(1)$, $b = 894.2(2)$, $c = 1407.5(2)$ Å, $\alpha = 80.23(2)$ º, $\beta = 86.86(2)^0$, $\gamma = 68.71(2)$º, $Z = 2$, $V = 0.8584(3)$ Å^3. The spectral behavior of the optimized structures of these compounds was reproduced by the hybrid DFT method B3LYP and HF method both with 6-31G basis set and some semi-empirical methods for comparison. The theoretical spectra were compared with the experimental ones.

Key words: 1,4-Dihydropyridines; Synthesis; X-Ray Diffraction Analysis; DFT, HF, AM1 and PM3 Study; UV-Vis and IR spectra.

INTRODUCTION

The nucleus of 1,4-dihydropyridine (1,4-DHP) is an important scaffold for calcium channel antagonism and other cardiovascular activities [1-5]. The structural requirement for such antihypertensive and antianginal properties has the envisaged importance of electron-withdrawing groups at a *meta* substituted phenyl ring, attached to the C4 of 1,4-DHP rings. Most of the known DHP drugs have symmetrical, as well as asymmetric structures with respect to the C3 and C5 positions. The m-NO$_2$ phenyl 1,4-DHPs were well-explored to obtain *Nimodipine*, *Nitrenedipine*, *Cilnidipine*, *Manidipine*, *Barnidipine* and *Efonidipine*. Along with well known cardiovascular effects of DHPs, there are additional data for antiinflammatory effects [6], antioxidant activity [7], K$_{ATP}$ channel activation activity [8], and atheroprotective effects [9]. Some DHPs have influence on rat paw edema [10]. The hydroxyl group as a substituent has not been well-explored in such DHP systems.

There are many different literature data about Hantzsch reaction [11–15]. Some of them, which we used, give good yields and purity of the resulting compounds, the reaction time is reduced in comparison with the classical type of the reaction and reaction conditions are in agreement with international conventions of green chemistry.

The crystal structures of hydroxyl substituted DHPs are not described in the literature until now. For this reason it was interesting to confirm the supposed structure, because our previous investigations showed that not every arylaldehyde reacts successfully in Hantzsch reaction and in many cases other products are obtained instead of 1,4-DHPs.

The literature data show the good prediction ability of quantum mechanics methods (*ab initio* and semi-empirical) by optimization of molecular geometry and calculation of UV-Vis and IR spectra and some physicochemical properties of 1,4-DHPs [16–19].

---

* To whom all correspondence should be sent:
E-mail: imanolov@gmx.net

EXPERIMENTAL

Materials and Methods

All starting materials were purchased from Merck and Sigma-Aldrich and were reagent grade. They were used without further purification. Melting points were measured in open capillary tubes on a Büchi 535 melting point apparatus. The elemental analysis was realized by atomic absorption spectrometry. The UV-Vis spectra were taken on a Hewlett-Packard 8452A UV-Vis spectrophotometer with a step of 2 nm, scanning speed of 1 s/spectrum with diode-array detector and quartz test tube of 1 cm thickness. The spectra were obtained in ethanol solutions against ethanol as a blank sample. The IR spectra were recorded on a FTIR Perkin-Elmer spectrometer in KBr tablets and frequencies were expressed in cm^{-1}.

General Procedures for the Preparation of 1,4-Dihydropyridines

The compounds diethyl 4-(4-hydroxyphenyl)-2,6-dimethyl-1,4-dihydropyridine-3,5-dicarboxylate (I) and its isomer diethyl 4-(3-hydroxyphenyl)-2,6-dimethyl-1,4,-dihydropyridine-3,5-dicarboxylate (II) (Fig. 1) were synthesized by the:

Fig. **1**. Chemical Structures of diethyl 4-(4-hydroxyphenyl)-2,6-dimethyl-1,4-dihydropyridine-3,5-dicarboxylate (I) and diethyl 4-(3-hydroxyphenyl)-2,6-dimethyl-1,4-dihydropyridine-3,5-dicarboxylate (II)

Experimental Procedure 1 (P1):

A reaction mixture of 3-, resp. 4-hydroxybenzaldehyde (1.22 g, 10 mmol) and ethyl acetoacetate (2.60 g, 20 mmol) was heated in ethanol under reflux until boiling. Then NH$_3$ (3 mL) was added and the mixture was heated for 5 h. After the end of the reaction distilled water (40 mL) was added to the mixture (slowly and carefully). After cooling a yellow precipitate was obtained. The precipitate was recrystallized.

Experimental Procedure 2 (P2):

A reaction mixture of 3-, resp. 4-hydroxybenzaldehyde (1.22 g, 10 mmol), ethyl acetoacetate (2.60 g, 20 mmol) and ammonium acetate (0.77 g, 10 mmol) was heated in water medium under reflux until a yellow precipitate was obtained (1.5 h). The precipitate was recrystallized from an appropriate solvent.

Synthesis of diethyl 4-(4-hydroxyphenyl)-2,6-dimethyl-1,4-dihydropyridine-3,5-dicarboxylate

Yellow crystals, m.p. 231.8-233.7^{0}C (methanol); Yield (P1, P2): 1.82 g (53 %), 3.0 g (87 %); FTIR (KBr): $\bar{\nu}$ = 3352, 3308, 1650, 1595, 1473, 1368, 1218, 1128, 1019 cm^{-1}; UV–Vis (EtOH): λ_{max} = 220, 272, 320, 374 nm; Anal.: C$_{19}$H$_{23}$NO$_5$ (345.38), calcd. % C 66.07, % H 6.71, % N 4.06, found % C 66.53, % H 6.49, % N 4.17.

Synthesis of diethyl 4-(3-hydroxyphenyl)-2,6-dimethyl-1,4-dihydropyridine-3,5-dicarboxylate

Yellow crystals, m.p. 185.8-187.0 ^{0}C (2-propanol); Yield (P1, P2): 1.78 g (52 %), 2.98 g (86 %); FTIR (KBr): $\bar{\nu}$ = 3347, 1662, 1591, 1488, 1369, 1226, 1130, 1021 cm^{-1}; UV-Vis (EtOH): λ_{max} = 220, 274, 320, 376 nm; Anal.: C$_{19}$H$_{23}$NO$_5$ (345.38), calcd. % C 66.07, % H 6.71, % N 4.06, found % C 66.54, % H 6.67, % N 4.11.

X-Ray Crystal Structure Analyses

The crystal structures of the compounds were determined by single crystal X-Ray diffraction. Data collection was carried out at -40 ^{0}C on an IPDS single crystal diffractometer (STOE, Darmstadt) using graphite-monochromated MoK_α radiation. The structures were solved by direct methods with the program SHELXS and refined with SHELXL, both from the SHELXL-97 program package [20]. All atom positions, including those of hydrogen atoms were localized from the electron density map. All non-hydrogen atoms were afterwards refined anisotropically.

Complete data collection parameters and details of the structures solutions and refinements are given in Table 1. The plots of the molecular structures were produced using the DIAMOND program (ver. 3.1) (CRYSTAL IMPACT GbR, Bonn, Germany).

Data of the crystal structures can be obtained from Cambridge Crystallographic Data Centre (CCDC number 701877 (I) and CCDC number 701878 (II)) free of charge via www.ccdc.cam.ac.uk/products/csd/request/.

METHODS OF COMPUTATION

All the calculations were performed on a single processor computer. Gaussian 03 (Frisch et al.) [21] software package was used for structure

Table 1. Crystal data and structure refinement for the two isomeric 1,4-dihydropyridines

Identification code	I	II
Chemical formula	$C_{19}H_{23}NO_5$	$C_{19}H_{23}NO_5$
Formula weight	345.38	345.38
Temperature [K]	230(2)	235(2)
Crystal system	monoclinic	Triclinic
Space group	$P2_1/c$	$P\bar{1}$
Unit cell dimension	$a = 739.0(1)$ pm; $\alpha = 90^0$	$a = 742.8(1)$ pm; $\alpha = 80.23(2)^0$
	$b = 2769.5(3)$ pm	$b = 894.2(2)$ pm
	$\beta = 104.24(2)^0$	$\beta = 86.86(2)^0$
	$c = 880.9(1)$ pm; $\gamma = 90^0$	$c = 1407.5(2)$ pm; $\gamma = 68.71(2)^0$
Cell volume [nm³]	1.7475(4)	0.8584(2)
Z	4	2
Density (calculated) [g cm⁻³]	1.313	1.336
Radiation type	Mo K_{α}	Mo K_{α}
Wavelength [pm]	71.073	71.073
Absorption coefficient [mm⁻¹]	0.095	0.097
$F(000)$	736	368
Crystal description	colorless block	colorless block
Crystal size [mm³]	$0.4 \times 0.3 \times 0.45$	$0.45 \times 0.3 \times 0.3$
Reflections collected	15146	8577
Independent reflections	3054 [R(int) = 0.0393]	2798 [R(int) = 0.0482]
Reflections observed [$I > 2\sigma(I)$]	2325	2176
θ range for data collection [deg]	2.50 to 24.94	2.48 to 25.88
Index ranges	$-8 \le h \le 8, -32 \le k \le 32,$	$-8 \le h \le 8, -10 \le k \le 10,$
	$-10 \le l \le 10$	$-15 \le l \le 15$
Data / parameters	3054 / 318	2798 / 318
Goodness-of-fit on F^2	0.959	1.059
Final R indices [$I > 2\sigma(I)$]	$R1 = 0.0361$; $wR2 = 0.0898$	$R1 = 0.0587$; $wR2 = 0.1361$
Final R indices (all data)	$R1 = 0.0482$; $wR2 = 0.0949$	$R1 = 0.0779$; $wR2 = 0.1450$
$(\Delta/\rho)_{max}$ [e.Å⁻³]	0.267	0.246
$(\Delta/\rho)_{min}$ [e.Å⁻³]	-0.184	-0.220
Measurement	STOE IPDS I	STOE IPDS I
Structure determination	SHELX-97	SHELX-97
Refinement	Full-matrix least-squares on F^2	Full-matrix least-squares on F^2

optimization and spectral behavior calculation. GaussView and ChemBio3D programs were utilized for visualization of all spectra. The hybrid DFT method B3LYP and RHF both with 6-31G basis set and some semi-empirical methods (AM1 and PM3) were used for geometry optimization and calculation of spectral and other properties.

RESULTS AND DISCUSSION

Chemistry

The corresponding two isomeric compounds were synthesized via classical type of Hantzsch reaction under two different reaction conditions. We found some serious advantages of using water as reaction medium in contrast to ethanol. The reaction time was vastly reduced (about 3.5 times); the end of the reaction was visually detected – when the reaction was completed, a precipitate of the target compound was obtained, because of its

low solubility in water. The resulting yield was about 30 % higher. Using of water is also in good agreement with the principles of green chemistry. The synthesized compounds were characterized by elemental analysis, IR and UV-Vis spectrometry and single crystal X-Ray diffractometry. The analytical data confirmed our hypothesis about the structure of I and II.

Crystal Structure

Colorless block-like crystals suitable for X-Ray diffraction analysis were grown by slow evaporation of a methanol, resp. 2-propanol solution of the corresponding compounds. Crystallographic data of the investigated crystals are listed in Table 1. The solid state structures of a molecule of the compounds (I) and (II) are shown in Figs. 2 and 3, respectively.

By comparison of the experimental data for (I) and (II) with the data for other similar compounds
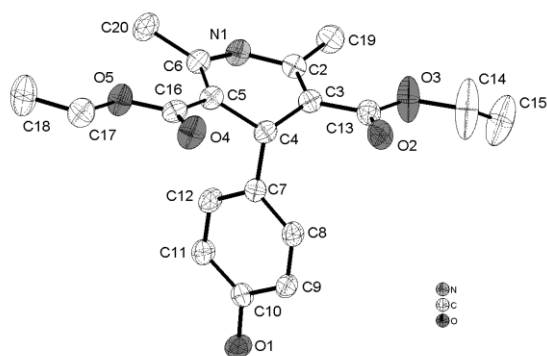
Fig. 2. Crystal structure of diethyl 4-(4-hydroxyphenyl)-2,6-dimethyl-1,4-dihydropyridine-3,5-dicarboxylate (I) (displacement ellipsoids for C and O with 50 % probability). (DIAMOND plot)
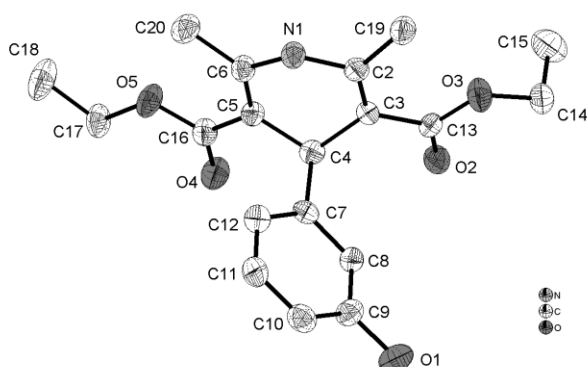

Fig. 3. Crystal structure of diethyl 4-(3-hydroxyphenyl)-2,6-dimethyl-1,4-dihydropyridine-3,5-dicarboxylate (II) (displacement ellipsoids for C and O with 50 % probability). (DIAMOND plot

[22] it can be stated that most of the bond lengths and angles for the described compounds agree very well with the standard values.

The 1,4-dihydropyridine rings have an expected flat boat conformation, with N1 and C4 at a distance of 277.1 Å (I) and 274.8 Å (II) through the four carbon atoms (C2, C3, C5 and C6), which define the base of the boat. The degree of ring distortions at N1 and C4 is directly reflected in the magnitude of the torsion angles emanating from these two atoms. The torsion-angle values of C2-C3-C4-C5: $-30.99(1)^0$ (I) and $35.20(1)°$ (II) or C3-C4-C5-C6 $28.60(1)°$ (I) and $-33.11(1)°$ (II) are higher in the DHP ring, which indicates that puckering is greater at C4 than at N1.

The structures have intra- and intermolecular hydrogen bonds of the type C-H---O, N-H---O and O-H---O, which help to stabilize the crystal structures. Every molecule is linked with other molecules into infinite chains by intermolecular hydrogen bonds between the amine H atom of a molecule and the carbonyl oxygen of a neighbouring molecule or between the hydroxyl H

atom of a molecule and the carbonyl oxygen of a neighbouring molecule.

THEORETICAL PART

Structure

Because the crystal structures of the two corresponding 1,4-DHPs were known, we wanted to check the correlation between X-Ray data and theoretical calculations. To this aim we generated theoretical models of (I) and (II) (ChemBio3D software package) and after molecular mechanics optimization of the structures using MM2 force field, full optimization of the molecular geometry was done *via* different *ab initio* (DFT and HF both with 6-31G basis set) and semi-empirical (AM1 and PM3) methods for comparison.

The calculated and selected bond lengths for I and II are given in Tables 2 and 3. The calculated and selected bond angles for I and II are given in Tables 4 and 5. There is a very good correlation between experimental and calculated values of bond lengths and angles, especially for I using the DFT B3LYP method which finds very broad usage in this kind of calculations. The molecular geometry parameters are very close to the data for other similar structures like diethyl 4-(3-bromophenyl)-2,6-dimethyl-1,4-dihydropyridine-3,5-dicarboxylate [22]. As a rule, the results obtained with semi-empirical methods are with bigger diversion from the experimental values of molecular geometry parameters, but these methods are vastly faster than *ab initio*. It may be concluded that DFT and HF methods with 6–31G basis set are appropriate for geometry optimization of the 1,4-DHPs.

UV-Vis Spectra

The excitation states of the corresponding compounds were calculated for singlet state and half-singlet / half-triplet state by B3LYP and RHF methods using a 6-31G basis set (Table 6). The values for λ_{max} obtained from hybrid DFT method B3LYP were higher than the HF values and there is very good approximation with some of the maxima in the experimental ones, especially for I (320 nm). All maxima obtained from the experiment or quantum mechanical calculations for the two compounds are very similar because of their similar structure. The reasons for some disagreements between experimental and theoretical data could be the specifics of the calculation methods or the fact that the experimental spectra were obtained in 95%

103

Table 2. Selected bond lengths [Å] for diethyl 4-(4-hydroxyphenyl)-2,6-dimethyl-1,4-dihydropyridine-3,5-dicarboxylate (I).

	X-Ray	B3LYP (6-31G)	HF (6-31G)	AM1	PM3
N 1 – C 2	137.7(2)	139.5(6)	138.5(7)	139.5(7)	143.2(3)
N 1 – C 6	138.2(2)	139.5(6)	138.5(7)	139.5(7)	143.2(3)
C 2 – C 3	135.9(2)	136.5(3)	134.4(1)	136.8(7)	135.0(1)
C 2 – C 19	150.4(2)	150.9(8)	150.8(5)	149.5(1)	149.1(2)
C 3 – C 13	146.6(2)	146.1(9)	146.1(7)	146.2(1)	148.9(5)
C 3 – C 4	151.9(2)	153.0(5)	152.3(6)	150.5(4)	150.4(2)
C 4 – C 5	151.5(2)	153.0(5)	152.3(6)	150.1(7)	150.4(2)
C 4 – C 7	153.0(2)	153.7(2)	153.2(1)	150.5(1)	151.0(3)
C 5 – C 6	135.3(2)	136.5(3)	134.4(1)	136.7(1)	135.0(1)
C 5 – C 16	147.1(2)	146.1(9)	146.1(7)	146.4(5)	148.9(5)
C 6 – C 20	149.8(2)	150.9(8)	150.8(6)	149.5(2)	149.1(2)
C 10 – O 1	136.2(8)	139.6(1)	138.0(1)	137.7(3)	136.8(4)
C 13 – O 2	121.1(2)	124.5(4)	122.1(1)	123.7(1)	121.5(7)
C 13 – O 3	132.0(2)	138.9(1)	135.1(7)	137.3(3)	136.4(2)
C 14 – O 3	145.8(2)	147.8(5)	145.4(5)	143.9(3)	142.9(1)
C 14 – C 15	135.8(4)	151.8(1)	151.2(1)	150.9(3)	151.6(6)
C 16 – O 4	121.0(2)	124.5(4)	122.1(1)	123.4(9)	121.5(7)
C 16 – O 5	133.5(2)	138.9(1)	135.1(7)	137.3(5)	136.4(2)
C 17 – O 5	145.5(2)	147.8(5)	145.4(5)	143.9(1)	142.9(1)
C 17 – C 18	148.2(2)	151.8(1)	151.2(1)	150.9(3)	151.6(6)

Table 3. Selected bond lengths [Å] for diethyl 4-(3-hydroxyphenyl)-2,6-dimethyl-1,4-dihydropyridine-3,5-dicarboxylate (II).

	X-Ray	B3LYP (6-31G)	HF (6-31G)	AM1	PM3
N 1 – C 2	139.1(2)	139.6(2)	138.3(1)	139.6(6)	143.1(8)
N 1 – C 6	138.5(2)	139.4(2)	138.5(1)	139.5(6)	143.1(8)
C 2 – C 3	135.1(2)	136.5(6)	134.5(5)	136.8(3)	135.0(6)
C 2 – C 19	150.0(2)	150.6(7)	150.6(9)	149.5(1)	149.1(2)
C 3 – C 13	146.5(2)	146.8(4)	146.0(3)	146.3(4)	149.0(1)
C 3 – C 4	152.9(2)	152.9(1)	152.1(4)	150.4(7)	150.3(8)
C 4 – C 5	149.0(3)	153.4(6)	152.6(4)	150.1(6)	150.3(8)
C 4 – C 7	154.0(2)	154.1(4)	153.4(5)	150.7(3)	151.2(2)
C 5 – C 6	136.4(2)	136.6(1)	134.4(9)	136.7(5)	135.0(6)
C 5 – C 16	147.2(2)	146.0(5)	146.1(5)	146.4(9)	149.0(1)
C 6 – C 20	149.0(3)	150.9(5)	150.8(7)	149.5(2)	149.1(2)
C 9 – O 1	137.0(2)	139.5(9)	137.9(5)	137.7(8)	136.9(7)
C 13 – O 2	121.8(2)	124.9(4)	122.6(6)	123.6(1)	121.4(5)
C 13 – O 3	133.2(2)	138.2(1)	134.4(4)	137.3(6)	136.9(1)
C 14 – O 3	143.9(2)	147.8(1)	145.3(5)	143.5(2)	142.2(1)
C 14 – C 15	149.5(3)	152.2(8)	151.6(4)	150.8(7)	151.7(1)
C 16 – O 4	121.7(2)	124.6(5)	122.1(6)	123.4(5)	121.4(5)
C 16 – O 5	133.3(2)	138.9(6)	135.1(3)	137.4(2)	136.9(1)
C 17 – O 5	146.3(2)	148.1(3)	145.6(6)	143.4(8)	142.2(1)
C 17 – C 18	148.5(4)	152.2(6)	151.6(4)	150.8(7)	151.7(1)

ethanol solutions (10^{-3} M) in contrast to theoretical, which were produced in solid state.

The excited states for half singlets and half triplets ("50-50") are very close to the experimental data, especially at λ_{max} = 320. These electronic transitions were with lower energy, because of the lower energy of the B3LYP virtual orbitals. The higher maxima obtained with the HF method are very close to the experimental ones.

The absorption maximum at λ_{max} = 220 nm both for I and II corresponds to aromatic double bonds from aryl ring at C4 position, which take part in π -> π^* transitions. Ester C=O groups absorb energy at 272 and 274 nm (n --> π^* transitions) for I and II, respectively. The absorption maximum at 320 nm corresponds to the transition of O-H group in the aryl ring of the compounds. The compound I has more intensive absorption than II.

Table 4. Selected angles [º] for diethyl 4-(4-hydroxyphenyl)-2,6-dimethyl-1,4-dihydropyridine-3,5-dicarboxylate (I).

	X-Ray	B3LYP(6-31G)	HF(6-31G)	AM1	PM3
C 2 – N 1 – C 6	123.9(1)	124.6(1)	124.3(1)	120.7(1)	118.0(1)
C 3 – C 2 – N 1	118.2(1)	118.4(1)	118.6(1)	120.1(1)	120.0(1)
C 3 – C 2 – C 19	128.6(1)	127.9(1)	128.1(1)	122.9(1)	124.6(1)
N 1 – C 2 – C 19	113.1(1)	113.7(1)	113.3(1)	117.0(1)	115.4(1)
C 2 – C 3 – C 13	125.7(1)	125.2(1)	124.6(1)	124.4(1)	122.2(1)
C 2 – C 3 – C 4	119.5(1)	120.8(1)	121.1(1)	121.4(1)	122.7(1)
C 13 – C 3 – C 4	114.8(1)	114.1(1)	114.3(1)	114.1(1)	115.0(1)
C 5 – C 4 – C 3	110.7(1)	111.3(1)	111.0(1)	111.2(1)	111.6(1)
C 5 – C 4 – C 7	112.0(1)	111.6(1)	111.6(1)	111.5(1)	110.8(1)
C 3 – C 4 – C 7	109.6(1)	111.6(1)	111.6(1)	110.3(1)	110.8(1)
C 6 – C 5 – C 16	125.4(1)	125.2(1)	124.6(1)	123.8(1)	122.2(1)
C 6 – C 5 – C 4	119.8(1)	120.8(1)	121.1(1)	121.7(1)	122.7(1)
C 16 – C 5 – C 4	114.6(1)	114.1(1)	114.3(1)	114.5(1)	115.0(1)
C 5 – C 6 – N 1	118.6(1)	118.4(1)	118.6(1)	120.0(1)	120.0(1)
C 5 – C 6 – C 20	128.3(1)	127.9(1)	128.1(1)	122.7(1)	124.6(1)
N 1 – C 6 – C 20	113.2(1)	113.7(1)	113.3(1)	117.3(1)	115.4(1)
C 8 – C 7 – C 4	120.8(1)	121.4(1)	121.5(1)	121.7(1)	121.2(1)
C 12 – C 7 – C 4	121.7(1)	120.3(1)	120.5(1)	119.0(1)	119.2(1)
O 1 – C 10 – C 11	122.6(1)	122.8(1)	122.6(1)	122.7(1)	123.0(1)
O 1 – C 10 – C 9	118.0(1)	117.0(1)	117.1(1)	116.6(1)	116.2(1)
O 2 – C 13 – O 3	121.7(1)	120.6(1)	120.3(1)	116.7(1)	119.7(1)
O 2 – C 13 – C 3	122.4(1)	123.9(1)	123.5(1)	127.3(1)	127.1(1)
O 3 – C 13 – C 3	115.9(1)	115.5(1)	116.2(1)	116.0(1)	113.2(1)
C 13 – O 3 – C 14	116.8(2)	116.1(1)	119.2(1)	116.2(1)	118.3(1)
C 15 – C 14 – O 3	111.7(2)	106.9(1)	106.9(1)	106.3(1)	106.4(1)
O 4 – C 16 – O 5	122.1(1)	120.6(1)	120.3(1)	117.1(1)	119.7(1)
O 4 – C 16 – C 5	123.7(1)	123.9(1)	123.5(1)	127.6(1)	127.1(1)
O 5 – C 16 – C 5	114.2(1)	115.5(1)	116.2(1)	115.3(1)	113.2(1)
C 16 – O 5 – C 17	117.0(1)	116.1(1)	119.2(1)	116.1(1)	118.3(1)
O 5 – C 17 – C 18	107.3(1)	106.9(1)	106.9(1)	106.3(1)	106.4(1)

Table 5. Selected angles [º] for diethyl 4-(3-hydroxyphenyl)-2,6-dimethyl-1,4-dihydropyridine-3,5-dicarboxylate (II).

	X-Ray	B3LYP(6-31G)	HF(6-31G)	AM1	PM3
C 2 – N 1 – C 6	123.2(2)	124.5	124.1	120.6	118.0
C 3 – C 2 – N 1	117.4(2)	118.8	119.0	120.1	120.0
C 3 – C 2 – C 19	129.7(2)	127.9	126.8	122.8	124.5
N 1 – C 2 – C 19	112.8(2)	113.3	114.1	117.1	115.5
C 2 – C 3 – C 13	124.6(2)	121.8	120.4	124.3	121.4
C 2 – C 3 – C 4	119.1(2)	120.3	121.2	121.4	122.7
C 13 – C 3 – C 4	116.3(1)	117.8	118.4	114.2	115.9
C 5 – C 4 – C 3	110.4(1)	111.3	110.8	111.1	111.6
C 5 – C 4 – C 7	113.2(1)	111.0	111.1	111.5	110.7
C 3 – C 4 – C 7	108.8(1)	112.0	111.7	110.1	110.7
C 6 – C 5 – C 16	124.6(2)	124.9	124.4	123.8	121.4
C 6 – C 5 – C 4	119.1(2)	120.6	121.3	121.6	122.7
C 16 – C 5 – C 4	116.1(1)	114.4	114.3	114.5	115.9
C 5 – C 6 – N 1	118.2(2)	118.2	118.7	120.0	120.0
C 5 – C 6 – C 20	129.6(2)	128.0	128.0	122.7	124.5
N 1 – C 6 – C 20	112.3(2)	113.8	113.3	117.3	115.5
C 8 – C 7 – C 4	119.2(2)	119.5	120.0	118.6	118.9
C 12 – C 7 – C 4	121.4(2)	121.3	121.1	121.5	121.2
O 1 – C 9 – C 8	122.1(2)	116.7	116.8	116.4	116.0
O 1 – C 9 – C 10	117.7(2)	122.4	122.3	122.5	123.0
O 2 – C 13 – O 3	123.2(2)	120.8	121.1	117.3	120.0
O 2 – C 13 – C 3	121.6(2)	127.9	126.2	127.0	127.8
O 3 – C 13 – C 3	115.2(1)	111.3	112.7	115.7	112.2
C 13 – O 3 – C 14	118.5(1)	117.7	121.0	117.5	119.7
C 15 – C 14 – O 3	110.0(2)	110.8	110.8	111.1	112.5
O 4 – C 16 – O 5	122.4(2)	120.9	120.6	117.5	120.0
O 4 – C 16 – C 5	122.1(2)	123.9	123.4	127.4	127.8
O 5 – C 16 – C 5	115.5(2)	115.2	116.0	115.1	112.2
C 16 – O 5 – C 17	117.7(2)	116.7	120.0	117.5	119.7
O 5 – C 17 – C 18	106.4(2)	111.0	111.0	111.1	112.5

Table 6. UV-Vis spectral data for diethyl 4-(4-hydroxyphenyl)-2,6-dimethyl-1,4-dihydropyridine-3,5-dicarboxylate (I) and 4-(3-hydroxyphenyl)-2,6-dimethyl-1,4-dihydropyridine-3,5-dicarboxylate (II).

Compound	Experimental λ_{max} [nm]	B3LYP (6-31G) λ_{max} singlet [nm]	B3LYP (6-31G) λ_{max} 50-50 [nm]	HF (6-31G) λ_{max} singlet [nm]	HF (6-31G) λ_{max} 50-50 [nm]
I	220, 272, 320, 374	286, 351, 353	320, 351, 353	204, 205, 253	253, 272, 275
II	220, 274, 320, 376	295, 337, 351	337, 351	202, 204, 254	254, 256, 270

Table 7. IR spectral data for diethyl 4-(4-hydroxyphenyl)-2,6-dimethyl-1,4-dihydropyridine-3,5-dicarboxylate (I) and 4-(3-hydroxyphenyl)-2,6-dimethyl-1,4-dihydropyridine-3,5-dicarboxylate (II).

Com-pound	Functional group	Experimental $\bar{\nu}$ [cm^{-1}]	B3LYP (6-31G) $\bar{\nu}$ [cm^{-1}]	B3LYP (6-31G) $\bar{\nu}$ [cm^{-1}] scaled	HF (6-31G) $\bar{\nu}$ [cm^{-1}]	HF (6-31G) $\bar{\nu}$ [cm^{-1}] scaled	AM1 $\bar{\nu}$ [cm^{-1}]	AM1 $\bar{\nu}$ [cm^{-1}] Scaled	PM3 $\bar{\nu}$ [cm^{-1}]	PM3 $\bar{\nu}$ [cm^{-1}] scaled
I	ν O–H	3308	3667	3594	4047	3723	3461	3299	3889	3796
	ν N–H	3352	3651	3578	3914	3601	3466	3304	3376	3295
	ν C=O		1663	1630	1829	1683	2059	1963	1976	1929
	ν C=O	1650	1662	1629	1828	1682	2046	1950	1968	1921
	ν C=C		1708	1674	1876	1726	1851	1764	1884	1839
	ν C=C		1694	1660	1853	1705	1821	1736	1856	1812
	ν C=C		1673	1640	1822	1676	1788	1704	1801	1758
	ν C=C	1595	1650	1617	1794	1650	1784	1701	1783	1740
	ν C=C	1473	1567	1536	1698	1562	1680	1601	1633	1594
II	ν O–H		3665	3592	4049	3725	3463	3301	3890	3797
	ν N–H	3347	3642	3569	3913	3600	3466	3304	3375	3294
	ν C=O	1662	1660	1627	1825	1679	2061	1965	1978	1931
	ν C=O		1654	1621	1797	1653	2050	1954	1974	1927
	ν C=C		1713	1679	1870	1720	1851	1764	1884	1839
	ν C=C		1697	1663	1856	1708	1821	1736	1853	1809
	ν C=C		1674	1641	1821	1675	1794	1710	1801	1758
	ν C=C	1591	1643	1610	1789	1646	1775	1692	1786	1743
	ν C=C	1488	1543	1512	1668	1535	1663	1585	1609	1571

[1] The characteristic vibrations of O-H and N-H bonds are very close

IR (vibrational) spectra

IR spectra of the two isomeric 1,4-DHPs were calculated. The data about vibration frequencies must be scaled by a scaling factor appropriate for the different methods, because the theoretical vibrations are harmonic and the experimental ones are anharmonic. The values of the scaling factor for DFT methods is 0.98 and for HF methods – 0.92, for AM1 – 0.9532 and for PM3 – 0.9761 [23]. Some of the characteristic IR frequencies for the two compounds are compared with the calculated ones in Table 7.

Some of the vibrations obtained by calculation are not very close to the experimental ones, which is due to fact, that the molecules of the corresponding compounds have several hydrogen bonds – intra- and intermolecular, which stabilize the structure of the corresponding compounds and the calculation methods have very low capability to describe hydrogen bonding. Some differences between results obtained with semi-empirical and

ab initio methods are due to the different type of IR vibrations calculated (the scaling factors of AM1 and PM3 try to reproduce the true fundamental frequencies; in contrast, the scaling factors for DFT B3LYP and HF try to reproduce the zero point energies).

Calculation of other physicochemical properties

Some other physicochemical constants for I and II, as dipole moments and energy of HOMO and LUMO, calculated by the quantum mechanical (*ab initio* and semi-empirical) methods, are given in Table 8.

From the calculated physicochemical parameters it can be seen that these two isomeric 1,4-DHPs are comparatively polar compounds. *Ab initio* calculations (DFT and HF) showed that I is more polar than II. In contrast, semi-empirical calculations (AM1 and PM3) showed that II is more polar than I. Because of their higher precision and accuracy, *ab initio* calculations can be qualified

Table 8. HOMO and LUMO energies [eV] and dipole moments (μ) [D] of diethyl 4-(4-hydroxyphenyl)-2,6-dimethyl-1,4-dihydropyridine-3,5-dicarboxylate (I) and 4-(3-hydroxyphenyl)-2,6-dimethyl-1,4-dihydropyridine-3,5-dicarboxylate (II).

Com-pound		B3LYP (6-31G)	HF (6-31G)	AM1	PM3
I	HOMO	- 0.203	- 0.291	- 0.319	- 0.321
	LUMO	- 0.051	0.092	- 0.011	- 0.001
	Dipole moment	5.30	6.15	5.54	3.13
II	HOMO	- 0.205	- 0.300	- 0.319	- 0.320
	LUMO	- 0.052	0.091	- 0.011	0.000
	Dipole moment	4.48	5.18	6.58	3.15

as more reliable than semi-empirical methods. The comparatively lower values of HOMO energy, negative values of LUMO energy and HOMO/LUMO gaps for I and II mean that they are good reductors, which is in very good correlation with experimental data. The reduction properties and light sensibility of 1,4-DHPs are due to double bonds in their DHP ring.

CONCLUSIONS

Two isomeric 1,4-DHPs, known in literature, with hydroxyphenyl ring at fourth position in the DHP ring were synthesized by two different experimental procedures. The products were characterized by different physicochemical methods of analysis – melting point elemental analysis, IR, UV-Vis and X-Ray single crystal diffractometry. The molecular geometry of these compounds was optimized using the hybrid DFT method B3LYP and HF method both with 6-31G basis set and semi-empirical methods – AM1 and PM3 for comparison. The methods gave good results, comparable with the experimental data and with the literature data for similar compounds.

The same methods were used for predicting the UV-Vis and IR properties of the compounds. The comparison with the experimental data showed that the use of scaling factors of 0.98, 0.92, 0.9532 and 0.9761 for DFT, HF, AM1 and PM3, respectively, is not suitable for all predicted frequencies in the IR spectra, but is appropriate for simulation of UV-Vis spectra. The calculated other physicochemical properties of the compounds can be used in additional QSAR analysis.

REFERENCES

1 W. Vater, G. Kroneberg, F. Hoffmeister, *Arzn. Forsch.* **22** (1), 1 (1972).
2 M. J. Brown, C. R. Palmer, A. Castaigne, *Lancet*, **356**(9227), 366 (2000).
3 P. A. Poole-Wilson, B. A. Kirwan, Z. Vokó, S. de Brouwer, F. J. van Dalen, J. Lubsen, *Cardiovas. Drugs Ther.*, **20**(1), 45 (2006).
4 B. Love, M. Goodman, K. Snader, R. Tedeschi, E. Macko, *J. Med. Chem.*, **17**, 956 (1974).
5 F. Bossert, H. Meyer, E. Wehinger, *Angew. Chem.* Int. Ed. Engl., **20**, 762 (1981).
6 S. Bahekar, D. Shinde, *Acta Pharm.*, **52**, 281 (2002).
7 H. Lob, A. C. Rosenkranz, T. Breitenbach, R. Berkels, G. Drummond, R. Roesen, *Pharmacology*, **76** (1), 8 (2006).
8 J. H. Li, *Cardiovascular Drug Reviews* **15** (3), 220 (2006)**.**
9 R. P. Mason, *Cerebrovasc. Dis.*, **16**(3), 11 (2003).
10 R. Meškys, A. Vaitkuvienė, E. Liutkevičius, G. Biziulevičienė, A. Ulinskaitė, A. Darinskas, *Biologija*, **3**, 96 (2006).
11 A. Hantzsch, *Ber.*, **14**, 1637 (1881).
12 M. F. Gordeev, D. V. Patel, E. M. Gordon, *J. Org. Chem.*, **61**, 924 (1996).
13 J. G. Breitenbucher, G. Figliozzi, G. *TetLett.*, **41**, 4311 (2000).
14 J. J. Vanden Eynde, A. Mayence, *Int. J. Med. Biol. Environ.,* **28**, 25 (2000).
15 P. A. Navarrete-Encina, J. A. Squella, J. Carbajo, B. Conde, L. J. Núñez-Vergara, *Synth. Commun.,* **37**(12), 2051 (2007).
16 A. P. Scott, L. Radom, *J. Phys. Chem.*, **100**, 16502 (1996).
17 L. F. Wang, H. Y. Zhang, L. Kong, Z. W. Chen, J. G. Shi, *Helv. Chim. Acta* **87**(6), 1515 (2004).
18 H. R. Memarian, H. Sabzyan, M. Abdoli-Senejani, *J. Mol. Struct.*, **813**, 39 (2007).
19 H. Novoa de Armas, N. M. Blaton, O. M. Peeters, C. J. de Ranter, M. Suarez, E. Ochoa, Y. Verdecia, E. Salfran, *J. Chem. Cryst.*, **30**(4), 237 (2000).
20 A. L. Spek, PLATON General Crystallographic Tool, Utrecht University, The Netherlands, 1998.
21 G. M. Sheldrick, SHELXL-97 program package for crystal structure solution and refinement, University of Göttingen, Germany, 1997.
22 M. Mahendra, B. H. Doreswamy, P. Adlakha, K. Raval, A. Shah, S. M. Anandalwar, J. S. Prasad, *Anal. Sci.,* **21**, 35 (2005).
23 M. J. Frisch, G. W. Trucks, H. B. Schlegel, G. E. Scuseria, M. A. Robb, J. R. Cheeseman, J. A. Jr. Montgomery, T. Vreven, K. N. Kudin, J. C. Burant, J. M. Millam, S. S. Iyengar, J. Tomasi, V. Barone, B. Mennucci, M. Cossi, G. Scalmani, N. Rega, G. A. Petersson, H. Nakatsuji, M. Hada, M. Ehara, K. Toyota, R. Fukuda, J. Hasegawa, M. Ishida, T. Nakajima, Y. Honda, O. Kitao, H. Nakai, M. Klene, X. Li, J. E. Knox, H. P.

Hratchian, J. B. Cross, C. Adamo, J. Jaramillo, R. Gomperts, R. E. Stratmann, O. Yazyev, A. Austin, R. Cammi, C. Pomelli, J. W. Ochterski, P. Y. Ayala, K. Morokuma, G. A. Voth, P. Salvador, J. J. Dannenberg, V. G. Zakrzewski, S. Dapprich, A. D. Daniels, M. C. Strain, O. Farkas, D. K. Malick, A. D. Rabuck, K. Raghavachari, J. B. Foresman, J. V. Ortiz, Q. Cui, A. G. Baboul, S. Clifford, J. Cioslowski, B. B. Stefanov, G. Liu, A. Liashenko, P. Piskorz, I. Komaromi, R. L. Martin, D. J. Fox, T. Keith, M. A. Al-Laham, C. Y. Peng, A. Nanayakkara, M. Challacombe, P. M. W. Gill, B. Johnson, W. Chen, M. W. Wong, C. Gonzalez, J. A. Pople, Gaussian, Inc., Pittsburgh PA, 2003.

СИНТЕЗ, КРИСТАЛНА СТРУКТУРА И ТЕОРЕТИЧНО ИЗСЛЕДВАНЕ НА ДВЕ ИЗОМЕРНИ ПОЛИЗАМЕСТЕНИ ПРОИЗВОДНИ НА 1,4-ДИХИДРОПИРИДИН

Стефан Дочев[1], Маркус Щрьобеле[2], Ханс-Юрген Майер[2], Илия Манолов[3]

[1]Изследователска група Миховилович, Изследователска група по Органична химия, Институт по Приложна Синтетична химия, Факултет по Техническа химия, Виенски Технологичен Университет, А-1060 Виена, Австрия
[2]Отдел по химия на твърдите тела и Теоретична Неорганична химия, Институт по Неорганична химия, Университет Тюбинген, Об дем Химелрайх 7, D-72074 Тюбинген, Германия
[3]Катедра по Фармацевтична химия, Фармацевтичен факултет, Медицински университет,ул. „Дунав" 2, BG-1000 София, България

(Резюме)

1,4-Дихидропиридините са добре известни блокери на калциевите канали с широко приложение като антихипертензивни агенти. Те имат интересни спектрални и химични свойства, които са изучени експериментално и теоретично. Два изомерни полизаместени 1,4-дихидропиридини са синтезирани по три различни едностадийни схеми. Веществата диетил 4-(4-хидроксифенил)-2,6-диметил-1,4-дихидроксипиридин-3,5-дикарбоксилат (**I**) and diethyl 4-(3- хидроксифенил)-2,6- диметил -1,4- дихидроксипиридин -3,5-дикарбоксилат (**II**) са охарактеризирани с т.т., елементен анализ, ИЧ- и УВ-спектроскопия, а структурата им е доказана чрез монокристален рентгеноструктурен анализ. Съединение (I) кристализира в моноклинна кристална система и пространствена група $P2_1/c$, с параметри на елементарната клетка $a = 739.1(1)$, $b = 2769.5(3)$, $c = 880.9(1)$ Å, $\alpha = 104.24(2)$ º, $\beta = \gamma = 90$º, $Z = 4$, $V = 1.7476(4)$ Å^3. Съединение (II) кристализира в триклинна кристална система и пространствена група $P\bar{1}$, с параметри на елементарната клетка $a = 742.8(1)$, $b = 894.2(2)$, $c = 1407.5(2)$ Å, $\alpha = 80.23(2)$ º, $\beta = 86.86(2)^0$, $\gamma = 68.71(2)$º, $Z = 2$, $V = 0.8584(3)$ Å^3. Спектралното поведение на оптимизираните структури е изучено с хибриден DFT метод, B3LYP and HF методи, последните два с 6-31G базисна мрежа и някои полуемпирични методи за сравнение. Теоретичните спектри са сравнени с експерименталните.

Synthesis and crystal structure of 4-hydroxy-3-[(3E)-3-(hydroxyimino)-1-(4-nitrophenyl)butyl]-2H-chromen-2-one

Ilia Manolov*[1] and Cecilia Maichle-Moessmer[2]

[1]Department of Pharmaceutical Chemistry, Faculty of Pharmacy, Medical University, 2, Dunav St, BG-1000 Sofia, Bulgaria,
[2]Institute of Inorganic Chemistry, Auf der Morgenstelle 18, D-72076 Tuebingen, Germany

The structure of 4-hydroxy-3-[(3E)-3-(hydroxyimino)-1-(4-nitrophenyl)butyl]-2H-chromen-2-one was determined by X-ray crystallography. The compound crystallizes in an orthorhombic crystal system and was characterized thus: Pbcn, a = 11.3411(8)Å, b = 10.0843 (14)Å, c = 33.170(3)Å, $\alpha = \beta = \gamma = 90°$, Z = 8, V = 3793.6(7)Å^3. The crystal structure was solved by direct methods and refined by full-matrix least-squares on F^2 to a final R1 of 0.0946.

Key words: 4-Hydroxy-3-[(3E)-3-(hydroxyimino)-1-(4-nitrophenyl)butyl]-2H-chromen-2-one, crystal structure, coumarin derivatives

INTRODUCTION

Coumarin is a structural fragment of different natural and synthetic compounds which demonstrated a wide range of pharmacological activities. The coumarin derivatives are of interest because of their properties as oral anticoagulants or rodenticides [1], photosensitizers [2], anti-HIV agents [3,4], and antibiotics [5]. There has been continuous interest in the synthesis of these compounds. The most widely used antithrombotic in European countries is racemic Acenocoumarol (Synthrom, Niffcoumar). Chemical modifications of the Acenocoumarol structure seem to be a promising route to obtain compounds with good biological activity, lower toxicity and fewer side effects.

EXPERIMENTAL

Synthesis and characterization

The title compound (**I**) was obtained according to the reaction scheme 1.
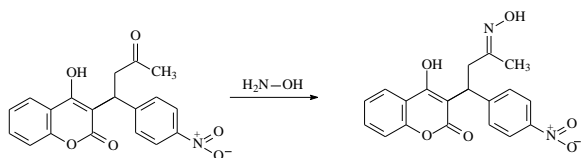
Fig.1. Reaction pathway

Melting point was measured on a Boetius hot plate microscope (Germany) and was uncorrected. IR spectra (nujol) were recorded on an IR-spectrometer FTIR-8101 M Shimadzu. ^{1}H NMR spectra were recorded at ambient temperature on a Bruker 250 WM (250 MHz) spectrometer in [D$_6$]-acetone. Chemical shifts are given in ppm (σ) relative to TMS used as an internal standard. Mass spectra were recorded on a Jeol JMS D 300 double focusing mass spectrometer coupled to a JMA 2000 data system. The compound was introduced by direct inlet probe, heated from 50 ºC to 400 ºC at a rate of 100 º/min. The ionization current was 300 mA, the accelerating voltage 3 kV and the chamber temperature 150 ºC. TLC was performed on precoated plates Kieselgel 60 F$_{254}$ Merck (Germany) with layer thickness of 0.25 mm and UV detection (254 nm). Yields of TLC-homogeneous isolated product are given. Elemental analysis was performed at the Faculty of Chemistry, University of Sofia. Analysis data indicated by the symbols of the elements were within ±0.4 % of the theoretical values.

X-ray crystallographic study (general procedure of the diffraction method by single crystal): Measurements [6] were made at 173(2) K on an Enraf-Nonius KAPPA CCD diffractometer with a graphite monochromated Mo- K$_\alpha$ (λ = 0.71069 Å). Crystal unit-cell and orientation parameters were obtained from the auto indexing procedure, as implemented in DENZO [7]. Intensities recorded up to a maximum 2θ value of 45.0° using the ω scan technique, were integrated with DENZO [7], scaled, and then reduced in Scalepack [7] after a

* To whom all correspondence should be sent:
E-mail: imanolov@gmx.net

post-refinement of the unit-cell parameters. The structure was solved by direct methods using SIR97 [8] and refined by full–matrix least–squares techniques on F^2 using SHELX-L 97 [9, 10]. All non-hydrogen atoms were anisotropically and fully refined at the calculated positions.

Acenocoumarol, synthesized by us, was treated with hydroxylamine hydrochloride at a molar ratio of 1:1 to produce the oxime derivative. Acenocoumarol (3.53 g, 10 mmol) was added to 150 ml ethanol containing hydroxylamine hydrochloride (0.7 g, 10 mmol). Three ml pyridine and 0.4 g sodium hydroxide were added to the reaction mixture. The solution was allowed to stand for 12 h and then refluxed for 6 h. After cooling the oxime crystallized out and was filtered off. The crude product was recrystallized from methanol. TLC (toluene/chloroform/acetone, 8:8:1). Yield 2.58 g (70 %), m.p. 191–193 ℃, R_f = 0.15. $C_{19}H_{16}N_2O_6$ (368): IR, cm^{-1}: 2994, 1673, 1620, 1568, 1497, 1452, 1399, 1215, 766. ^{1}H NMR ([D_6]-acetone): 1.84 s (3H), 3.1–3.3 d (2H – side chain), 4.9–5.1 t (1H), 7.2–8.1 m (8H- arom), 10.9 s (2H – two hydroxyl groups). MS: 368 (0.3), 351 (3.2), 310 (0.6), 296 (0.6), 205 (100), 163 (6.4), 162 (52), 159 (58), 143 (20), 142 (15), 120 (77), 92 (46) [11].

RESULTS AND DISCUSSION

We investigated the reaction of 4-hydroxy-3-[1-(4-nitrophenyl)-3-oxobutyl]-2*H*-chromen-2-one (acenocoumarol) with hydroxylamine hydro-chloride at a molar ratio of 1:1 in ethanol in the presence of pyridine and sodium hydroxide. The aim of the investigation was to synthesize 4-hydroxy-3-[(3E)-3-hydroxyimino)-1-(4-nitrophenyl) butyl]-2H-chromen-2-one, m. p. 191–193 ℃ [10]. It is known that the oximes of the aromatic ketones readily undergo a similar to Beckmann rearrangement to produce different cyclo-derivatives [12]. We established that the only product in this case is the title compound (Fig. 1).

Colourless thin needle-like crystals, sufficiently suitable for X-ray diffraction analysis, were grown by slow evaporation of an ethyl acetate solution. The crystal belongs to the orthorhombic system, chiral space group Pbcn and the structure solution unveils that the asymmetric unit is composed of one diastereomeric molecule corresponding to the title compound, 4-hydroxy-3-[(3E)-3-(hydroxyimino)-1-(4-nitrophenyl)butyl]-2H-chromen-2-one.

An examination of the bond lengths revealed that the atoms retained the character expected for the open-side chain (hydroxyimino) compound.

Table 1. Crystal and experimental data

Empirical formula	$C_{19}H_{16}N_2O_6$
Formula weight	368.34
Temperature	173(2) K
Wavelength	0.71073 A
Crystal system	Orthorhombic
group	Pbcn
Unit cell dimensions	a = 11.3411(8) Å α = 90º
	b = 10.0843(14) Å β = 90º
	c = 33.170(3) Å γ = 90º
Volume	3793.6(7) Å^3
Z	8
Calculated density	1.290 Mg/m^3
Absorption coefficient	0.098 mm^{-1}
F(000)	1536
Crystal size	0.30 × 0.15 × 0.10 mm
θ range for data collection	5.89 to 24.70 deg.
Index ranges	−13≤h≤13, -11≤k≤10, −38≤l≤38
Reflections collected / unique	31770 / 3177 [R(int) = 0.1598]
Completeness to 2 θ = 24.70	86.7%
Absorption correction	None
Refinement method	Full-matrix least-squares on F^2
Data / restraints / parameters	3177 / 0 / 308
Goodness-of-fit on F^2	1.235
Final R indices [I>2σ (I)]	R1 = 0.0946, wR2 = 0.1667
R indices (all data)	R1 = 0.1339, wR2 = 0.1814
Largest diff. peak and hole	0.222 and −0.175 e.A^{-3}

The O21–C2 bond length of 1.348(5)Å is close to that of the phenolic C-O bond. Moreover, the bond lengths between C02–C03 and between C03-C04 are 1.502(6) and 1.490(7), respectively, close to the expected values for C–C bonds adjacent to a C=N-group. In the structure of the investigated compound there is no bond between C03 and O21. Within the coumarin system, the length of the double bond C1-C2, 1.359(6) Å is suitable for a C=C bond conjugated to a carbonyl, and the adjacent C10–C1 bond of 1.437(6) Å is slightly shorter than expected because of resonance. Two near disposed planarities of the coumarin ring system and the aromatic nucleus formed an angle of 110.4(4)º between C11 – C01 – C1. The compound crystallized in the open-chain ketimino form and had only one asymmetric center at C01. No hemiketimino ring was formed in the investigated compound.

All hydrogen atoms were located in different electron-density maps, but refined as riding, with C—H= 0.93 Å and 0.96 Å for the benzene and methyl H atoms, respectively.(Fig. 2).
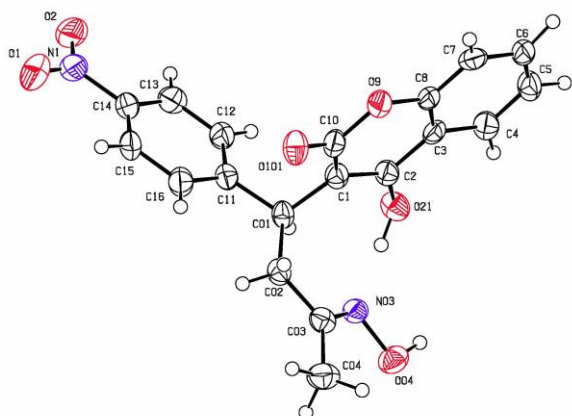
Fig. 2. View of the molecular structure of compound (I), showing the atom-numbering scheme. Displacement ellipsoids for non-H atoms are drawn at the 50% probability level and H are shown as small spheres of arbitrary radii.

Table 2. Atomic coordinates ($\times 10^4$) and equivalent isotropic displacement parameters (A^2 $\times 10^3$) for the compound. U(eq) is defined as one third of the trace of the orthogonalized Uij tensor.

Atom	x	y	z	U(eq)
C 01	5892(4)	−981(5)	3967(1)	32(1)
C 1	6004(4)	−661(4)	3519(1)	33(1)
C 2	6159(4)	−1602(4)	3231(1)	33(1)
C 02	4625(4)	−910(5)	4122(1)	35(1)
C 3	6352(4)	−1240(4)	2817(1)	32(1)
C 03	3843(4)	−2047(5)	4004(1)	35(1)
C 4	6551(4)	−2151(5)	2509(1)	39(1)
C 04	2582(5)	−2014(7)	4128(2)	49(1)
C 5	6719(4)	−1713(6)	2120(1)	42(1)
C 6	6690(4)	−391(6)	2028(1)	42(1)
C 7	6473(4)	527(6)	2328(1)	40(1)
C 8	6320(4)	94(5)	2720(1)	35(1)
C 10	5891(4)	706(5)	3402(1)	36(1)
C 11	6802(4)	-214(4)	4208(1)	32(1)
C 12	7975(4)	-571(5)	4157(1)	39(1)
C 13	8861(5)	65(5)	4364(1)	42(1)
C 14	8556(4)	1061(5)	4625(1)	42(1)
C 15	7414(5)	1448(5)	4681(1)	44(1)
C 16	6526(5)	789(5)	4471(1)	42(1)
N 1	9494(5)	1757(5)	4850(1)	57(1)
N 03	4318(3)	−3009(4)	3811(1)	35(1)
O 1	9209(4)	2671(5)	5071(1)	85(2)
O 2	10515(4)	1384(4)	4797(1)	68(1)
O 04	3514(3)	−4040(3)	3724(1)	45(1)
O 9	6094(3)	1051(3)	3008(1)	39(1)
O 21	6157(3)	−2913(3)	3309(1)	42(1)
O 101	5616(3)	1610(3)	3624(1)	45(1)

Table 3. Selected bond lengths [Å] for the compound.

C 01 – C 11	1.518(6)
C 01 – C 1	1.525(6)
C 01 – C 02	1.528(6)
C 1 – C 2	1.359(6)
C 1 – C 10	1.437(6)
C 2 – O 21	1.348(5)
C 2 – C 3	1.436(6)
C 02 – C 03	1.502(6)
C 03 – N 03	1.280(6)
C 03 – C 04	1.490(7)
C 8 – O 9	1.381(5)
C 10 – O 101	1.214(5)
C 10 – O 9	1.374(5)
C 14 – N 1	1.478(6)
N 1 – O 1	1.219(6)
N 1 – O 2	1.231(6)
N 03 – O 04	1.413(5)

Table 4. Selected bond angles [º] for the compound.

C 11 – C 01 – C 1	110.4(4)
C 11 – C 01 – C 02	116.0(4)
C 1 – C 01 – C 02	113.4(4)
C 2 – C 1 – C 10	119.4(4)
C 2 – C 1 – C 01	123.2(4)
C 10 – C 1 – C 01	117.3(4)
O 21 – C 2 – C 1	123.3(4)
O 21 – C 2 – C 3	115.7(4)
C 03 – C 02 – C 01	115.5(4)
C 4 – C 3 – C 2	123.9(4)
N 03 – C 03 – C 04	124.0(5)
N 03 – C 03 – C 02	117.4(4)
C 04 – C 03 – C 02	118.5(4)
O 9 – C 8 – C 7	116.8(4)
O 9 – C 8 – C 3	121.6(4)
O 101 – C 10 – O 9	115.5(4)
O 101 – C 10 – C 1	125.4(4)
O 9 – C 10 – C 1	119.1(4)
C 16 – C 11 – C 12	119.2(4)
C 16 – C 11 – C 01	123.7(4)
C 12 – C 11 – C 01	117.1(4)
C 13 – C 14 – N 1	119.1(5)
O 1 – N 1 – O 2	124.5(5)
O 1 – N 1 – C 14	118.2(5)
O 2 – N 1 – C 14	117.3(5)
C 03 – N 03 – O 04	112.8(4)
C 10 – O 9 – C 8	120.8(3)

Symmetry transformations used to generate equivalent atoms.

Table 5. Anisotropic displacement parameters ($A^2 \times 10^3$) for the compound. The anisotropic displacement factor exponent takes the form: $-2 \pi^2 [h^2 a^{*2} U11 + ... + 2 h k a^* b^* U12]$

	U11	U22	U33	U23	U13	U12
C 01	35(3)	33(3)	29(2)	-6(2)	0(2)	5(2)
C 1	29(2)	39(3)	31(2)	-4(2)	-1(2)	2(2)
C 2	27(2)	39(3)	33(2)	-5(2)	1(2)	3(2)
C 02	35(3)	40(3)	30(2)	-6(2)	3(2)	3(2)
C 3	23(2)	39(3)	34(2)	-7(2)	-4(2)	-5(2)
C 03	31(2)	41(3)	32(2)	7(2)	-1(2)	3(2)
C 4	29(2)	50(3)	38(2)	-9(2)	1(2)	6(2)
C 04	38(3)	56(4)	53(3)	7(3)	4(3)	-4(3)
C 5	34(3)	58(4)	35(3)	-14(2)	1(2)	2(2)
C 6	29(3)	66(4)	30(2)	-7(2)	0(2)	-7(2)
C 7	30(3)	46(3)	44(3)	6(2)	-1(2)	13(2)
C 8	24(2)	50(3)	30(2)	-7(2)	0(2)	-8(2)
C 10	5(3)	41(3)	32(2)	-7(2)	-6(2)	0(2)
C 11	36(3)	34(3)	26(2)	-1(2)	1(2)	1(2)
C 12	36(3)	46(3)	33(2)	-6(2)	2(2)	-1(2)
C 13	33(3)	56(3)	38(2)	8(2)	-2(2)	3(3)
C 14	43(3)	55(3)	27(2)	6(2)	-6(2)	12(2)
C 15	56(3)	47(3)	28(2)	-8(2)	-2(2)	-7(3)
C 16	41(3)	51(3)	34(2)	-5(2)	-2(2)	0(3)
N 1	58(3)	75(4)	38(2)	12(2)	-8(2)	-26(3)
N 03	36(2)	37(2)	33(2)	5(2)	-2(2)	-5(2)
O 1	82(3)	103(4)	70(3)	-32(3)	-3(2)	-39(3)
O 2	46(2)	106(3)	52(2)	17(2)	-16(2)	
O 04	48(2)	35(2)	52(2)	3(2)	-4(2)	-8(2)
O 9	44(2)	37(2)	35(2)	-4(1)	-3(1)	-5(2)
O 21	50(2)	35(2)	40(2)	-3(2)	9(2)	6(2)
O 101	58(2)	37(2)	40(2)	-10(2)	-6(2)	6(2)

Table 6. Hydrogen coordinates ($\times 10^4$) and isotropic displacement parameters ($A^2 \times 10^3$) for the compound.

	X	Y	Z	U(eq)
H 01	6100(3)	1850(4)	3999(11)	22(11)
H 02A	4630(5)	790(6)	4386(17)	72(18)
H 02B	4260(3)	100(4)	4042(11)	21(10)
H 4	6520(4)	3230(5)	2566(13)	43(13)
H 04	4030(7)	4660(8)	3540(2)	130(3)
H 04A	2380(4)	2660(5)	4351(14)	44(13)
H 04B	2050(5)	2170(6)	3921(17)	71(18)
H 04C	2490(6)	1090(9)	4290(2)	120(3)
H 5	6860(4)	2360(5)	1911(14)	46(13)
H 6	6860(4)	50(5)	1756(15)	56(14)
H 7	6410(3)	1360(4)	2268(11)	16(11)
H 12	8220(4)	1240(4)	3989(12)	33(12)
H 13	9630(4)	200(5)	4329(13)	43(14)
H 15	7210(4)	2210(5)	4843(13)	48(14)
H 16	5830(5)	1050(6)	4517(16)	64(19)
H 21	5580(5)	3130(5)	3503(15)	54(15)

REFERENCES

1 M. A. Hermodson, W. M. Barker, K.P. Link, *J. Med. Chem.* **1971**, 14, 176.

2 H. Wulf, H. Rauer, T. During, C. Hanselmann, K. Ruff, A. Wrisch, S. Grissmer, W. Hansel. *J. Med. Chem.* **1998**, 41, 4542.

3 H. I. Skulnick, P. D. Johnson, P. A. Aristoff, J. K. Morris, K. D. Lovasz. *J. Med. Chem.* **1997**, 40, 1149.

4 C. Spino, M. Dodier, S. Sotheeswaren. *Bioorganic & Med. Chem. Lett.* **1998**, 8, 3475.

5 F. W. Crow, W. K. Duholke, K. A. Farley, C. E. Hadden, D. A. Hahn, B. D. Kaluzny, C. S. Mallory, G. E. Martin, R. F. Smith, T. J. Tamann. *J. Heterocycl. Chem.* **1999**, 36, 365.

6 B. V. Nonius, *"Collect" data collection software*, **1999.**

7 A. A. Ajees, S. Manikandan, and R. Raghunathan, *Acta Cryst.* **2002**, E58, 802 [doi: 10.1107/S1600536802010863].

8 M. R. Lutz Jr, M. Zeller, and D. P. Becker, Acta Cryst., **2007**, E63, 4390 [doi: 10.1107/S16005368007051136].

9 Z. Otwinovski and W. Minor, " Macromolecular Crystallography, Part A Methods in Enzymology", Academic Press, New York, **1997**, 307.

10 G. M. Sheldrick, *SHELX97*. Program for the Refinement of Crystal Structures from Diffraction Data, University of Göttingen, Germany, **1997**.

11 I. Manolov, N. D. Danchev. *Arch. Pharm. Pharm. Med. Chem.* **1999**, 332 (7), 243.

12 A. Penkova, P. Retailleau, I. Manolov. X-Ray Structure Analysis Online **2009**, 25, 125.

СИНТЕЗА И КРИСТАЛНА СТРУКТУРА НА 4-ХИДРОКСИ-3-[(3E)-3-(ХИДРОКСИИМИНО)-1-(4-НИТРОФЕНИЛ)БУТИЛ]-2H-ХРОМЕН-2-ОН

И. Манолов[1] , Ч. Майхле-Мьосмер[2]

[1]*Катедра по Фармацевтична химия, Фармацевтичен факултет, Медицински университет,ул. „Дунав" 2, 1000 София, България*
[2]*Институт по неорганична химия, Моргенщеле-18, Тюбинген 72076, Германия*

(Резюме)

Структурата на 4-хидрокси-3-[(3E)-3-(хидроксиимино)-1-(4-нитрофенил)бутил]-2H-хромен-2-он е определена чрез монокристален рентгеноструктурен анализ. Съединението кристализира в орторомбична кристална система и пространствена група Pbcn, с параметри на елементарната клетка a = 11.3411(8)Å, b = 10.0843 (14)Å, c = 33.170(3)Å, α = β = γ= 90º, Z = 8, V = 3793.6(7)Å^3. Кристалната структура е доказана с директни методи и точно определена с помощта на метода на най-малките квадрати за F^2 до стойност R1 = 0.0946.

Chemical transformations of *β*-hydroxyethyl esters of n-2-hydroxyalkyl carbamic acids

V. A. Mitova[1], R. Ts. Cherkezova[2], K. D. Troev[1]*

[1] *Institute of Polymers, Bulgarian Academy of Sciences, Acad. G. Bonchev St., Bl. 103A, 1113 Sofia, Bulgaria*
[2] *Medical University "Prof. Dr. Paraskev Stoyanov" Varna, Tsar Osvoboditel Blvd. 76, Varna, 9000 Bulgaria*

The reactivity of *β*–hydroxyethyl esters of N-2-hydroxyalkyl carbamic acids at different temperatures was examined. It was established that *β*–hydroxyethyl esters of N-2-hydroxyalkyl carbamic acids at 45ºC undergo several chemical transformations resulting in the formation of 2-oxazolidinones, 1,2-propandiol, 2-aminoethanol, N-2-hydroxyethyl carbamic acid and substituted 3-(2-hydroxyethyl) 2-oxazolidinones. At elevated temperatures (>150ºC) these esters afforded bis(2-hydroxyethyl) urea and N-(2-hydroxyethyl)-imidazolidinone. The reactivity enhancement of *β*–hydroxyethyl esters of N-2-hydroxyalkyl carbamic acids may probably be explained through hydrogen bonding. The role of the hydroxyl group in these reactions may be regarded as intramolecular catalysis.

Key words: *β*–Hydroxyethyl esters of N-2-hydroxyalkyl derivatives of carbamic acid, chemical transformations.

INTRODUCTION

It has been recently reported that the reaction of H- phosphonic acid diesters {$(RO)_2P(O)H$, R = CH_3, C_2H_5, C_3H_7, i-C_3H_7, C_4H_9 and C_6H_5} with a mixture of 1-methyl-2-hydroxyethyl-N-2'-hydroxyethyl carbamate and 2-methyl-2-hydroxyethyl-N-2'-hydroxyethyl carbamate at elevated temperatures (>160ºC) resulted in 3-ethyl-2-hydroxy-2-oxo-1,4,2-oxazaphosphorinane [1–3].
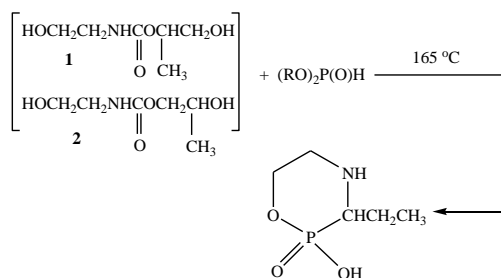
The formation of this cyclic aminophosphonic acid in 21% yield is unexpected having in mind the structure of the starting compounds. Obviously, the secondary reaction products resulting from the chemical transformations of the initial esters of carbamic acid react with the diesters of H-phosphonic acid to give 3-ethyl-2-hydroxy-2-oxo-1,4,2-oxazaphosphorinane.

It is well known that amino alcohols of short chain length, when reacted with 1,3-dioxolan-2-on yielded *β*–hydroxyethyl esters of N-2-hydroxyalkyl carbamic acids and the product distilled, gave cyclic urethanes [4,5]. For instance, 2-aminoethanol and 1,3-dioxolan-2-on at 45ºC yielded 2-oxazolidinone [4]; 4-amino-2-butanol and 3-amino-1-propanol gave six-membered cyclic urethanes. Facilitation of the alkaline hydrolysis of 1,2-diol monoesters is a well-established fact [6–9]. On the other hand it is known that the hydroxyl group in the esters of carboxylic acids plays an important role in amide-forming reactions [6–9].

In the present communication the chemical transformations of *β*–hydroxyethyl esters of N-2-hydroxyalkyl carbamic acid are studied.

EXPERIMENTAL

Materials:

Propylene carbonate (4-methyl-1,3-dioxolan-2-on) and ethylene carbonate (1,3-dioxolan-2-on) (Aldrich) were dried under vacuum. 2-Aminoethanol, 1-amino-2-propanol and 2-(methylamino)ethanol were purchased from Aldrich and were used as supplied.

NMR spectra were measured on a Bruker spectrometer at 250 MHz in $CDCl_3$ at 25ºC using TMS as an internal standard. FAB spectra were measured on a MAT 8200 spectrometer in glycerol.

---

* To whom all correspondence should be sent:
 E-mail: ktroev@polymer.bas.bg

General procedure for the synthesis of β –hydroxyethyl esters of N-2-hydroxyalkyl carbamic acids

β−Hydroxyethyl esters of N-2-hydroxyalkyl carbamic acids were synthesized by reacting an equimolar amount of alkylene carbonate with aminoalcohol. Alkylene carbonate was added to aminoalcohol at temperatures below 10 ºC. After that the reaction mixture allowed to stay at 45ºC for 6 h.

Synthesis of 1-methyl-2-hydroxyethyl-N-2'-hydroxyethyl carbamate (1) and 2-methyl-2-hydroxyethyl-N-2'-hydroxyethyl carbamate (2)

A mixture of (**1**) and (**2**) was synthesized by reacting 4-methyl-1,3-dioxolan-2-on with 2-aminoalcohol.

1-Methyl-2-hydroxyethyl-N-2'-hydroxyethyl carbamate (**1**): ^{1}H NMR: δ = 1.20 (d, ^{3}J(H,H)=6.3 Hz, 3H, CH_3), 3.29 (q, ^{3}J(H,H)=5.04 Hz, 2H, CH$_2$CH_2NH), 3.64 (t, ^{3}J(H,H)=5.4 Hz, 2H, CH$_2$CH_2OH), 3.63–3.66 (dd, ^{3}J(H,H)=2.8 Hz, 2H, CHCH_2OH), 3.96–4.01 (m, 1H, CH), 4.24 (br s, OH), 6.19 ppm (t, ^{3}J(H,H)=5.4 Hz, NH); ^{13}C {H}NMR: δ = 16.83 (*C*H3), 43.67 (N*C*H$_2$), 61.63 (*C*H$_2$OH), 65.80 (CH*C*H$_2$OH), 72.72 (*C*H), 157.86 ppm (*C*=O).

2-Methyl-2-hydroxyethyl-N-2'-hydroxyethyl carbamate (**2**): ^{1}H NMR: δ = 1.17 (d, ^{3}J(H,H)=6.3 Hz, CH_3), 3.29 (q, ^{3}J(H,H)=5.04 Hz, 2H, CH$_2$CH_2NH), 3.64 (t, ^{3}J(H,H)=5.4 Hz, 2H, CH$_2$CH_2OH), 3.82–3.88 (m, 1H, CH), 4.04 , 4.07 (dd, ^{3}J(H,H)=2.8 Hz, 2H, OCH_2CH), 4.24 (brs, OH), 6.06 ppm (t, ^{3}J(H,H) = 5.4 Hz, 1H, NH). ^{13}C {H}NMR: δ =19.30 (*C*H$_3$), 43.61 (N*C*H$_2$), 61.63 (*C*H$_2$OH), 66.30 (*C*HOH), 70.30 (*C*H$_2$OC), 157.80 ppm (*C*=O); FAB-MS m/z=164.2.

Synthesis of 2-hydroxyethyl-N-2'-hydroxyethyl carbamate (3)

2-Hydroxyethyl-N-2'-hydroxyethyl carbamate (**3**) was synthesized from 1,3-dioxolan-2-on and 2-aminoethanol.

2-Hydroxyethyl-N-2'-hydroxyethyl carbamate (**3**): ^{1}H NMR: δ =3.29 (t, ^{3}J(H,H)=5.7 Hz, 2H, NHCH_2), 3.62 (t, ^{3}J(H,H)=5.8 Hz, 2H, CH_2OH), 3.74 (t, ^{3}J(H,H)=4.6 Hz, 2H, CH_2OH), 4.13 (t, ^{3}J(H,H)=5.6 Hz, 2H, (C(O)CH_2OH), 4.89 ppm (br s, 3H, OH and NH); ^{13}C {H} NMR: δ=37.29 (N*C*H$_2$), 59.64 (*C*H$_2$OH), 61.34 (CO*C*H$_2$), 157.99 ppm (*C*=O); FAB-MS m/z=150.1.

Synthesis of 1-methyl-2-hydroxyethyl-N-methyl-N-2'-hydroxyethyl carbamate (4) and 2-methyl-2-hydroxyethyl-N-methyl-N-2'-hydroxyethyl carbamate (5)

A mixture of (**4**) and (**5**) was synthesized by reacting 4-methyl-1,3-dioxolan-2-on with 2-(methylamino)ethanol.

1-Methyl-2-hydroxyethyl-N-methyl-N-2'-hydroxyethyl carbamate (**4**): ^{1}H NMR: δ =1.19 (d, ^{3}J(H,H)=6.3 Hz, 3H, CH_3), 3.18 (s, 3H, N-CH_3), 3.28 (t, ^{3}J(H,H)=5.1 Hz, 2H, CH_2N), 3.61 (t, ^{3}J(H,H)=5.4 Hz, 2H, CH_2OH), 3.66–3.68 (m, 2H, CHCH_2), 4.12– 4.15 (m, 1H, CH), 4.25 ppm (b.s. 2H, OH); ^{13}C {H} NMR: δ=16.79 (*C*H$_3$), 31.71 (N*C*H$_3$), 47.11 (NCH2), 59.78 (*C*H$_2$OH), 61.98 (CH*C*H$_2$OH), 70.81 (O*C*H), 157.22 ppm (*C*=O).

2-Methyl-2-hydroxyethyl-N-methyl-N-2'-hydroxyethyl carbamate (**5**): ^{1}H NMR: δ =1.17 (d, ^{3}J(H,H)=6.3 Hz, 3H, CH_3), 3.18 (s, 3H, N-CH_3), 3.28 (t, ^{3}J(H,H)=5.1 Hz, 2H, CH_2N), 3.61 (t, ^{3}J(H,H)=5.4 Hz, 2H, CH_2OH), 3.81–3.91 (m, 1H, CH), 4.07–4.09 (m, 2H, OCH_2CH), 4.25 ppm (b.s. 2H, OH); ^{13}C {H} NMR: δ=19.07 (*C*H$_3$), 31.71 (N*C*H$_3$), 47.11 (N*C*H$_2$), 59.78 (*C*H$_2$OH), 61.98 (CH*C*H$_2$OH), 68.51 (O*C*H), 157.18 ppm (*C*=O); FAB-MS m/z = 178.1.

Synthesis of 2-hydroxyethyl-N-2'-hydroxypropyl carbamate (6)

2-Hydroxyethyl-N-2'-hydroxypropyl carbamate (**6**) was synthesized by reacting 1,3-dioxolan-2-on with 1-amino-2-propanol.

2-Hydroxyethyl-N-2'-hydroxypropyl carbamate (**6**): ^{1}H NMR: δ =1.16 (d, ^{3}J(H,H)=6.3 Hz, 3H, CH_3), 2.97-3.03 and 3.18-3.27 (m, 2H, CHCH_2NH), 3.75 (t, ^{3}J(H,H)=4.4 Hz, 2H, CH_2OH), 3.83–3.93 (m, 1H, CH), 4.15 (t, ^{3}J(H,H)=5.0 Hz, 2H, COCH_2), 4.28 (b.s., 2H, OH), 6.18 ppm (t, ^{3}J(H,H)=5.7 Hz, 1H, NH); ^{13}C {H} NMR: δ=20.38 (*C*H$_3$), 48.21 (N*C*H$_2$), 60.81 (*C*H$_2$OH), 66.45 (C(O)*C*H$_2$), 66.83 (*C*HOH), 157, 64 ppm (*C*=O); FAB-MS m/z = 164.1.

Reactivity of β–hydroxyethyl esters of N-2-hydroxyalkyl carbamic acids

1-Methyl-2-hydroxyethyl-N-2'-hydroxyethyl carbamate (1) and 2-methyl-2-hydroxyethyl-N-2'-hydroxyethyl carbamate (2) At 110 ºC

13.2 g (0.08 mol) of **1** and **2** were put into a three-necked flask equipped with a condenser, magnetic stirrer and thermometer. The reaction

mixture was heated at 110ºC for 1 h. After that the reaction mixture was allowed to cool to room temperature and was subjected to distillation.

Chemical transformations of *β*-hydroxyethyl esters of n-2-hydroxyalkyl carbamic acids *1,2-Propanediol* [2.4 g, 0.03 mol, 18,2 %, b.p. 34ºC $(4.10^{-2}$ mm Hg)]; ^{1}H NMR: δ =1.13 (d, ^{3}J(H,H)=6.6 Hz, 3H), 3.22 – 3.49 (m, 2H), 3.70 –3.80 (m, 1H), 4.24 ppm (br s); ^{13}C NMR: δ =19.11 (CH_3), 68.19 (CH_2), 68.63 ppm (CH); *2-Oxazolidinone* [1.9 g, 0.022 mol, 14.4 %, b.p. 89ºC $(4.10^{-2}$ mm Hg)]; ^{1}H NMR: δ =3.48–3.56 (m, 2H, NCH_2), 4.28–4.36 (m, 2H, OCH_2), 6.68 ppm (br s, 1H, N*H*); ^{13}C NMR: δ =42.01 (C4), 65.43 (C5), 161.15 ppm (C2); *2-Aminoethanol* [2.4 g, 0.04 mol, 18.2 %, b.p. 28 ºC $(4.10^{-2}$ mm Hg)] were distilled. *Residue*, 6.5g.

At 155ºC

13.1 g, (0.08 mol) of **1** and **2** were heated at 155ºC for 2 h. During the heating CO_2 was evolved. After that the reaction mixture was allowed to cool to room temperature and was subjected to distillation.

1,2 –Propanediol [3.1 g, 0.04 mol, 23.7 %], *2-oxazolidinone* [3.4 g, 0.04 mol, 25.9 %] and a mixture of *5-methyl-3-(2-hydroxyethyl)-2-oxazolidinone* and *4-methyl-3-(2-hydroxyethyl)-2-oxazolidinone* [1.9 g, 0.01 mol, 16.4 %, b.p. 105 ºC $(2.10^{-2}$ mm Hg)] were distilled; *5-Methyl-3-(2-hydroxyethyl)-2-oxazolidinone*, ^{13}C {H} NMR: δ =20.83 (*C*H$_3$), 44.02 (NCH_2), 46.88 (C4), 65.42 (*C*H$_2$OH), 70.96 (C5), 159.23 ppm (*C*=O). *4-Methyl-3-(2-hydroxyethyl)-2-oxazolidinone*, ^{13}C {H} NMR: δ =20.83 (CH$_3$), 52.48 (NCH$_2$), 44.02 (C4), 65.42 (*C*H$_2$OH), 59.86 (C5), 159.23 ppm (C=O). Residue, (3.5 g, 26.7 %).

1 and **2** were heated at 165ºC for 15 and 22 h. FAB-MS spectral data are given in Table 1.

2-Hydroxyethyl-N-2'-hydroxyethyl carbamate (3)

10.8 g (0.07 mol) of **3** were heated at 165ºC for 5 h. During the heating CO_2 was evolved. After that the reaction mixture was allowed to cool to room temperature and was subjected to distillation; *2-oxazolidinone* [1.5 g, 0.017 mol, 13.9%] and N-(2-hydroxyethyl)-2-oxazolidinone [0.8 g, 0.006 mol, 7.4 %, b.p. 112ºC $(3.10^{-2}$ mm Hg)] were distilled. *N-(2-hydroxyethyl)-2-oxazolidinone* ^{13}C NMR: δ=44.02 (NCH_2), 46.88 (C4), 65.42 (*C*H$_2$OH), 70.96 (C5), 159.23 ppm (*C*=O). Residue, 8.2 g.

1-Methyl-2-hydroxyethyl-N-methyl-N-2'-hydroxyethyl carbamate (4) and 2-methyl-2-hydroxyethyl-N-methyl-N-2'-hydroxyethyl carbamate (5)

11.3 g (0.064 mol) of **4** and **5** were heated at 165ºC for 5 h. During the heating CO_2 was evolved. After that the reaction mixture was allowed to cool to room temperature and was subjected to distillation; *1,2-propanediol* (<0.5 g), *2-(methylamino)ethanol* [1.4 g, 0.018 mol, 12.4%] and *3-methyl-2- oxazolidinone* [3.5 g, 0.034 mol, 31.3%] were distilled. *3-Methyl-2-oxazolidinone* ^{1}H NMR: δ =3.48 -3.56 (m, 2H, NCH_2), 4.28–4.36 (m, 2H, OCH_2), 3.82 ppm (s, 3H, N-CH_3); ^{13}C{H} NMR: δ =47.80 (N-CH$_3$), 42.01 (C4), 65.43 (C5), 161.15 ppm (C2). Residue, 5.1 g.

2-Hydroxyethyl-N-2'-hydroxypropyl carbamate (6)

11.4 g (0.07 mol) of **6** was heated at 165ºC for 5 h. After that the reaction mixture was allowed to cool to room temperature and was subjected to distillation; *ethylene glycol* [1.6 g, 0.026 mol, 14.0%] and 5-methyl-2-oxazolidinone [2.5 g, 0.02 mol, 22.0%, b.p. 88 ºC $(2.10^{-2}$ mm Hg)] were distilled. *5-Methyl-2-oxazolidinone*, ^{1}H NMR: δ=1.45 (d, ^{3}J(H,H)=3.8 Hz, 3H, CH_3), 3.65–3.71 (m, 2H, NCH_2), 4.73–4.81 (m, 1H, C*H*), 6.8 ppm (br. s, 1H, N*H*); ^{13}C {H} NMR: δ=20.84 (*C*H$_3$), 47.78 (N*C*H2), 73.90 (*C*H), 160.91 ppm (*C*=O). Residue, 7.3 g.

RESULTS AND DISCUSSION

Chemical transformations of 1-methyl-2-hydroxyethyl-N-2'-hydroxyethyl carbamate and 2-methyl-2-hydroxyethyl-N-2'-hydroxyethyl carbamate
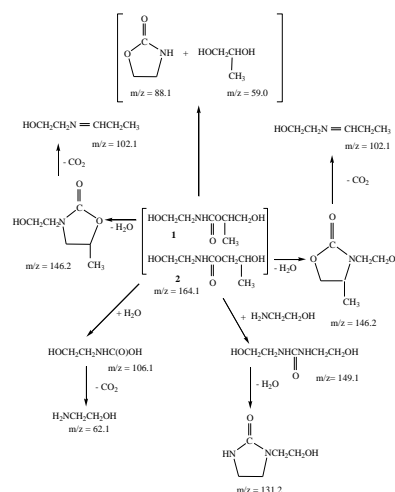
Scheme 1. Chemical transformations of **1** and **2**.

Table 1. FAB-MS spectral data of the products obtained after heating of **1** and **2** at 45ºC, 110ºC, 155ºC and 165ºC. Peak intensities are given in parentheses.

Compound	$[M + H]^+$	45 ºC	110 ºC	155 ºC	165 ºC 15 h	22 h
1 and **2**	164.2	(100)	(100)	(65.7)	(20.7)	(3.3)
2-Oxazolidinone	88.1	(9.5)	(58.8)	(71.5)	(40.4)	(28.5)
1,2-Propanediol	59.1*	(3.2)	(17.5)	(12.1)	(9.8)	(6.4)
N-2-hydroxyethyl carbamic acid	106.1	(9.3)	(25.8)	(5.0)	(2.0)	(0.0)
2-Aminoethanol	62.1	(10.1)	(65.4)	(34.5)	(18.1)	(2.7)
Bis(2-hydroxyethyl) urea	149.1	(0.0)	(2.9)	(74.8)	(72.1)	(3.5)
N-2-hydroxyethyl imidazolidinone	131.2	(0.0)	(1.0)	(45.1)	(94.4)	(100)
5-Methyl-3-(2-hydroxy-ethyl)-2-oxazolidinone and 4-Methyl-3-(2-hydroxy-ethyl)-2-oxazolidinone	146.2	(6.8)	(10.5)	(84.4)	(100)	(27.4)
$HOCH_2CH_2N = CHCH_2CH_3$ (Shiff base)	102.1	(0.0)	(3.8)	(8.8)	(17.4)	(26.8)

* At the FAB conditions 1,2-propanol undergoes dehydration resulting in the formation of a cation with m/z = 59.1.

Study of the mixture of 1-methyl-2-hydroxyethyl-N-2'-hydroxyethyl carbamate **1** and 2-methyl-2-hydroxyethyl-N-2'-hydroxyethyl carbamate **2** (m/z=164.2) after heating by FAB-MS revealed that depending on the temperature, several chemical reactions take place, resulting in the formation of new compounds (Scheme 1). The FAB-MS spectrum of the starting mixture of **1** and **2** showed that at 45ºC formation of a few compounds with m/z=88.1, 106.1, 146.2 proceeds. The mixture of **1** and **2** was heated at 165ºC for 15 and 22 h. FAB-MS spectral data are given in Table 1.

NMR studies of **1** and **2** after heating confirmed that several chemical reactions proceeded. ^{13}C {H}NMR spectrum (Fig. 1) revealed that several new carbonyl compounds are formed as a result of heating of **1** and **2**. The new signals at 159.02 ppm, 160.36 ppm, 161.1 ppm, and 164.04 ppm, characteristic for carbonyl carbon atoms appear after heating (Fig. 1b). The signals at 16.42 and 18.88 ppm for CH$_3$ carbon atoms of **1** and **2** (Fig. 1a) disappear (Fig. 1b). New signals at 18.68 ppm and 20.45 ppm which can be assigned to CH$_3$ carbon atoms appear (Fig. 1b). The intensity of the signal for NCH$_2$ carbon atoms of **1** and **2** (43.25 ppm and 43.31ppm) strongly decreases. New signals appear in the region 38.08 ppm – 46.48 ppm
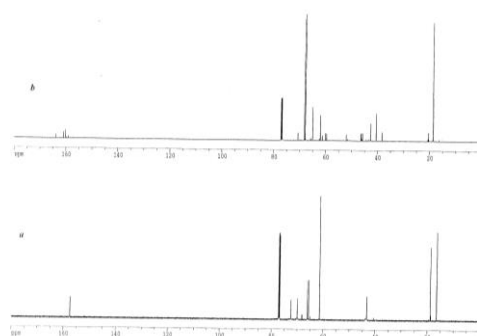
Fig. 1. ^{13}C {H}NMR spectrum of a mixture of **1** and **2**: (a) at 45 ºC and (b) after heating at 165ºC for 15 h.

which are characteristics for NCH$_2$ carbon atoms. Signals at 69.98 ppm and 72.44 ppm for C(O)OCH$_2$ and C(O)OCH carbon atoms disappear. In the ^{1}H NMR spectrum two doublets for CH$_3$ protons at 1.15 ppm and 1.18 ppm of **1** and **2** disappear. A new signal for CH$_3$ protons appears at 1.07 ppm. The characteristic signals at 5.82 and 5.98 ppm for C(O)NH protons of **1** and **2** disappear. A new signal at 5.95 ppm for NH protons appears. A few compounds were isolated by distillation. The intramolecular transesterification of **1** and **2** (by nucleophilic attack of 2'- hydroxyl group at the carbonyl group) yielded 2-oxazolidinone and 1,2-propanediol (eq.1).

117

$$\left[\begin{array}{l} HOCH_2CH_2NHCOCHCH_2OH \\ \mathbf{1} \quad\quad\quad \underset{O}{\|} \; \underset{CH_3}{|} \\[2mm] HOCH_2CH_2NHCOCH_2CHOH \\ \mathbf{2} \quad\quad\quad \underset{O}{\|} \quad \underset{CH_3}{|} \end{array}\right] \rightleftharpoons \underset{m/z = 88.1}{\boxed{O{-}C({=}O){-}NH}} + HOCH_2CHOH\;(CH_3) \qquad \text{eq.1}$$
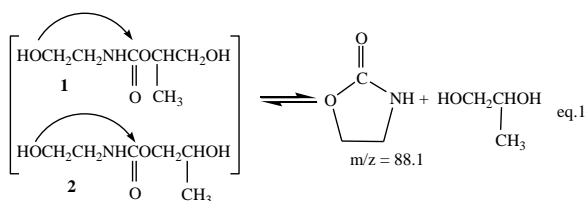
The signal at 161.1 ppm in the ^{13}C {H}NMR spectrum (Fig. 1b) can be assigned to the carbonyl atom of 2-oxazolidinone. The doublet at 1.13 ppm with $^3J(H,H)=6.6$ Hz can be assigned to the CH_3 group of 1,2-propanediol. 2-Oxazolidinone and 1,2-propanediol were isolated by vacuum distillation. The experimental results showed that the intramolecular transesterification proceeds at 45ºC. The reactivity enhancement of β-hydroxyethyl esters of N-2-hydroxyalkyl carbamic acids is explicable in terms of hydrogen bonding of the β-hydroxyl group to the alcoholic oxygen. Such hydrogen bonding makes the carbonyl atom a stronger electrophilic center and favors the transesterification reaction at mild conditions.

$$\begin{array}{c} H \\ | \\ CH_2 - O \quad\; O \quad\; H - O \\ | \qquad\quad \| \qquad\quad | \\ CH_2 - N \; C \; O \; CH - CH \\ \qquad\qquad\qquad\quad | \quad\; | \\ \qquad\qquad\qquad\quad X \quad\; Y \end{array}$$
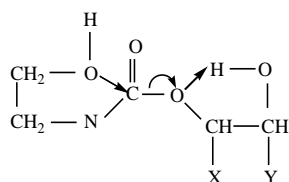
The hydrolysis of **1** and **2** at 45ºC yielded N-2-hydroxyethyl carbamic acid (m/z 106.1). This acid decomposes at temperatures higher than 110ºC to 2-aminoethanol (m/z=62.1) and CO_2 (eq.2).

$$\left[\begin{array}{l} HOCH_2CH_2NHCOCHCH_2OH \\ \mathbf{1} \quad\quad\quad \underset{O}{\|} \; \underset{CH_3}{|} \\[2mm] HOCH_2CH_2NHCOCH_2CHOH \\ \mathbf{2} \quad\quad\quad \underset{O}{\|} \quad \underset{CH_3}{|} \end{array}\right] \xrightarrow[\;+H_2O\;]{} \underset{m/z = 106.1}{HOCH_2CH_2NHC(O)OH} \xrightarrow[-CO_2]{140\,ºC} \underset{m/z = 62.1}{H_2NCH_2CH_2OH} \qquad \text{eq. 2}$$
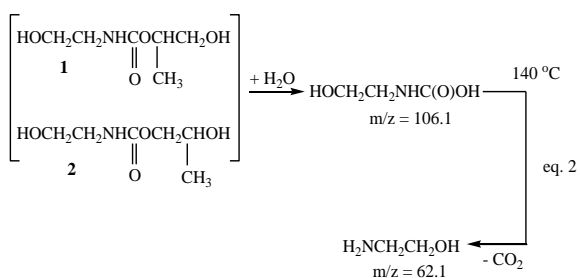
The peak with m/z=149.1 can be assigned to bis(2-hydroxyethyl)urea. This compound can be obtained *via* transesterification of **1** and **2** with ethanolamine (eq.3) or as a result of the reaction of 2-oxazolidinone with 2-aminoethanol (eq.4).

$$\left[\begin{array}{l} HOCH_2CH_2NHCOCHCH_2OH \\ \mathbf{1} \quad\quad\quad \underset{O}{\|} \; \underset{CH_3}{|} \\[2mm] HOCH_2CH_2NHCOCH_2CHOH \\ \mathbf{2} \quad\quad\quad \underset{O}{\|} \quad \underset{CH_3}{|} \end{array}\right] + HOCH_2CH_2NH_2 \xrightarrow[-HOCH_2CHOH(CH_3)]{} \qquad \text{eq. 3}$$

$$\underset{m/z = 149.1}{HOCH_2CH_2NHCNHCH_2CH_2OH \; (\underset{O}{\|})} \xrightarrow[-H_2O]{} \underset{m/z = 131.2}{HN{-}C({=}O){-}NCH_2CH_2OH}$$

$$\underset{}{\boxed{O{-}C({=}O){-}NH}} + H_2NCH_2CH_2OH \xrightarrow{\qquad} \qquad \text{eq.4}$$

$$\underset{m/z = 149.1}{HOCH_2CH_2NHCNHCH_2CH_2OH \;(\underset{O}{\|})}$$
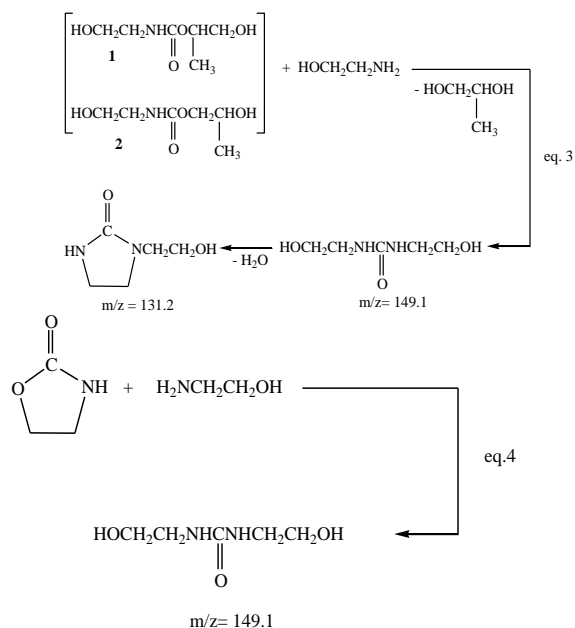
The experimental results revealed that the formation of bis(2-hydroxyethyl)urea *via* eq.4 is more acceptable at elevated temperatures.

The dehydration of bis(2-hydroxyethyl)urea, which starts at 110ºC, furnished N-(2-hydroxyethyl) imidazolidinone (m/z=131.2). At 165ºC after 22 h heating N-(2-hydroxyethyl) imidazolidinone was the main product (Table 1). It is known that higher temperatures [10] accelerate the dehydration of N-(2-hydroxyethyl)ureas to imidazolidinones. The experimental results showed that when heating at 165ºC is realized in the presence of a few drops of H_2SO_4 the main peak has m/z=131.2. We accept that H_2SO_4 catalyses the intramolecular transesterification of **1** and **2**, the transesterification of 2-oxazolidinone with 2-aminoethanol to form bis(2-hydroxyethyl)urea and its dehydration to N-(2-hydroxyethyl) imidazolidinone (m/z=131.2).

The FAB-MS spectrum showed a peak with m/z=146.2 which is the main peak at 165ºC and can be assigned to substituted 3-(2-hydroxyethyl)-2-oxazolidinones. 5-Methyl-3-(2-hydroxyethyl)-2-oxazolidinone and 4-methyl-3-(2-hydroxyethyl)-2-oxazolidinone result from the dehydration of **1** and **2** (eq.5).

$$\underset{\mathbf{1}}{HOCH_2CH_2NHCOCHCH_2OH\,(\underset{O}{\|}\,\underset{CH_3}{|})} \xrightarrow[-H_2O]{} \underset{\substack{CH_3 \\ m/z = 146.2}}{O{-}C({=}O){-}NCH_2CH_2OH} \qquad \text{eq.5}$$

$$\underset{\mathbf{2}}{HOCH_2CH_2NHCOCH_2CHOH\,(\underset{O}{\|}\,\underset{CH_3}{|})} \xrightarrow[-H_2O]{} \underset{CH_3}{O{-}C({=}O){-}NCH_2CH_2OH}$$
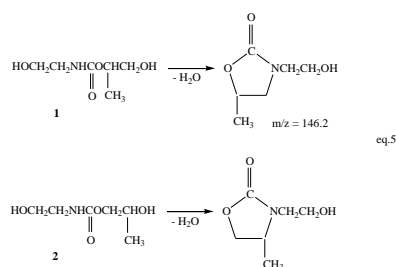
The experimental results showed that the dehydration reaction starts at 45ºC and higher temperatures favour the dehydration of **1** and **2**. The participation of the NH proton in the hydrogen bonding with the oxygen atom of the β –hydroxyl group, favours the dehydration reaction, to yield substituted 3-(2-hydroxyethyl) -2-oxazolidinones.
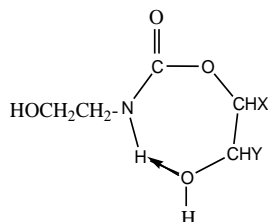
The substituted 3-(2-hydroxyethyl)-2-oxazolidinones are thermally unstable. The experimental results revealed that their content decreases (Table 1) from 100 % to 27.4 % at 165ºC after 22 h heating and their decomposition is accompanied by evolution of CO_2. The following reaction scheme for the decomposition of the substituted 3-(2-hydroxyethyl)-2-oxazolidinones can be accepted (eq. 6),

eq.6
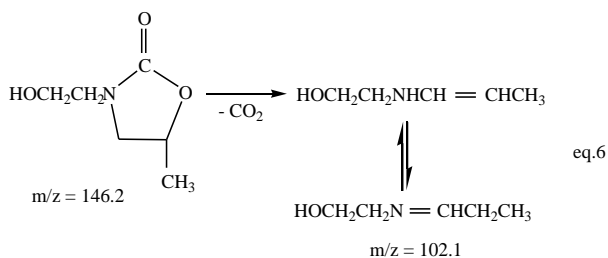
In the FAB-MS spectrum a peak with m/z=102.1 appears which can be assigned to the Schiff base resulting from the decomposition of the substituted 3-(2-hydroxyethyl)-2-oxazolidinones. From the FAB-MS studies it can be seen that the content of this compound increases with the temperature increase. Unfortunately, we had no chance to isolate this compound. Indirect evidence for its formation is the isolated 3-ethyl-2-hydroxy-2-oxo-1,4,2-oxazaphosphorinane (eq.7).

eq.7
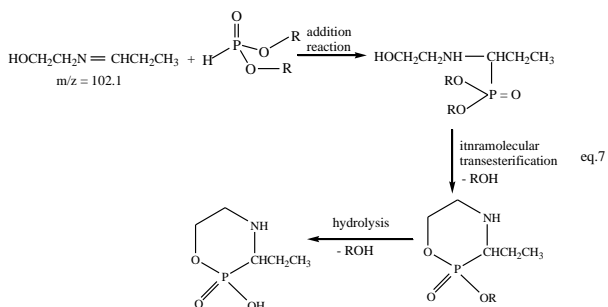
Reactivity of 2-hydroxyethyl-N-2'-hydroxyethyl carbamate (3)

The experimental results show that 2-hydroxyethyl-N-2'-hydroxyethyl carbamate **3** undergoes the same reactions as **1** and **2**. The FAB-MS spectrum showed that during the synthesis of **3** (45ºC) there proceeds intramolecular transesterification yielding 2-oxazolidinone (m/z = 88). The FAB-MS spectral data showed that the main compound which forms at 165˚C is N-2-hydroxyethyl-imidazolidinone (m/z = 131.1).

Reactivity of 1-methyl-2-hydroxyethyl-N-methyl-N-2'-hydroxyethyl carbamate (4) and 2-methyl-2-hydroxyethyl-N-methyl-N-2'-hydroxyethyl carbamate (5)

The mixture of 1-methyl-2-hydroxyethyl-N-methyl-N-2'-hydroxyethyl carbamate and 2-methyl-2-hydroxyethyl-N-methyl-N-2'-hydroxyethyl carbamate was studied mainly because of the lack of NH proton in these carbamates. The experimental results showed that **4** and **5** undergo the same chemical transformation as **1**, **2** and **3**. The only difference with **1**, **2** and **3** is the absence of 3-substituted-2-oxazolidinones.

This result is a direct evidence for the participation of the NH proton of β–hydroxyethyl esters of N-2-hydroxalkyl derivatives of carbamic acid in a dehydration reaction yielding substituted 3-(2-hydroxyalkyl) 2-oxazolidinones.

Reactivity of 2-hydroxyethyl-N-2'-hydroxypropyl carbamate (6)

In 2-hydroxyethyl-N-2'-hydroxypropyl carbamate one of the hydroxyl groups is secondary. Therefore it was of interest to study the reactivity of this carbamate. 5-Methyl-2-oxazolidinone (m/z = 102) is the main compound which forms at 165ºC. The intramolecular transesterification of 2-hydroxyethyl-N-2'-hydroxypropyl carbamate starts at 45ºC.

CONCLUSION

The results obtained demonstrate that β–hydroxyethyl esters of N-2-hydroxyalkyl carbamic acids are very reactive compounds at different temperatures. At mild conditions they undergo several chemical transformations. The specific reactivity of these esters of carbamic acids is determined by the presence of a β –hydroxyl group. The reactivity enhancement of β–hydroxyethyl esters of N-2-hydroxyalkyl carbamic acids may be probably explained through

hydrogen bonding. The role of the hydroxyl group in these reactions may be regarded as intramolecular catalysis. The reaction temperature has an effect on the reactivity of the β–hydroxyethyl esters of N-2-hydroxyalkyl carbamic acids. Temperatures lower than 150ºC promote the intramolecular transesterification reaction resulting in the formation of oxazolidinones while temperatures higher than 150ºC favor the dehydration reaction leading to the formation of substituted 3-(2-hydroxyethyl) 2-oxazolidinones. Probably the decarboxylation of the substituted-3-(2-hydroxyethyl)-2-oxazolidinone at elevated temperatures furnished a Schiff base which reacted with H-phosphonic acid diesters to give 1,4,2-oxazaphosphorinane.

REFERENCES

1. K. Troev, *Phosphorus, Sulfur Silicon Relat. Elem.*, **127**, 167 (1997).
2. K.Troev, Sh. Cremer, G. Hagele, *Heteroat. Chem.*, **10**, 627 (1999).
3. K.Troev, G. Hagele, K. Kreidler, R. Olschner, C. Verwey, D. M. Roundhill, *Phosphorus, Sulfur Silicon Relat. Elem.*, **148**, 161 (1999).
4. E. Dyer, H. Scott, *J. Am. Chem. Soc*., **79**, 672 (1957).
5. a) S. Gabriel, *Ber.*, **21**, 569 (1888); b) P. Vieles, J. Seguin*, Bull. Soc. Chim. France,* 287 (1953); c) R. Delaby, R. Damines, G. d'Huyteza, *Compt. Rend*., **239**, 674 (1954); d) J. B. Bell, L. Silver, J. D. Malkemus, *US Patent* 2755286 (1956); e) E. Dyer, R. Read, *J. Org. Chem*., **24**, 1788 (1959); f) A. Homeyer, *US Patent* 2399118 (1946); j) J. R. Caldwell, *US Patent* 2656328 (1953); h) M.-J. Viard, GB Patent 689705 (1953).
6. N.Ogata, K. Sanui, H. Nakamura, *Polym. J.*, **10**, 499 (1978).
7. H.Nakamura, H. Sakuma, N. Ogata, *Polym. J.*, **11**, 279 (1979.
8. H.Puntambekar, D. Naik, A. Kapadi, *Indian J. Chem.*, **32B**, 684 (1993).
9. F. M. Menger, J. H. Smith, *J. Am. Chem. Soc*., **91**, 5346 (1969).
10. G. S. Poindexter, D. A. Owens, P. L. Dolan, E. Woo, *J. Org. Chem*., **57**, 6257 (1992)

ХИМИЧНИ ТРАНСФОРМАЦИИ НА β-ХИДРОКСИЕТИЛОВИ ЕСТЕРИ НА N-2-ХИДРОКСИАЛКИЛ КАРБАМИНОВИ КИСЕЛИНИ

В.А. Митова[1], Р.Ц. Черкезова[2], К.Д. Троев[1]

[1] Институт по полимери,Българска академия на науките, ул.Акад. Г. Бончев, блок 103А, 1113 София
Меицински университет „Проф. Парашкев Стоянов“, бул. Ц. Освободител 76, 9000 Варна

(Резюме)

Изследвана е реактивоспособността на β-хидроксиетилови естери на N-2-хидроксиалкил карбаминови киселини при различни температури. Установено е че β-хидроксилестерите of N-2-хидроксиакил карбаминови киселини при 45ºС претърпяват няколко химични трансформации, даващи 2-оксазолидони, 1,2-пропандиол, 2-сминоетанол, N-2-хидроксиетил карбаминова киселина и заместени 3-(2-хидроксиетил) 2-оксазолидони. При по-високи температури (>150ºC) тези естери these esters afforded бис(2-хидроксиетил) карбамид и N-(2-хидроксиетил)-имидазолидон. Повишаването на реактивоспособността на β-хидроксиетиловите естери на N-2-хидроксиалкил карбаминовите киселини вероятно може да се обясни чрез образуване на водородни връзки. Ролята на хидроксилните групи при тези реакции може да се отнесат към интрамолекулния катализ.

.

BULGARIAN CHEMICAL COMMUNICATIONS

Instructions about Preparation of Manuscripts

General remarks: Manuscripts are submitted in English by e-mail or by mail (in duplicate). The text must be typed double-spaced, on A4 format paper using Times New Roman font size 12, normal character spacing. The manuscript should not exceed 15 pages (about 3500 words), including photographs, tables, drawings, formulae, etc. Authors are requested to use margins of 3 cm on all sides. For mail submission hard copies, made by a clearly legible duplication process, are requested. Manuscripts should be subdivided into labelled sections, e.g. **Introduction, Experimental, Results and Discussion**, *etc.*

The title page comprises headline, author's names and affiliations, abstract and key words.

Attention is drawn to the following:

a) **The title** of the manuscript should reflect concisely the purpose and findings of the work. Abbreviations, symbols, chemical formulas, references and footnotes should be avoided. If indispensable, abbreviations and formulas should be given in parentheses immediately after the respective full form.

b) **The author**'s first and middle name initials, and family name in full should be given, followed by the address (or addresses) of the contributing laboratory (laboratories). **The affiliation** of the author(s) should be listed in detail (no abbreviations!). The author to whom correspondence and/or inquiries should be sent should be indicated by asterisk (*).

The abstract should be self-explanatory and intelligible without any references to the text and containing not more than 250 words. It should be followed by key words (not more than six).

References should be numbered sequentially in the order, in which they are cited in the text. The numbers in the text should be enclosed in brackets [2], [5, 6], [9−12], etc., set on the text line. References, typed with double spacing, are to be listed in numerical order on a separate sheet. All references are to be given in Latin letters. The names of the authors are given without inversion. Titles of journals must be abbreviated according to Chemical Abstracts and given in italics, the volume is typed in bold, the initial page is given and the year in parentheses. Attention is drawn to the following conventions:

a) The names of all authors of a certain publications should be given. The use of "*et al.*" in the list of references is not acceptable.

b) Only the initials of the first and middle names should be given.

In the manuscripts, the reference to author(s) of cited works should be made without giving initials, e.g. "Bush and Smith [7] pioneered...". If the reference carries the names of three or more authors it should be quoted as "Bush *et al.* [7]", if Bush is the first author, or as "Bush and co-workers [7]", if Bush is the senior author.

Footnotes should be reduced to a minimum. Each footnote should be typed double-spaced at the bottom of the page, on which its subject is first mentioned.

Tables are numbered with Arabic numerals on the left-hand top. Each table should be referred to in the text. Column headings should be as short as possible but they must define units unambiguously. The units are to be separated from the preceding symbols by a comma or brackets.

Note: The following format should be used when figures, equations, *etc.* are referred to the text (followed by the respective numbers): Fig., Eqns., Table, Scheme.

Schemes and figures. Each manuscript (hard copy) should contain or be accompanied by the respective illustrative material as well as by the respective figure captions in a separate file (sheet). As far as presentation of units is concerned, SI units are to be used. However, some non-SI units are also acceptable, such as °C, ml, l, etc.

The author(s) name(s), the title of the manuscript, the number of drawings, photographs, diagrams, etc., should be written in black pencil on the back of the illustrative material (hard copies) in accordance with the list enclosed. Avoid using more than 6 (12 for reviews, respectively) figures in the manuscript. Since most of the illustrative materials are to be presented as 8-cm wide pictures, attention should be paid that all axis titles, numerals, legend(s) and texts are legible.

The authors are asked to submit **the final text** (after the manuscript has been accepted for publication) in electronic form either by e-mail or mail on a 3.5'' diskette (CD) using a PC Word-

processor. The main text, list of references, tables and figure captions should be saved in separate files (as *.rtf or *.doc) with clearly identifiable file names. It is essential that the name and version of the word-processing program and the format of the text files is clearly indicated. It is recommended that the pictures are presented in *.tif, *.jpg, *.cdr or *.bmp format, the equations are written using "Equation Editor" and chemical reaction schemes are written using ISIS Draw or ChemDraw programme.

The authors are required to submit the final text with a list of three individuals and their e-mail addresses that can be considered by the Editors as potential reviewers. Please, note that the reviewers should be outside the authors' own institution or organization. The Editorial Board of the journal is not obliged to accept these proposals.

EXAMPLES FOR PRESENTATION OF REFERENCES

REFERENCES

1. D. S. Newsome, *Catal. Rev.–Sci. Eng.*, **21**, 275 (1980).
2. C.-H. Lin, C.-Y. Hsu, *J. Chem. Soc. Chem. Commun.*, 1479 (1992).
3. R. G. Parr, W. Yang, Density Functional Theory of Atoms and Molecules, Oxford Univ. Press, New York, 1989.
4. V. Ponec, G. C. Bond, Catalysis by Metals and Alloys (Stud. Surf. Sci. Catal., vol. 95), Elsevier, Amsterdam, 1995.
5. G. Kadinov, S. Todorova, A. Palazov, in: New Frontiers in Catalysis (Proc. 10th Int. Congr. Catal., Budapest, 1992), L. Guczi, F. Solymosi, P. Tetenyi (eds.), Akademiai Kiado, Budapest, 1993, Part C, p. 2817.
6. G. L. C. Maire, F. Garin, in: Catalysis. Science and Technology, J. R. Anderson, M. Boudart (eds), vol. 6, Springer-Verlag, Berlin, 1984, p. 161.
7. D. Pocknell, *GB Patent* 2 207 355 (1949).
8. G. Angelov, PhD Thesis, UCTM, Sofia, 2001.
9. JCPDS International Center for Diffraction Data, Power Diffraction File, Swarthmore, PA, 1991.
10. CA **127**, 184 762q (1998).
11. P. Hou, H. Wise, *J. Catal.*, in press.
12. M. Sinev, private communication.
13. http://www.chemweb.com/alchem/articles/1051611477211.html.

CONTENTS

СЪДЪРЖАНИЕ